Enclosure 2
MIDUS Transportation Package Safety Analysis Report,
Document No. TYC01-1600, Revision 3, March 2016
Public Version
(1 paper copy)

MIDUS Transportation Package Safety Analysis Report

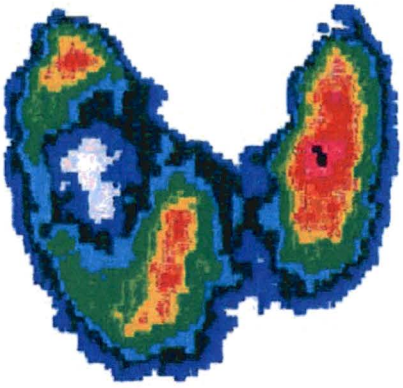

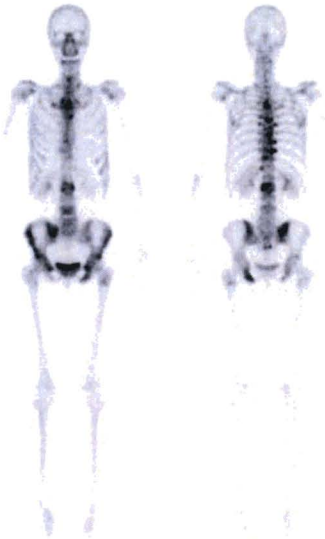

TYC01-1600
Docket No. 71-9320

ENERGYSOLUTIONS

MIDUS Transportation Package
Safety Analysis Report

Revision 3
March 2016

Document No. TYC01-1600
Docket No. 71-9320

Prepared by:
Energy*Solutions*
Campbell, CA

This page intentionally blank.

Table of Contents

Table of Contents (continued)

Table of Contents (continued)

Table of Contents (continued)

Table of Contents (continued)

Table of Contents (continued)

Table of Contents (continued)

Table of Contents (continued)

List of Tables

List of Tables (continued)

List of Tables (continued)

List of Tables (continued)

List of Figures

List of Figures (continued)

List of Figures (continued)

List of Figures (continued)

Nomenclature

ALARA	At least as low as reasonably achievable
ASME	American Society of Mechanical Engineers
B&PV	Boiler and Pressure Vessel Code, the ASME B&PV Code
CMS	Computational modeling software
DU	Depleted uranium, the DU alloy used to construct MIDUS
HAC	Hypothetical accident conditions: the tests specified in 10 CFR 71.73, or the condition of the packaging after such tests
LMC	Least material condition
MIDUS	Medical Isotope Depleted Uranium Shielded
MNOP	Maximum normal operating pressure
NCT	Normal conditions of transport: the tests specified in 10 CFR 71.71, or the condition of the packaging after such tests
Package	The packaging with its radioactive contents, or payload, as presented for transport. For MIDUS, the package includes the packaging plus the payload internals (the radioactive product, product container(s), and optional dunnage)
Packaging	The MIDUS cask assembly (cask body, shield plug, cask closure lid, cask shield lid, and fasteners) and overpack assembly (overpack base, overpack lid, and fasteners)
Product	Radioactive payload
SAR	Safety Analysis Report
Shield Lid	A shielded lid that installs onto the cask closure lid to provide additional gamma shielding in the post-HAC configuration
Shield Plug	The cylindrical plug that provides gamma shielding for normal operating conditions
T.I.	Transport index, as defined in 10 CFR 71.4

1 GENERAL INFORMATION

1.1 Introduction

This Safety Analysis Report (SAR) describes a reusable Type B(U) package design named MIDUS, which stands for Medical Isotope Depleted Uranium Shielded Transport Package. MIDUS will be used to transport ^{99}Mo, which decays to ^{99m}Tc, an important source for medical imaging. The package will deliver enough ^{99}Mo for millions of annual patient doses. The package is also suitable for other radioisotope sources as defined in Section 1.2.2.

The package is designed for non-exclusive use conveyance. The contents are normal or special form, non-fissile, and are Category II as defined by Regulatory Guide 7.11 [1.1].

The package is designed and manufactured in accordance with the Energy*Solutions*' 10 CFR 71, Subpart H quality assurance program, NRC approval number 0935.

This SAR demonstrates that the package meets the applicable requirements of 10 CFR 71. The basis for qualification is the safety analysis contained herein, supplemented by the results of full-scale confirmatory testing. The testing validates the analytical tools used in the safety analyses, and it physically demonstrates the robustness of the design. The complete test report is included in this SAR in Section 2.12.4.

1.2 Package Description

1.2.1 Packaging

Due to the short half-life of ^{99}Mo, the package is designed to be as small and light as possible to allow conveyance by land or air. The overall dimensions are 520 mm diameter by 551 mm high, and the maximum weight is 330 kg.

Drawing TYC01-1601 in Section 1.3.2 shows the package general arrangement, including the payload specification, major cask features, and packaging markings. The remainder of the drawings include general arrangements of the overpack and cask assemblies, containment system, closure devices, gamma shielding, heat transfer features, energy absorbing features, and lifting and tie-down features.

1.2.1.1 Overpack

Drawing TYC01-1602 in Section 1.3.2 shows the general arrangement of the overpack, including overall dimensions, material specifications, and weld callouts for the shells.

The overpack is a two-piece stainless steel shell filled with polyurethane foam. The foam is discussed in Section 1.2.1.7. The lid unit has four welded stainless steel lugs used for lifting and tie-down purposes. The base unit has a bottom flange with four integral lugs that may be used for additional tie-downs as needed. The outer shell is relatively thick for resistance to the normal

wear and tear of frequent use. The inner shell is relatively thinner to obtain the desired response to the hypothetical accident condition (HAC) specified in 10 CFR 71.51. This package crushes from the inside-out during the drop.

The inside radius at the top end of the overpack base unit is chamfered to provide lead-in for insertion of the cask during loading operations. The overpack flange is dog-leg shaped to provide a barrier for moisture and dirt. The flange mates snugly at the bolting ring to provide shear resistance in the drop.

Eight recessed alloy steel bolts fasten the overpack lid to the base unit. The design of the overpack closure is described below in Section 1.2.1.4.

Each of the lid and base units have four holes leading into the foam cavity. The holes are plugged with nylon screws intended to melt during the HAC fire test, providing pressure relief from the hot gas generated by the foam. This feature helps prevent the overpack shell from bursting during the fire, thus keeping the foam from direct contact with the flames. The thermal relief plugs have elastomeric O-rings to protect the foam from weather.

The overpack base unit has a copper thermal shunt, the thermal spider, which is brazed to the inner and outer shell. The thermal spider is described in Section 1.2.1.6 below.

Polymeric dunnage may be placed in the annular space between the cask assembly and overpack as needed to minimize scuffing or other wear.

A tamper-indicating security seal provides assurance that the package cannot be opened inadvertently and provides evidence of unauthorized opening if it occurs.

1.2.1.2 Cask Assembly

Drawing TYC01-1602 in Section 1.3.2 shows the cask assembly general arrangement, including overall dimensions, material specifications, and weld callouts for the shells.

The cask assembly includes a cask body, closure lid, shield plug, contents, and a separate shield lid that is installed on top of the closure lid.

The cask body is constructed from stainless steel and depleted uranium (DU). It has three main structural pieces and two DU parts. The containment shell is a monolithic, machined component that includes the cask inner shell, cask flange, and bolting circle. This part is described in detail in Section 1.2.1.3 below. The cask outer shell is welded to the containment shell and bottom shell, capturing the radial and bottom DU gamma shields. These shields are described below in Section 1.2.1.5.

The cask flange has two O-ring seals: an inner containment seal, and an outer test seal. The flange has a recessed step on the edge that forms a shear lip for the closure lid and prevents the closure bolts from shearing under transverse impact loads.

The shield plug is a DU core clad in stainless steel. It has a tapered bottom to assist remote insertion and reduce gamma streaming. The tapered surface has a "cleanliness" O-ring that serves two purposes. First, it provides a housekeeping seal which is useful as a redundant barrier for the ^{99}Mo production facility. Second, it provides enough compliance so that the shield plug protrudes slightly above the plane of the cask flange. When the cask lid is bolted shut, the cleanliness seal compresses, assuring that the shield plug is in close contact with the closure lid. This feature reduces the potential volume of fluid that can collect between the shield plug and closure lid in the worst-case HAC scenario, thus reducing the accident dose rates to as low as reasonably achievable.

The cask closure lid is secured by eight recessed alloy steel bolts, which are described in Section 1.2.1.4. The lid has a test port that communicates with the space between the test and containment O-rings. The test port has an elastomeric seal to protect the cask O-ring interspace from dust and moisture. The closure lid has two tapped holes with threaded inserts used for lifting the cask to and from the overpack. Two more threaded holes with thread inserts are located near the outer perimeter of the lid for attaching the shield lid. The closure lid's top surface has a warning marking to remind operators that the shield lid must be installed before closing the overpack.

The shield lid is a stainless steel-clad DU plate designed to maintain dose rates within allowable limits under the worst-case HAC scenario. If the product were to breach the product container(s) and the shield plug cleanliness seal, then the product could migrate up and around the shield plug, thereby bypassing most of the package's top end gamma shielding. The shield lid provides the extra required top end axial shielding *outside* the containment boundary. The shield lid is fastened to the cask closure lid using two captive bolts. The captive bolts are an operational aid, serving as a lift point and helping to minimize damage and loss of the bolts. By preventing separation of the shield lid in an end drop event, the shield lid fasteners also prevent radiation streaming between the shield lid and cask assembly.

1.2.1.3 Containment System

Drawing TYC01-1604 in Section 1.3.2 shows the specifications for the package containment system, including the location of the containment boundary, and the specifications for materials of construction, surface finishes, and key dimensions and tolerances.

The containment boundary has no welds, valves, pressure relief devices, or penetrations of any kind. Chapter 4 discusses the containment design in further detail.

1.2.1.4 Closure Devices

Drawing TYC01-1605 in Section 1.3.2 shows the specifications for the package closure devices.

The cask body closure is designed to protect the eight closure bolts from damage due to puncture and shear. The closure bolts are recessed in the lid to minimize damage by direct impact. The closure lid has a shear lip feature to prevent the bolts from being loaded in shear by transverse impact loads. The bolt holes are fitted with threaded inserts for improved maintenance.

The overpack closure is designed to protect its eight closure bolts in a similar fashion. The bolts are recessed, and the overpack lid has a shear lip, similar to the cask body. The closure is designed with shear pockets to further prevent shear loading of the bolts in oblique drops. The overpack closure bolt holes are also fitted with threaded inserts for improved maintenance.

1.2.1.5 Gamma Shielding

Drawing TYC01-1606 in Section 1.3.2 shows the specifications for the package gamma shielding.

Two DU parts provide the primary gamma shielding in the cask body: one radial piece, and an interlocking bottom piece. The joint is a stepped design to reduce radiation streaming. The shield plug has a third DU block. The removable shield lid has the fourth DU block in the form of a disk.

1.2.1.6 Heat Transfer Features

Drawing TYC01-1607 in Section 1.3.2 shows the specifications for the package heat transfer features.

The package generates a small amount of heat, which must be dissipated. Section 3.1.2 discusses the package heat generation. Heat flows from package top end through the steel in the overpack flange. The thermal spider provides the corresponding heat flow path through the bottom end of the packaging.

The thermal spider is constructed from copper and brazed to the bottom of the overpack inner shell. The legs are brazed to the overpack outer shell, near the base flange. The base flange provides a relatively large thermal mass of stainless steel that helps distribute the heat evenly.

The overpack foam serves as both an energy absorbing material and as thermal protection in the HAC fire event. The foam is discussed in Section 1.2.1.7 below.

During the fire, the thermal relief plugs discussed in Section 1.2.1.1 above are designed to melt and blow out of the overpack shell, reducing the overpack cavity pressure and allowing heat to escape via mass transfer.

1.2.1.7 Energy Absorbing Features

Drawing TYC01-1608 in Section 1.3.2 shows the specifications for the package's energy absorbing features. The polyurethane foam in the overpack is the primary energy absorbing feature for the free HAC drop.

The only penetrations through the overpack shells are the thermal relief plug ports, which have O-ring seals for weather and dust protection. The shells protect the foam from deterioration due to sunlight, atmospheric pollutants, or biological matter.

1.2.1.8 Lifting and Tie-Down Devices

Drawing TYC01-1609 in Section 1.3.2 shows the specifications for the package lifting and tie-down features.

There are four lifting/tie-down lugs on the overpack lid and four tie-down lugs on the overpack base. The lugs are sized for a standard-sized anchor shackle. Sections 2.5.1 and 2.5.2 describe the design and analysis of the lifting and tie-downs.

1.2.2 Contents

The contents of the MIDUS package are discussed in the following subsections. The MIDUS package was first designed for a natrium molybdate solution containing up to 4,400 Ci of ^{99}Mo, as described in Section 1.2.2.1 below. This payload is now referred to as Content #01 and all subsequent MIDUS payloads shall be identified with a unique sequential number. The safety analyses presented in Chapters 2 through 8 are for Content #01. For clarity, the chapter material is not revised for additional contents. Instead, evaluations to demonstrate that the additional contents comply with the applicable performance requirements of 10 CFR 71 are provided in the SAR addenda beginning with Chapter 9.

1.2.2.1 Content #01 - ^{99}Mo as Natrium Molybdate Solution

Content #01 is a liquid payload, or product, consisting of ^{99}Mo with its daughter products as natrium molybdate ($NaNO_3$ 1M / NaOH 0.2M). This payload is non-fissile and does not generate neutrons. The specification for Content #01 is provided on Drawing No. TYC01-1601 in Section 1.3.2 and discussed below.

The maximum product activity is 4,400 Ci of ^{99}Mo at the time of shipment. Section 5.2.1 discusses the photon source term calculations, including all significant equilibrium daughter products. Section 3.1.2 discusses the payload's maximum calculated thermal source term. The maximum product *specific* activity is 60 Ci/ml ^{99}Mo at the time of shipment. The specific activity affects the concentration of the potential radiological source terms for HAC. Section 5.3.1.2 describes the shielding assumptions made for HAC.

The product generates gas by radiolytic decomposition. This gas production affects package internal pressures and the composition of the internal gas mixture. The safety evaluations are based on experimental data for ^{99}Mo product solution produced by Mallinckrodt Medical, B.V., therefore the activity specifications above are only valid for Mallinckrodt-produced product solution.

The product volume may vary from 0 to 150 ml. The product volume affects potential gas pressures in the product bottle and cask containment. The package's maximum normal operating pressure (MNOP) is discussed further in Section 3.3.2.

The package materials of construction have been evaluated and are compatible with the chemical form of the product. Section 2.2.2 discusses the materials evaluation in further detail.

The payload internals for Content #01 include a user-supplied product bottle, secondary container, and snap ring, illustrated in Figure 1-1. These items are important for the ^{99}Mo manufacturing process and will always be present during shipping. Optional dunnage may be included in the form of a spacer to reduce vibration of the secondary container during shipment.

The product bottle is a stainless steel flask with a stainless steel cap sealed by a compression fitting metal-to-metal seal. It has a one-piece body with a welded base ring for stability. The design pressure for the product bottle is much higher than the package MNOP and the metal-to-metal seal offers containment-grade closure, although no credit is taken for this as containment.

The secondary container serves a housekeeping function in the ^{99}Mo manufacturing process. It is constructed from stainless steel and it provides a second barrier to the payload solution when its lid is installed. The lid is also constructed from stainless steel, and the seal is an elastomeric O-ring.

The snap ring has a threaded stud that screws into the bottom of the package's shield plug. It allows the other payload internals to be handled remotely in the ^{99}Mo production facility hot cell by use of spring-loaded detent-balls that engage the groove on top of the secondary container lid. The snap ring is constructed from stainless steel.

The maximum volume of the product bottle, secondary container, secondary container O-ring, snap ring, and dunnage is 125 ml. This is the volume of the materials of construction, not counting enclosed spaces. It is necessary to specify this volume because it impacts the pressure buildup during shipment.

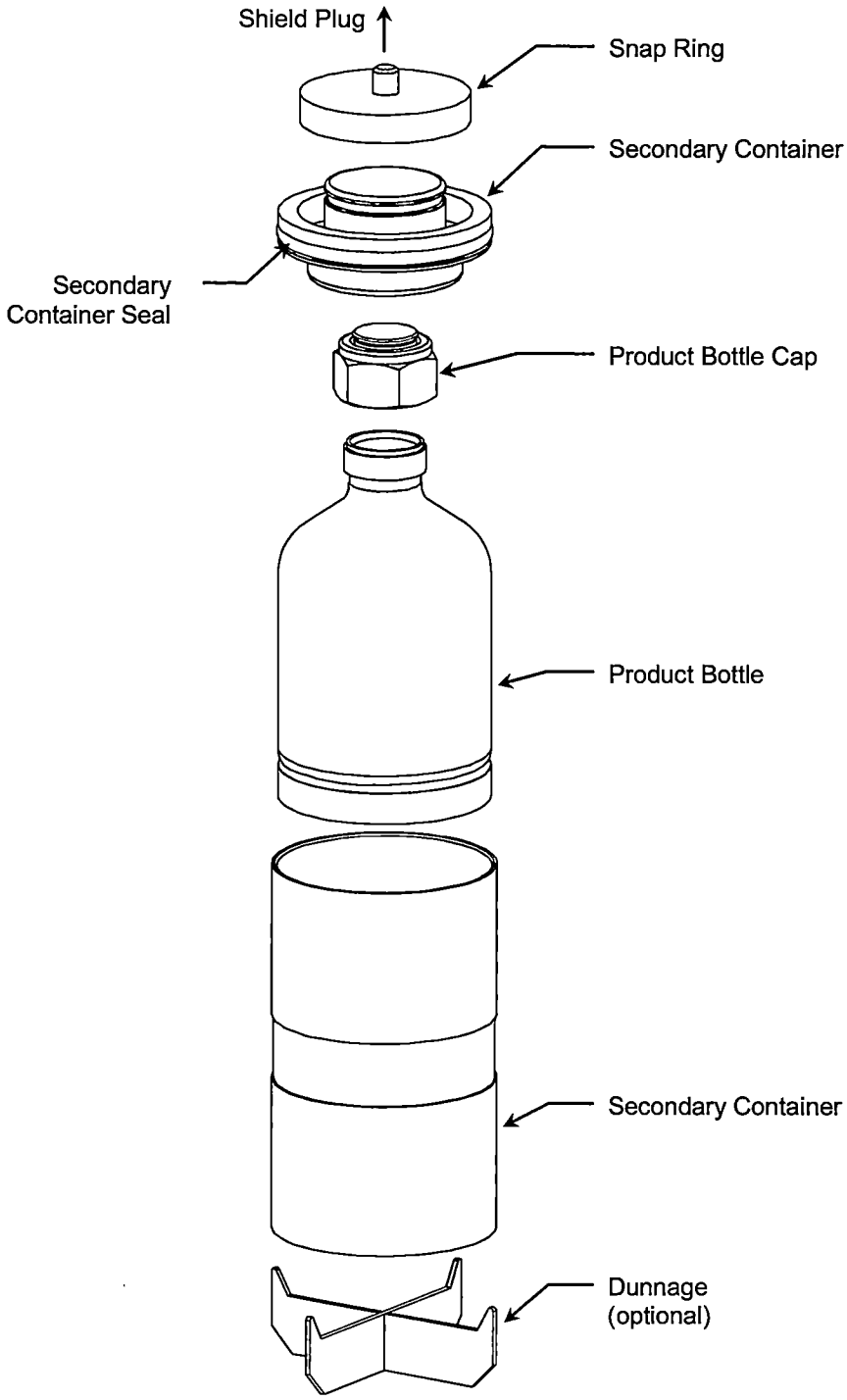

Figure 1-1 – Content #01 Payload Internals

1.2.2.2 Content #02 - ^{99}Mo as Metallic Molybdenum

Content #02 is specified on Drawing No. TYC01-1601 in Section 1.3.2, and described further in Section 9.1. Chapter 9 contains the safety evaluations for Content #02.

1.2.3 Special Requirements for Plutonium

Not applicable.

1.2.4 Operational Features

The package has no special or complex operational features. All operational features are described in the general arrangement drawings in Section 1.3.2. Chapter 7 describes the operational steps, including use of the package's operational features.

1.3 Appendix

1.3.1 References

[1.1] Regulatory Guide 7.11, *Fracture Toughness Criteria of Base Material for Ferritic Steel Shipping Cask Containment Vessels with a Maximum Wall Thickness of 4 Inches (0.1 m)*, U.S. Nuclear Regulatory Commission, June 1991.

[1.2] NUREG/CR-5502, *Engineering Drawings for 10 CFR Part 71 Package Approvals*, U.S. Nuclear Regulatory Commission, May 1998.

1.3.2 Drawings

Drawings 1601 through 1609 show the package's general arrangement and design features in accordance with NUREG/CR-5502 [1.2]. The drawings refer to material specifications, welding requirements, inspection and test requirements, and dimensions as necessary to support the safety analyses.

Drawing No.	Title	Rev.
TYC01-1601	General Arrangement of Packaging and Contents	1
TYC01-1602	General Arrangement of Cask Assembly	1
TYC01-1603	General Arrangement of Overpack Assembly	1
TYC01-1604	Containment System	2
TYC01-1605	Closure Devices	0
TYC01-1606	Gamma Shielding	1
TYC01-1607	Heat Transfer Features	0
TYC01-1608	Energy Absorbing Features	0
TYC01-1609	Lifting and Tie-Down Devices	0

Drawings withheld on the basis that they are Security-Related Information

2 STRUCTURAL EVALUATION

The structural evaluation of the MIDUS package demonstrates compliance with the applicable performance requirements of 10 CFR 71. The structural evaluation presented in the body of this chapter is for the liquid payload (i.e., Content #01) described in Section 1.2.2.1. For clarity, the body of this chapter is not revised extensively for additional contents. Instead, the structural evaluation of each additional payload is presented in SAR addenda, starting in Chapter 9. Compliance with the applicable general standards (§71.43) and lifting and tie-down standards (§71.45) is demonstrated in Sections 2.4 and 2.5, respectively. The structural evaluation for NCT tests (§71.71) and HAC tests (§71.73) presented in Sections 2.6 and 2.7, respectively, demonstrates that the structural components of the package satisfy the applicable structural design criteria of Subsections WB [2.1] and NF [2.2] of the ASME Boiler and Pressure Vessel Code. Furthermore, under NCT tests (§71.71), the package will experience no loss or dispersal of radioactive contents, no significant increase in external surface radiation levels, and no substantial reduction in the effectiveness of the packaging. Therefore, the package satisfies the requirements of §71.43(f) and §71.51(a)(1). The structural evaluation also shows that the cumulative package damage resulting from the HAC test sequence (§71.73) does not result in escape of other radioactive material exceeding a total amount of A_2 in one week, nor does it result in an external radiation dose rate that exceeds 10 mSv/h at 1 m from the external surface of the package. Thus, the package satisfies the requirements of §71.51(a)(2).

The structural evaluation of the package is performed by analysis using computational modeling software (CMS) and classical closed-form solutions (hand calculations). The analytic techniques used for the structural evaluation comply with guidance provided in Regulatory Guide 7.9 [2.3], as supplemented by Interim Staff Guidance – 21 (ISG-21) [2.4]. The ANSYS Mechanical and ANSYS LS-DYNA PC computer programs are used for the structural evaluation of the package. These computer programs are well-benchmarked and widely used for structural analyses of transportation packages for radioactive materials. Descriptions of these computer programs, including discussion of validation of the computer codes, are provided in Section 2.12.2. The computer models used for the structural evaluation are identified and described in the following sections.

The adequacy of the analytic techniques used to evaluate the package dynamic response to NCT and HAC free drop and puncture drop impacts is demonstrated by comparison to results of full-scale confirmatory drop tests. The confirmatory tests performed, along with comparisons to pretest predictions determined using the same analytic techniques used for the structural analysis of the package, are discussed in Section 2.12.4. The results confirm that the computer model developed to evaluate the dynamic response of the package for NCT and HAC drop tests provides accurate predictions of the cask rigid-body response, the structural response of the overpack assembly, and the extent of damage sustained by the overpack.

2.1 Description of Structural Design

2.1.1 Discussion

The principal structural members that are important to the safe operation of the package are the cask assembly, shield lid assembly, and overpack assembly. The cask is the central component of the package that provides containment of the radioactive contents, radiation shielding, and structural support. The shield lid provides supplemental shielding on the top end of the cask. The overpack limits the impact loads imparted to the cask under NCT and HAC free drop tests and insulates the cask from the effects of the HAC thermal test. The structural design of these assemblies is described in the following sections.

2.1.1.1 Cask Assembly

The cask assembly includes a cask body assembly, a shield plug assembly, a closure lid assembly, and eight cask closure bolts. The shield plug is placed in the top end of the cask body and captured by the closure lid and closure bolts. The internal cylindrical cavity volume, which is formed by the cask body and shield plug, houses the payload.

The cask body consists of a stainless steel shell assembly that encases the cask body gamma shield components. The cask body shell assembly is constructed entirely from austenitic stainless steel material and is formed from three pieces: a containment shell, an outer shell, and an outer bottom. The containment shell and outer bottom are both machined from solid pieces of steel. The containment shell forms the inner shell for the cask cavity and shield plug regions, as well as the bolting flange for the cask closure. The top plate of the containment shell includes grooves that accommodate the containment and leak-test O-rings. A 3:1 taper transition is included between the containment shell wall that surrounds the shield plug cavity and the top flange to minimize stress concentration at the structural discontinuity. The containment shell bolting flange includes eight closure bolt holes, fitted with threaded inserts. The cask body outer shell is rolled from plate and formed with a full-penetration longitudinal seam weld. The outer shell is connected to the containment shell and outer bottom with full-penetration circumferential groove welds.

The cask body gamma shield, which is sealed inside the cask body shell, consists of two pieces: a bottom shield and radial shield. Both the cask body bottom shield and radial shield are fabricated from depleted uranium (DU) that is alloyed with 2% molybdenum by weight (U-2% Mo). A stepped interface is provided between the DU bottom shield and radial shield to minimize radiation streaming through the interface. The cask body assembly is designed with nominal radial clearances of 0.65 mm between the containment shell and radial shield and 0.35 mm between the outer shell and radial shield. The larger clearance on the inside of the radial shield assures that the containment shell will not support the weight of the radial shield when subjected to transverse loads, such as a side drop. A longitudinal clearance of 0.7 mm is provided between the bottom end of the cask containment shell and the top surface of the bottom shield to assure that the cask containment shell does not support the weight of the bottom shield when subjected to loads such as a top-end drop or top-corner drop.

The shield plug consists of U-2% Mo shielding material that is fully encased in stainless steel. The shield plug top plate has an integral lifting boss located on the centerline. The bottom end of the shield plug includes a pocket that accommodates the top end fitting of the payload hardware. The bottom corner of the shield plug casing is chamfered and includes a groove that houses an elastomeric "cleanliness" O-ring seal, whose function is to prevent radioactive material from contaminating the cavity spaces that surround the shield plug. The cleanliness O-ring seal is compressed when the closure lid is bolted to the cask body.

The closure lid is a circular plate that is equipped with a test port, holes for the closure bolts, and threaded holes for lifting the cask and attaching the shield lid. The eight equally spaced holes that accommodate the cask closure bolts include a recess for heads of the closure bolts. The two holes used for lifting the cask are fitted with threaded inserts. Two additional holes located near the perimeter of the closure lid are used to attach the shield lid to the cask. The closure lid includes an integral shear lip on the outer bottom edge that interfaces with the top end of the cask body. The closure lid shear lip is designed to resist all shear forces resulting from NCT and HAC impact loads, thereby protecting the closure bolts from shear failure. A shear pocket is machined into the outer top edge of the closure lid to accommodate the shield lid shear lip.

The cask containment system, which is designed for a maximum normal operating pressure (MNOP) of 700 kPa, is formed by the cask body containment shell, closure lid, containment O-ring seal, and eight closure bolts. There are no welds in the cask containment system since the cask containment shell is machined from a single, solid piece of steel. Furthermore, the containment boundary does not include any ports, valves, or pressure relief devices. The leak-test port in the cask closure lid is used to perform helium leak tests on the containment system during fabrication and pre-shipment pressure rise or drop leakage tests following cask assembly. A sealed plug is installed in the leak-test port prior to shipment to prevent debris or water from entering the leak-test port cavity.

2.1.1.2 Shield Lid Assembly

The shield lid assembly, which provides additional shielding on the top end of the package, is bolted to the top end of the cask prior to installing the overpack lid. The shield lid consists of DU shield plate that is fully encased in a stainless steel shell assembly. The shield lid has an integral shear lip on the outer bottom edge that interfaces with the top end of the closure lid. The shield lid is attached to the top end of the closure lid by two captured socket head cap screws that are fabricated from austenitic stainless steel. The shield lid is lifted and handled using the two capture attachment bolts. The shield lid must be installed on the cask after its placement in the overpack base cavity. When the shield lid is installed, the cask lifting attachments and leak-test port on the closure lid are not accessible.

2.1.1.3 Overpack Assembly

The overpack assembly consists of a base assembly and a lid assembly that are bolted together. The overpack has a flat bottom-end that provides a stable base for transport. Four high-strength steel lugs are attached to the overpack lid for lifting and tie-down of the package. The base of the

overpack also includes four integral lugs that may be used for additional tie-down attachments, but only in combination with the lid lugs, as described in Section 2.5.2.

The overpack base and lid assemblies are constructed in a similar manner. Both consist of a water-tight stainless steel shell assembly, inside which polyurethane foam is placed. The overpack base and lid shell are fabricated entirely from mild austenitic stainless steels, with the exception of the overpack lid lugs, which are fabricated from higher strength stainless steel material. The overpack base and lid shell are filled with LAST-A-FOAM® FR-3714 polyurethane foam with a nominal density of 13.5 lb/ft^3. The foam is placed in-situ with the direction of foam rise parallel to the longitudinal axis of the package. Following foam placement, stainless steel covers are welded over the foam pour holes to protect the foam from water intrusion and contamination.

The overpack base and lid both have 6 mm thick outer shells and 3.0 mm thick inner shells. The thicker outer shells provides a rugged exterior that is resistant to damage from normal handling and that prevents penetration and perforation under NCT and HAC loading. The thin inner shell of the overpack protects the foam from damage due to normal handling, but is designed to deform under NCT and HAC free drops, allowing the polyurethane foam to absorb energy and limit the impact loads imparted to the cask.

The overpack bolted closure, which includes the overpack base and lid bolting flanges and eight closure bolts made from high strength alloy steel bolting material, is designed to withstand all NCT and HAC tests without significant permanent deformation or bolt failure. The overpack base and lid bolting flanges are relatively large in comparison to the package size to accommodate a shear relief pocket on the overpack base flange for each closure bolt. The use of longer closure bolts and shear relief pockets allows the overpack closure bolts to flex without breaking under severe impact loads. Furthermore, the bolting flange also includes an integral shear lip that is designed to withstand shear loads resulting from impacts and to protect the overpack closure bolts from shear failure.

Thermal relief plugs are provided in the both the overpack base and lid to prevent over-pressurization of the shell assemblies during the HAC thermal test. The thermal relief plugs are nylon thumb screws with elastomeric O-ring seals that prevent water from intruding into the foam cavities under normal conditions, but are designed to melt under the extreme temperatures of a fire and to allow gasses generated by the foam to escape. Four thermal relief plugs are equally spaced around both the overpack lid bolting flange and overpack base tie-down flange. The number and locations of the thermal relief ports are designed to preclude blockage that could prevent pressure relief.

2.1.2 Design Criteria

The design criteria used for the structural design of the package is selected in accordance with the codes and standards identified in Section 2.1.4. Structural analyses of the package are performed for the applicable NCT tests [§71.71] and HAC tests [§71.73]. The combination of initial conditions used for the structural evaluation of each NCT and HAC test are discussed in Section 2.1.2.1. The stresses in the package structural components are calculated for the NCT

and HAC load combinations and compared to the allowable stress design criteria described in Section 2.1.2.2. Other structural failure modes, such as brittle buckling, fatigue, and brittle fracture, are evaluated using the design criteria discussed in Sections 2.1.2.3 through 2.1.2.5.

2.1.2.1 Load Combinations

The load combinations used for the structural evaluation of the package are developed in accordance with Regulatory Guide 7.8 [2.5]. The load combinations are based on Table 1 of Regulatory Guide 7.8, with additional load combinations for intermediate initial conditions that could possibly create a more limiting case for the package design. The NCT and HAC load combinations are summarized in Table 2-1 and Table 2-2.

2.1.2.2 Allowable Stresses

The pressure-retaining components of the cask containment system, which consist of the cask containment shell, closure lid, and closure bolts, are designed in accordance with the requirements of Subsection WB of the ASME Code [2.1]. In addition, the non-pressure-retaining circumferential weld that attaches the cask outer shell to the cask containment shell, is designed in accordance with the applicable requirements of Subsection WB of the ASME Code. The containment component stress intensity limits for NCT and HAC, which are developed in accordance with Figures WB-3221-1 and WB-3224-1, respectively, are summarized in Table 2-3.

With the exception of the overpack assembly, all package structural components that are not relied upon for containment are designed in accordance with the allowable stress design criteria for Class 2 plate- and shell-type supports from Subsection NF of the ASME Code [2.2]. The NCT and HAC allowable stress design criteria for the package non-containment components are summarized in Table 2-4.

Subsections NF and WB of the ASME Code impose stress limitations on primary membrane, local membrane, membrane (primary or local) plus bending, and primary plus secondary stress intensities. To demonstrate conformance to the ASME Code limits, it is necessary to determine the required code stress intensities at the critical cross-sections of the cask. Since the critical cross-section locations are load-condition-dependent, several "stress evaluation sections" are established to ensure that all critical locations have been evaluated for every load condition. The stress evaluation sections selected for the cask containment system and non-containment components are illustrated in Figure 2-1 and Figure 2-2, respectively. Multiple sections are selected in the high stress regions near the ends of the shells. For evaluation of conditions producing a stress distribution in the cask that is not axisymmetric, section stress evaluations are performed at multiple circumferential locations to assure that the maximum stresses are captured. For the cask shell buckling evaluation, membrane stress components at the mid-length of the cask inner and outer shell (sections C5 and N5) are used.

The section stresses at each stress evaluation location are obtained using the ANSYS "stress linearization" post-processing feature. The stress linearization provides membrane, bending, membrane plus bending, peak, and total stress intensities at each section. These stresses are

classified in accordance with the ASME Code for comparison to the applicable allowable stress design criteria as follows:

Membrane Stress Intensity

The membrane stress intensities are classified as primary membrane (P_m) or local membrane (P_l) based upon the location in the structure and the nature of the stress. Membrane stresses occurring at a structural discontinuity (e.g., at the transition inner shell thickness transitions and at the shell-to-flange transitions) are classified as local membrane, provided that the distance over which the membrane stress intensity exceeds the P_m limit does not exceed $1.0(Rt)^{1/2}$, where R is the minimum mid-surface radius of curvature and t is the minimum thickness in the region considered. Membrane stresses at all other sections are classified as primary.

Membrane Plus Bending Stress Intensity

The membrane plus bending stress intensities at each section are classified as either primary (P_m+P_b) or secondary (P_m+P_b+Q) based upon the location in the structure. Bending stresses at gross structural discontinuities, such as flange-to-shell junctions and junctions between shells of different diameters or thickness, are classified as secondary. Membrane plus bending stress intensities at all other stress sections are classified as primary.

Total Stress Intensity

Total stress intensities include primary plus secondary plus peak stresses. In accordance with the ASME Code, these stresses are objectionable only as a possible source of a fatigue crack or a brittle fracture. As shown in Section 2.1.2.4, evaluation of cyclic loading is not required for the cask components other than bolts.

Using the critical sections from each load case, minimum design margins are calculated and reported for all bounding load combinations. The design margin (D.M.) is defined as follows:

$$\text{D.M.} = \left(\frac{\text{Allowable Value}}{\text{Calculated Value}} \right) - 1;$$

where the allowable and calculated values are in consistent units.

The overpack shell is designed to deform plastically and absorb the kinetic energy when subjected to the NCT free drop, HAC free drop, and HAC puncture drop load conditions. Therefore, a strain-based design criteria is used for the overpack. The maximum crush depth of the polyurethane foam in the overpack is generally limited to 70% of the nominal foam section thickness. In cases of highly localized foam crush, e.g., that due to the HAC hot top-corner drop impact, the maximum foam crush depth may not exceed 80% of the nominal foam section thickness. The maximum strain in the overpack stainless steel shell components is limited to the lower-bound maximum elongation from the ASME material specifications for all material options.

The overpack closure bolts are designed to satisfy the Service Level A allowable stress design criteria for Class 2 supports from Subsection NF of the ASME Code for NCT. The bolt allowable stress design criteria for NCT is summarized in Table 2-3. However, a strain-based design criteria is used for the overpack closure bolts for HAC free drop and HAC puncture drop load conditions. The maximum strain in the overpack closure bolts is limited to the bolt material maximum elongation from the ASME material specification. In addition, the average shear stress in the overpack closure bolts for HAC is limited to the lesser of $0.6S_y$ and $0.42S_u$ in accordance with Appendix F [2.6] of the ASME Code.

2.1.2.3 Buckling

The cask inner and outer shells are evaluated for buckling in accordance with the requirements of ASME Code Case N-284-1 [2.7]. The geometric parameters of the cask inner and outer shells used for the buckling evaluation are summarized in Table 2-5. Capacity reduction factors are calculated in accordance with Section -1511 of ASME Code Case N-284-1 to account for possible reductions in the capacity of the shells due to imperfections and nonlinearity in geometry and boundary conditions. Plasticity reduction factors, which account for nonlinear material properties when the product of the classical buckling stresses and capacity reduction factors exceed the proportional limit, are calculated in accordance with Section -1610 of ASME Code Case N-284-1. The theoretical buckling stresses of the cask inner and outer shells under uniform stress fields are calculated in accordance with Section -1712.1.1 of ASME Code Case N-284-1. Cask shell lower-bound material properties at an upper bound temperature of 93°C are conservatively used to determine the buckling factors and theoretical buckling stresses. The capacity reduction factors, plasticity reduction factors, and theoretical buckling stresses for the cask inner and outer shells are summarized in Table 2-6.

The allowable elastic and inelastic buckling stresses for NCT and HAC are calculated in accordance with the formulas given in Section -1713.1.1 and Section -1713.2.1 of ASME Code Case N-284-1. The allowable buckling stresses include factors of safety of 2.0 for NCT and 1.34 for HAC in accordance with Section -1400 of ASME Code Case N-284-1. Table 2-7 provides a summary of the cask inner and outer shell elastic and inelastic buckling stresses for NCT and HAC. Buckling interaction ratios are calculated for the cask inner and outer shells for all NCT and HAC tests that load the shells in compression. The interaction ratios for elastic buckling and inelastic buckling are calculated using the highest values of compressive stress and shear stress from the finite element analysis solutions in accordance with the formulas given in Section -1713.1.1 and Section -1713.2.1 of ASME Code Case N-284-1.

2.1.2.4 Fatigue

2.1.2.4.1 Structural Components, Other Than Bolts

Analysis of the package structural components for cyclic service is not required because the conditions stipulated in WB-3221.9(d)(1) through (6) are met. The analysis is conservatively based on the assumption that the package will be used for 20 years of service and be used for one shipment per week, for a total of 1,040 shipments. This analysis is summarized as follows:

1. The number of atmospheric-to-operating pressure cycles, which is equal to the number of shipments (1,040 cycles), is less than 13,688 cycles, corresponding to an S_a value of $3S_m = 414$ MPa for Type 304 and Type 316 stainless steel over the temperature range of interest. Thus, condition (1) of WB-3221.9(d) is met.

2. Normal operating pressure fluctuation cycles in the package result from diurnal fluctuations in ambient conditions (temperature and insolation). Thus, it is assumed that the cask will experience one normal operating pressure fluctuation per day, or 7,300 cycles over its 20-year service life. The thermal analysis of the package shows that the maximum temperature fluctuation of the cavity gas due to diurnal cycles is approximately 10°C, which results in a pressure change of approximately 20 kPa based on the ideal gas law. The 20 kPa pressure change is much less than the significant pressure fluctuation (SPF) of 330 kPa, which is based on a bounding design pressure of 700 kPa gauge, an S_a value of 195 MPa at 10^6 cycles per Table I-9.1 of Appendix I [2.8] of the ASME Code, and S_m of 138 MPa for Type 304 and Type 316 stainless steel over the temperature range of interest. Thus, condition (2) of WB-3221.9(d) is met.

3. The temperature difference between any two adjacent points on the cask shell during startup and shutdown is limited to 127°C. This is based on an S_a value of 758 MPa for 1,040 startup-shutdown cycles and the elastic modulus and mean coefficient of thermal expansion for the cask shell Type 304 and Type 316 stainless steel material at room temperature. The thermal evaluation of the package shows that the temperature difference between any two adjacent points on the cask does not exceed 127°C under any NCT thermal condition. Thus, condition (3) of WB-3221.9(d) is met.

4. Normal operating temperature fluctuation cycles in the package result from diurnal fluctuations in ambient conditions (temperature and insolation). Thus, it is assumed that the cask will experience one normal operating temperature fluctuation per day, or 7,300 cycles over its 20-year service life. The package's significant temperature fluctuation (STF) is 33°C based on an S_a value of 195 MPa at 10^6 cycles and the elastic modulus and mean coefficient of thermal expansion for the cask shell Type 304 and Type 316 stainless steel material at room temperature. The thermal evaluation of the package shows that the temperature difference in the cask does not vary significantly under NCT and is less than 33°C. Thus, condition (4) of WB-3221.9(d) is met.

5. With the exception of the closure bolts, the only dissimilar materials used in the construction of the cask are austenitic stainless steel and DU. DU has a lower coefficient of thermal expansion that the austenitic stainless steel materials of the components that encase the DU. Under elevated temperatures, differential thermal expansion between these materials results in growth of the clearance between the DU and cask shells. However, differential thermal expansion at reduced temperatures produces interference-related stresses in the cask. The STF for temperature difference in dissimilar material of the cask is 102°C based on a total of 7,300 temperature cycles and the cask material properties at a lower-bound temperature of -40°C. The thermal evaluation of the

package shows that the temperature difference in the cask does not vary significantly under NCT and is less than 102°C. Thus, condition (5) of WB-3221.9(d) is met.

6. The only significant cyclic mechanical loads, excluding pressure, that the package is subjected to during normal operation are those resulting from handling and NCT vibration. The only handling operation that creates any significant stress in the cask is the cask lift. The number of cask lift operations performed for each shipment is small, but conservatively assumed to be 10 or less per shipment for a maximum of 10,400 lifting cycles of the 20-year service life. As discussed in Section 2.6.5, a bounding 10*g* vertical vibration load is conservatively assumed for the package evaluation. It is conservatively assumed that the package will experience a total of 10^6 cycles of vibration loading per shipment with a magnitude of 10*g*, or 1.04E10 cycles over the 20-year service life. The value of S_a for 1E10 cycles and higher, for austenitic stainless steels is 94 MPa per Figure I-9.2.2 (curve C) of Appendix I [2.8] of the ASME Code. As discussed in Section 2.5.1.2 and Section 2.6.5, the maximum stress intensity in the cask due to the cask lift and NCT vibration loads are 9 MPa and 11 MPa, respectively. These stresses are less than one-eighth of the S_a value for the total number mechanical load cycles. Thus, condition (6) of WB-3221.9(d) is met.

2.1.2.4.2 Cask Closure Bolts

The cask closure bolts are subjected to cyclic loading due to startup-shutdown cycles of bolt preload, temperature, and pressure loading, normal fluctuation cycles of pressure and temperature, and cyclic loading due to vibration normally incident to transport. The cask closure bolts are evaluated for fatigue failure due to cyclic loading using the methods of WB-3221.9(e) in accordance with the requirements of WB-3232(d)(2). In accordance with the requirements of WB-3232(d)(2)(d), a fatigue strength reduction factor of 4.0 is used for the cask closure bolt fatigue evaluation.

Startup-Shutdown Cycles

The package is conservatively assumed to undergo 1,040 startup-shutdown cycles over its 20-year design life. The maximum stress in the cask closure bolt due to the maximum bolt preload, MNOP, and NCT heat loading is 209 MPa. The minimum stress in the closure bolt for startup-shutdown cycles is zero. Thus, the alternating stress in the closure bolts for startup-shutdown cycles, including a fatigue reduction factor of 4, is 418 MPa. The allowable number of startup-shutdown cycles for an alternating stress of 418 MPa is 1,678 per Figure I-9.4 of Appendix I [2.8] of the ASME Code. Therefore, the cask closure bolt usage factor for startup-shutdown cycles is 0.62 (1,040/1,678).

Thermal and Pressure Fluctuations – Normal Operating Cycles

Normal operating temperature and pressure fluctuations in the cask result from diurnal ambient temperature fluctuations. The package is conservatively assumed to undergo one normal operating cycle for every day of its 20-year design life, or 7,300 cycles. The maximum temperature fluctuations of the cask in the region of the closure bolts (e.g., the cask seals) and the

bulk average temperature of the cask cavity gas in the cask cavity both fluctuate by approximately 10°C during each diurnal cycle. This temperature fluctuation produces an alternating stress in the closure bolts.

The maximum stress in the cask closure bolt due to the maximum bolt preload, MNOP, and NCT heat loading (based on a bounding bolt temperature of 68.3°C) is 209 MPa. At room temperature (21°C) the bolt stress due to the maximum preload of 7,219 N is 92 MPa. Thus, a temperature change of 47.3°C combined with an internal pressure load of 700 kPa gauge increases the bolt stress by 117 MPa (209 MPa – 92 MPa). The stress range due to a 10°C temperature fluctuation is 25 MPa (=117 x 10/47.3). Thus, the alternating stress in the closure bolts for normal operating thermal and pressure cycles, including a fatigue reduction factor of 4, is 50 MPa. The allowable number of normal operating cycles for an alternating stress of 50 MPa is 184,062 per Figure I-9.4 of Appendix I [2.8] of the ASME Code. Therefore, the cask closure bolt usage factor for normal operating thermal and pressure cycles is 0.04 (7,300/184,062).

Vibration Cycles

The results of the cask closure bolt evaluation show that NCT vibration loading results in only a 1 MPa increase in the closure bolt stress. Thus, the alternating stress in the closure bolts for NCT vibration cycles, including a fatigue reduction factor of 4, is S_{alt3} = 2.0 MPa. The value of S_a at 1E6 cycles is 37 MPa per Figure I-9.4 of Appendix I [2.8] of the ASME Code. Since S_{alt3} is much lower that S_a at the endurance limit of 1E6 cycles, the usage factor for NCT vibration is insignificant (i.e., $U_3 = 0.00$).

Cumulative Usage Factor

The cumulative usage factor for cyclic loading of the cask closure bolts is:

$$U = U_1 + U_2 + U_3$$
$$= 0.62 + 0.04 + 0.00 = 0.66$$

Since the cumulative usage factor is less than 1.0, the cask closure bolt will not fail due to fatigue during their 20-year design life.

2.1.2.5 Brittle Fracture

The cask is designed in accordance with the fracture toughness requirements of Regulatory Guide 7.11 [2.9] and NUREG/CR-1815 [2.10] for Category II containers, since it is designed to transport normal form content with a maximum activity between 3,000 A_2 and 30 A_2 and not greater than 1.11 PBq (30,000 Ci). The criteria for Category II containers assures that the fracture toughness is sufficient to prevent fracture initiation of preexisting cracks under dynamic loading.

With the exception of the cask closure bolts and overpack closure bolts, all structural components of the package are fabricated of austenitic stainless steels. These materials do not undergo a ductile-to-brittle transition in the temperature range of interest for load conditions that

involve impact loads, i.e., down to -20°F (-29°C), and, thus, do not need to be evaluated for brittle fracture. As stated in Regulatory Guide 7.11 [2.9], "Since austenitic stainless steels are not susceptible to brittle failure at temperatures encountered in transport, their use in containment vessels is acceptable to the staff and no tests are needed to demonstrate resistance to brittle fracture."

The cask closure bolts and overpack closure bolts are fabricated from SA-320 and A320, Grade L43 bolting material, respectively. In accordance with Section 5 of NUREG/CR-1815 [2.10], bolts are generally not considered as fracture-critical components because multiple load paths exist and bolting systems are generally redundant, as is the case with the cask and overpack closure bolts. However, for purposes of comparison, the nil-ductility transition (NDT) temperature of the closure bolts is calculated and compared with the requirements of NUREG/CR-1815.

The closure bolt material is required to have a minimum impact energy absorption of 27 N-m (20 ft-lbf) at a temperature of -101°C (-150°F). The Charpy impact measurement may be transformed into a fracture toughness value by using the empirical relationship from Section 4.2 of NUREG/CR-1815:

$$K_{ID} = \sqrt{5C_v E} = 59\ \text{MPa}\sqrt{\text{m}}\ \ (54\ \text{ksi}\sqrt{\text{in}}\,)$$

where E is 199 MPa (28.8 X 10^6 psi) at -101°C (-150°F) from Table TM-1, Material Group B of Section II, Part D, of the ASME Code [2.11].

The dynamic fracture toughness is conservatively translated to an equivalent NDT temperature by using the Design Reference K_{ID} curve provided in Figure 2 of NUREG/CR-1815. By interpolation, the temperature relative to NDT (i.e., T - NDT) is approximately 18°C (32°F). Accordingly, the NDT temperature is:

$$\text{NDT} = -101°\text{C} - (18°\text{C}) = -119°\text{C}\ (-182°\text{F})$$

For Category II fracture critical components with a minimum section thickness of 15.9 mm (0.625 inches) and a yield strength of 690 MPa (100 ksi), Figure 7 of NUREG/CR-1815 gives the minimum offset "A" as approximately 0°C (0°F). Thus, for Lowest Service Temperature (LST) of -29°C (-20°F), the maximum NDT temperature value is:

$$T_{NDT} = \text{LST} - \text{A} = -29°\text{C} - 0°\text{C} = -29°\text{C}\ (-20°\text{F})$$

The closure bolts experience a ductile-to-brittle transition temperature at -119°C, whereas the criterion of NUREG/CR-1815 prescribes a maximum NDT temperature of -29°C. The 90°C margin provides conservative assurance that brittle fracture will not occur in the closure bolts.

The shielding components of the package are fabricated from DU alloyed with 2% molybdenum by weight (U-2% Mo). This material was selected for the MIDUS package design because the addition of 2% molybdenum results in the formation of a second phase that increases the yield strength of DU and provides good ductility over the temperature range of interest [2.12]. Since the ductile-to-brittle transition temperature of U-2% Mo falls within the package operating

temperature range, four additional measures are taken to assure that the DU will not be susceptible to brittle fracture.

All the DU components receive inspections for fracture toughness, chemical composition, and density. The specified fracture toughness is a minimum Charpy V-notch impact energy of 6 ft-lb at 70 °F. The chemical composition is tested to assure that alloy meets specifications because unalloyed DU is more susceptible to brittle fracture then the 2% Mo alloy. Density measurements are performed on each DU component to assure that the material is free of significant voids that might affect shielding or promote brittle fracture. Lastly, visual inspections are performed on each part after final machining to assure that the surfaces are free of voids, cracks, or porosity. The visual inspection gives assurance that no significant material flaws exist which might promote brittle fracture. The DU casting process does not favor the creation of cracking, and any cracks which might form during cooling are preferentially located on the surface of the part. The critical flaw size required for fracture is very large, about ¼ or more of the part thickness, and so visual inspection is a reliable testing method.

Since the maximum stress in the DU shield for all NCT and HAC tests is very low (i.e., less than 40% of the yield strength of U-2% Mo at -29°C), the lower-bound critical flaw size that must exist for fracture is calculated to be 17 mm using the following equation from SAND80-1836 [2.12]:

$$K \approx 2\sigma\sqrt{a}$$

Where;

K = $K_{IC(min)}$ or 42.3 MPa·$m^{1/2}$, lower-bound value of the critical stress intensity factor for plane strain failure at -40°C [2.12]

σ = 162 MPa, maximum stress intensity in the DU shield for all NCT and HAC tests (resulting from the HAC top oblique drop)

a = crack depth (m)

2.1.3 Weights and Centers of Gravity

The nominal mass properties of the package, including each of the major individual packaging subassemblies and contents, are summarized in Table 2-8. The mass, center of gravity, and moment of inertia of each major individual subassembly and the package are provided. The reference point for all centers of gravity is the bottom centerline of the overpack base, as shown in Figure 2-3. Moments of inertia are taken about the local center of gravity of each major individual subassembly and the package. The package has a total nominal mass of 320.6 kg and a center of gravity located at 267 mm above the bottom end of the overpack base. The mass moment of inertia of the package is 8.91E+06 kg-mm^2.

2.1.4 Identification of Codes and Standards for Package Design

The package, which is designed to transport normal form content with a maximum activity between 3,000 A_2 and 30 A_2 and not greater than 30,000 Ci, is designed, fabricated, tested, and maintained in accordance with codes and standards that are appropriate for transportation packages with Category II container contents. The codes and standards are selected based on guidance provided in Regulatory Guide 7.6 [2.13] and NUREG/CR-3854 [2.14].

The package containment system is designed in accordance with the applicable requirements of the ASME Code, Section III, Division 3, Subsection WB [2.1]. The non-containment structural components of the package are designed in accordance with the applicable requirements for plate- and shell-type Class 2 supports from the ASME Code, Section III, Division 1, Subsection NF [2.2]. The design criteria for the package is discussed in Section 2.1.2. The load combinations used in the package structural evaluation are developed in accordance with Regulatory Guide 7.8 [2.5], as discussed in Section 2.1.2.1. The buckling evaluation of the cask cylindrical shells is performed in accordance with ASME Code Case N-284-1 [2.7], as discussed in Section 2.1.2.3. Fracture toughness of the package components is evaluated in accordance with the requirements of Regulatory Guide 7.11 [2.9] and NUREG/CR-1815 [2.10] for Category II containers.

The package containment system is fabricated in accordance with the applicable requirements of Subsections WA and WB of Section III, Division 3, of the ASME Code [2.1]. The non-containment structural components of the package are fabricated in accordance with the applicable requirements of Subsection NF [2.2] of the ASME Code for plate- and shell-type Class 2 supports. The exceptions taken to the ASME Code design and fabrication requirements, along with the alternate compliance basis, are summarized in Table 2-9 and Table 2-10. The weld that connects the cask outer shell to the cask containment shell is fabricated and inspected in accordance with the applicable requirements of Subsections WA and WB of Section III, Division 3, of the ASME Code [2.1]. All other package welds are fabricated and inspected in accordance with the applicable requirements of Subsection NF [2.2] of the ASME Code.

The package DU alloy gamma shield components are fabricated, installed, and tested in accordance with standard industry practices. Testing of the DU alloy gamma shield material is performed to assure that it satisfies the requirements for chemical composition and fracture toughness. In addition, the soundness of the DU alloy material used for the gamma shielding components is demonstrated through measurement of the component densities (i.e., weight and volume) and visual inspection of the component surfaces for unacceptable flaws (e.g., voids, cracks, or porosity.)

The polyurethane foam material that fills the overpack base and lid shells is fabricated, installed, and tested in accordance with the foam vendors' standard practices. The foam is installed in the overpack shells in-situ, with the foam rise parallel to the longitudinal axis of the package. Foam specimens from each foam batch are tested to assure that the foam has the specified physical characteristics, including density, crush strength, flame retardency, intumescences, and leachable chlorides.

Table 2-1 – Load Combinations for Normal Conditions of Transport

Normal or Accident Condition	Initial Conditions[1]								
	Ambient Temperature		Insolation[2]		Decay Heat		Internal Pressure[3]		Fabrication Stress[4]
	38°C	-29°C	Max.	Zero	Max.	Zero	Max.	Min.	
Hot Environment (38°C ambient temp.)			X		X		X		X
Cold Environment (-40°C ambient temp.)				X		X		X	X
Reduced External Pressure	X		X		X		X		X
Increased External Pressure		X		X		X		X	X
Vibration	X		X		X		X		X
		X		X		X		X	X
Free Drop	X		X		X		X		X
		X		X		X		X	X

Notes:
1. Initial cask temperature distributions are considered to be at steady-state.
2. Maximum insolation in accordance with §71.71(c)(1).
3. Internal pressure is consistent with the other initial conditions being considered. Minimum internal pressure is taken as atmospheric pressure.
4. Stresses due to assembly of the major components of the packaging, including stresses due to closure bolt preload.

Table 2-2 – Load Combinations for Hypothetical Accident Conditions

Normal or Accident Condition	Initial Conditions[1]								
	Ambient Temperature		Insolation[2]		Decay Heat		Internal Pressure[3]		Fabrication Stress[4]
	38°C	-29°C	Max.	Zero	Max.	Zero	Max.	Min.	
Free Drop	X		X		X		X		X
		X		X		X		X	X
Puncture	X		X		X		X		X
		X		X		X		X	X
Thermal	X		X		X		X[5]		X

Notes:
1. Initial cask temperature distributions are considered to be at steady-state.
2. Maximum insolation in accordance with §71.71(c)(1).
3. Internal pressure is consistent with the other initial conditions being considered. Minimum internal pressure is taken as atmospheric pressure.
4. Stresses due to assembly of the major components of the packaging, including stresses due to closure bolt preload.
5. Maximum internal pressure for the HAC thermal condition includes increased pressure due to increased fill gas temperatures during the fire transient.

Table 2-3 – Containment System Allowable Stress Design Criteria

Stress Type	Allowable Stress Limits[1]	
	NCT	HAC
Other Than Bolts		
Primary Membrane Stress Intensity (P_m)	S_m	Lesser of $2.4S_m$ and $0.7S_u$
Primary + Bending Stress Intensity (P_L or $P_L + P_b$)	$1.5S_m$	Lesser of $3.6S_m$ and S_u
Primary + Secondary Stress Intensity ($P_L + P_b + Q$)	$3.0S_m$	N/A[2]
Average Bearing Stress	S_y	Not required
Pure Shear Stress	$0.6S_m$	$0.42S_u$
Bolts		
Average Shear Stress	$0.4S_y$	Lesser of $0.42S_u$ and $0.6S_y$
Average Stress[3]	$2S_m$[4]	Lesser of $3S_m$ and $0.7S_u$
Maximum Stress[5]	$3S_m$	[6]

Notes:
1. Stress limits applicable for components and systems evaluated using elastic system analysis.
2. Evaluation of secondary stress is not required for HAC.
3. The axial stress component averaged across the bolt cross-section and neglecting stress concentrations.
4. The stress due to internal pressure and gasket seating loads (e.g., bolt torque) shall not exceed one times S_m.
5. The maximum value of stress intensity at the periphery of the bolt cross-section resulting from direct tension plus bending, neglecting stress concentrations.
6. Evaluation of maximum bolt stress not required for HAC.

Table 2-4 – Non-Containment Component Allowable Stress Design Criteria

Stress Type	Allowable Stress Limits[1]	
	NCT	HAC
Other Than Bolts		
Primary Membrane Stress Intensity (P_m)	S_m	Greater of $1.2S_y$ and $1.5S_m$, but $\leq 0.7S_u$
Primary Membrane + Bending Stress Intensity (P_L or $P_m + P_b$)	$1.5S_m$	150% of P_m allowable
Average Bearing Stress	S_y	[2]
Pure Shear Stress	$0.6S_m$	$0.42S_u$
Bolts		
Tensile Stress (f_t)	$F_{tb} = S_u/2$ (ferritic steels) or $F_{tb} = S_u/3.33$ (austenitic steels)	Lesser of $0.7S_u$ and S_y[3][4]
Shear Stress (f_v)	$F_{vb} = 0.62S_u/3$ (ferritic steels) or $F_{vb} = 0.62S_u/5$ (austenitic steels)	Lesser of $0.42S_u$ and $0.6S_y$
Combined Tensile & Shear Stress	$\frac{f_t^2}{F_{tb}^2} + \frac{f_v^2}{F_{vb}^2} \leq 1$	$\frac{f_t^2}{F_{tb}^2} + \frac{f_v^2}{F_{vb}^2} \leq 1$[4]

Notes:
1. Stress limits applicable for components and systems evaluated using elastic system analysis.
2. Evaluation of secondary stress is not required for HAC.
3. Limit applies to average tensile stress across the entire bolt cross-section. For high-strength bolts ($S_u > 100$ ksi), the maximum value of tensile stress at the periphery of the bolt cross-section resulting from direct tension plus bending and excluding stress concentrations shall not exceed S_u.
4. Stress limit is not applicable to the overpack closure bolts, since they are evaluated for HAC tests using plastic-system analysis.

Table 2-5 – Cask Shell Buckling Geometric Parameters

Geometric Parameter	Inner Shell	Outer Shell
Outside Diameter (mm)	90.0	225.0
Inside Diameter (mm)	85.0	217.0
Length, L (mm)	134.0	221.0
Mean Radius, R (mm)	43.8	110.5
Shell Thickness, t (mm)	2.5	4
R/t	17.5	27.6
Unsupported Axial Length, l_ϕ (mm)	134.0	220.5
Unsupported Circumferential Length, l_θ (mm)	274.9	694.3
$M_\phi = l_\phi/\sqrt{Rt}$	12.81	10.49
$M_\theta = l_\theta/\sqrt{Rt}$	26.28	33.02
M = smaller of M_ϕ and M_θ	12.81	10.49

Table 2-6 – Buckling Reduction Factors and Theoretical Buckling Stresses

Calculation	Parameter	Inner Shell	Outer Shell
Capacity Reduction Factors (-1511)	$\alpha_{\phi L}$	0.269	0.269
	$\alpha_{\theta L}$	0.800	0.800
	$\alpha_{\phi\theta L}$	0.800	0.800
Plasticity Reduction Factors (-1610)	$\Delta=\alpha_{\phi L}*\sigma_{\phi eL}/\sigma_y$	10.257	6.498
	$\Delta=\alpha_{\theta L}*\sigma_{\theta eL}/\sigma_y$	3.988	3.157
	$\Delta=\alpha_{\phi\theta L}*\sigma_{\phi\theta eL}/\sigma_y$	10.610	7.488
	η_ϕ	0.097	0.154
	η_θ	0.250	0.307
	$\eta_{\phi\theta}$	0.057	0.080
Theoretical Buckling Values (-1712.1.1)	C_ϕ	0.605	0.605
	$\sigma_{\phi eL}$	6,579 MPa	4,168 MPa
	$C_{\theta r}$	0.0790	0.0987
	$\sigma_{\theta eL} = \sigma_{reL}$	859 MPa	680 MPa
	$C_{\theta h}$	0.0756	0.0934
	$\sigma_{\theta eL} = \sigma_{heL}$	822 MPa	643 MPa
	$C_{\phi\theta}$	0.2102	0.2342
	$\sigma_{\phi\theta eL}$	2,286 MPa	1,614 MPa

Table 2-7 – Cask Shell Allowable Buckling Stresses

Buckling Regime	Stress Type	Allowable Buckling Stress (MPa)			
		Inner Shell		Outer Shell	
		NCT	HAC	NCT	HAC
Elastic Buckling	Axial Compression, σ_{xa}	884	1,319	560	836
	Hydrostatic Pressure, σ_{ha}	329	491	257	384
	Hoop Compression, σ_{ra}	344	513	272	406
	In-Plane Shear, $\sigma_{\tau a}$	914	1,365	645	963
Inelastic Buckling	Axial Compression, σ_{xc}	86	129	86	129
	Radial External Pressure, σ_{rc}	86	128	84	125
	In-Plane Shear, $\sigma_{\tau c}$	52	77	52	77

Table 2-8 – Package Mass Properties Summary

Package Component or Assembly	Mass (kg)	Center of Gravity[1] (mm)	Moment of Inertia[2] (kg-mm^2)
Cask Body Assembly	167.5	235	1.70E+06
Cask Shield Plug Assembly	13.8	354	1.81E+04
Closure Lid Assembly	5.8	409	1.83E+04
Cask Payload	1.1	247	1.72E+03
Misc. Cask Hardware	0.3	402	5.00E+01
Cask Assy. Subtotals	**188.5**	**250**	**2.08E+06**
Shield Lid Assembly	13.6	430	4.22E+04
Cask & Shield Lid Subtotals	**202.1**	**262**	**2.53E+06**
Overpack Base Assy.	83.1	197	3.77E+06
Overpack Lid Assy.	35.1	464	8.12E+05
Misc. Overpack Hardware	0.4	410	1.03E+02
Package Totals	**320.6**	**267**	**8.91E+06**

Notes:
1. Longitudinal distance from the bottom end of the overpack base to the center of gravity of the individual packaging subassembly or assembly, as shown in Figure 2-3.
2. Moment of inertia about the center of gravity of the associated component or assembly.

Table 2-9 – MIDUS Package ASME BPVC Section III, Division 1, Requirements Compliance Summary (4 Pages)

Item	ASME Code Requirement or Issue	Alternative Compliance Basis	ASME BPVC Sections
1	ASME BPVC Section III, Division 1, uses the following terminology that is not consistent with the terminology used for the MIDUS package:	The equivalent terminology or compliance basis used for the MIDUS package are as follows:	
	(a) "Owner's Certificate"	(a) Energy*Solutions* will notify the USNRC of the intent to design and fabricate the package, but will not seek an Owner's Certificate from the ASME.	NCA-1210 & NCA-3230
	(b) "Design Specification"	(b) The information typically contained in the ASME BPVC Design Specification shall be included in the MIDUS Transportation Package Safety Analysis Report (SAR).	NCA-1210 & NCA-3250
	(c) "Review of Design Report" and "Design Report"	(c) The information typically contained in an ASME BPVC Design Report shall be included in the MIDUS Transportation Package SAR and submitted for review and approval by the USNRC.	NCA-1210, NCA-3260 & NCA-3350
	(d) "Certificate Holder" or "Owner"	(d) Energy*Solutions* bears the responsibilities associated with a "Certificate Holder" or "Owner" relative to the package, with the exceptions as noted.	Throughout
	(d) "Certificate of Authorization"	(d) Replaced by USNRC-issued Certificate of Compliance (CofC).	Throughout
	(e) "Data Report" and "Stamping"	(e) Replaced by a Final Records Package and Energy*Solutions'* CofC for each fabricated package.	NCA-1210 & NCA-8000
2	Metallic materials shall be manufactured to an SA, SB, or SFA Specification, or any other material specification permitted by this Section. Such material shall be manufactured, identified, and certified in accordance with the requirements of this Section.	As permitted by USNRC NUREG/CR-3854 via NUREG-1609, ASTM materials may be used for the fabrication/construction of the non-containment structural components of the package otherwise governed by the applicable requirements of ASME BPVC Section III, Division 1, Subsection NF.	NCA-1221

Table 2-9 – MIDUS Package ASME BPVC Section III, Division 1, Requirements Compliance Summary (4 Pages)

Item	ASME Code Requirement or Issue	Alternative Compliance Basis	ASME BPVC Sections
3	Metallic materials produced under an ASTM designation may be accepted as complying with the corresponding ASME Specification, provided that the ASME Specification is designated as being identical with the ASTM Specification for the grade, class, or type produced and provided that the material is confirmed as complying with the ASTM Specification by a certified Material Test Report or Certificate of Compliance from the Material Organization.	See Items 2 & 8.	NCA-1221.1
4	The package overpack assembly (i.e., impact limiter) is constructed to the requirements of Subsection NF, but not designed to the requirements of Article NF-3000 or Appendix NF-III.	The package overpack assembly is designed by analysis and confirmed by scaled test to provide sufficient crush strength and structural integrity.	NF-3000, Appendix NF-III
5	The maximum temperature of the metal shall not exceed the maximum temperatures listed in the applicable tables of Section II, Part D, Subpart 1. However, the package is designed for a HAC fire that is not within the scope of the loading conditions typically considered for components designed in accordance with ASME BPVC Subsection NF.	The short-term allowable temperature limits for the package materials that are used for the HAC evaluation shall be defined in the system's calculation packages and SAR.	NF-3112.1
6	The ASME BPVC requires that the Design Specification be certified by one or more Registered Professional Engineers.	The Design Specification for the package (i.e., its SAR per Item 1(b)) shall be prepared and verified by personnel qualified in accordance with the USNRC-approved Energy*Solutions* QA Program.	NCA-3255
7	The ASME BPVC requires that the Owner or his designee review the Design Report for compliance with the Design Specification.	The Design Report for the package (i.e., its SAR per Item 1(c)) shall be prepared and verified by personnel qualified in accordance with the USNRC-approved Energy*Solutions* QA Program.	NCA-3260

Table 2-9 – MIDUS Package ASME BPVC Section III, Division 1, Requirements Compliance Summary (4 Pages)

Item	ASME Code Requirement or Issue	Alternative Compliance Basis	ASME BPVC Sections
8	Subsection NF requires the Certificate Holder to certify, by application of the appropriate Code symbol and completion of the appropriate Data Report in accordance with NCA-8000, that the materials used comply with all the requirements of NF-2000 and that the fabrication and installation complies with the requirements of NF-4000.	The package will be purchased, identified, controlled, and manufactured in accordance with the USNRC-approved Energy*Solutions* QA Program based on NQA-1 and USNRC Regulatory Guide 7.10 and NUREG/CR-6407 criteria. Therefore, Code symbol stamping will not be applied to the fabrication and installation of the package.	NCA-1281, NCA-3800, NCA-8000 & NF-4121
9	The ASME BPVC requires the use of an Authorized Inspection Agency (AIA) to provide inspection and audit services during the construction and installation of the supports.	The activities associated with the AIA, including the Authorized Nuclear Inspector (ANI), will be replaced by the auditing and inspection activities of the QA/QC organization performing the fabrication with oversight by the Design Owner (Energy*Solutions*).	NCA-5000, NCA-8000 & NF-4121
10	Material for supports shall conform to the requirements of the specifications for materials listed in the tables of Section II, Part D applicable to the Class of construction.	See Item 2.	NF-2121
11	Only those welding processes which are capable of producing welds in accordance with the welding procedure qualification requirements of ASME BPVC Section IX and this Subsection shall be used for welding support material or attachments thereto.	As permitted by USNRC NUREG/CR-3019 via NUREG-1609, welding criteria of ASME BPVC Section VIII, Division 1, may also be used for non-containment structural component welding.	NF-4311

Table 2-10 – MIDUS Package ASME BPVC Section III, Division 3, Requirements Compliance Summary (3 Pages)

Item	ASME Code Requirement or Issue	Alternative Compliance Basis	ASME BPVC Sections
1	ASME BPVC Section III, Division 3, uses the following terminology that is not consistent with the terminology used for the MIDUS package: (a) "N3 Certificate Holder" (b) "Packaging Owner" (c) "Design Specification" (d) "Design Report" (e) "Fabrication Specification" (f) "Certificate of Authorization"	The equivalent terminology and compliance basis used for the MIDUS package are as follows: (a) Energy*Solutions* has the responsibility of the N3 Certificate Holder, with the exceptions as noted. (b) Energy*Solutions* has the responsibility of the Packaging Owner, with the exceptions as noted. (c) The information typically contained in an ASME BPVC Design Specification will be included in the MIDUS Transportation Package Safety Analysis Report (SAR) to be submitted to the USNRC for review and approval. (d) The information typically contained in an ASME BPVC Design Report will be included in the MIDUS Transportation Package SAR. (e) Replaced by Energy*Solutions'* fabrication specification, quality category assessment, and procurement drawing documentation. (f) Replaced by USNRC-issued C of C.	Throughout Subsections WA and WB
2	The ASME BPVC Edition and Addenda dates shall be established in the Design Specification.	The ASME BPVC Edition and Addenda to be used for the design and fabrication of the package shall be the 2001 Edition with Addenda through 2003.	WA-1140(a)

Table 2-10 – MIDUS Package ASME BPVC Section III, Division 3, Requirements Compliance Summary (3 Pages)

Item	ASME Code Requirement or Issue	Alternative Compliance Basis	ASME BPVC Sections
3	ASME BPVC Section III, Division 3, requires that the N3 Certificate Holder use a NPT Certificate Holder to construct the containment system. The following Code requirements apply to the NPT Certificate Holder:	A NPT Certificate Holder is not required to construct the containment system (i.e., cask assembly) of the package.	WA-3420.
	(a) The NPT Certificate Holder shall construct the containment system under the provisions of a Quality Assurance (QA) Program that has been accepted by the Society. The QA Program shall meet the requirements of the latest Division 3 Edition and Addenda issued at the time that the containment system is constructed.	(a) The package will be purchased, identified, controlled, and manufactured in accordance with the USNRC-approved Energy*Solutions* QA Program based on NQA-1, USNRC Regulatory Guide 7.10, and NUREG/CR-6407 criteria.	WA-1140(b), WA-3111, WA-3113 & WA-3420(e)
	(b) The NPT Certificate Holder shall obtain an N-type Certification of Authorization and apply a Code Symbol Stamp to the completed containment system of the transportation packaging.	(b) See Item 3(a).	WA-3111, WA-3113, WA-3130 & WA-3470
4	The ASME BPVC requires that the Design Specification, Design Report, and Fabrication Specification be certified by one or more Registered Professional Engineers, competent in the applicable field of construction and related transport packaging requirements of ANSI/ASME N626.3.	The design and fabrication documents for the package shall be prepared and verified by personnel qualified in accordance with the USNRC-approved Energy*Solutions* QA Program.	WA-3351.4,WA-3356 & WA-3361.3

Table 2-10 – MIDUS Package ASME BPVC Section III, Division 3, Requirements Compliance Summary (3 Pages)

Item	ASME Code Requirement or Issue	Alternative Compliance Basis	ASME BPVC Sections
5	The ASME BPVC requires the use of an Authorized Inspection Agency (AIA) to provide inspection and audit services during the construction and installation of the containment system. Other requirements related to the use of an AIA are as follows:	The activities associated with the AIA, including the Authorized Nuclear Inspector (ANI), will be replaced with auditing and inspection activities of the QA/QC organization performing the fabrication with oversight by the Design Owner (Energy*Solutions*).	WA-5000 & WB-6113
	(a) The N3 and NPT Certificate Holder shall obtain written agreement with an AIA to provide inspection and audit services prior to application.	(a) The agreement with an AIA is replaced with auditing and inspection activities of the QA/QC organization performing the fabrication with oversight by the Design Owner (Energy*Solutions*).	WA-3320(o), WA-3420(h) & WA-8130
	(b) The N3 and NPT Certificate Holder shall file copies of the QA Manual with the AIA.	(b) Instead of an AIA, the QA Manual of the Design Owner (Energy*Solutions*) is filed with and has been reviewed and approved by the USNRC.	WA-3373 & WA-3461
6	The containment system shall be designed to account for buckling due to compressive stresses. However, the rules for evaluating buckling are under development.	The inner and outer shells of the cask are designed to withstand compressive loads without buckling in accordance with the design criteria of ASME BPVC Code Case N-284-1.	WB-3211(c) & WB-3133
7	Stress Limits for Bolts	The closure bolts are evaluated in accordance with the guidance and design criteria provided in NUREG/CR-6007.	WB-3230

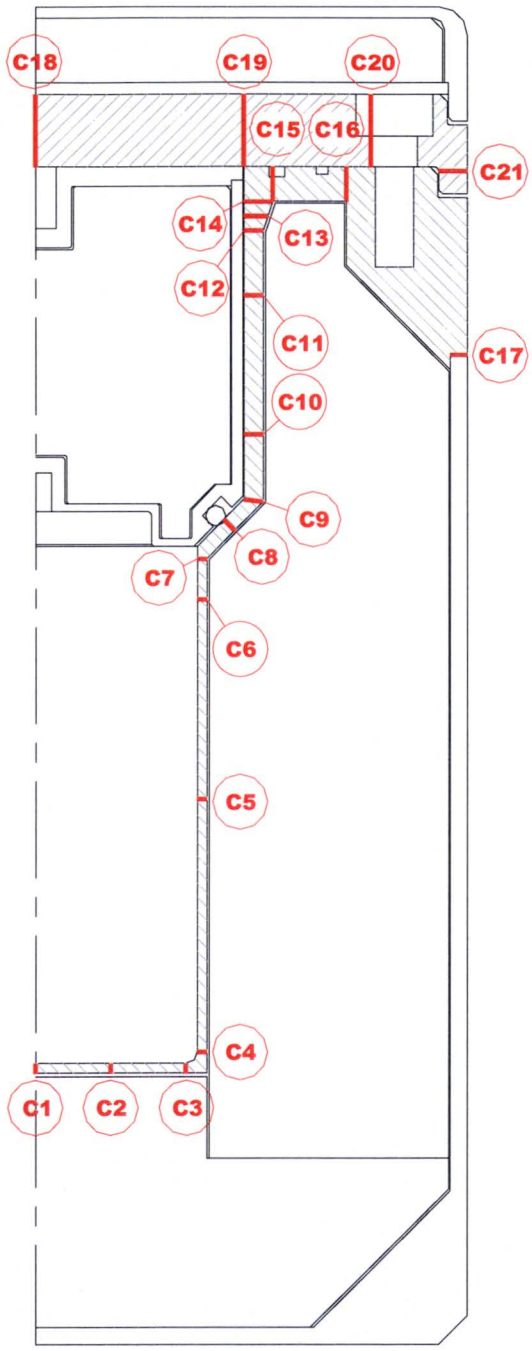

Figure 2-1 – Cask Containment Component Stress Evaluation Locations

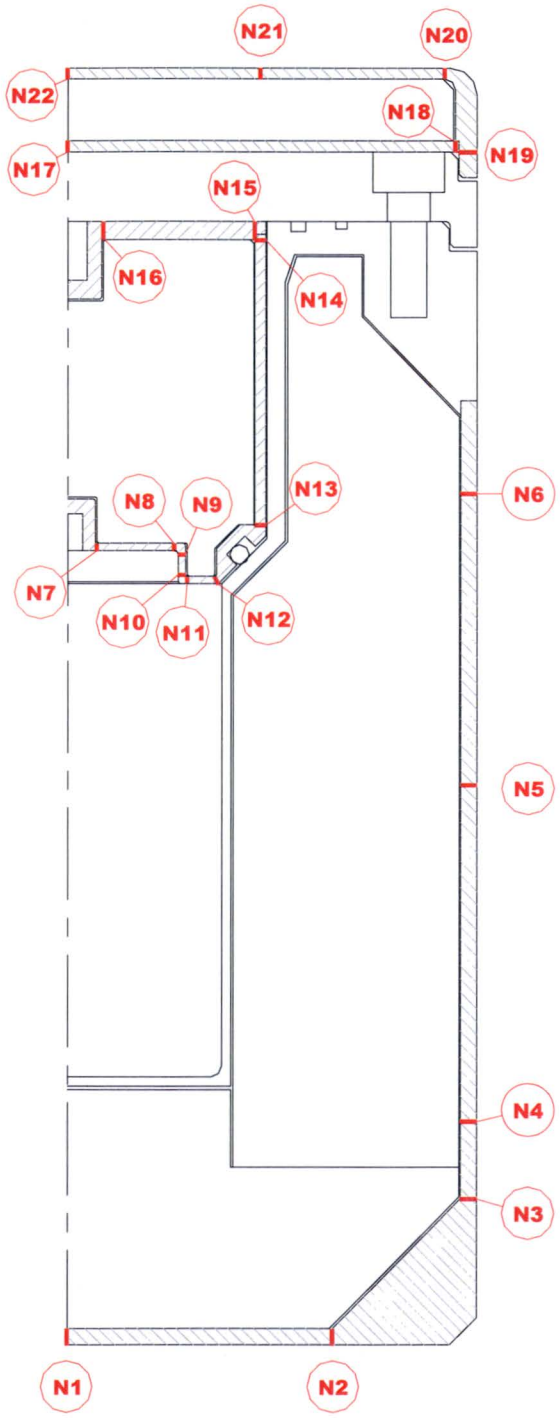

Figure 2-2 – Cask Non-Containment Component Stress Section Locations

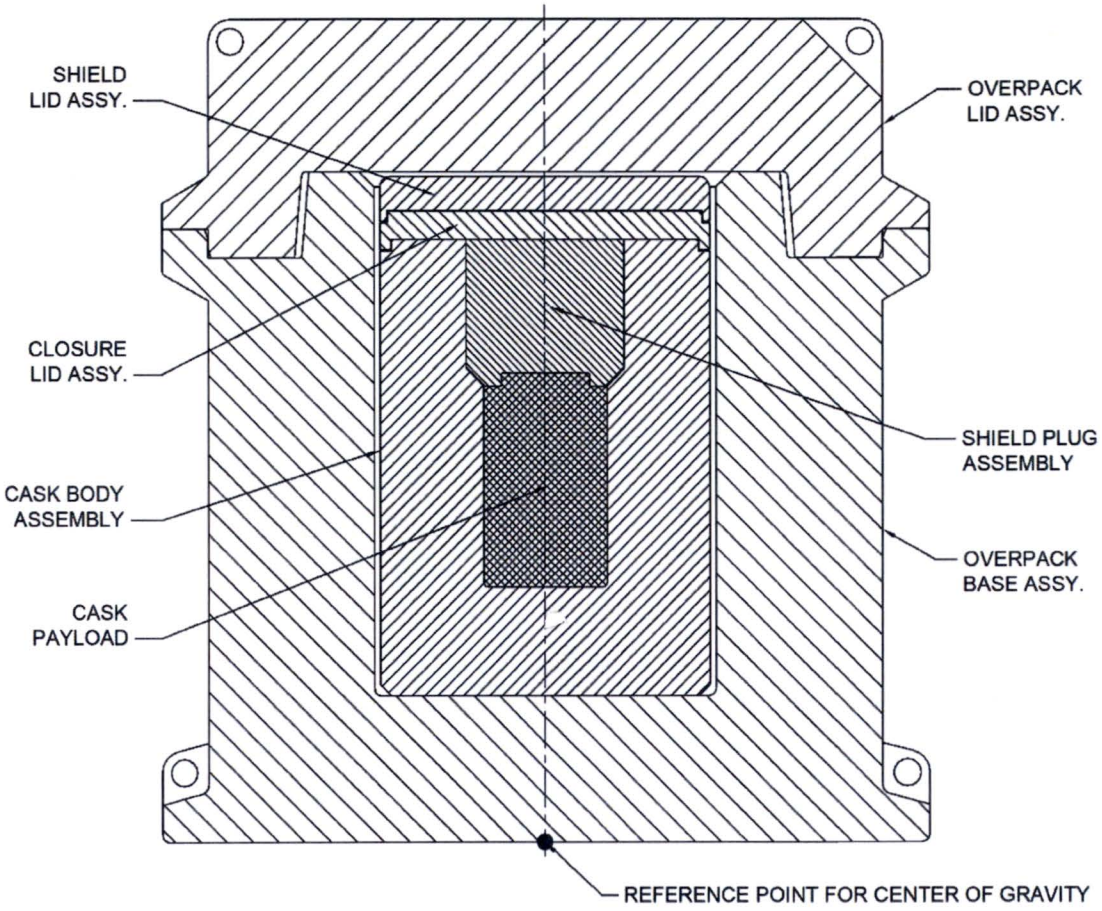

Figure 2-3 – MIDUS Package Mass Properties Schematic

2.2 Materials

2.2.1 Material Properties and Specifications

The specifications for the package materials of construction are summarized in Table 2-11. The mechanical properties of the package materials that are used in the structural evaluation are described in this section. The material properties for all steel components of the packaging are described in Section 2.2.1.1. The material properties of DU shielding material are described in Section 2.2.1.2. The crush strength properties of the overpack foam material are described in Section 2.2.1.3. The material properties of other materials considered in the structural evaluation are described in Section 2.2.1.4.

2.2.1.1 Structural Materials

The structural components of the package are fabricated from stainless steel material and alloy steel bolting material. Type 304 and/or Type 316 austenitic stainless steel, in either bar (SA-479/A479) or plate (SA-240/A240) form, is used to fabricate the structural components of the cask body, shield plug, closure lid, shield lid, and overpack. The shield lid attachment bolts are fabricated from A193, Grade B8 stainless steel material. The cask closure bolts and overpack closure bolts are fabricated from high-strength SA-320/A320, Grade L43 alloy bolting steel material.

The structural evaluation of the package is performed using mechanical properties of materials that are appropriate for the anticipated service conditions. The temperature range of interest for NCT is -40°C to 93°C. A mass density of 8,030 kg/m^3 and a Poisson's ratio of 0.3 are used for all stainless steel materials. A mass density of 7,865 kg/m^3 and a Poisson's ratio of 0.3 are used for the cask and overpack closure bolts. Temperature-dependent mechanical properties for the structural material of the package, including design stress intensity (S_m), yield strength (S_y), tensile strength (S_u), modulus of elasticity (E), and mean coefficient of thermal expansion (α), are obtained from the ASME Code, Section II, Part D [2.11] and summarized in Table 2-12 through Table 2-18.

The mechanical properties of Type 304 and Type 316 stainless steel material are summarized in Table 2-12 and Table 2-13, respectively. Since many of the package's structural components may be fabricated using either Type 304 or Type 316 stainless steel material, the structural evaluation of the package is performed using the most conservative mechanical properties of these materials for the condition being analyzed. As shown in Table 2-12 and Table 2-13, the only differences between the mechanical properties of Type 304 and Type 316 stainless steel over the temperature range of interest are the yield and ultimate strengths at 93°C. Thus, the allowable stresses that depend on the yield and/or ultimate strength of Type 304 and Type 316 stainless steel at 93°C are calculated based on the lower strength values. The mechanical properties of A240, Type XM-19 stainless steel, which is used only for the overpack lid lugs, are summarized in Table 2-14. The mechanical properties of SA-320/A320, Grade L43 alloy bolting steel material, which is used for the cask closure bolts and overpack closure bolts, and A193,

Grade B8 stainless steel bolting material, which is used for the shield lid attachment bolts, are summarized in Table 2-15 and Table 2-16, respectively.

Elastic-plastic true stress-strain properties are used for overpack shell stainless steel material in the structural evaluation of the overpack for NCT free drop, HAC free drop, and HAC puncture tests. The stainless steel materials that form the overpack shells are modeled using a piecewise linear plasticity model. The data points on the true stress-strain curves are developed using the Ramberg-Osgood relationship [2.15] as follows:

$$\frac{\varepsilon}{\varepsilon_o} = \frac{\sigma}{\sigma_o} + \alpha\left(\frac{\sigma}{\sigma_o}\right)^n$$

where;

ε = true strain

σ = true stress

ε_o = S_y/E, true yield strain

σ_o = S_y, true yield stress

S_y = Yield strength

E = Elastic modulus

$$\alpha = \left[\frac{\ln(1+e_u)}{\ln\left(1+{}^{S_y}\!/_{E}\right)} - \frac{S_u(1+e_u)}{S_y\left(1+{}^{S_y}\!/_{E}\right)}\right]\left[\frac{S_u(1+e_u)}{S_y\left(1+{}^{S_y}\!/_{E}\right)}\right]^{-n}$$

S_u = Ultimate tensile strength

e_u = Ultimate strain

n = $1/[\ln(1+e_u)]$

Using this relationship, and the material properties from Table 2-12 and Table 2-13, the upper-bound and lower-bound true stress-strain curves are developed for all of the overpack shell stainless steel materials (except for the lid lug Type XM-19 material) over the temperature range of interest (-20°F to 200°F). The resulting stress-strain curves are shown in Figure 2-4 along with enveloping upper-bound and lower-bound stress-strain curves used for the overpack NCT and HAC free drop structural analyses. The enveloping upper-bound and lower-bound true stress-strain design data used for the overpack stainless steel shells in the drop loads analysis are summarized in Table 2-17. The lower-bound curve is developed based on the minimum yield

and ultimate strength values from Table 2-12 and Table 2-13 at an upper-bound temperature of 93°C and the lowest maximum elongation for all product forms and material types permitted for the fabrication of the overpack shell assembly components (i.e., 30% for A479, Type 304 and Type 316 stainless steels). However, the upper-bound design curve is based on a yield strength of 310 MPa and a tensile strength of 655 MPa since the values given in Table 2-12 and Table 2-13 represent the minimum expected values at temperature. In addition, the upper-bound design curve is conservatively extended beyond the failure strain of the overpack shell materials to a maximum strain of approximately 60%. This is done to avoid material failure that may lead to non-conservative predictions of the upper-bound drop loads.

The structural evaluation of the overpack for the HAC free drop and HAC puncture tests is performed using a plastic kinematic material model for the overpack closure bolts. The material model is defined by an elastic modulus, yield stress, tangent slope, and failure strain. The tangent modulus (E_t) is calculated based upon the yield stress (S_y), yield strain (ε_y), ultimate tensile stress (S_u), and failure strain (ε_u) as follows:

$$E_t = \frac{S_u - S_y}{\varepsilon_u - \varepsilon_y}$$

Where;

ε_y = $(S_y/E) + 0.002$

S_y = Yield stress (0.2% offset)

E = Elastic modulus

The upper-bound and lower-bound plastic-kinematic material properties for the overpack closure bolt material used for the structural evaluation of the package for the HAC free drop and HAC puncture tests are summarized in Table 2-18.

2.2.1.2 Shielding Material

The shielding components of the package are fabricated from DU that is alloyed with 2% molybdenum by weight (U-2% Mo). The addition of molybdenum results in the formation of a second phase that increases the yield strength of DU and improves the ductility of the material. The mechanical properties of DU over the temperature range of interest are summarized in Table 2-19.

2.2.1.3 Overpack Foam

The overpack base and lid assemblies are filled with rigid, closed-cell LAST-A-FOAM® FR-3714 polyurethane foam having a nominal density of 13.5 pcf (216 kg/m^3). The polyurethane foam is installed in-situ in the overpack shells, with foam rise parallel to the longitudinal axis of the package. The nominal static crush strength data of the polyurethane foam at room

temperature, both parallel and perpendicular to the direction of foam rise, are summarized in Table 2-20.

The dynamic stress versus strain curves for the polyurethane foam material, which are used for the NCT and HAC free drop test evaluations, are developed based on data provided by the foam manufacturer [2.16]. Upper-bound and lower-bound dynamic stress versus strain curves are developed considering the effects of crush direction, i.e., parallel or perpendicular to the direction of foam rise; temperature; strain rate; and tolerance on foam crush strength. The minimum and maximum foam temperatures considered are -29°C and 82°C, respectively. These temperatures bound the range of temperatures that the foam will experience under all initial conditions for the NCT and HAC free drop tests. The dynamic crush strength ($\sigma_{Dynamic}$) of foam is proportional to the static crush strength (σ_{Static}) and is predicted by the following equations:

$$\sigma_{Dynamic} = (Y_{Int})(\sigma_{Static})^{S}$$

Where Y_{Int} and S are the dynamic crush strength regression coefficients provided by the foam manufacturer ([2.16], Table 8). The static crush strength of foam at the lower- and upper-bound temperatures of -29°C and 82°C are calculated based on temperature correlation factors (C_T) provided by the foam manufacturer ([2.16], Tables 6 and 7).

The average static compressive strength of the polyurethane foam at room temperature is required to be within ± 10% of the nominal value for crushing parallel and perpendicular to the direction of foam rise. Therefore, the maximum and minimum static crush strengths at each strain value are taken as 110% and 90% of the nominal crush strength value.

The dynamic crush strength versus strain data for foam temperatures of -29°C and 82°C are summarized in Table 2-21. The data shows that the dynamic crush strength of polyurethane foam parallel to the direction of foam rise is slightly higher than the perpendicular to rise dynamic crush strength in all cases. For design purposes, upper-bound and lower-bound dynamic stress versus strain curves are developed and used for all drop analyses, regardless of crush orientation. The bounding design dynamic crush strength data is summarized in Table 2-22 and shown in Figure 2-5 along with the maximum and minimum dynamic crush strength values at temperature.

2.2.1.4 Other Materials

The overpack base thermal spider is a non-structural component that is fabricated from SB-152 copper sheet material. The function of the thermal spider is to conduct heat through the overpack base sidewall. Although the thermal spider is not relied upon for structural support, it is included in the structural evaluation of the overpack because its stiffness has a minor effect on the drop loads that are imparted to the cask. A plastic kinematic material model is used for the thermal spider. The material model is defined by an elastic modulus, yield stress, tangent slope, and failure strain. The elastic modulus, yield strength, and failure strain of SB-152 copper sheet material over the temperature range of interest are obtained from the ASME Code, Section II, Part B [2.17] and Part D [2.11]. The tangent modulus is calculated as described in Section 2.2.1.1. The upper-bound and lower-bound plastic-kinematic material properties for the

thermal spider material used for the structural evaluation of the package for the NCT free drop, HAC free drop, and HAC puncture tests are summarized in Table 2-23.

2.2.2 Chemical, Galvanic, or Other Reactions

The package's materials of construction are evaluated for possible chemical, galvanic, or other reactions considering the contact of dissimilar materials and the operating environments as shown in Table 2-24.

DU/steel interactions are considered, including galvanic corrosion, stress corrosion cracking, and eutectic formation. Eutectic formation does not affect package performance because the service temperatures are lower than the eutectic formation temperature. No significant DU interactions are found to occur that would affect package performance.

Hydrogen generation production by chemical and galvanic reactions is evaluated and found not to affect package effectiveness. The payload generates hydrogen through radiolysis, as discussed in Section 3.3.2.

The package has no significant chemical, galvanic, or other reactions that affect package performance.

2.2.3 Effects of Radiation on Materials

The package is designed using materials that will withstand damaging effects from radiation. Durable materials of construction such as austenitic stainless steel, ferritic bolting steel, and DU are unaffected by the radiation levels in this package.

The polyurethane foam material used for the overpack cores is unaffected by gamma radiation exposure up to 2×10^8 rads, equivalent to 1,000 rads/hour for a period of 20 years. At radiation exposure up to 2×10^8 rads, testing shows no effect on density or crush strength ([2.16], Table 4). Furthermore, the resistance of the polyurethane foam material to water absorption is unaffected by radiation exposure up to 1×10^7 rads ([2.16], Table 5).

The ethylene propylene O-ring material has good radiation-resistance properties [2.18]. Most elastomers exhibit unacceptable compression set after 10^8 rads. Ethylene propylene O-rings tested to 10^7 rads exhibit moderate compression set, and exposures to 10^6 rads produce little effect on all elastomer O-ring materials. The package containment and test O-rings only receive direct radiation from the payload momentarily as the package is loaded. Many hundreds of loading cycles would be required to reach 10^6 rads, therefore normal wear is the main factor affecting their replacement frequency. The cleanliness seal is more directly irradiated by the payload since it is inside the shielded region of the cask assembly. The cleanliness seal is therefore replaced every shipment to assure that it is not adversely affected by radiation.

The O-rings are coated with a thin film of silicone-based lubricant to help protect the O-ring from damage by abrasion, pinching, or cutting. The lubricant also helps to seat the O-ring properly and protect the polymer from environmental damage. Because the O-ring lubricant is

frequently cleaned and replaced, and because most of the lubricant's benefit occurs during installation, radiation damage is not a concern.

A nickel-based thread lubricant is specified for threaded fasteners. This material is commonly used for nuclear applications and is suitable for use in radiation environments. None of the package fasteners are located in high exposure areas, and the lubricant is frequently cleaned and replaced, so the lubricant is not subject to radiation damage.

Table 2-11 – Packaging Material Specifications (2 Pages)

Packaging Assembly	Packaging Component	Material Specification	Reference Section
Cask Body Assembly	Containment Shell	SA-479, Type 304 or Type 316	2.2.1.1
	Outer Shell and Bottom	A240, Type 304 or Type 316	2.2.1.1
	Radial and Bottom Shields	DU Alloy	2.2.1.2
	Threaded Insert, Closure Bolt Holes	Type 304 Stainless Steel	2.2.1.1
Closure Lid Assembly	Closure Lid	SA-240 or SA-479, Type 304 or Type 316	2.2.1.1
Cask Closure Bolts	---	SA-320, Grade L43	2.2.1.1
Shield Plug Assembly	Casing and Top Plate	A240 or A479, Type 304 or Type 316	2.2.1.1
	Shield Plug Core	DU Alloy	2.2.1.2
	Threaded Insert, Lifting Hole	Type 304 Stainless Steel	2.2.1.1
Shield Lid Assembly	Top Plate	A240 or A479, Type 304 or Type 316	2.2.1.1
	Casing Plate	A240, Type 304 or Type 316	2.2.1.1
	Shield lid	DU Alloy	2.2.1.2
	Attachment Bolts	A193, Grade B8	2.2.1.1
Overpack Base Assembly	Inner Bottom, Outer Bottom, Flange, and Pour Hole Covers	A240 or A479, Type 304 or Type 316	2.2.1.1
	Inner and Outer Shells	A240, Type 304 or Type 316	2.2.1.1
	Threaded Inserts, Overpack Bolting Flange	Type 304 Stainless Steel	2.2.1.1
	Thermal Spider	Copper, B152	2.2.1.4
	Inner Foam Core	LAST-A-FOAM® FR-3714 Polyurethane Foam	2.2.1.3

Table 2-11 – Packaging Material Specifications (2 Pages)

Packaging Assembly	Packaging Component	Material Specification	Reference Section
Overpack Lid Assembly	Outer Top, Flange, and Pour Hole Covers	A240 or A479, Type 304 or Type 316	2.2.1.1
	Lugs	A240, Type XM-19	2.2.1.1
	Inner Foam Core	LAST-A-FOAM® FR-3714 Polyurethane Foam	2.2.1.3
Overpack Closure Bolts	---	A320, Grade L43	2.2.1.1

Table 2-12 – Mechanical Properties of Type 304 Stainless Steel

Temp. (°C)	Design Stress Intensity, S_m[2] (MPa)	Yield Strength, S_y[3] (MPa)	Tensile Strength, S_u[4] (MPa)	Modulus of Elasticity, E[5] (MPa X 10^3)	Mean Coef. Of Thermal Expansion, α[6] (m/m/°C x 10^{-6})
-40	138	207	517	*199*	*14.7*
-29	138	207	517	*198*	*14.8*
21	138	207	517	195	15.3
38	138	207	517	*194*	15.5
93	138	172	490	190	16.0

Notes:
1. Values for SA-240/A240 and SA-479/A479 product specifications.
2. ASME Code, Section II, Part D [2.11], Table 2A.
3. ASME Code, Section II, Part D [2.11], Table Y-1.
4. ASME Code, Section II, Part D [2.11], Table U.
5. ASME Code, Section II, Part D [2.11], Table TM-1, Material Group G.
6. ASME Code, Section II, Part D [2.11], Table TE-1, Group 3, Coefficient B (mean from 70°F).
7. Values shown in *italics* are calculated using linear interpolation or linear extrapolation.

Table 2-13 – Mechanical Properties of Type 316 Stainless Steel

Temp. (°C)	Design Stress Intensity, S_m[2] (MPa)	Yield Strength, S_y[3] (MPa)	Tensile Strength, S_u[4] (MPa)	Modulus of Elasticity, E[5] (MPa X 10^3)	Mean Coef. Of Thermal Expansion, α[6] (m/m/°C x 10^{-6})
-40	138	207	517	*199*	*14.7*
-29	138	207	517	*198*	*14.8*
21	138	207	517	195	15.3
38	138	207	517	*194*	15.5
93	138	179	517	190	16.0

Notes:
1. Values for SA-240/A240 and SA-479/A479 product specifications.
2. ASME Code, Section II, Part D [2.11], Table 2A.
3. ASME Code, Section II, Part D [2.11], Table Y-1.
4. ASME Code, Section II, Part D [2.11], Table U.
5. ASME Code, Section II, Part D [2.11], Table TM-1, Material Group G.
6. ASME Code, Section II, Part D [2.11], Table TE-1, Group 3, Coefficient B (mean from 70°F).
7. Values shown in *italics* are calculated using linear interpolation or linear extrapolation.

Table 2-14 – Mechanical Properties of A240, Type XM-19 Stainless Steel

Temp. (°C)	Design Stress Intensity, S_m[2] (MPa)	Yield Strength, S_y[3] (MPa)	Tensile Strength, S_u[4] (MPa)	Modulus of Elasticity, E[5] (MPa X 10^3)	Mean Coef. Of Thermal Expansion, α[6] (m/m/°C x 10^{-6})
-40	*230*	*379*	*690*	*199*	*14.3*
-29	230	379	690	*198*	*14.4*
21	230	379	690	195	14.8
38	230	379	690	*194*	14.8
66	229	343	*688*	*192*	15.1
93	228	325	685	190	15.3

Notes:
1. ASME Code, Section II, Part D [2.11], Table 2A.
2. ASME Code, Section II, Part D [2.11], Table Y-1.
3. ASME Code, Section II, Part D [2.11], Table U.
4. ASME Code, Section II, Part D [2.11], Table TM-1, Material Group G.
5. ASME Code, Section II, Part D [2.11], Table TE-1, Group 4, Coefficient B (mean from 70°F).
6. Values shown in *italics* are calculated using linear interpolation or linear extrapolation.

Table 2-15 – Mechanical Properties of SA-320/A320, Grade L43 Bolting Steel

Temp. (°C)	Design Stress Intensity, S_m[1] (MPa)	Yield Strength, S_y[2] (MPa)	Tensile Strength, S_u[3] (MPa)	Modulus of Elasticity, E[4] (MPa X 10^3)	Mean Coef. Of Thermal Expansion, α[5] (m/m/°C x 10^{-6})
-40	241	724	862	*195*	*11.1*
-29	241	724	862	*194*	*11.1*
21	241	724	862	192	11.5
38	241	724	862	*191*	11.7
93	228	683	862	187	12.1

Notes:
1. ASME Code, Section II, Part D [2.11], Table 4.
2. In accordance with ASME Code, Section II, Part D [2.11], Table 4, General Note (a), the yield strength is equal to 3 times the allowable stress value, S_m.
3. Minimum tensile strength from ASME Code, Section II, Part D [2.11], Table 4. The tensile strength is assumed to remain constant up to 93°C.
4. ASME Code, Section II, Part D [2.11], Table TM-1, Material Group B.
5. ASME Code, Section II, Part D [2.11], Table TE-1, Group 1, Coefficient B (mean from 70°F).
6. Values shown in *italics* are calculated using linear interpolation or linear extrapolation.

Table 2-16 – Mechanical Properties of A193, Grade B8 Bolting Steel

Temp. (°C)	Design Stress Intensity, S_m[1] (MPa)	Yield Strength, S_y[2] (MPa)	Tensile Strength, S_u[3] (MPa)	Modulus of Elasticity, E[4] (MPa X 10^3)	Mean Coef. Of Thermal Expansion, α[5] (m/m/°C x 10^{-6})
-40	69	207	517	*199*	*14.7*
-29	69	207	517	*198*	*14.8*
21	69	207	517	195	15.3
38	69	207	517	*194*	15.5
93	57	172	490	190	16.0

Notes:
1. ASME Code, Section II, Part D [2.11], Table 4.
2. ASME Code, Section II, Part D [2.11], Table Y-1.
3. ASME Code, Section II, Part D [2.11], Table U.
4. ASME Code, Section II, Part D [2.11], Table TM-1, Material Group G.
5. ASME Code, Section II, Part D [2.11], Table TE-1, Group 3, Coefficient B (mean from 70°F).
6. Values shown in *italics* are calculated using linear interpolation or linear extrapolation.

Table 2-17 – Stainless Steel True Stress-Strain Design Data

Lower-Bound Curve		Upper-Bound Curve	
True Strain	**True Stress (Pa)**	**True Strain**	**True Stress (Pa)**
0.00055	5.99E+07	0.00049	8.81E+07
0.00250	1.20E+08	0.00153	1.76E+08
0.00718	1.80E+08	0.00434	2.64E+08
0.01593	2.39E+08	0.01077	3.52E+08
0.03004	2.99E+08	0.02328	4.40E+08
0.05083	3.59E+08	0.04485	5.28E+08
0.07959	4.19E+08	0.07901	6.17E+08
0.11761	4.79E+08	0.12982	7.05E+08
0.16616	5.39E+08	0.20181	7.93E+08
0.22653	5.99E+08	0.30000	8.81E+08
0.30000	6.59E+08	0.42991	9.69E+08
---	---	0.59749	1.06E+09

Notes:
1. Lower-bound data calculated based on the lowest yield and ultimate strength of all overpack shell stainless steel materials at an upper-bound temperature of 93°C and an ultimate strain of 40%. The stress-strain data is terminated at a strain of 30%, equal to the lowest maximum elongation for all product forms and material types permitted for the fabrication of the overpack shell assembly components.
2. Upper-bound data based on an upper-bound yield strength 310 MPa, an upper-bound ultimate strength of 655 MPa, and an ultimate strain of 30%. The upper-bound stress-strain data is extended to a strain of approximately 60% to avoid material failure that may lead to non-conservative predictions of the upper-bound drop loads.

Table 2-18 – SA-320/A320, Grade L43 Alloy Bolting Steel Plastic-Kinematic Properties

Parameter	Upper Bound, -29°C	Lower Bound, 93°C
Elastic Modulus, $E^{(1)}$ (MPa)	1.94E5	1.87E5
Yield Strength, $S_y^{(1)}$ (MPa)	724	683
Tensile Strength, $S_u^{(1)}$ (MPa)	862	862
Tangent Modulus, E_t (MPa)	894	1,158
Failure Strain, $\varepsilon_u^{(2)}$	0.16	0.16

Notes:
1. Values from Table 2-15 at temperature.
2. Maximum elongation of SA-320, Grade L43 alloy bolting steel from ASME BPVC, Section II, Part A [2.19], Specification SA-320. Table 1.

Table 2-19 – Mechanical Properties of DU Alloy

Temperature (°C)	Yield Strength, S_y[1] (MPa)	Tensile Strength, S_u[1] (MPa)	Modulus of Elasticity, E[2] (MPa X 10^3)	Mean Coef. Of Thermal Expansion, α[3] (m/m/°C x 10^{-6})
-40	420	850	---	11.5
-29	420	850	---	11.7
21	405	810	172	12.7
38	400	780	---	13.0
93	380	690	---	14.1

Notes:
1. Yield and ultimate strength of U-2% Mo from Figure 5 of [2.12].
2. Average tension modulus of DU from [2.20].
3. Properties from Figure I-2 of [2.21]. Values shown in *italics* are calculated by linear extrapolation.

Table 2-20 – Overpack Foam Static Stress-Strain Data at Room Temperature

Strain	Static Crush Strength (psi)	
	Parallel-to-Rise	Perpendicular-to-Rise
10%	464	472
20%	469	490
30%	500	524
40%	560	591
50%	695	734
60%	1,003	1,059
65%	1,306	1,377
70%	1,821	1,910

Notes:
1. Properties from [2.16].

Table 2-21 – Foam Dynamic Stress-Strain Properties

Strain	Dynamic Crush Strength (psi)			
	Cold (-29°C/-20°F)		Hot (82°C/180°F)	
	Nominal	Upper-Bound	Nominal	Lower-Bound
Parallel-to-Rise				
0.10	1,005	1,109	450	403
0.20	939	1,033	442	398
0.30	964	1,060	477	429
0.40	1,038	1,142	514	462
0.50	1,236	1,359	617	556
0.60	1,649	1,811	834	752
0.65	2,169	2,384	1,091	983
0.70	2,406	2,636	1,334	1,206
Perpendicular-to-Rise				
0.10	1,015	1,120	458	411
0.20	981	1,080	462	416
0.30	1,010	1,111	492	443
0.40	1,112	1,224	542	488
0.50	1,295	1,424	652	587
0.60	1,713	1,881	880	793
0.65	2,215	2,434	1,168	1,052
0.70	2,346	2,570	1,376	1,244

Table 2-22 – Overpack Foam Upper- and Lower-Bound Dynamic Stress-Strain Data

Strain	Dynamic Crush Strength (psi)	
	Upper Bound	Lower Bound
0.05[1]	1,120 (7.72 MPa)	398 (2.74 MPa)
0.10	1,120 (7.72 MPa)	398 (2.74 MPa)
0.20	1,120 (7.72 MPa)	398 (2.74 MPa)
0.30	1,120 (7.72 MPa)	429 (2.96 MPa)
0.40	1,225 (8.45 MPa)	462 (3.19 MPa)
0.50	1,430 (9.86 MPa)	556 (3.83 MPa)
0.60	1,890 (13.03 MPa)	752 (5.19 MPa)
0.65	2,440 (16.82 MPa)	980 (6.76 MPa)
0.70	2,640 (18.20 MPa)	1,220 (8.41 MPa)

Notes:
1. The foam manufacturer's crush strength data [2.16] is provided at 10% strain increments. However, the foam manufacturer's literature indicates that the foam crush strength typically reaches the yield strength at strains of approximately 5%. Therefore, the foam crush strength is assumed to increases linearly from zero at 0% strain to the 10% strain crush strength value at 5% strain.

Table 2-23 – SB-152 Copper Sheet Plastic-Kinematic Properties

Parameter	Upper Bound, -29°C	Lower Bound, 93°C
Elastic Modulus, $E^{(1)}$ (MPa)	1.19E5	1.14E5
Yield Strength, $S_y^{(2)}$ (MPa)	69	56
Tensile Strength, $S_u^{(3)}$ (MPa)	207	188
Tangent Modulus, E_t (MPa)	345	330
Failure Strain, $\varepsilon_u^{(4)}$	0.40	0.40

Notes:
1. ASME BPVC, Section II, Part D [2.11], Table TM-4, Material C12200.
2. ASME BPVC, Section II, Part D [2.11], Table Y-1.
3. ASME BPVC, Section II, Part D [2.11], Table U.
4. Maximum elongation of ASME BPVC, Section II, Part B [2.17], Specification SB-152, Section 8.1.

Table 2-24 – Summary of MIDUS Material Interactions

	Decon Fluid	DU	E-P O-rings	Nylon (screw)	O-ring lubricant	Foam	Product	Stainless Steel	Ni-Cr-Mo Fasteners	Thread Lubricant	Copper	Brazing Metal
Decon Fluid		--	S	S	S	--	S	S	S	S	--	--
DU			--	--	--	--	--	NHS	--	--	--	--
EP O-rings				NHS	NHS	NHS	H	NHS	--	--	--	--
Nylon Screw					NHS	NHS	--	NHS	--	--	--	--
O-ring lubricant						--	H	NHS	--	--	--	--
Foam							--	NHS	--	--	NHS	NHS
Product								NHS	--	--	--	--
Stainless Steel									NHS	NHS	NHS	NHS
Ni-Cr-Mo Fastener										NHS	--	--
Thread Lubricant											--	--
Copper												NHS

Notes:

N = normal conditions of transportation; H = hypothetical accident conditions; S = service conditions at medical isotope facilities.

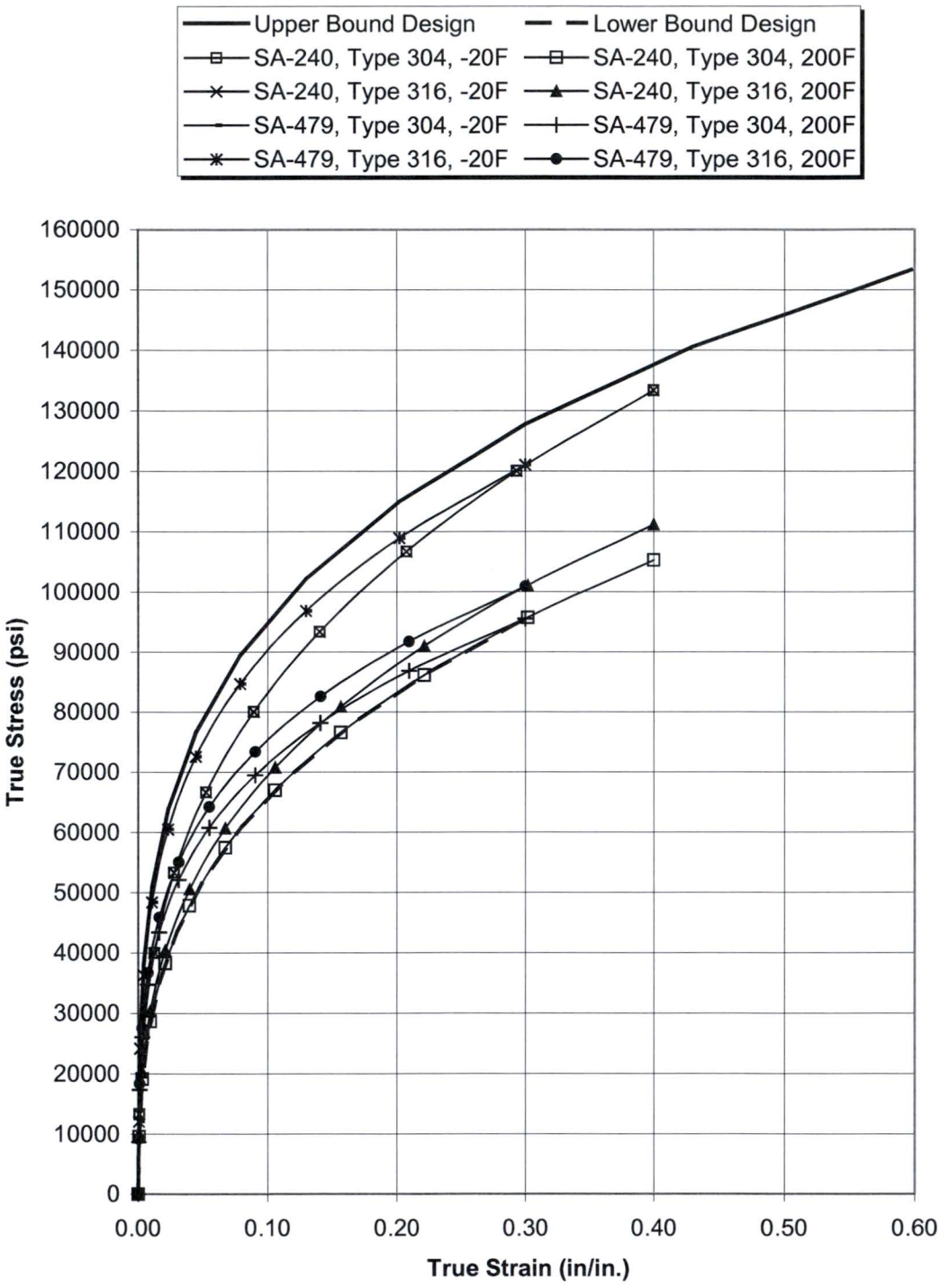

Figure 2-4 – Stainless Steel True Stress-Strain Design Curves

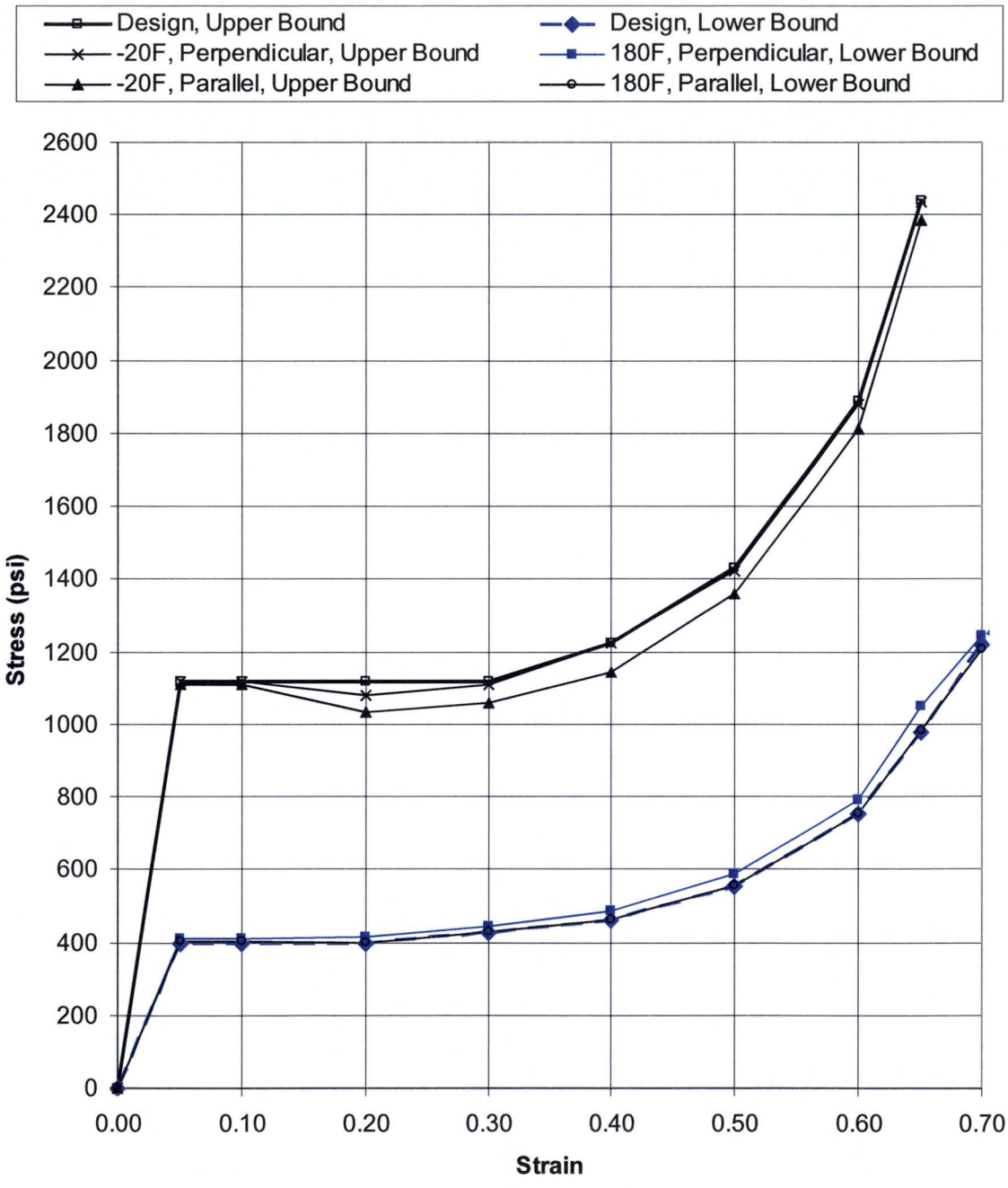

Figure 2-5 – Overpack Foam Dynamic Stress-Strain Curves

2.3 Fabrication and Examination

2.3.1 Fabrication

All work performed to fabricate the package is performed under Energy*Solutions*' 10 CFR 71, Subpart H quality assurance program, NRC approval number 0935. The package containment system is fabricated in accordance with the applicable requirements of Subsections WA and WB of Section III, Division 3 of the ASME Code [2.1]. Use of an NPT Certificate Holder and an Authorized Inspection Agency is not required for the construction of the package containment system. The non-containment structural components of the package are fabricated in accordance with the applicable requirements of Subsection NF [2.2] of the ASME Code for plate- and shell-type Class 2 supports. Standard industry practices are used for the fabrication of the DU alloy gamma shield components, the overpack base thermal spider and its brazed connections to the overpack base shells, and the overpack base and lid assembly polyurethane foam cores.

All components that form the package containment system are fabricated from materials permitted by Subsection WB [2.1] of the ASME Code and included in Section II, Part D, of the ASME Code [2.11]. All other non-containment structural components of the package are fabricated from ASTM materials that are equivalent to ASME materials, as permitted by NUREG/CR-3854 [2.14]. All package welds, with the exception of the overpack lid lug attachment welds, are made with SFA-5.9 ER308L, ER308LSi, or ER316L weld filler metal. The overpack lid lug attachment welds are made with SFA-5.9 ER309L or ER309LSi weld filler metal. All weld filler metal is required to have a minimum delta ferrite content of 5 FN. The quality category of the weld material is required be equal to or greater than the higher quality category of the components being joined. A certified material test report (CMTR) is provided for all steel materials, including weld filler metals, used to fabricate the package.

Consumables, such as threaded inserts and elastomeric O-rings, are procured from commercial suppliers and commercially dedicated in accordance with the requirements of the Energy*Solutions* QA program, commensurate with their safety functions.

All materials, components, and assemblies used for the fabrication of the package, including the weld filler metal, are labeled to maintain control and traceability of materials throughout the fabrication process. Marking of materials, components, and assemblies is done using permanent methods that do not result in harmful contamination or sharp discontinuities, or infringe upon the minimum required material thickness.

All operations associated with the fabrication and assembly of the package are included in written shop instructions, e.g., fabrication travelers and/or procedures. All welding and brazing is performed in accordance with a written welding procedure specification (WPS) or brazing procedure specification (BPS) that is qualified in accordance with the applicable requirements of the ASME Code. All personnel performing welding or brazing are qualified to use the welding or brazing procedure, and their qualifications are documented in accordance with the applicable requirements of Section IX of the ASME Code [2.22]. Only GTAW and GMAW welding processes are permitted for the fabrication of the package.

The general processes used to fabricate each finished assembly of the package are described as follows:

Cask Body Assembly

The cask body assembly is constructed from a containment shell, outer bottom, outer shell, bottom shield, radial shield, and threaded inserts. The DU alloy material is cast into molds that are slightly larger than the finished dimensions of the cask body gamma shield components. The DU alloy castings are heat-treated in a vacuum induction furnace to obtain the desired mechanical properties. The heat-treated DU alloy castings are then precision-machined to the dimensions shown on the general arrangement drawings in Section 1.3.2.

The cask body containment shell and outer bottom are both fabricated by machining solid pieces of bar or plate material. This minimizes the amount of welding and/or forming operations required to fabricate the package, which results in less weld distortion and residual stress. The cask body outer shell is fabricated from rolled steel plate with a full-penetration longitudinal seam weld to form a cylinder. The use of a backing bar made from similar material is permitted for the longitudinal seam weld, provided that it is removed for the finished assembly. The cask body outer shell may be rolled to the required finished dimensions or formed from thicker plate that is machined to achieve the required dimensions. The outer shell is aligned with the containment shell and outer bottom and attached using full-penetration circumferential seam welds, sealing the DU-alloy gamma shield components inside the cask body shell.

Some of the critical features of the cask body, such as the top face of the cask bolting flange, the leak-test and containment O-ring grooves, and closure bolt holes may be machined to the final dimensions shown on the general arrangement drawings in Section 1.3.2 after completing the cask body welds. Following completion of machining operations, threaded inserts are installed in the closure bolt holes in accordance with the manufacturer's recommendations for bottoming taps.

Shield Plug Assembly

The cask shield plug assembly is constructed from a casing shell, top plate, DU core, and a threaded insert. The processes used to fabricate the DU core of the shield plug are the same as those described above for the cask body DU shield components. The shield plug casing shell and top plate are both fabricated by machining solid pieces of bar or plate material to minimize the amount of welding and/or forming operations required to fabricate the finished shield plug. The DU core is placed inside the casing shell, and the top plate is attached using a full-penetration circumferential seam weld. After completing the weld, the shield plug assembly is machined to the final dimensions shown on the general arrangement drawings in Section 1.3.2. Following completion of machining operations, the threaded insert is installed in the shield plug lifting hole in accordance with the manufacturer's recommendations for bottoming taps.

Closure Lid Assembly

The closure lid assembly is constructed from a closure lid, test port plug, and threaded inserts. The closure lid is fabricated by machining a solid piece of bar or plate material to the dimensions shown on the general arrangement drawings in Section 1.3.2. Following completion of machining operations, the threaded inserts are installed in the cask lifting attachment holes and shield lid attachment holes in accordance with the manufacturer's recommendations for bottoming taps. The test port plug is installed in the leak-test port of the closure lid after coating the test port plug O-ring seal and the associated sealing surface in the leak-test port of the closure lid with O-ring lubricant in accordance with the O-ring manufacturer's recommendations.

Shield Lid Assembly

The shield lid assembly is constructed from a top plate, casing plate, DU shield plate, and two shield lid attachment bolts. The processes used to fabricate the DU alloy core of the shield lid are the same as those described above for the cask body DU shield components. The shield lid top plate is fabricated by machining a solid piece of bar or plate material, whereas the shield lid top plate is fabricated from a single piece of plate. The shield lid core is placed inside the shield lid top plate and the casing plate is attached using a full-thickness, all-around, partial-penetration groove weld to seal the DU alloy gamma shield inside the cask body shell. The shield lid attachment bolts are fabricated from M10 X 1.5 socket heat cap screws that are machined as shown on the general arrangement drawings in Section 1.3.2. The shield lid attachment bolts are threaded through the tapped holes in the shield lid top plate, making them captured hardware.

Overpack Base Assembly

The overpack base assembly is constructed from a shell assembly that is filled with polyurethane foam. The shell assembly is constructed from an outer bottom, outer shell, flange, inner shell, inner bottom, thermal spider, and thermal relief plugs. The outer bottom, flange, and inner bottom are all fabricated from a solid piece of bar or plate material that is machined to the dimensions shown on the general arrangement drawings in Section 1.3.2. The inner and outer shells are both fabricated from rolled steel plate with a full-penetration longitudinal seam weld to form a cylinder. The use of backing bars made from similar material is permitted for the shell longitudinal seam welds. The shells may be rolled to the required finished dimensions or formed from thicker plate and machined to achieve the required dimensions. The thermal spider is fabricated from copper sheet or plate material that is cut to size and mechanically formed to the dimensions shown on the general arrangement drawings in Section 1.3.2. The outer shell, flange, inner shell, and inner bottom are aligned and attached with all-around, full-penetration, circumferential seam welds, as shown on the general arrangement drawings in Section 1.3.2. Prior to welding the outer bottom in place, the thermal spider is brazed to the inner bottom and outer shell. The outer bottom is then aligned with the outer shell and attached with a full-penetration, circumferential seam weld.

Some features of the overpack base that are not required for foam installation, such as the finished dimensions of the bolting flange, the overpack bolt holes, and the holes for the tamper-indicating device, may be machined before or after completing the foam installation

process. However, the four nylon thermal relief plugs must be installed in the corresponding threaded holes of the overpack base shell prior to installing the polyurethane foam core. The polyurethane foam core of the overpack base is installed in-situ at the foam manufacturer's facility. The overpack base shell is positioned upside-down and filled with the liquid foam mixture through two pour holes located on the bottom plate of the shell . The foam is allowed to cure completely before welding the steel cover plates over the pour holes. Final machining operations of the overpack base features not completed prior to foam installation are then performed. Following completion of machining operations, threaded inserts are installed in each of the overpack base closure bolt holes in accordance with the manufacturer's recommendations and two locating pins are installed in the flange to facilitate overpack lid assembly installation operations.

Overpack Lid Assembly

The processes used to fabricate the overpack lid assembly are similar to those used to fabricate the overpack base. The overpack lid is constructed from a shell assembly that is filled with polyurethane foam. The shell assembly consists of a lid flange, outer top, four lid lugs, and four thermal relief plugs. The overpack lid flange and outer top are both fabricated from single, solid pieces of bar or plate material that are machined to the dimensions shown on the general arrangement drawings in Section 1.3.2. The lid flange and outer top are positioned and joined using an all-around, full-penetration, circumferential weld. The lid lugs, which are machined from plate material, are positioned and welded to the overpack lid outer top. The outer surfaces of the overpack lid may be machined to the finished dimensions following attachment of the lid lugs. Some features of the overpack lid that are not required for foam installation, such as the finished dimensions of the bolting flange, overpack bolt holes, and the holes for the tamper-indicating device, may be machined before or after completing the foam installation process. However, the four nylon thermal relief plugs must be installed in the corresponding threaded holes of the overpack base shell prior to installing the polyurethane foam core. The polyurethane foam core of the overpack lid is installed in-situ at the foam manufacturer's facility. The overpack lid shell is positioned upside-down and filled through two pour holes located on the overpack lid bottom plate with the liquid foam mixture. The foam is allowed to cure completely before welding the steel cover plates over the pour holes. Final machining operations of the overpack lid features not completed prior to foam installation are then performed.

2.3.2 Examination

Examination and testing of the package is performed under Energy*Solutions*' NRC-approved QA program. The components and assemblies of the package are inspected to assure that the package satisfies the dimensional requirements shown on the general arrangement drawings in Section 1.3.2 and are examined using non-destructive techniques to assure quality of workmanship. In addition, materials, components, and assemblies are tested to assure that they have the required critical characteristics and that they satisfy the acceptance criteria for all required functional tests. All operations associated with the examination and testing of the package are included in written shop instructions, e.g., fabrication travelers and/or procedures,

and performed by personnel that are trained and qualified in accordance with the requirements of the Energy*Solutions* QA program and the requirements of the applicable codes and standards using calibrated measuring and test equipment (M&TE). Witness and hold points are included in the written shop instructions for activities that require QA inspection or oversight. Copies of all written shop instructions, personnel training and qualification records, and M&TE calibration records are maintained with the final records package.

The processes used for the examination and testing of the package are described as follows:

Material Tests

The steel materials used to fabricate the components and assemblies of the package are furnished with CMTRs that assure that the materials possess the critical characteristics that are required to perform their safety functions. No additional examination or testing of these steel materials is required prior to fabrication.

The DU alloy material used to fabricate the gamma shield components of the package is tested to assure that it has the 2.0% ± 0.2% molybdenum by weight, a maximum carbon content of 0.2% by weight, and a minimum Charpy V-notch impact energy of 6 ft-lb at 70°F (21°C). The density of the finished DU alloy components, as determined from the measured weight and volume, is tested to assure that it is not less than 18.65 g/cc.

The polyurethane foam used to fill the overpack base and lid is tested to assure that it has the required density, static crush strength, flame retardancy, and intumescence. Assurance of the physical properties of each batch of foam used to fill the overpack base and lid is provided through specimen testing performed by the foam manufacturer in accordance with standard procedures. The average density of the test specimens from each batch of foam must be within ±10% of the nominal foam density (13.5 pcf). The average static compressive strength of each batch of foam, tested both parallel-to-rise and perpendicular-to-rise, is required to be within ±10% of the nominal crush strength values at 10%, 30%, and 50% strain levels. Following application of a 816°C flame for at least 60 seconds, the foam must not sustain a flame for more than 15 seconds. The intumescence of the foam specimens shall not be less than 100%. Furthermore, the foam specimens are tested to assure they have no more than 1 ppm of leachable chlorides. Conformance with these testing requirements is certified by the foam manufacturer.

Fabrication Tests and Examinations

The dimensions of the components and assemblies of the package are measured with calibrated M&TE to assure compliance with the dimensional requirements shown on the general arrangement drawings in Section 1.3.2. In addition, the weight of the finished cask and packaging are measured to assure that they meet the weight requirements.

All welded joints receive a workmanship visual examination and liquid penetrant (PT) non-destructive examination (NDE) to assure that they do not include visible defects, such as lack of fusion, lack of penetration, linear or crack-like indications, or porosity. All accessible surfaces of brazed joints are visually examined to assure adequate flow of brazing metal through

the joint. Examinations of welded and brazed joints are performed in accordance with the applicable requirements of the ASME Code. Areas of surface defect removal and completed weld repairs require thickness checks, using either a mechanical or ultrasonic testing (UT) device, by qualified personnel to verify compliance with the minimum thickness requirements. Written reports of each weld examination are prepared and maintained with the final records package.

Prior to assembly of the cask body, the containment shell is leak-tested in accordance with ANSI N14.5 to demonstrate a leak rate of the base metal that is less than or equal to 1.0×10^{-7} ref-cm^3/s. The components of the finished cask that form the containment system, i.e., the cask body, closure lid, cask closure bolts, and containment O-ring seal are leak-tested in accordance with ANSI N14.5 to demonstrate a leak rate less than or equal to 1.0×10^{-7} ref-cm^3/s. The cask is also tested for an internal pressure not less than 1,050 kPa in accordance with the requirements of WB-6220 to verify the structural integrity of the cask containment system at 150% MNOP.

Functional Tests

Functional tests are performed to assure proper fit-up of the packaging components. The shield plug assembly, with the cleanliness O-ring installed, must fit within the cask body and its entire top surface must protrude above the top surface of the cask body. This test is performed to assure that the cleanliness O-ring will be compressed when the closure lid is installed, thereby minimizing the air space between the shield plug and closure lid where radioactive product could potentially collect following the HAC free drop or puncture drop tests.

2.4 General Requirements for All Packages

2.4.1 Minimum Package Size

In accordance with the requirement of §71.43(a), the smallest overall dimension of a package may not be less than 10 cm. The package has an overall height of 55.1 cm and an outside diameter of 52 cm. Therefore, the package meets the minimum package size requirement of §71.43(a).

2.4.2 Tamper-Indicating Feature

In accordance with the requirement of §71.43(b), the outside of a package must incorporate a feature, such as a seal, that is not readily breakable and that, while intact, would be evidence that the package has not been opened by unauthorized persons. The outside of the package includes a one-piece wire cable tamper-indicating seal that is looped through holes in the bolting flange of the assembled package and secured in place. The location of the seal and its materials of construction minimize the potential for accidental damage during transport. The tamper-indicating seal must be removed to open the package and cannot be removed by unauthorized persons without damaging the seal or the package. Thus, the package satisfies the tamper-indicating feature requirements of §71.43(b). The tamper-indicating seal is not required to be installed for empty shipments.

2.4.3 Positive Closure

In accordance with the requirement of §71.43(c), the package must include a containment system securely closed by a positive fastening device that cannot be opened unintentionally or by a pressure than may arise within the package. The cask is completely enclosed inside the overpack, which includes a tamper-indicating seal, as discussed in Section 2.4.2. The tamper-indicating seal will prevent the overpack from being unintentionally opened. Furthermore, the containment system includes a closure lid that is secured to the cask body by eight closure bolts. Since tools are required to remove these bolts, the cask containment system cannot be unintentionally opened. The containment system does not include any covers, valves, or other access that could be inadvertently opened.

The cask containment system is evaluated for internal pressure loads that arise during NCT and HAC in Section 2.6.3 and Section 2.7.4.3, respectively. The evaluations demonstrate that the cask closure bolts satisfy the applicable allowable stress design criteria and that the containment seal remains intact under NCT and HAC. Hence, the package containment system satisfies the positive closure requirements of §71.43(c).

2.5 Lifting and Tie-down Standards for All Packages

2.5.1 Lifting Devices

In accordance with the requirements of §71.45(a), the lifting attachments that are structural parts of the package are designed with a minimum factor of safety of three against yield when used to lift the package in the intended manner. The lifting attachments are also designed so that failure of any lifting device under excessive load would not impair the ability of the package to meet the other requirements of 10 CFR 71 Subpart E.

2.5.1.1 Package Lift

The package is intended to be lifted vertically using the four lifting lugs that are integral to the overpack lid. The nominal mass of the package is 320.6 kg. It is conservatively assumed that the package is lifted using only two diametrically opposed lifting lugs, as shown in Figure 2-6. Each lifting lug must support one half of the package weight, or a vertical force (Fv) of 1,619 N, conservatively based on an upper-bound package mass of 330 kg. The resultant lug force (Fr) is a function of the lift angle (α). Conservatively assuming a minimum lift angle of 30°, the maximum resultant lug force is 3,238 N. The average bearing stress and shear tear-out stress in the overpack lid lug and the maximum stress intensity in the lug attachment weld due to the maximum resultant lug force are determined using hand calculations and shown to satisfy the requirements of §71.45(a).

Average Bearing Stress

The maximum resultant lug force produces an average bearing stress in the lifting lug of 10 MPa, based on the projected area of a 16 mm diameter shackle pin inside the hole of the 20 mm thick overpack lid lug. The yield strength of the overpack lid lug Type XM-19 material at a bounding design temperature of 93°C is 324 MPa. The average bearing stress in the lifting lug due to the maximum resultant lug force is less than one-third of the lug material yield strength (108 MPa). The minimum design margin for average bearing stress in the lid lifting lug is +9.80. Therefore, the stress limit requirement of §71.45(a) is satisfied.

Shear Tear-Out Stress

The shear tear-out stress in the lifting lug due to the lifting load is conservatively calculated using the resultant lug load and the smallest shear tear-out area, as follows.

$$f_v = \frac{Fr}{A_v} = 13 \text{ MPa}$$

Where:

A_v = $2b(R_o - R_h)$, shear tear-out area of lifting lug hole
= 240 mm^2

b = 20.0 mm, lifting lug thickness

R_o = 15.0 mm, corner radius lifting lug

R_h = 9.0 mm, lifting lug hole radius

The allowable shear stress for lifting devices is taken as 60% of the allowable stress for the base material, or 65 MPa for Type XM-19 material at a bounding design temperature of 93°C. The maximum shear tear-out stress in the overpack lid lug is less than 65 MPa. The minimum design margin for shear tear-out stress in the lid lifting lug is +4.00. Therefore, the stress limit requirement of §71.45(a) is satisfied.

Lug Attachment Weld Stress

Each overpack lifting lug is attached to the top outer shell of the overpack lid by a two-sided full thickness groove weld with 4 mm cover fillet welds. Under the lifting loads, the lifting lug attachment weld is subjected to tensile, shear, and bending loads, as shown in Figure 2-7. The weld loads are calculated as follows.

$$Vw = Fr \cdot \cos(15^\circ) = 3{,}128 \text{ N}$$

$$Nw = Fr \cdot \sin(15^\circ) = 838 \text{ N}$$

$$Mw = Vw \cdot e = 51{,}612 \text{ N-mm}$$

$$e = \frac{53.3}{\sqrt{2}} - 15.0 \cdot \sqrt{2} = 16.5 \text{ mm}$$

The stresses in the overpack lifting lug attachment weld due to the lifting loads are calculated as follows.

$$f_a = \frac{Nw}{A_w} = 0.6 \text{ MPa}$$

$$f_v = \frac{Vw}{A_w} = 2.1 \text{ MPa}$$

$$f_b = \frac{Mw}{S_w} = 2.7 \text{ MPa}$$

Where:

A_w = bd, Weld area
= 1,508 mm^2

S_w = $bd^2/6$, Weld area
= 18,951 mm^3

b = 20 mm, weld thickness (assumed equal to lifting lug thickness)

d = 75.4 mm, weld length

The resulting maximum stress intensity in the lifting lug attachment weld is:

$$P_m + P_b = \frac{f_a + f_b}{2} + \sqrt{\left(\frac{f_a + f_b}{2}\right)^2 + f_v^{\,2}} = 4.3 \text{ MPa}$$

The allowable weld stress is equal to one third of the yield strength of the weaker base material. The lower-bound yield strength of the overpack lid top plate Type 304 and Type 316 stainless steel at 93°C is 172.4 MPa. Therefore, the allowable stress for the lifting lug attachment weld is 57.5 MPa and the minimum design margin is +12.7. The results demonstrate that the overpack lifting lug attachment weld satisfies the lifting standards of §71.45(a).

The results of the package lifting evaluation show that the lowest design margin is +4.00 for shear tear-out stress. Therefore, under excessive load, the overpack lid lug is expected to fail by shear tear-out. Shear tear-out failure of the overpack lid lug would not significantly affect the structural or thermal performance of package under NCT and HAC loadings, nor would it impair the ability of the package to meet the other requirements of 10 CFR 71 Subpart E.

2.5.1.2 Cask Assembly Lift

The cask, without the shield lid attached, is intended to be lifted in a vertical orientation by two threaded holes located on the top of the closure lid for insertion or removal from the overpack. The nominal mass of the cask assembly is 188.5 kg. An upper-bound cask mass of 195 kg is conservatively assumed for the cask lifting analysis. Each lifting attachment must support half of the cask weight, or 956 N. The cask assembly lift structural evaluation demonstrates that the stresses in the cask lifting attachment threads, the cask closure lid, and the cask closure bolts satisfy the requirements of §71.45(a).

Lifting Attachment Thread Shear Stress

The cask assembly is lifted by two M10 x 1.5 x 10 mm deep threaded inserts located on a 94.0 mm bolt circle on the centerline of the closure lid. Each lifting attachment must support half of the cask weight, or a force of 956 N. The thread shear stress in the cask lid lifting attachment resulting from a 956 N lifting load is 6.4 MPa, based on an internal thread shear area of 150 mm^2 for the M10 x 1.5 threaded insert with a minimum engagement length of 7.0 mm.

The allowable shear stress for lifting devices is taken as 60% of the allowable stress for the base material, conservatively neglecting the higher strength of the threaded insert material. The lowest yield strength of closure-lid stainless steel material at 93°C is 172.4 MPa. Therefore the

allowable shear stress for the closure lid at a bounding design temperature of 93°C is 34.5 MPa. The corresponding minimum design margin for the thread shear stress is +4.39. Therefore, the cask lifting attachment satisfies the lifting standards of §71.45(a).

Closure Lid Stresses

The stresses in the cask closure lid resulting from the cask lift load are determined using the 3-D quarter-symmetry finite element model of the closure lid shown in Figure 2-8. The finite element model includes the closure lid, closure bolts, and the top face of the cask bolting flange. The closure lid, closure bolt heads, and cask bolting flange are modeled using 3-D structural solid elements. The closure bolt shanks are modeled using 3-D beam elements. Surface-to-surface contact elements are used to model the nonlinear interfaces between the bolt heads and closure lid and between the cask flange and closure lid and capture prying effects on the closure bolts. The closure lid is modeled using the linear-elastic material properties for Type 304 or 316 stainless steel at a bounding design temperature of 93°C. The closure bolts are modeled using the material properties of SA-320, Grade L43 bolting steel at 93°C.

Symmetry boundary displacement constraints are applied to the nodes lying on the quarter-symmetry planes. The nodes located on the underside of the cask bolting flange face are restrained from vertical translation. In addition, the nodes at the base of each bolt beam element are restrained in all degrees of freedom. A total upward force of 478 N, which is equivalent to ¼ of the cask upper bound mass (195 kg), is applied to the closure plate at the centerline of the lifting attachment hole. A linear-elastic static analysis is performed using the ANSYS Mechanical finite element program.

The finite element analysis results show that the maximum stress intensities due to the vertical lift loads occur in the top plate near the lifting post. The results show that the maximum stress intensity in the closure lid due to the vertical lift is 9 MPa. The allowable stress is equal to one third of the material yield strength. The lower-bound yield strength of Type 304 and Type 316 stainless steel at an upper-bound design temperature of 93°C is 172 MPa. Therefore the allowable stress for the closure lid is 57 MPa and the minimum design margin is +5.33. Therefore, the closure lid satisfies the lifting standards of §71.45(a).

Closure Bolt Stress

The maximum closure-bolt reaction force due to the cask lifting load is shown to be 449 N from the results of the closure-lid finite element analysis. For the M10 x 1.5 closure bolt, with a stress area of 54.7 mm^2 based on a minor diameter of 8.344 mm, the bolt tensile stress is 8 MPa.

The allowable closure-bolt tensile stress is equal to one third of the material yield strength. The SA-320, Grade L43 closure bolt material has a yield strength of 683 MPa at 93°C. Therefore, the allowable tensile stress for the closure bolt is 228 MPa. The corresponding minimum design margin in the closure bolt is +27.5.

The thread shear stress in the cask closure bolt due to the 449 N lifting load is 2 MPa based on the external thread shear area of 296 mm^2 for the M10 x 1.5 closure bolt with an engagement length of 19.0 mm.

The allowable shear stress for lifting devices is taken as 60% of the allowable stress for the base material, conservatively neglecting the higher strength of the threaded insert material. The yield strength of SA-320, Grade L43 bolting steel at 93°C is 683 MPa. Therefore, the allowable closure-bolt thread shear stress is 137 MPa and the minimum design margin for the closure bolt thread shear stress is +67.5. Therefore, the closure bolt satisfies the applicable allowable stress design criteria for normal lifting loads.

The shear stress in the cask flange base metal due to the maximum bolt tensile force for the cask lift is evaluated for the maximum bolt tensile load of 449 N resulting from the cask lift. The maximum thread shear stress in the cask flange closure bolt attachment is 1.7 MPa based on an internal thread shear area of 269 mm^2 for the M10 x 1.5 thread of the cask flange base metal and a thread engagement length of 17.0 mm.

The allowable shear stress for lifting devices is taken as 60% of the allowable stress for the cask flange base material. The lower-bound yield strength of the cask bolting flange stainless steel material at an upper-bound design temperature of 93°C is 172.4 MPa. Therefore, the allowable shear stress for the closure lid is 34.5 MPa, and the minimum design margin for the thread shear stress is +19.3. These results demonstrate that the cask flange closure bolt attachment satisfies the lifting standards of §71.45(a).

The results of the cask lifting evaluation show that the lowest design margin is +4.39 for thread shear stress in the closure lid lifting attachments. Therefore, under excessive load, the closure lid lifting attachments threads are expected to fail in shear, which does not result in a loss of containment nor significantly affect the structural or thermal performance of the package under NCT and HAC loadings. Thus, it does not impair the ability of the package to meet the other requirements of 10 CFR 71 Subpart E.

2.5.2 Tie-Down Devices

The package tie-down system is comprised of the lugs that are integral to the bottom ring of the overpack base plus the four lugs that are integral to the overpack lid. The acceptable package tie-down configuration is shown in Figure 2-9. The package must be tied down using four tension-only members, e.g., cables or slings, attached to overpack lid lugs. The base of the package may be tied down by the four bottom lugs, blocked, or left unrestrained. The tie-down analysis conservatively assumes that the base of the package is left unrestrained. As shown in Figure 2-9, the angle of the four tie-down attachments is allowed to vary by ±22.5° from radial and between 35° and 65° from vertical to provide operational flexibility.

The tie-down loads are calculated based on a bounding package mass of 330 kg. The horizontal load is conservatively taken as the resultant of the 10*g* horizontal and 5*g* transverse loads for a maximum horizontal load of 11.18*g* or 36,193 N. In addition, a 2*g* upward vertical load, or 6,475 N, is applied to the package center of gravity. A lower-bound value of 0.09 for the

coefficient of sliding friction between the bottom of the package and the supporting surface is conservatively assumed for the tie-down evaluation. The tie-down evaluation is performed for a range of acceptable tie-down configurations, both with and without tie-down pretension loads, to assure that the applicable design requirements are satisfied. Six different tie-down configurations expected to cause the highest stresses in the package tie-down attachments are evaluated, as shown in Figure 2-10.

The reaction loads at each of the package tie-down attachment points for each tie-down configuration considered are determined using the finite element model shown in Figure 2-11. The model includes the package, the tie-down contact surface, and the tie-downs. The package is modeled using rigid, massless 3-D beam elements and a rigid, massless solid bottom end for a contact surface. The ends of the beam elements on the top of the package are located at the center of the lid lug holes. A single 3-D mass element is included in the model at the location of the package center of gravity. The nonlinear contact between the bottom surface of the package and the supporting tie-down surface is modeled using surface-to-surface contact elements. The tie-downs are modeled using 3-D tension-only spar elements. These elements are oriented in accordance with the angles specified in Figure 2-10 for each case analyzed.

For each evaluation, the lower ends of the tie-downs are fixed and an initial strain is applied to the tie-down elements to account for tie-down pretension loads. For each tie-down configuration, analyses are performed for essentially no tie-down pretension and for a maximum tie-down pretension load of 22.3 kN. The tie-down reaction loads for cases 1 through 6 are summarized in Table 2-25. The maximum bearing stress and shear tear-out stress in the overpack lid lug and the maximum stress intensity in the overpack lid lug attachment weld are calculated by hand for the maximum tie-down reaction loads from each tie-down case.

The maximum bearing stress, resulting from case 1, is 195 MPa. The allowable bearing stress, which is equal to the yield strength of Type XM-19 stainless steel at the overpack lid lug upper-bound design temperature of 66°C, is 343 MPa. Thus, the minimum design margin for bearing stress in the package tie-down attachment is +0.76.

The maximum shear tear-out stress in the tie-down lug subjected to the maximum tie-down load is calculated by hand using the maximum tie-down reaction loads in each case. The maximum shear tear-out stress, resulting from case 3, is 189 MPa. The allowable shear tear-out stress is taken as 60% of the allowable stress for the base material, or 206 MPa. The corresponding minimum design margin for shear stress in the lug is +0.09.

Each overpack lid lug is attached to the overpack lid outer shell by a full thickness weld with 4 mm cover fillet welds on both sides. The weld stresses are calculated at two sections, as shown in Figure 2-12. Section 1 is the smaller section that passes through the higher strength lug base material. Section 2 is the larger section located at the base of the lug weld adjacent to the weaker outer shell base material. The maximum tie-down reaction is used to calculate the normal stress, shear stress, and bending stress on each section as follows:

$$f_{a,i} = \frac{F_y}{A_i} = \frac{F_{max}\sin(a-45^\circ)\cos(b)}{c_i d_i}$$

$$f_{v,i} = \frac{F_v}{A_i} = \frac{\sqrt{F_x^{\,2} + F_z^{\,2}}}{c_i d_i} = \frac{\sqrt{\left(F_{max}\sin(b)\cos(a-45^\circ)\right)^2 + \left(F_{max}\cos(b)\cos(a-45^\circ)\right)^2}}{c_i d_i}$$

$$f_{b,i} = \frac{M_{x,i}}{S_{x,i}} + \frac{M_{z,i}}{S_{z,i}} = \frac{6(F_z e_i)}{c_i d_i^{\,2}} + \frac{6(F_x e_i)}{c_i^{\,2} d_i}$$

Where;

F_{max} = Maximum tie-down reaction from Table 2-25.

a = Vertical tie-down angle from Figure 2-10.

b = Radial tie-down angle from Figure 2-10.

c_i = Section width (see Figure 2-12).
= 20.0 mm at Section 1
= 28.0 mm at Section 2

d_i = Section length (see Figure 2-12).
= 67.4 mm at Section 1
= 75.4 mm at Section 2

e_i = Moment arm to section (see Figure 2-12).
= 12.5 mm at Section 1
= 16.5 mm at Section 2

The resulting stresses on each weld section from tie-down cases 1 and 2 are calculated as described above and summarized in Table 2-26. The results show that the maximum stress intensities at both sections result from case 1. The maximum stress intensities at sections 1 and 2 are 87 MPa and 60 MPa, respectively. The allowable stress is equal to the material yield strength. At section 1, the yield strength of the Type XM-19 base material at an upper bound temperature of 93°C is 325 MPa. Therefore, the minimum design margin at section 1 is +2.74. At section 2, the yield strength of the weaker Type 304 or 316 stainless steel base material at an upper-bound temperature of 93°C is 172 MPa. Therefore, the minimum design margin at section 2 is +1.87.

The results of the tie-down stress analysis show that the minimum design margin for shear tear-out stress in the lug is less than the minimum design margin for stresses in the lug attachment weld. Therefore, under excessive loading, the lug will fail due to shear tear-out instead of failure at the lug welded connection. Shear tear-out failure of the lug will not impair the ability of the package to meet other requirements of 10 CFR 71.

Table 2-25 – Tie-Down Reaction Loads

Tie-Down Case	Tie-Down Pretension	Tie-Down Reaction Forces (kN)			
		F_A	F_B	F_C	F_D
1	Minimum	0.0	5.4	67.5	43.4
	Maximum	0.0	8.9	62.9	46.1
2	Minimum	0.0	20.7	52.5	21.2
	Maximum	4.2	23.2	50.9	25.5
3	Minimum	12.1	20.3	60.5	51.2
	Maximum	11.1	18.9	55.7	47.2
4	Minimum	13.7	31.2	50.0	29.0
	Maximum	13.3	30.6	47.0	28.8
5	Minimum	0.0	21.6	51.9	21.6
	Maximum	2.1	26.5	50.9	26.5
6	Minimum	13.5	30.9	48.2	30.9
	Maximum	13.7	29.8	46.0	29.8

Table 2-26 – Overpack Lid Lug Weld Stresses

Stress Type	Weld Section	Tie-Down Case					
		1	2	3	4	5	6
Normal Stress, f_a (MPa)	1	8.0	6.3	14.2	11.7	6.7	12.2
	2	5.1	4.0	9.1	7.5	4.3	7.8
Shear Stress, f_v (MPa)	1	49.3	38.4	42.2	34.9	37.9	33.6
	2	31.5	24.5	26.9	22.3	24.2	21.5
Bending Stress, f_b (MPa)	1	50.7	39.4	43.4	35.8	42.1	37.3
	2	38.2	29.7	32.7	27.0	31.8	28.1
Maximum Stress Intensity, P_m+P_b (MPa)	1	87	67	80	66	70	67
	2	60	47	55	45	48	46

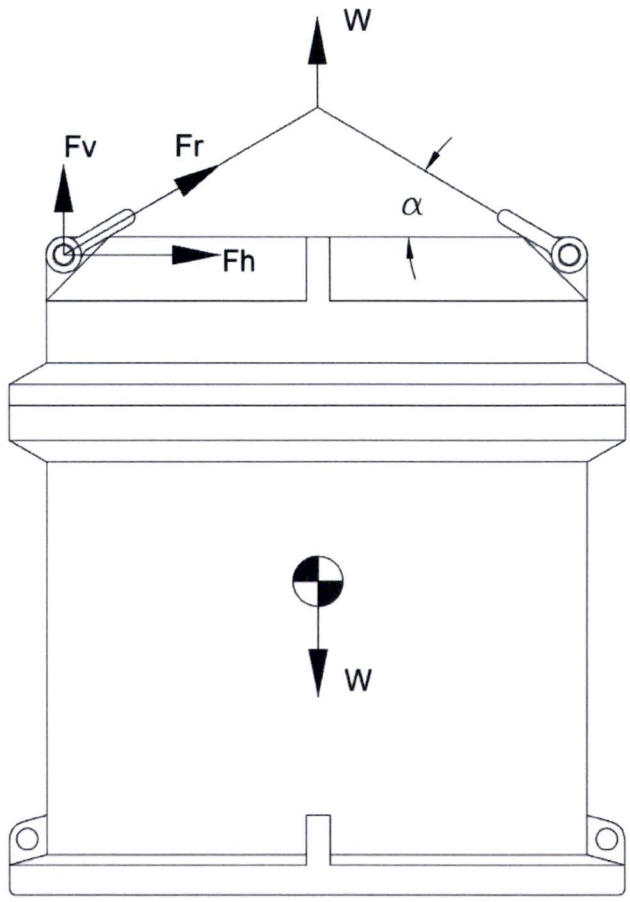

Figure 2-6 – Package Lifting Free Body Diagram

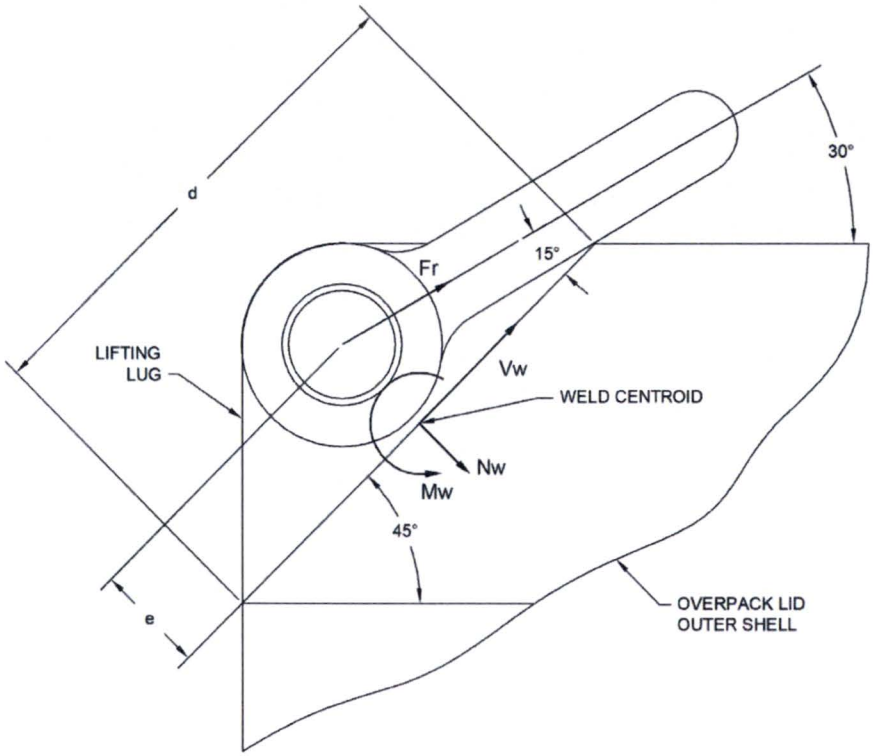

Figure 2-7 – Overpack Lifting Lug Weld Lifting Loads

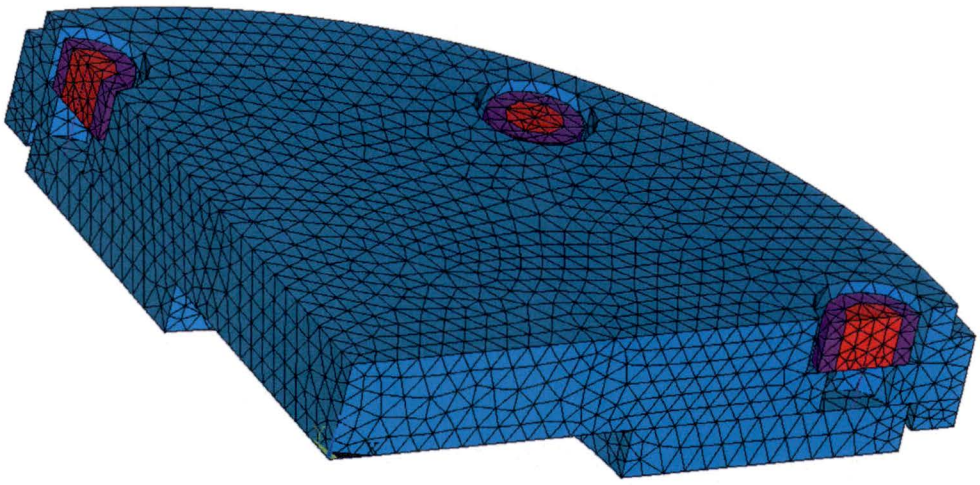

Figure 2-8 – Cask Closure Lid Quarter-Symmetry Finite Element Model

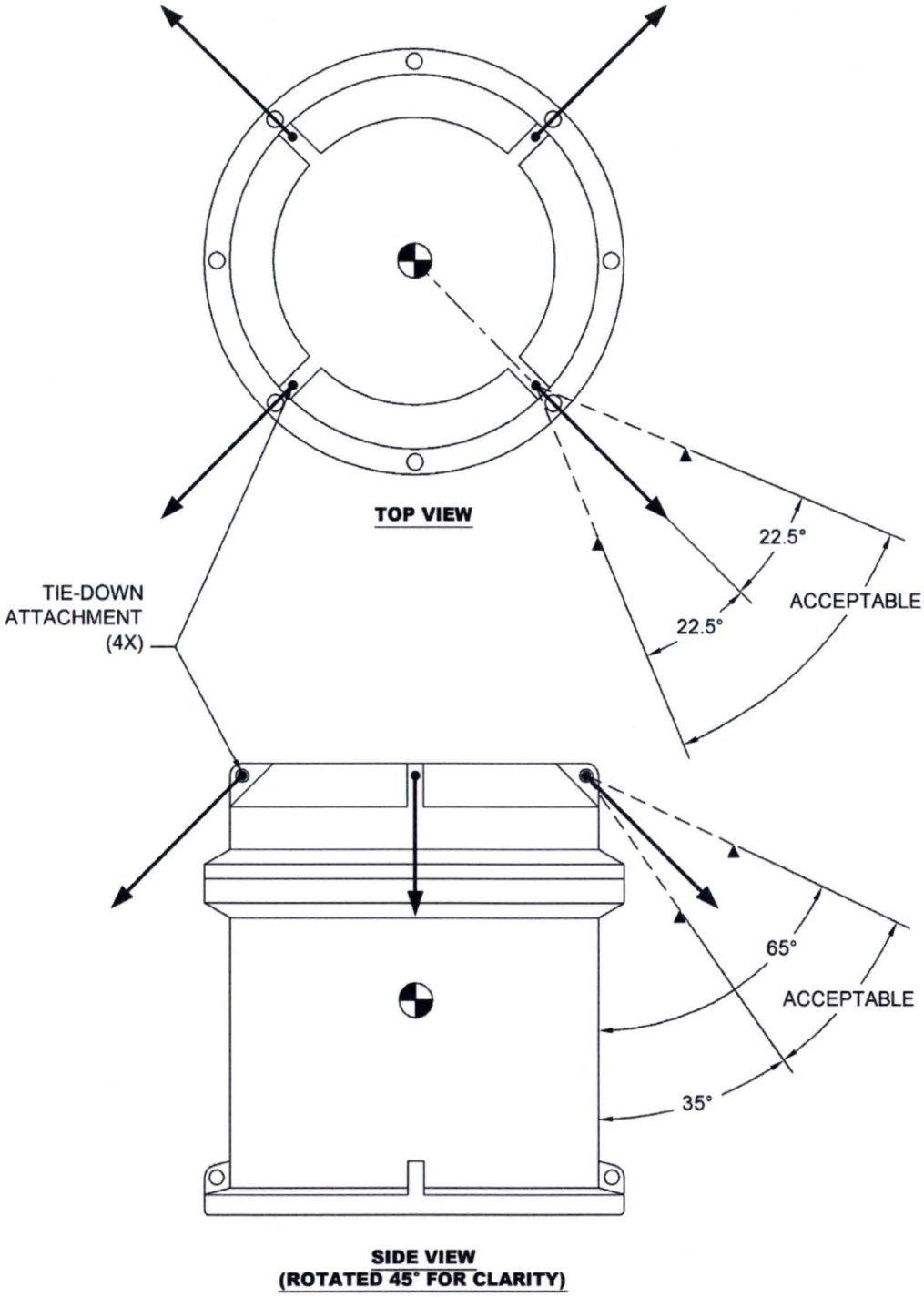

Figure 2-9 – Acceptable Package Tie-Down Configuration

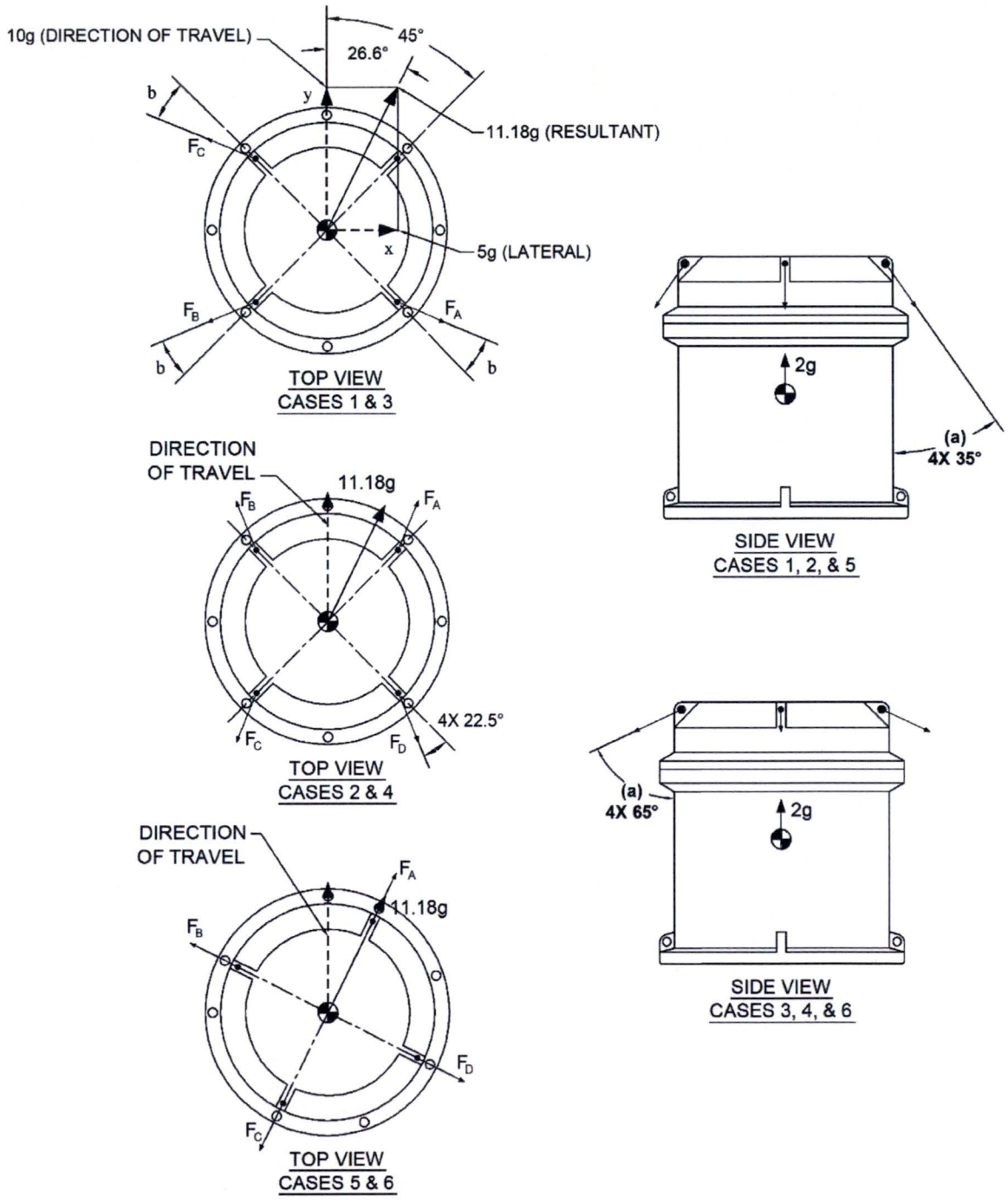

Figure 2-10 – Tie-Down Cases Evaluated

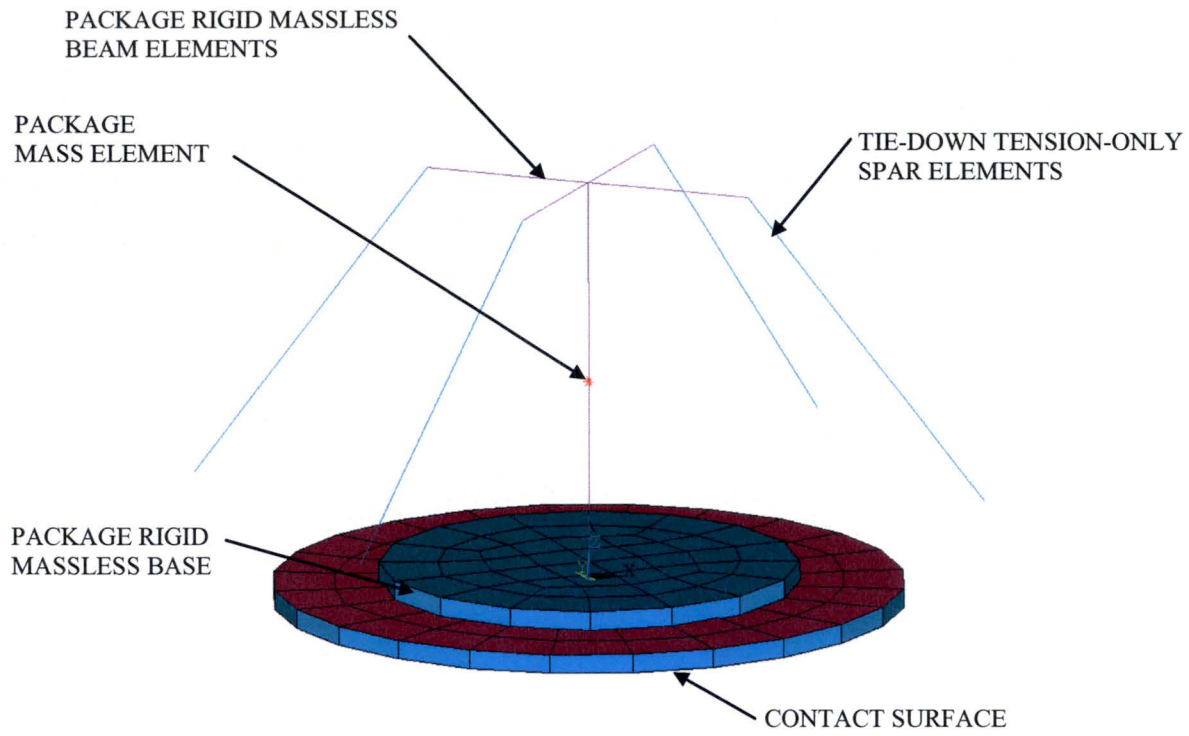

Figure 2-11 – MIDUS Package Tie-Down Finite Element Model

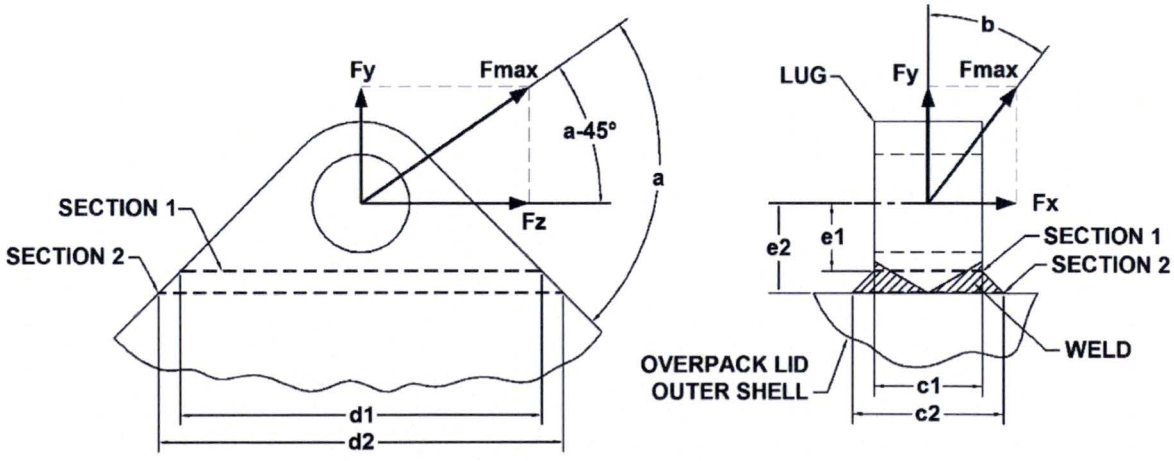

(Note: Lug rotated 45° for clarity)

Figure 2-12 – Overpack Lid Lug Weld Tie-Down Loading Diagram

2.6 Normal Conditions of Transport

This section presents the structural evaluation of the package that demonstrates compliance with the requirements of §71.43(f) and §71.51(a)(1) when subjected to the NCT tests specified in §71.71. The package is evaluated for each NCT test individually based on the most unfavorable initial conditions, including an ambient temperature between -29°C and +38°C and an internal pressure between zero and the MNOP. The structural evaluation shows that there would be no loss or dispersal of radioactive contents, no significant increase in external surface radiation levels, and no substantial reduction in the effectiveness of the packaging.

2.6.1 Heat

In accordance with §71.71(c)(1), the package is subjected to an ambient temperature of 38°C in still air and insolation. The cask maximum internal pressure and temperatures resulting from NCT heat conditions are summarized in Section 2.6.1.1. Differential thermal expansion between the various components of the package under NCT heat loading is evaluated in Section 2.6.1.2. The cask stresses due to NCT heat loading are evaluated in Section 2.6.1.3. The results of the NCT heat structural evaluation demonstrate that the cask satisfies the applicable structural design criteria.

2.6.1.1 Summary of Pressures and Temperatures

The maximum temperatures of the cask for NCT thermal conditions from Chapter 3 are summarized in Table 3-1. The maximum package temperatures result from the NCT hot thermal condition. The maximum temperature of the cask, not including the cask cavity gas or overpack, is 72°C. The allowable stress intensities used for the evaluation of the cask are conservatively based on an upper bound temperature of 74°C.

As discussed in Section 3.3.2, the maximum gauge pressure that would develop in the cask containment system in a period of one year under the heat conditions (MNOP) is less than 700 kPa. A bounding internal pressure of 700 kPa is used to perform the cask structural analysis for NCT.

2.6.1.2 Differential Thermal Expansion

Differential thermal expansion of the packaging components is evaluated considering possible interference resulting from a reduction in gap sizes. The differential thermal expansion evaluation includes radial and longitudinal differential thermal expansion between the cask assembly and the overpack cavity. In addition, radial and longitudinal differential thermal expansion between the cask body DU shield and shells is evaluated. The results of the evaluation of differential thermal expansion show that the cask expands freely within the overpack cavity under NCT thermal loading.

The package is designed with sufficient clearances between the overpack cavity and the outside surfaces of the cask and shield lid to permit free thermal expansion of the cask under NCT and

HAC. Nominal axial and radial clearances of 5 mm and 2.5 mm are provided between the overpack cavity and the outside surfaces of the cask and shield lid. The results of the NCT heat finite element analysis show that the maximum thermal expansion of the cask and shield lid is 0.20 mm in the longitudinal direction and 0.08 mm in the radial direction. Since the thermal expansion of the cask and shield lid is less than the nominal clearances provided, no interference will result from differential thermal expansion between the overpack and the cask and shield lid.

The cask body is designed with a nominal axial clearance of 0.7 mm between the DU bottom shield and the bottom end of the containment shell (i.e., below the cavity). The cask body design also provides nominal radial clearances of 0.65 mm and 0.35 mm on the inside radius and outside radius of the DU radial shield. Under NCT heat loading, differential thermal expansion caused by thermal gradients (i.e., the cask inner shell becomes hotter than the outer shell) and dissimilar materials (i.e., the coefficient of thermal expansion of DU is less than that of the stainless steel shells) causes a reduction in the clearances provided between the cask body DU and shells.

Differential thermal expansion between the cask body components is evaluated using the results of the finite element analysis described in Section 2.6.1.3. The clearances between the cask body DU and stainless steel shells under NCT heat loading are determined based on the minimum gap sizes of contact elements modeled between the adjacent surfaces. The results, which are summarized in Table 2-27, show that no interference will result from differential thermal expansion between the cask DU shield stainless steel shells under NCT heat loading. The amount of differential thermal expansion between the cask body DU shield and the adjacent cask shell components is small in comparison to the nominal design clearances.

2.6.1.3 Stress Calculations

The cask is designed to withstand the effects of heat loading in accordance with §71.71(c)(1). Per Table 2-1, heat loading is evaluated in combination with maximum decay heat, insolation, maximum internal pressure, and fabrication stresses.

The stresses in the cask body, closure lid, and shield lid due to the NCT heat loading are calculated using the axisymmetric finite element model shown in Figure 2-13. The model is comprised of a total of 2,012 nodes and 2,135 elements, representing all of the major structural and shielding components of the cask and shield lid. The model geometry is based on the nominal component dimensions. Design features such as fillets, chamfers, and bolt holes are not included in the model to simplify the finite element mesh.

All components of the packaging, with the exception of the closure bolts and O-rings, are modeled using 2-D structural solid axisymmetric elements. The closure bolts are modeled using 2-D spar elements. The closure-bolt element real constants are used to define the closure-bolt cross-section area and initial strain due to preload. The closure-bolt area is calculated based on the nominal bolt diameter of 10 mm. The containment O-ring, leak test O-ring, and cleanliness O-ring are all modeled using 3-D combination spring elements. The elastomeric O-ring linear spring stiffness constants are determined based on manufacturer's data for compressive loads versus percent compression and O-ring durometer over the range of compression permitted by

the O-ring groove design (i.e., up to approximately 25%). The nonlinear contact interface between the various components of the cask and shield lid are modeled using surface-to-surface contact elements. Figure 2-14 shows the surfaces on which contact elements are modeled.

All steel components of the cask and shield lid are modeled with a density of 8030 kg/m^3, Poisson's ratio of 0.3, and the temperature-dependent modulus of elasticity for Type 304/316 stainless steel from Table 2-12 and Table 2-13. The closure bolts are modeled with a density of 8030 kg/m^3, Poisson's ratio of 0.3, and the temperature-dependent modulus of elasticity for SA-320, Grade L43 bolting steel from Table 2-15. The DU shielding material in the cask body, shield plug, and shield lid is modeled with an elastic modulus of 172 MPa, an assumed Poisson's ratio of 0.3, and a mass density of 18,800 kg/m^3.

The cask body is restrained from longitudinal translation at a single node located on the bolting flange face at the bolt circle radius. In addition, coupled node sets are used to prevent rigid-body displacement of the cask body DU shields, shield plug DU shield, and the shield lid components. This is necessary for numerical stability since these components become unconstrained as differential thermal expansion between the cask stainless steel shells and DU shields creates gaps at the longitudinal contact surfaces.

The bounding NCT heat temperature gradient shown in Figure 2-15 is applied to the finite element model in combination with the internal pressure and maximum initial bolt preload. A bounding internal pressure load of 700 kPa gauge is applied to the inner surfaces of the cask containment boundary. The maximum bolt preload is 7.2 kN per bolt. The bolt preload is applied on a 360° basis as an initial strain in the cask closure bolt elements that produces a total preload (for eight closure bolts) of 57.8 kN on the closure lid.

The results of the NCT heat stress analysis show that the maximum total (P_m+P_b+Q) stress intensity in the cask due to NCT heat loading is 97 MPa, occurring at the center of the containment shell bottom plate (section C1 in Figure 2-1). This stress is due almost entirely to the internal pressure loading and not to the NCT heat temperature gradient. The maximum P_m+P_b+Q stress intensity in the cask containment system for NCT is limited to $3.0S_m$. The minimum value of S_m for the cask shell materials at a bounding design temperature of 74°C is 138 MPa. Therefore, the allowable P_m+P_b+Q stress intensity for the containment system is 414 MPa and the minimum design margin in the cask containment system due to NCT heat loading is +3.27.

The stresses in the cask closure bolts due to NCT heat loading are determined using the 3-D quarter-symmetry finite element model described in Section 2.5.1.2. The NCT hot temperature loading for the cask closure bolt analysis is applied as a uniform elevated temperature load of 68.3°C. This conservatively bounds the maximum temperature of the cask closure bolt for the NCT heat of 67°C. Elevated temperature produces differential thermal expansion between the closure bolts and closure lid, due to the differences in their material model coefficient of thermal expansion values, thereby causing thermal stress. Thermal stresses in the closure bolts due to closure plate through-thickness temperature gradients are not considered since these temperature gradients are very small and they create bolt-prying loads that oppose those due to internal pressure. Therefore, they are conservatively neglected. In combination with the NCT heat

loading, a maximum bolt preload of 7221 N is applied to each closure bolt and an internal pressure is applied as a uniform pressure load of 700 kPa on the inner surface of the closure plate over the entire area inside the containment O-ring.

The maximum average stress (i.e., axial stress) and maximum stress (i.e., axial plus bending stress) in the closure bolts due to NCT heat loading are 201 MPa and 209 MPa, respectively. The average axial stress due to internal pressure and gasket seating loads (i.e., bolt torque) must not exceed one times the tabulated values of S_m at the corresponding design temperature for NCT. The allowable maximum stress for NCT is limited to $3S_m$. The value of S_m for SA-320, Grade L43 bolting steel at a bounding closure bolt design temperature of 68.3°C is 234 MPa. Therefore, the allowable average stress and maximum stress are 234 MPa and 701 MPa, respectively. The maximum closure bolt stress ratios for NCT heat loading are 0.86 for average stress and 0.30 for maximum stress.

The results of the NCT heat structural evaluation demonstrate that the cask containment system satisfies the applicable NCT allowable stress design criteria. NCT heat loading does not cause any permanent deformation of the package, nor does it substantially reduce the effectiveness of the packaging. Furthermore, since the evaluation shows that the containment seal is maintained under NCT heat loading, there would be no loss or dispersal of radioactive contents. Finally, the configuration of the package under NCT heat loading is the same as that considered in the shielding evaluation. Therefore, NCT heat loading does not cause any significant increase in external surface radiation levels. The package thus complies with the requirements of §71.43(f) and §71.51(a)(1) when subjected to the NCT heat test specified in §71.71(c)(1).

2.6.1.4 Comparison with Allowable Stresses

The results of the NCT heat structural evaluation demonstrate that the cask containment system satisfies the applicable NCT allowable stress design criteria. The minimum design margins due to NCT heat loading are +0.16 for average tensile stress in the closure bolts and +3.27 primary plus secondary stress intensity in all other cask components. NCT heat loading does not cause any permanent deformation of the package, nor does it substantially reduce the effectiveness of the packaging. Furthermore, since the evaluation shows that the containment seal is maintained under NCT heat loading, there would be no loss or dispersal of radioactive contents. Finally, the configuration of the package under NCT heat loading is the same as that considered in the shielding evaluation. Therefore, NCT heat loading does not cause any significant increase in external surface radiation levels. Therefore, the package complies with the requirements of §71.43(f) and §71.51(a)(1) when subjected to the NCT heat test specified in §71.71(c)(1).

The structural evaluation of the package for reduced external pressure, increased external pressure, vibration normally incident to transport, and NCT free drop tests is discussed in the following sections. Each NCT test is evaluated in combination with the initial conditions expected to cause maximum package damage. The structural evaluation demonstrates that the package satisfies the applicable performance requirements specified in the regulations under all NCT tests. The evaluation of the cask for cyclic service under NCT, which is presented in Section 2.1.2.4, demonstrates that the package satisfies the applicable fatigue design criteria of the ASME Code.

Table 2-27 – Cask Body Differential Thermal Expansion Summary

Cask Body DU Shield Clearances	Nominal Design Clearance (mm)	Clearance Under NCT Heat Loading (mm)	Differential Thermal Expansion (mm)
Axial (Under Cavity)	0.70	0.54	-0.16
Outer Radius	0.35	0.36	+0.01
Inner Radius	0.65	0.63	-0.02

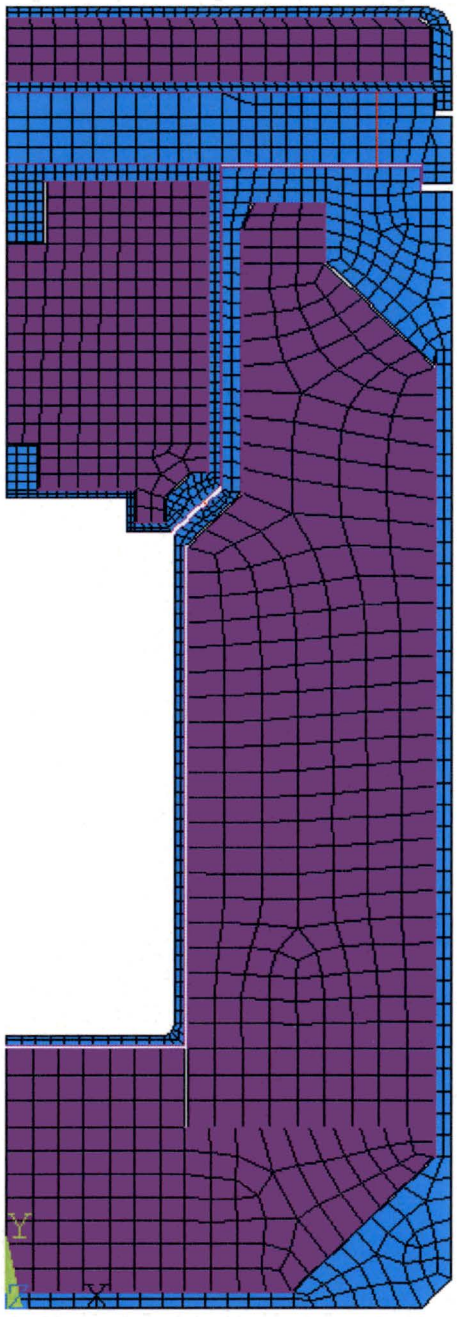

Figure 2-13 – MIDUS Cask Assembly Axisymmetric FE Model

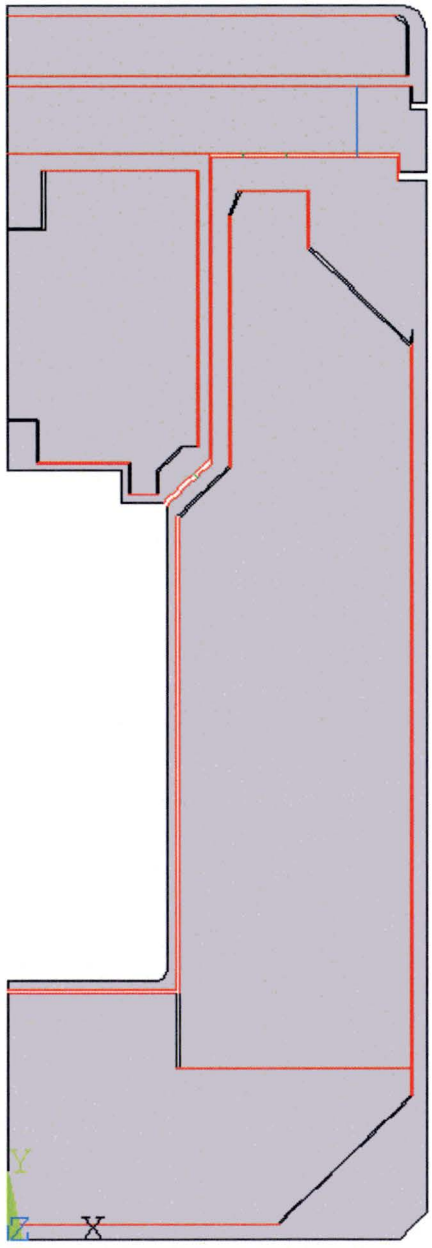

(Note: Contact surfaces shown in red)

Figure 2-14 – Axisymmetric FE Model Contact Surfaces

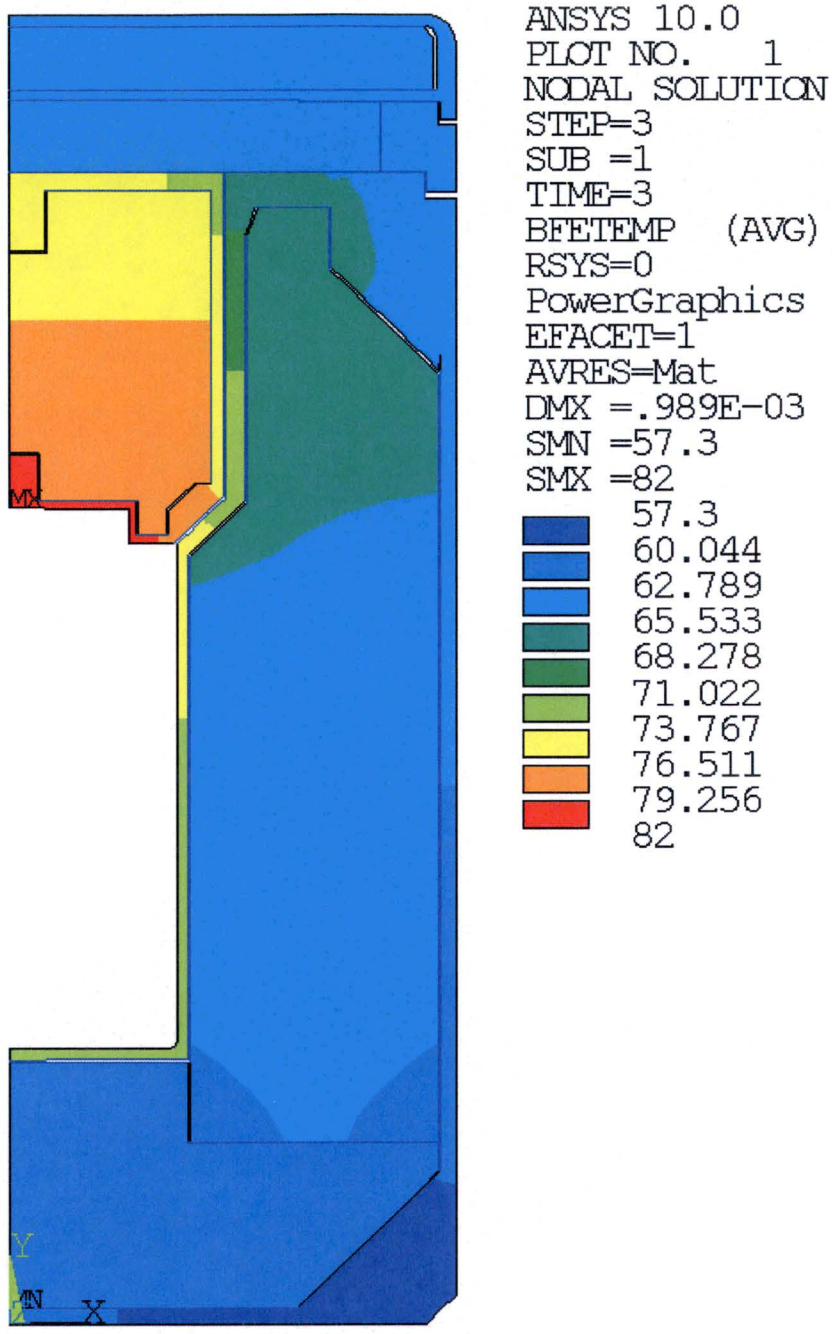

Figure 2-15 – Bounding NCT Heat Temperature Distribution

2.6.2 Cold

The cask is designed to withstand the effects of a steady-state ambient temperature of -40°C in still air and shade in accordance with §71.71(c)(2). Per Table 2-1, the NCT cold environment is evaluated in combination with zero insolation, zero decay heat, and zero internal pressure. The NCT cold environment with zero insolation and zero decay heat results in a uniform temperature of –40°C throughout the package. The cask body, shield plug, and shield lid all include DU shield cores that are encased in austenitic stainless steel. Because the coefficient of thermal expansion of austenitic stainless steel is higher than that of DU, reduced temperatures cause the stainless steel casing to contract more than the DU cores. The resulting differential thermal expansion produces thermal stress in the cask and shield lid.

The stresses in the cask body, closure lid, and shield lid due to the NCT cold loading are calculated using the axisymmetric finite element model described in Section 2.6.1.3. A uniform temperature of –40°C is applied to the finite element model in combination with the maximum initial bolt preload. The results of the NCT cold linear-elastic static analysis show that the highest stress intensities in the cask containment system and non-containment components are 26 MPa (at section C17 in Figure 2-1) and 60 MPa (at section N3 in Figure 2-2), respectively.

Per WB-3213.13, general thermal stress, neglecting stress concentrations, is classified as secondary stress (Q). The NCT allowable P_m+P_b+Q stress intensities for the cask containment system components at -40°C is 414 MPa and the minimum design margin in the cask containment system due to NCT cold loading is +14.9 (=414/26 - 1). Therefore, the cask satisfies the applicable NCT allowable stress design criteria under NCT cold conditions.

Evaluation of secondary stresses is not required for the cask non-containment components, which are designed in accordance with Subsection NF of the ASME Code. However, the maximum stress intensity in the cask non-containment components due to NCT cold loading is much less than the shell material minimum yield strength at -40°C of 207 MPa. Therefore, NCT cold loading will not cause any yielding of the cask non-containment components.

The stresses in the cask closure bolts due to NCT cold loading are determined using the 3-D quarter-symmetry finite element model described in Section 2.5.1.2. NCT cold loading is applied in combination with maximum internal pressure and minimum bolt preload to assure that the minimum bolt preload is sufficient to maintain the minimum required gasket load under the worst-case combination of loads. The combination of minimum bolt preload and NCT cold temperature loading produces the lowest possible value of non-prying tensile bolt force because temperature change associated with the NCT cold thermal condition produces differential thermal expansion between the closure bolts and closure lid that relaxes the initial bolt preload. (The maximum internal pressure loading produces the highest outward-acting non-prying tensile force on the closure bolts.) The NCT cold temperature loading is applied to the finite element model as a uniform temperature load of -40°C. The minimum bolt preload of 5,366 N is applied to each bolt, and a uniform pressure load of 700 kPa is applied on the inner surface of the closure plate over the area inside the containment O-ring.

The maximum average stress (i.e., axial stress) and maximum stress (i.e., axial plus bending stress) in the closure bolts due to NCT cold loading are 14 MPa and 39 MPa, respectively. The average axial stress due to internal pressure and gasket seating loads, i.e., bolt torque, is limited to one times the tabulated values of S_m at the corresponding design temperature for NCT. The allowable maximum stress for NCT is limited to $3S_m$. The value of S_m for SA-320, Grade L43 bolting steel at 68.3°C is 234 MPa based on linear interpolation of the S_m values shown in Table 2-15. Therefore, the allowable average stress and maximum stress are 234 MPa and 701 MPa, respectively. The corresponding minimum design margins in the closure bolt for NCT cold loading are +15.7 for average stress and +17.0 for maximum stress.

The maximum gap separation at the inside edge of the bolting flange due to the NCT cold loading is approximately 0.013 mm, or 1.5% of the O-ring compression. For the cask closure to maintain containment under these conditions, the elastomeric O-ring must have sufficient elasticity to expand to fill the gap, considering potential material degradation due to environmental effects such as radiation and temperature. This is satisfied provided that the maximum compression set does not exceed 98% (i.e., (0.88-0.013)/0.88). As shown in Section 3.9.14 of the Parker O-Ring Handbook [2.18], the compression set in ethylene propylene O-rings after exposure to 10^7 rads of gamma radiation at room temperature ranges from 28.6% to 46.6%, based on the compound. The data also shows that these materials will take on a compression set of less than 18% when exposed to a maximum temperature of 100°C for 70 hours ([2.18], Figure 2-13). This data suggests that the maximum O-ring compression set due to the combined effects of temperature and radiation will be sufficient to maintain a tight seal for the NCT cold loading.

The results of the NCT cold structural evaluation demonstrate that the cask containment system satisfies the applicable NCT allowable stress design criteria. NCT cold loading does not cause any permanent deformation of the package, nor does it substantially reduce the effectiveness of the packaging. Furthermore, since the evaluation shows that the containment seal is maintained under NCT cold loading, there would be no loss or dispersal of radioactive contents. Finally, the configuration of the package under NCT cold loading is the same as that considered in the shielding evaluation. Therefore, NCT cold loading does not cause any significant increase in external surface radiation levels. The package thus complies with the requirements of §71.43(f) and §71.51(a)(1) when subjected to the NCT cold test specified in §71.71(c)(2).

2.6.3 Reduced External Pressure

In accordance with §71.71(c)(3), the package is designed to withstand the effects of a reduced external pressure of 25 kPa absolute. Per Table 2-1, reduced external pressure loading is considered in combination with maximum internal pressure, and NCT hot thermal loading (i.e., 38°C ambient temperature, maximum decay heat, and maximum insolation). Under these conditions, the maximum internal pressure is less than 700 kPa. Therefore, the greatest pressure difference between the inside and outside of the containment system is 775 kPa.

The stresses in the cask due to reduced external pressure loading are determined using the axisymmetric finite element model described in Section 2.6.1.3. A bounding internal pressure

load of 795 kPa is applied in combination with maximum bolt preload and NCT heat temperature loading. The stresses in the cask are calculated assuming linear-elastic static behavior.

The maximum stress intensities in the cask containment system and non-containment components are summarized in Table 2-28, along with the corresponding allowable stress intensities and minimum design margins. The results show that the maximum stress intensities in the cask due to reduced external pressure loading are lower than the corresponding allowable stress intensities. The minimum design margin for reduced external pressure loading is +0.88 for primary membrane plus bending stress intensity (P_m+P_b) at the center of the cask containment shell bottom plate (section C1 in Figure 2-1).

The results of the NCT reduced external pressure structural evaluation demonstrate that the cask containment system satisfies the applicable NCT allowable stress design criteria. Reduced external pressure loading does not cause any permanent deformation of the package, substantially reduce the effectiveness of the packaging, result in any loss or dispersal of radioactive contents, or cause any significant increase in external surface radiation levels. Therefore, the package complies with the requirements of §71.43(f) and §71.51(a)(1) when subjected to the NCT reduced external pressure test specified in §71.71(c)(3).

Table 2-28 – Reduced External Pressure Stress Summary

Cask System	Stress Type	Maximum Stress Intensity (MPa)	Stress Location[1]	Allowable Stress Intensity[2] (MPa)	Minimum Design Margin[3]
Containment System	P_m	25	C4	138	+4.52
	P_m+P_b	110	C1	207	+0.88
	P_m+P_b+Q	110	C1	414	+2.76
Non-Containment Components	P_m	31	N11	138	+3.45
	P_m+P_b	85	N7	207	+1.44
	P_m+P_b+Q	91	N7	N/A[4]	N/A[4]

Notes:

1. Containment system and non-containment component stress locations are shown in Figure 2-1 and Figure 2-2, respectively.
2. Allowable stresses are based on the lower-bound strength properties of all cask shell material alternatives at an upper-bound design temperature of 74°C.
3. Design margin is calculated as (Allowable S.I./Maximum S.I) – 1.
4. Evaluation of secondary stress is not required for non-containment components.

2.6.4 Increased External Pressure

In accordance with §71.71(c)(4), the package is designed to withstand the effects of an increased external pressure of 140 kPa absolute. Per Table 2-1, increased external pressure loading is considered in combination with an ambient temperature of -29°C, zero decay heat, and zero insolation, minimum internal pressure, and fabrication stresses. The minimum internal pressure for the cask is zero. Therefore, under these conditions the greatest pressure difference between the inside and outside of the containment system is 140 kPa gauge.

The stresses in the cask due to increased external pressure loading are determined using the axisymmetric finite element model described in Section 2.6.1.3. An external pressure load of 140 kPa is applied to the outside of the cask containment system, conservatively taking no credit for any pressure-retaining ability of the cask outer shell. In addition, the maximum bolt preload and NCT cold temperature loading (i.e., a uniform temperature of -29°C) are applied to the model. The stresses in the cask for increased external pressure loading are calculated assuming linear-elastic static behavior.

The maximum stress intensities in the cask assembly containment system and non-containment components for increased external pressure loading are summarized in Table 2-29, along with the corresponding allowable stress intensities and minimum design margins. The results show that the maximum stress intensities in the cask due to increased external pressure loading are lower than the corresponding allowable stress intensities. The minimum design margin for increased external pressure loading is +3.31 for primary membrane plus bending stress intensity (P_m+P_b) in the cask outer shell (section N3). Furthermore, since all of the stresses in the cask are below the material yield strength, no plastic deformation occurs under increased external pressure loading.

Buckling of the containment shell for the increased external pressure loading is evaluated in accordance with ASME Code Case N-284-1 [2.7]. A factor of safety of 2.0 against buckling is used for NCT in accordance with the requirements of ASME Code Case N-284-1. The results of the increased external pressure stress analysis for the cask show that only the cask containment shell is loaded in compression. The outer shell is loaded in tension due to thermal stresses arising from differential thermal expansion between the cask body DU and the stainless steel outer shell at reduced temperatures. The axial and hoop compressive stresses in the cask containment shell due to increased external pressure loading are 1,296 kPa and 2,524 kPa, respectively. The corresponding maximum buckling interaction ratio is 0.03. The cask containment shell satisfies the buckling design criteria of Code Case N-284-1 for increased external pressure loading because the maximum buckling interaction ratio does not exceed 1.0.

The results of the NCT increased external pressure structural evaluation demonstrate that the cask containment system satisfies the applicable NCT allowable stress design criteria. NCT increased external pressure loading does not cause any permanent deformation of the package, nor does it substantially reduce the effectiveness of the packaging. Increased external pressure loading will not result in any loss or dispersal of radioactive contents. Finally, the configuration of the package under NCT increased external pressure loading is the same as that considered in

the shielding evaluation. Therefore, NCT increased external pressure loading does not cause any significant increase in external surface radiation levels. The package thus complies with the requirements of §71.43(f) and §71.51(a)(1) when subjected to the NCT increased external pressure test specified in §71.71(c)(4).

Table 2-29 – Increased External Pressure Stress Summary

Cask System	Stress Type	Maximum Stress Intensity (MPa)	Stress Location[1]	Allowable Stress Intensity[2] (MPa)	Minimum Design Margin[3]
Containment System	P_m	14	C17	138	+8.86
	P_m+P_b	20	C17	207	+9.35
	P_m+P_b+Q	20	C17	414	+19.7
Non-Containment Components	P_m	29	N3	138	+3.76
	P_m+P_b	48	N3	207	+3.31
	P_m+P_b+Q	48	N3	N/A[4]	N/A[4]

Notes:
1. Containment system and non-containment component stress locations are shown in Figure 2-1 and Figure 2-2, respectively.
2. Allowable stresses are based on the lower-bound strength properties of all cask shell material alternatives at an upper-bound design temperature of 74°C.
3. Design margin is calculated as (Allowable S.I./Maximum S.I) – 1.
4. Evaluation of secondary stress is not required for non-containment components.

2.6.5 Vibration

In accordance with §71.71(c)(5), the package is subjected to vibration normally incident to transport. The package is transported by truck and air in a vertical orientation. The package is supported by the bottom end of the overpack base and tied down by the four lugs on the overpack lid. Table 2 of ANSI N14.23 [2.23] shows peak vibration accelerations of a trailer bed as a function of the package and tie-down system natural frequency. The maximum peak accelerations (99% level) for light packages (< 15 tons) are 2.0*g* in the vertical direction, 1.3*g* in the longitudinal direction, and 0.5*g* lateral. To provide a conservative, yet simple analysis, the longitudinal and transverse vibration loads are neglected and a bounding ±10*g* vertical acceleration load is used for the cask vibration stress evaluation. This load is expected to bound the vibration loads resulting from both truck and air transport.

The stresses in the cask and shield lid resulting from a 10*g* NCT vibration load are determined using the axisymmetric finite element model described in Section 2.6.1.3. The applied loading for the NCT vibration consist of a 10*g* equivalent-static acceleration load to account for the inertial load of the modeled components, a pressure load to account for the payload, and a reaction pressure load for static equilibrium. The load on the cask cavity due to the payload is conservatively modeled as a uniformly distributed pressure over the cavity bottom end. The magnitude of the payload pressure load is modeled as 22.0 kPa based on an upper-bound payload mass of 1.1 kg and a cavity bottom-end surface area of 4,902 mm^2. The NCT vibration reaction load is modeled as a uniformly distributed pressure load on the bottom end of the cask assembly. The magnitude of the reaction pressure load is modeled as 574.5 kPa based on the modeled combined mass of the cask and shield lid of 202.6 kg and a cask bottom-end surface area of 34,636 mm^2.

The maximum bolt preload of 7.2 kN per bolt is applied to the model on a 360° basis, producing a total preload (for eight closure bolts) of 57.8 kN on the closure lid. A uniform temperature of 75°C, which bounds the maximum cask temperature under the NCT heat thermal condition, is also applied to the model.

A linear-elastic static analysis is performed for NCT vibration loading. The membrane, membrane plus bending, and total stress intensity at each of the stress evaluation locations shown in Figure 2-1 and Figure 2-2 are evaluated for NCT vibration loading. The maximum stress intensities in the cask containment system and non-containment components due to NCT vibration loading are summarized in Table 2-30, along with the corresponding allowable stress intensities and minimum design margins. The results show that the maximum stress intensities in the cask due to NCT vibration loading are lower than the corresponding allowable stress intensities. The minimum design margin for NCT vibration loading is +19.7 for primary membrane plus bending stress intensity (P_m+P_b). Therefore, the cask and shield lid satisfy the applicable NCT allowable stress design criteria for the NCT vibration.

A detailed stress analysis of the cask closure bolts for NCT vibration loading is performed using the 3-D quarter-symmetry finite element model described in Section 2.5.1.2. A 10*g* acceleration load is applied to the model to account for the inertia load from the closure lid. In addition, a

uniform pressure load is applied to the underside of the closure lid to account for the loading from the combined mass of the shield plug and payload. For modeling simplicity, a uniform pressure load is applied over the entire area inside the containment O-ring diameter. Although the O-ring diameter upon which the pressure load is calculated is approximately 18% larger than the outside diameter of the shield plug, it does not significantly affect the solution results. In fact, the assumption of a uniform pressure distribution is conservative; the load from the shield plug will concentrate at its outer edge because the shield plug is relatively stiff compared to the closure plate. Thus, the prying moment resulting from the assumed uniform pressure load distribution is conservative.

NCT vibration loading is applied in combination with NCT heat temperature loading, maximum internal pressure, and maximum bolt preload. The NCT heat temperature loading is applied to the finite element model as a uniform temperature load of 68.3°C. The maximum bolt preload of 7.2 kN is applied to each bolt and a uniform pressure load of 700 kPa is applied on the inner surface of the closure plate over the area inside the containment O-ring.

The maximum average stress (i.e., axial stress) and maximum stress (i.e., axial plus bending stress) in the closure bolts due to NCT vibration loading are 201 MPa and 210 MPa, respectively. The average axial stress and maximum stress are limited to $2S_m$ and $3S_m$, respectively. The value of S_m for SA-320, Grade L43 bolting steel at 68.3°C is 234 MPa based on linear interpolation of the S_m values shown in Table 2-15. Therefore, the allowable average stress and maximum stress are 468 MPa and 701 MPa, respectively. The corresponding minimum design margins in the closure bolt for NCT vibration loading are +1.33 for average stress and +2.34 for maximum stress.

The results of the NCT vibration structural evaluation demonstrate that the cask satisfies the applicable NCT allowable stress design criteria. NCT vibration loading does not cause any permanent deformation of the package, nor does it substantially reduce the effectiveness of the packaging. Furthermore, the evaluation shows that NCT vibration loading does not result in any significant lid separation. Thus, under NCT vibration loading, the containment seal is maintained, and no loss or dispersal of radioactive contents occurs. Finally, the configuration of the package under NCT vibration loading is the same as that considered in the shielding evaluation. Therefore, NCT vibration loading does not cause any significant increase in external surface radiation levels. The package thus complies with the requirements of §71.43(f) and §71.51(a)(1) when subjected to the NCT vibration test specified in §71.71(c)(5).

Table 2-30 – Cask Stress Summary, NCT Vibration

Cask System	Stress Type	Maximum Stress Intensity (MPa)	Stress Location[1]	Allowable Stress Intensity[2] (MPa)	Minimum Design Margin[3]
Containment System	P_m	5	C16	138	+26.6
	P_m+P_b	10	C13	207	+19.7
	P_m+P_b+Q	11	C20	414	+36.6
Non-Containment Components	P_m	4	N13	138	+33.5
	P_m+P_b	4	N13	207	+50.8
	P_m+P_b+Q	5	N13	N/A[4]	N/A[4]

Notes:
1. Containment system and non-containment component stress locations are shown in Figure 2-1 and Figure 2-2, respectively.
2. Allowable stresses are based on the lower-bound strength properties of all cask shell material alternatives at an upper-bound design temperature of 74°C.
3. Design margin is calculated as (Allowable S.I./Maximum S.I) – 1.
4. Evaluation of secondary stress is not required for non-containment components.

2.6.6 Water Spray

In accordance with the requirements of §71.71(c)(6), the package must be subjected to a water spray that simulates exposure to rainfall of approximately 5 cm/h for at least 1 hour. Quenching effects due to the water spray test will not significantly affect the package. The cask assembly is isolated from the quenching effects of the water spray by the overpack assembly, which insulates the cask from sudden environmental changes. Furthermore, the thermal mass of the cask is large enough to significantly slow the thermal response to sudden external temperature changes. Therefore, this condition is not significant in the structural design of the cask and is not analyzed.

2.6.7 Free Drop

In accordance with §71.71(c)(7), the package, which weighs less than 5,000 kg, is subjected to a free drop through a distance of 1.2 m "*onto a flat, essentially unyielding, horizontal surface, striking in a position for which maximum damage is expected.*" The package is evaluated for seven different NCT free drop orientations, as shown in Figure 2-16. They include a bottom end drop, top end drop, bottom corner drop, top corner drop, horizontal side drop, bottom end oblique drop, and top end oblique drop. For the oblique drop impacts, a primary impact angle of 5° from horizontal is assumed (i.e., 85° for the bottom oblique impact and 95° for the top oblique impact) because it is expected to result in the worst-case NCT free drop secondary (slapdown) impact loads.

The dynamic response of the package to the NCT free drop test conditions is determined using explicit dynamic finite element analysis methods. The ANSYS LS-DYNA PC computer code, which is described in Section 2.12.2.2, is used for this analysis. The explicit dynamic finite element analysis of the package is used to predict the rigid-body response of the cask to each NCT free drop test. In addition, this analysis demonstrates the structural adequacy of the overpack assembly for the NCT free drop tests. The maximum stresses in the overpack closure bolts are shown to satisfy the applicable allowable stress design criteria of Subsection NF of the ASME Code. Furthermore, the maximum crush depth of the overpack polyurethane foam due to each NCT free drop is much less than the allowable crush depth. The drop loads analysis of the package is discussed further in Section 2.6.7.1.

A detailed stress analysis of the cask and shield lid is performed using linear-elastic static finite element analysis methods. The ANSYS Mechanical computer program, which is described in Section 2.12.2.1, is used for this analysis. Bounding equivalent-static acceleration design loads are applied to the cask finite element model for each NCT free drop orientation. The bounding equivalent-static acceleration design loads are determined by multiplying the cask peak rigid-body accelerations determined in Section 2.6.7.1 by dynamic load factors (DLFs) to account for possible dynamic amplification within the cask. The maximum stresses in the cask and shield lid due to each NCT free drop are calculated and shown to satisfy the applicable allowable stress design criteria of Subsections NF [2.2] and WB [2.1] of the ASME Code. In addition, the compressive stresses in the cask cylindrical shells due to each NCT free drop are evaluated in accordance with ASME Code Case N-284-1 [2.7] and shown to satisfy the

applicable buckling design criteria. The cask NCT free drop stress analysis and buckling analysis are discussed further in Sections 2.6.7.2 and 2.6.7.3, respectively.

The worst-case initial conditions are considered in accordance with §71.71(b) and Regulatory Guide 7.8 [2.5]. For the overpack analysis, which determines the cask rigid-body acceleration time-history response and evaluates the structural adequacy of the overpack components, the "cold" thermal condition (i.e., an ambient temperature of -29°C with zero decay heat and no insolation) is the worst case since it results in the lowest package temperatures, the highest crush strength of the overpack foam, and the highest cask acceleration loads. The "hot" thermal condition (i.e., an ambient temperature of 38°C with maximum decay heat and insolation), for which the package temperatures are highest and the foam crush strength is lowest, are not considered in the NCT free drop impact analysis since the cask accelerations will be bounded by those under "cold" thermal conditions and because there is no potential for the cask to "bottom-out" due to NCT free drop impacts.

For the cask NCT free drop stress evaluation, initial conditions include both "hot" and "cold" thermal conditions. However, the maximum cask accelerations calculated for the "cold" thermal conditions are conservatively used for all cask NCT free drop stress analyses. Furthermore, lower-bound allowable stresses are used for the cask NCT free drop stress evaluation, which are conservatively based on a design temperature that bounds the peak cask temperature under the "hot" thermal conditions. Further discussion of the load combinations considered in the stress evaluation is provided in Section 2.6.7.2.

The results of the NCT free drop structural evaluation demonstrate that the cask satisfies the applicable NCT allowable stress design criteria. NCT free drop loading does not cause any significant permanent deformation of the package, nor does it substantially reduce the effectiveness of the packaging. Furthermore, since the evaluation shows that the containment seal is maintained under NCT free drop loading, there would be no loss or dispersal of radioactive contents. Finally, the configuration of the package under NCT free drop loading is the same as that considered in the shielding evaluation. Therefore, NCT free drop loading does not cause any significant increase in external surface radiation levels. The package thus complies with the requirements of §71.43(f) and §71.51(a)(1) when subjected to the NCT free drop test specified in §71.71(c)(7).

2.6.7.1 Overpack Evaluation

The structural evaluation of the overpack for the NCT free drop test is performed using the ANSYS LS-DYNA PC finite element code and the 3-D half-symmetry finite element model shown in Figure 2-17. The finite element model, which consists of 27,973 elements and 36,382 nodes (not including the impact target), includes detailed representations of the overpack base, overpack lid, and the overpack closure bolts. All components are modeled based on the nominal design dimensions. Minor design features that do not affect the structural response of the package, such as small fillet radii on the overpack shells, thermal relief plug holes, drain holes, tamper-indicating feature holes, and foam pour hole covers, are not included in the model.

The exterior components of the overpack base and lid are all modeled using explicit 3-D structural solid elements, whereas the inner shells are modeled using explicit 4-node shell elements. Shell-to-solid constraints are used to "tie" the edge of the inner shell element nodes to the outer shell solid element nodes at the interfaces. The overpack inner and outer shells are modeled using a piecewise-linear plasticity material model, as discussed in Section 2.2.1.1. For the NCT free drop, the upper-bound stress-strain design curve shown in Figure 2-4 is conservatively used.

The overpack base and lid foam cores are modeled using explicit 3-D structural solid elements with a crushable foam material model. The foam stress-strain curves are developed as described in Section 2.2.1.3, considering foam crush strength tolerance, temperature effects, and dynamic (strain-rate) effects. The overpack analyses for all NCT free drop tests are conservatively performed using the upper-bound foam stress-strain curve shown in Figure 2-5.

The thermal spider, which connects the overpack base outer shell to the overpack base inner bottom plate, is also included in the model. Each leg of the thermal spider is modeled using explicit 3-D beam elements. The inside end of each leg is connected to the bottom corner of the overpack base inner shell and the outer end of the leg is connected to the inside of the overpack base outer shell. The thermal spider beam elements are modeled using the upper-bound bilinear kinematic material model for copper described in Section 2.2.1.4.

The overpack closure bolts are modeled using explicit 3-D beam elements, which support axial, shear, and bending loads. The bolt element cross-section properties are based on the overpack closure bolt nominal diameter. The cross-section properties of the bolts located on the half-symmetry plane are equivalent to that of the bolt half-circle. The bolts are modeled using the bilinear kinematic material model for A320, Grade L43 bolting steel, as described in Section 2.2.1.1. Each bolt is modeled using two elements: one spanning the length of thread engagement in the overpack base flange, and the other spanning from the top of the threads to the node located at the base of the bolt head.

The cask and shield lid are modeled using explicit 4-node shell elements. For the purpose of the drop loads analysis, these assemblies are treated as a single rigid-body having an outside diameter of 225.0 mm and a total height of 347.0 mm. The rigid-body is also modeled with a 7.5 mm by 45° chamfer on the bottom corner and a 7.5 mm radius on the top corner. The mass properties of the cask/shield lid rigid-body are defined by its mass, center of gravity, and a mass moment of inertia. The center of gravity of the cask/shield lid rigid-body is located on its centerline at a distance of 262 mm from the bottom end of the overpack assembly. The mass moment of inertia of the cask/shield lid rigid-body is defined relative to its local center of gravity. For the NCT free drop evaluation, the cask/shield lid rigid-body is modeled using lower-bound mass and mass moment of inertia, which results in upper-bound cask accelerations. The lower-bound mass properties of the cask and shield lid rigid-body are 2.5% lower than the nominal mass properties shown in Table 2-8.

The nonlinear contact between the various components of the package finite element model are modeled using the surface-to-surface contact type. All of the package contact surfaces are modeled without friction for the NCT free drop analyses. The results of a sensitivity study shows

that the frictionless surface contact assumption produces bounding results for the package response, including higher peak cask rigid-body accelerations, higher overpack sidewall foam crush, and higher overpack bolt stresses. Therefore, the frictionless surface contact assumed for the free drop analyses is conservative and bounding.

Each NCT free drop time-history analyses is started at the moment of initial contact between the package outer surface and the impact surface. An initial vertical velocity of 4.85 m/s, corresponding to a free-fall velocity from a height of 1.2 m, is applied to the package in all cases. In addition, a constant gravitational acceleration of 9.81 m/s^2 is applied to the model. For stable drop orientations (i.e., end, side, and corner drops), the duration of the time-history analysis is sufficient to capture the primary impact. The durations of the time-history analysis for the oblique drop impacts are sufficient to capture both the primary and secondary (slapdown) impacts.

The maximum rigid-body accelerations resulting from each NCT free drop test are summarized in Table 2-31. The results show that the highest longitudinal cask acceleration (262*g*) results from the NCT bottom end drop and the highest transverse cask acceleration (-573*g*) results from the NCT bottom oblique drop. Table 2-31 also summarizes the maximum foam crush, as a percentage of the total foam thickness, that results from each NCT free drop test. The maximum overpack foam crush for NCT free drop of 15% is much lower than the general limit of 70%.

The maximum axial stress, shear stress, and combined stress (i.e., interaction ratio) in the overpack closure bolts for each NCT free drop test are evaluated in accordance with the Service Level A allowable stress design criteria for Class 2 supports from Subsection NF [2.2] of the ASME Code. The overpack closure bolt maximum axial stress, shear stress, stress interaction ratio, and minimum design margins resulting from each NCT free drop test are summarized in Table 2-32. The minimum design margin in the overpack closure bolts is +0.35 due to the maximum axial bolt stress resulting from the NCT bottom oblique drop. Thus, the overpack closure bolts satisfy the applicable allowable stress design criteria for the NCT free drop.

The overpack damage resulting from the NCT free drop is minimal and will not affect the ability of the package to withstand the HAC tests required by §71.73. The most noticeable overpack damage for all NCT free drop cases evaluated results from the NCT top-corner drop. As shown in Figure 2-18, the extent of damage to the overpack resulting from the NCT top-corner drop is limited to the impacted overpack lid lug and the outer shell adjacent to the lug. In this case, the overpack lid outer shell at the base of the lug is permanently deformed inward by less than 15 mm. Although slightly more overpack damage results from the "hot" thermal condition with lower-bound material strength properties, this damage does not affect the ability of the package to withstand the HAC tests required by §71.73.

2.6.7.2 Cask Stress Evaluation

The stresses in the cask and shield lid due to NCT free drop loading are determined using finite element analysis methods. Equivalent-static linear-elastic analyses are performed for those NCT free drop orientations expected to cause maximum damage to the package. The equivalent-static acceleration loads for each NCT free drop orientation are equal to the peak rigid-body

accelerations of the cask multiplied by a DLF that accounts for possible dynamic amplification within the cask. As discussed in Section 2.12.3, upper-bound DLFs are conservatively applied to all NCT free drop longitudinal and transverse rigid-body accelerations, respectively. Table 2-33 provides a summary of the equivalent-static acceleration loads used for the structural evaluation of each NCT free drop orientation.

In accordance with Regulatory Guide 7.8 [2.5], NCT free drop loads are evaluated in combination with internal pressure, thermal, and fabrication stresses. As discussed in Section 2.6.1.1, a bounding internal design pressure of 700 kPa gauge is conservatively used for the structural evaluation of the cask. NCT cold and NCT hot thermal loadings are considered in combination with NCT free drop loading. The only significant fabrication stresses in the cask are those resulting from closure bolt preload. Therefore, the following load combinations are considered for each NCT free drop load orientation evaluated:

(A) NCT Free Drop + Bolt Preload

(B) NCT Free Drop + Bolt Preload + Maximum Internal Pressure

(C) NCT Free Drop + Bolt Preload + Max. Internal Pressure + NCT Heat[1]

(D) NCT Free Drop + Bolt Preload + NCT Cold[1]

Thermally induced stress intensities are classified as secondary in accordance with the ASME Code since they are self-limiting. Therefore, the stress intensities obtained from load combinations C and D are compared to the stress limits for primary plus secondary (P_m+P_b+Q) stress intensity.

The stress analyses for the NCT end drops are performed using the axisymmetric finite element model described in Section 2.6.1.3. For all other NCT free drop analysis, the stresses are calculated using the 3-D half-symmetry finite element model shown in Figure 2-19. The 3-D half-symmetry finite element model, which has the same basic cross-section geometry as the axisymmetric finite element model described in Section 2.6.1.3, is comprised of a total of 35,248 nodes and 35,504 elements, representing all of the major structural and shielding components of the cask and shield lid. With the exception of the closure bolts and O-rings, the model is constructed entirely of 3-D structural solid elements. The closure bolts are modeled using 3-D elastic beam elements with no credit taken for the bolt bending stiffness. The closure bolt element real constants are used to define the closure bolt cross-section properties and initial strain due to preload. The closure bolt area is calculated based on the nominal bolt diameter of 10 mm.

[1] Load combinations including NCT heat and NCT cold temperature loading are not evaluated for the NCT side, corner, and oblique drops. The results of the NCT end drop analyses show that these temperature loads do not cause any significant increase in the cask's maximum stress intensities.

The containment O-ring, leak test O-ring, and cleanliness O-ring are all modeled using a series of 3-D node-to-node gap elements in the 3-D half-symmetry finite element model. These O-ring gap elements transfer only compressive loads across the O-ring interface. Each O-ring gap element's contact stiffness is calculated based its tributary width (circumference) and the O-ring spring stiffness constants that are determined based on the manufacturer's data for O-ring compressive loads versus percent compression. The O-ring gap elements located on the symmetry plane have half the contact stiffness of those not located on the symmetry plane. Since the shield plug and closure lid are modeled at the initial positions of contact with the O-rings, the O-ring gap elements are all modeled as initially closed.

In the 3-D half-symmetry finite element model, the nonlinear contact interface between the various components of the cask components are modeled using 3-D surface-to-surface contact elements. Contacts are modeled on the same surfaces shown in Figure 2-14 and revolved around the circumference. Additional contact surfaces are modeled on the shield lid shear lip and between the outer diameter of the shield lid DU and the inner diameter of the shield lid casing side plate.

The material properties modeled in the 3-D half-symmetry finite element model are the same as those used for the cask axisymmetric finite element model, as described in Section 2.6.1.3.

The applied loading for each NCT free drop analysis consists of the equivalent-static acceleration design loads from Table 2-33, which account for the inertial load of the modeled components, pressure-loading to account for the payload mass, and reaction pressure-loads for static equilibrium. As shown in Table 2-33, the magnitude of the transverse acceleration varies along the length of the cask for the NCT side and oblique drop impacts. The axially-varying transverse acceleration loads are modeled by applying a uniform transverse acceleration load, equal to the average of the accelerations at the top and bottom ends of the cask, and a rotational acceleration around the mid-length of the cask.

The longitudinal loading on the cask cavity from the payload mass is applied as a uniformly distributed pressure on the end of the cask cavity nearest the impacted end of the package for the NCT end, corner, and oblique drops. The magnitude of the longitudinal payload pressure load is calculated based on the longitudinal equivalent-static acceleration design load from Table 2-33, a maximum payload mass of 1.1 kg, and the area of the surface over which the load is applied. The longitudinal reaction loads for the NCT end, corner, and oblique drops are modeled as uniformly distributed pressure loads on the impacted end of the cask. The magnitude of the longitudinal reaction pressure loads are calculated based on the longitudinal equivalent-static acceleration design loads from Table 2-33, a total cask and shield lid mass of 202.3 kg, and an end-surface area of 34,636 mm^2.

The transverse loading from the cask payload for the NCT side, corner, and oblique drops is applied as an axially-uniform pressure load on the impacted side of the cask cavity. The applied transverse pressure loads are calculated assuming a cosine distribution around the circumference as follows:

$$p = p_o \cos(90\theta/\theta_o),$$

where p_o is the maximum pressure amplitude based on the included mass and the transverse equivalent-static acceleration load at the payload center of gravity, θ is the angle from the point of maximum pressure, and θ_o is the half-angle over which the pressure load is applied (assumed to be 45°).

The transverse reaction loads on the cask closure lid and shield lid are applied as pressure loads on the impacted side of the cask. The reaction pressure loads are assumed to be uniformly distributed over the length and have a cosine distribution over a 45° half-angle of the circumference. The reaction pressures are calculated in the same manner as the payload inertia pressure loads, as discussed above.

The transverse reaction loads on the cask body are also applied as pressure loads on the impacted side of the cask. The pressure load is applied with a cosine distribution over a 45° half-angle of the circumference. For the NCT corner drops, the magnitude of the cask body reaction pressure is uniform along the length of the cask body. For the NCT side and oblique drops, the reaction pressure loading on the cask body is applied as a series of stepped uniform pressure loads over six axial zones. The axial distribution of the pressure loading is determined such that it balances the applied inertia loads due to the applied transverse and angular acceleration loads. The net transverse load on each axial zone is determined based on the principle of static equilibrium.

For all NCT free drop analyses, the maximum bolt preload of 7.2 kN per bolt is applied to the model. For the NCT end drop analyses, the bolt preload is applied on a 360° basis resulting in a total preload (for eight closure bolts) of 57.8 kN on the closure lid. For all other NCT free drop analyses, a bolt preload of 7.2 kN is applied to each individual bolt element (3.6 N for the bolts on the half-symmetry plane).

For those load combinations that include internal pressure, a pressure load of 700 kPa gauge is applied to the inside surfaces of the cask containment boundary. The internal pressure load is added to the payload pressure load acting on the impacted end of the cask cavity.

For the NCT free drop load combinations that do not include temperature loading, a uniform temperature of 75°C is applied to the model. For those NCT free drop load combinations that do include temperature loading, the bounding NCT heat temperature distribution shown in Figure 2-15 is applied to the model.

For the axisymmetric finite element model, a single node on the outer edge at the impacted end of the cask is restrained from vertical translation. For the 3-D half-symmetry finite element model, symmetry boundary displacement constraints are applied on all nodes located on the cask half-symmetry plane. The 3-D half-symmetry finite element model is also pinned at a single node at the top and bottom ends of the cask body to prevent rigid-body translation and rotation. The pinned boundary conditions applied to the models are required only for numerical stability since the applied inertial loads are balanced by equal and opposite applied reaction loads.

A linear-elastic equivalent-static analysis is performed for each of the NCT free drop impact orientations. The membrane, membrane plus bending, and total stress intensity at each of the stress evaluation locations shown in Figure 2-1 and Figure 2-2 are evaluated for each NCT free drop load combination. The maximum stress intensities resulting from each NCT free drop test, along with the location of the maximum stress intensity, the corresponding allowable stress intensity, and the resulting minimum design margin, are summarized in Table 2-34. The minimum design margin for primary stress intensities (P_m and P_m+P_b) due to NCT free drop loading is +0.06 for primary membrane plus bending (P_m+P_b) stress intensity due to the NCT bottom end drop. The lowest design margin for local membrane and primary plus secondary stress intensities for all NCT free drops is +0.02 for local membrane (P_l) stress intensity due to the NCT bottom oblique drop.

A detailed stress analysis of the cask closure bolts for NCT free drop loading is performed using the 3-D quarter-symmetry finite element model described in Section 2.5.1.2. Analyses are performed for the NCT top end drop and NCT top corner drop because these impact orientations result in the highest outward-acting forces on the closure lid and closure bolts. Transverse loads due to NCT free drops are not included in the closure bolt evaluation since the cask includes a shear lip to protect the closure bolts from shear loading.

The applied NCT top end drop and NCT top corner drop loads are based on the maximum calculated equivalent-static longitudinal accelerations from Table 2-33 of 253*g* and 98*g*, respectively. The inertia load from the closure lid self-weight due to the NCT free drop longitudinal acceleration is accounted for by applying the equivalent-static acceleration load to the model. In addition, a uniform pressure load is applied to the underside of the closure lid to account for the loading from the combined mass of the shield plug and payload. For modeling simplicity, a uniform pressure load is applied over the entire area inside the containment O-ring diameter. Although the O-ring diameter upon which the pressure load is calculated is approximately 18% larger than the outside diameter of the shield plug, it does not significantly affect the solution results. In fact, the assumption of a uniform pressure distribution is conservative; the load from the shield plug will concentrate at its outer edge because it is relatively stiff compared to the closure plate. Thus, the prying moment resulting from the assumed uniform pressure load distribution is conservative.

NCT free drop loading is applied in combination with NCT heat temperature loading, maximum internal pressure, and maximum bolt preload. The NCT heat temperature loading is applied to the finite element model as a uniform temperature load of 68.3°C. The maximum bolt preload of 7.2 kN is applied to each bolt and a uniform pressure load of 700 kPa is applied on the inner surface of the closure plate over the area inside the containment O-ring.

The maximum average stress (i.e., axial stress) and maximum stress (i.e., axial plus bending stress) in the closure bolts and the maximum gap lid separation at the inside edge of the bolting flange due to NCT top end drop and NCT top corner drop loading are summarized in Table 2-35. The maximum average stress and maximum stress in the cask closure bolts, which result from the NCT top end drop condition, are 242 MPa and 311 MPa, respectively. The average axial stress and maximum stress are limited to $2S_m$ and $3S_m$, respectively. The value of S_m for SA-320,

Grade L43 bolting steel at 68.3°C is 234 MPa based on linear interpolation of the S_m values shown in Table 2-15. Therefore, the allowable average stress and maximum stress are 468 MPa and 701 MPa, respectively. The corresponding minimum design margins in the closure bolt for NCT free drop loading are +0.93 for average stress and +1.25 for maximum stress.

The maximum lid separation at the inside edge of the bolting flange, resulting from the NCT top end drop loading, is approximately 0.047 mm, or 5.3% of the O-ring compression. For the cask closure to maintain containment under these conditions, the elastomeric O-ring must have sufficient elasticity to expand to fill the gap, with consideration of potential material degradation due to environmental effects such as radiation and temperature. This is satisfied provided that the maximum compression set does not exceed 94.7% (i.e., (0.88-0.047)/0.88). As shown in Section 3.9.14 of the Parker O-Ring Handbook [2.18], the compression set in ethylene propylene O-rings after exposure to 10^7 rads of gamma radiation at room temperature ranges from 28.6% to 46.6%, based on the compound. The data also shows that these materials will take on a compression set of less than 18% when exposed to a maximum temperature of 100°C for 70 hours ([2.18], Figure 2-13). This data shows that the maximum O-ring compression set due to the combined effects of temperature and radiation will be sufficient to maintain a tight seal for the NCT free drop loading.

2.6.7.3 Cask Shell Buckling Evaluation

Buckling evaluations of the cask containment shell and outer shell are performed for each NCT free drop test in accordance with the requirements of ASME Code Case N-284-1 [2.7]. The maximum compressive stresses and shear stresses near the mid-lengths of the cask inner shell and outer shell (i.e., Sections C5 and N5 in Figure 2-1 and Figure 2-2) are used for the buckling evaluation. As discussed in Section 2.1.2.3, elastic and inelastic buckling interaction ratios are calculated based on the NCT allowable buckling stresses shown in Table 2-7, which include a factor of safety of 2.0. The maximum interaction ratios must not exceed 1.0.

The maximum calculated cask shell stresses and the resulting maximum buckling interaction ratios are summarized in Table 2-36. The maximum buckling interaction ratio in the cask inner shell is 0.18, resulting from the NCT side drop. The maximum buckling interaction ratio in the cask outer shell is 0.41, resulting from the NCT bottom end drop. Therefore, the cask satisfies the buckling design criteria of ASME Code Case N-284-1 for the NCT free drop.

Table 2-31 – NCT Free Drop Loads Summary

NCT Drop Case I.D.	Case Description[1]	Maximum Overpack Foam Crush[2]	Cask Peak Rigid-Body Accelerations[3]		
			Transverse		
			Top End	Bottom End	Longitudinal
N1	Bottom End Drop	9%	[4]	[4]	+262g
N2	Top End Drop	9%	[4]	[4]	-230g
N3	Bottom Corner Drop	5%	-128g	-128g[5]	+144g
N4	Top Corner Drop	15%	-116g	-116g[5]	-89g
N5	Side Drop	8%	-394g	-265g[6]	[4]
N6	Bottom Oblique Drop - Primary Impact - Secondary Impact	7%	 +75g[6] -573g	 -279g +139g[6]	 +14g[6] +77g[6]
N7	Top Oblique Drop - Primary Impact - Secondary Impact	7%	 -517g +108g	 -47g[6] -280g	 -12g[6] -32g

Notes:
1. Impact orientations shown in Figure 2-16.
2. Value equal to the maximum deformation divided by the nominal foam thickness in the corresponding direction.
3. The highest peak accelerations on either the top or bottom centerline of the cask/shield lid rigid-body in the transverse (X) and longitudinal (Y) directions are reported, unless otherwise noted.
4. Peak accelerations are insignificant.
5. Conservatively assumed equal to higher peak acceleration at the other end of the cask.
6. Acceleration occurring at the same time as the highest peak transverse acceleration.

Table 2-32 – Overpack Closure Bolt NCT Free Drop Stress Summary

NCT Drop Case I.D.	Case Description[1]	Maximum Axial Stress (MPa)	Maximum Shear Stress (MPa)	Maximum Stress Interaction Ratio[2]	Minimum Bolt Design Margin[3]
N1	Bottom End Drop	241	45	0.31	+0.79
N2	Top End Drop	151	9	0.13	+1.85
N3	Bottom Corner Drop	78	67	0.14	+1.66
N4	Top Corner Drop	156	74	0.17	+1.41
N5	Side Drop	311	84	0.54	+0.39
N6	Bottom Oblique Drop	320	92	0.56	+0.35
N7	Top Oblique Drop	298	93	0.55	+0.45

Notes:
1. Impact orientations shown in Figure 2-16.
2. Calculated per Table 2-4.
3. The minimum design margin is calculated as (Allowable Value/Maximum Value) – 1, where the allowable axial and shear stresses for A320, Grade L43 bolting steel at an upper-bound temperature of 93°C are 431 MPa and 178 MPa, respectively. The allowable value for the stress interaction ratio is 1.0.

Table 2-33 – NCT Free Drop Equivalent-Static Acceleration Design Loads

NCT Free Drop Orientation[1]	Equivalent-Static Accelerations (g)					
	Calculated Loads			Applied Loads		
	Transverse			Transverse[2] (g)		
	Top End	Bottom End	Longitudinal	Top End	Bottom End	Longitudinal
Bottom End (N1)	---	---	288	---	---	290
Top End (N2)	---	---	253	---	---	290
Bottom Corner (N3)	-141	---	158	180	---	160
Top Corner (N4)	-128	---	98	130	---	100
Side (N5)	-445	-299	---	-460	-300	---
Bottom Oblique (N6)	-647	+162	+87	-650	+50	+90
Top Oblique (N7)	-584	-53	-14	-585	-55	-85

Notes:
1. Impact orientations shown in Figure 2-16.
2. The transverse loads are applied as an average transverse linear acceleration and a rotation acceleration about the cask mid-length.

Table 2-34 – NCT Free Drop Stress Summary

NCT Free Drop Orientation (Case I.D.)	Stress Type	Maximum Stress Intensity (MPa)	Stress Location[1]	Allowable Stress Intensity[2] (MPa)	Minimum Design Margin[3]
Bottom End (N1)	P_m	95	N13	138	+0.45
	P_l	120	C6	207	+0.73
	P_m+P_b	195	C1	207	+0.06
	P_m+P_b+Q	197	C7	414	+1.10
Top End (N2)	P_m	72	N9	138	+0.92
	P_l	72	N9	207	+1.88
	P_m+P_b	147	N9	207	+0.41
	P_m+P_b+Q	88	C1	414	+3.70
Bottom Corner (N3)	P_m	123	C6, 60°	138	+0.12
	P_l	171	C7, 67.5°	207	+0.21
	P_m+P_b	153	C6, 90°	207	+0.35
	P_m+P_b+Q	230	C7, 67.5°	414	+0.80
Top Corner (N4)	P_m	40	N4, 0°	138	+2.45
	P_l	89	N3, 0°	207	+1.33
	P_m+P_b	89	C1, 0°	207	+1.33
	P_m+P_b+Q	101	C14, 0°	414	+3.10
Side Drop (N5)	P_m	121	C11, 37.5°	138	+0.14
	P_l	170	C13, 0°	207	+0.22
	P_m+P_b	191	C11, 37.5°	207	+0.08
	P_m+P_b+Q	379	C13, 0°	414	+0.09
Bottom Oblique Drop (N6)	P_m	118	C11, 37.5°	138	+0.17
	P_l	203	C14, 0°	207	+0.02
	P_m+P_b	190	C11, 37.5°	207	+0.09
	P_m+P_b+Q	320	C13, 0°	414	+0.29
Top Oblique Drop (N7)	P_m	112	C11, 37.5°	138	+0.23
	P_l	174	C14, 0°	207	+0.19
	P_m+P_b	173	C11, 37.5°	207	+0.20
	P_m+P_b+Q	260	C13, 0°	414	+0.59

Notes:
1. Containment system and non-containment component stress locations are shown in Figure 2-1 and Figure 2-2, respectively. For cases N3 through N6, the circumferential location of the maximum stress intensity is shown, where 0° is at the side of impact.
2. Allowable stress intensities are based on an upper-bound design temperature of 74°C.
3. Design margin is calculated as (Allowable S.I./Maximum S.I) – 1.

Table 2-35 – Cask Closure Bolt NCT Free Drop Stress Summary

NCT Free Drop	Max. Average Stress			Maximum Stress			Maximum Lid Separation (mm)
	Max. (MPa)	Limit (MPa)	D.M.	Max. (MPa)	Limit (MPa)	D.M.	
Top End Drop	242	468	+0.93	311	701	+1.25	0.047
Top Corner Drop	207	468	+1.26	226	701	+2.10	0.017

Table 2-36 – NCT Free Drop Buckling Evaluation Summary

NCT Free Drop Orientation (Case I.D.)	Inner Shell[1]				Outer Shell[2]			
	Maximum S.I.[3] (kPa)			Maximum Buckling IR	Maximum S.I.[3] (kPa)			Maximum Buckling IR
	Axial	Hoop	Shear		Axial	Hoop	Shear	
Bottom End (N1)	0[4]	0[4]	0	0.00	35,670	59	0	0.41
Top End (N2)	2,431	8	0	0.03	7,782	35	0	0.09
Bottom Corner (N3)	4,846	985	7,596	0.08	25,229	13,309	7,293	0.31
Top Corner (N4)	4,803	543	4,037	0.06	9,230	12,616	4,306	0.16
Side (N5)	10,246	2,107	12,901	0.18	8,939	22,701	8,594	0.30
Bottom Oblique (N6)	11,063	1,187	7,846	0.15	25,384	34,418	14,436	0.49
Top Oblique (N7)	8,077	1,433	8,634	0.12	19,511	18,529	9,957	0.26

Notes:
1. Maximum stress intensities at section C5 in Figure 2-1 at all locations around the inner shell circumference.
2. Maximum stress intensities at section N5 in Figure 2-2 at all locations around the outer shell circumference.
3. The maximum compressive axial and hoop stress intensities and maximum in-plane shear stress intensities are reported.
4. Zero stress is assumed for the buckling evaluation since all stresses are tensile.

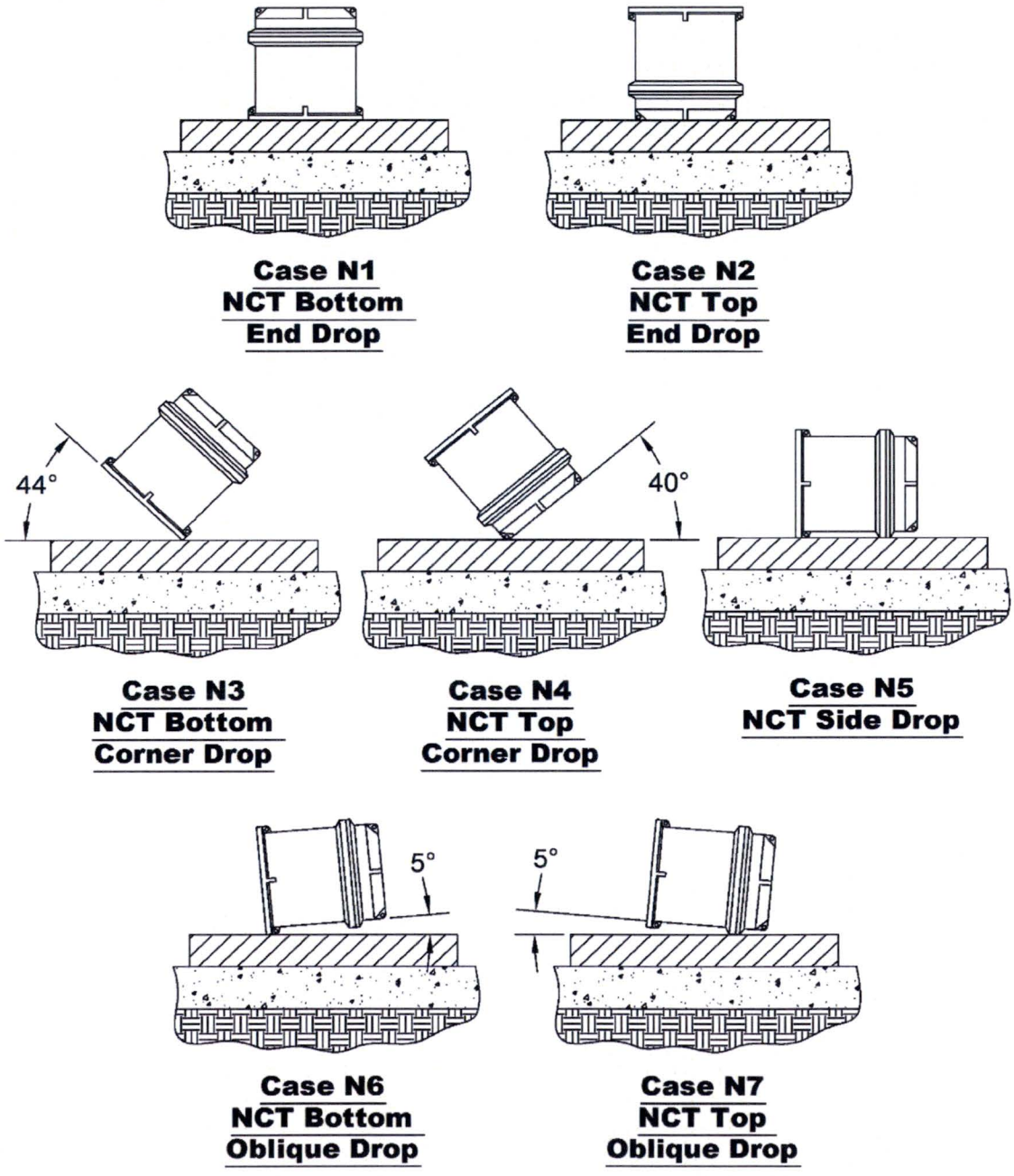

Figure 2-16 – NCT Free Drop Impact Orientations

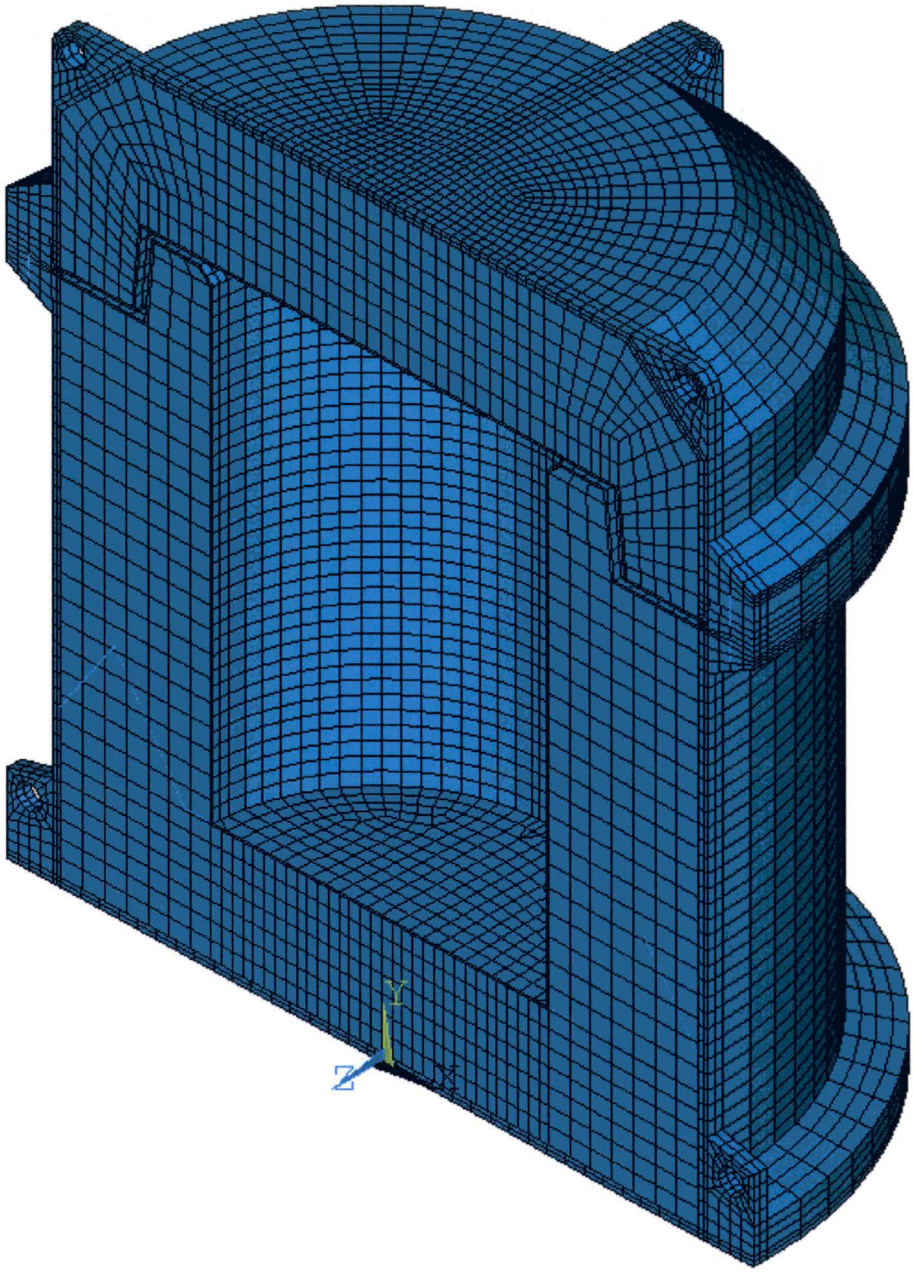

(Note: Cask/shield-lid rigid-body not shown)

Figure 2-17 – MIDUS Overpack 3-D Half-Symmetry Finite Element Model

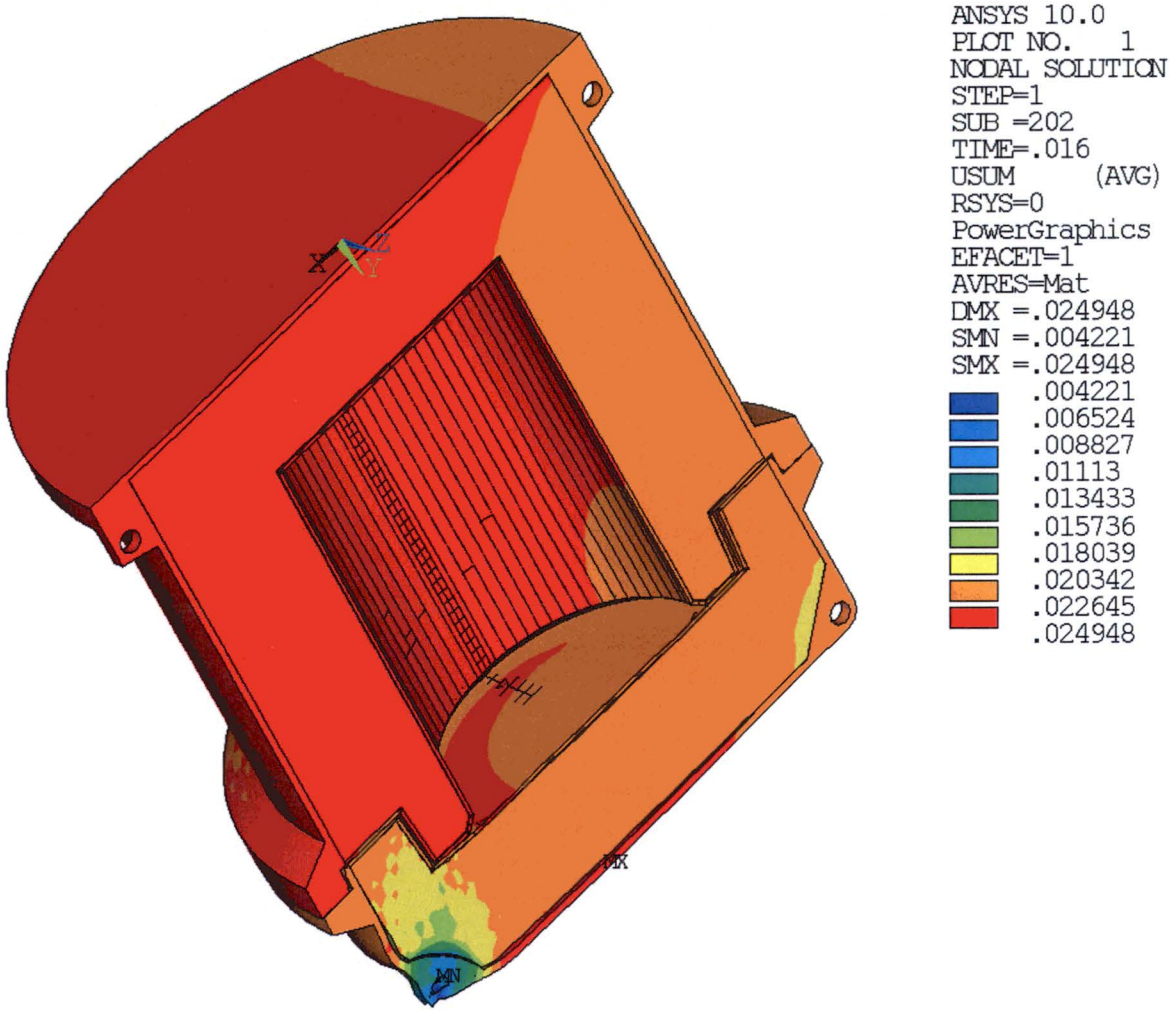

(Notes: Displacement units are meters. Deformed shape shown at 1:1 scale.)

Figure 2-18 – Overpack Permanent Deformation, NCT Top Corner Drop (Case N4)

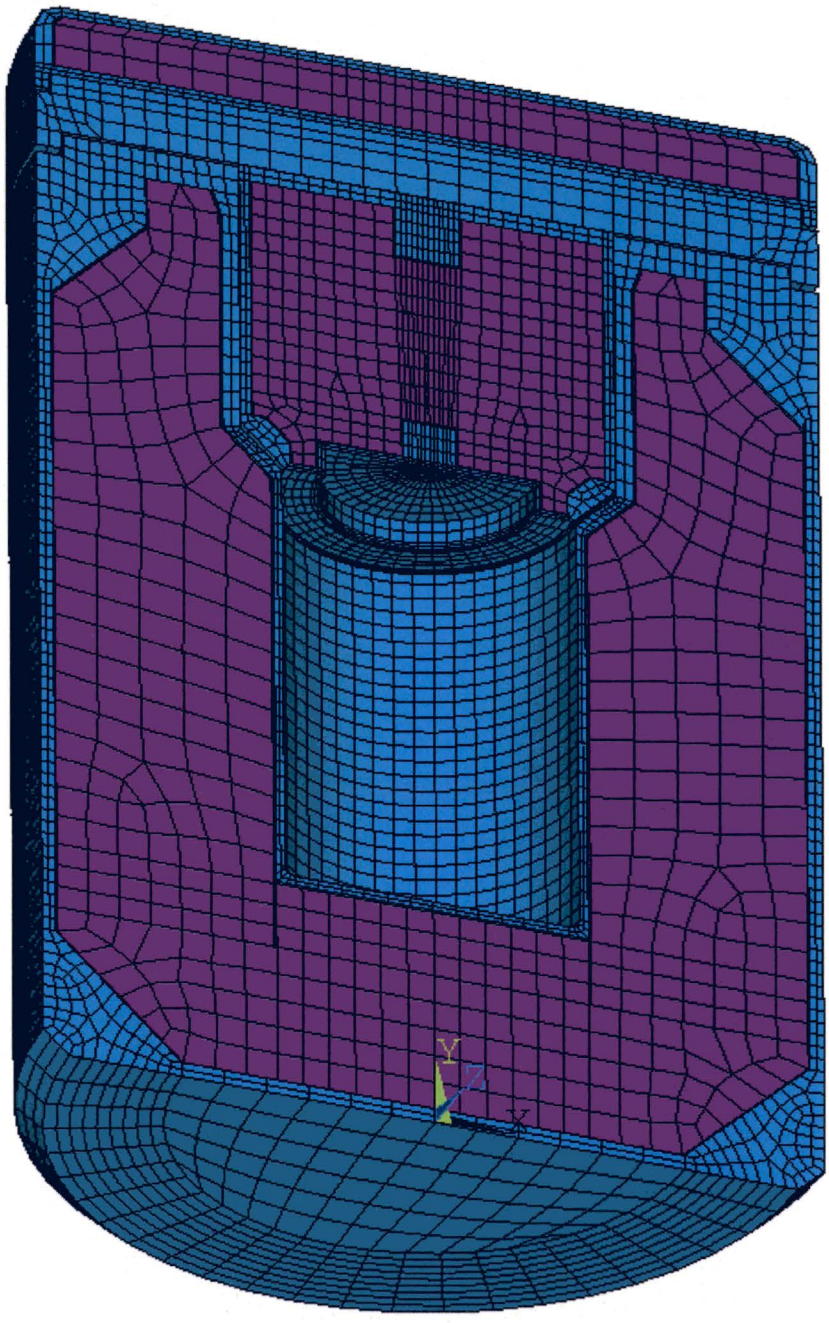

Figure 2-19 – MIDUS Cask Assembly Half-Symmetry FE Model

2.6.8 Corner Drop

In accordance with §71.71(c)(8), fiberboard, wood, or fissile material rectangular packages not exceeding 50 kg (110 lbs) and fiberboard, wood, or fissile material cylindrical packages not exceeding 100 kg (220 lbs) must be subjected to a free drop onto each corner of the package in succession, or in the case of a cylindrical package onto each quarter of each rim, from a height of 0.3 m (1 ft) onto a flat, essentially unyielding, horizontal surface. The package is not a fiberboard, wood, or fissile material package and it weighs more than 100 kg (220 lbs). Therefore, the corner drop test of §71.71(c)(8) is not applicable to the package.

2.6.9 Compression

In accordance with §71.71(c)(9), the package is subjected to a compressive load, applied uniformly to the top and bottom of the package in a position in which the package would normally be transported, for a period of 24 hours. The compressive load is equal to the greater of the equivalent of: (1) 5 times the weight of the package, and (2) 13 kPa multiplied by the vertically projected area of the package.

The package is evaluated for the NCT compression load using the ANSYS Mechanical quarter-symmetry finite element model of the overpack outer shell shown in Figure 2-20. The model includes only the external components of the overpack base and lid, conservatively neglecting structural support provided by the overpack foam cores and inner shells. The finite element model includes 8,763 nodes and 5,890 elements. The overpack shell components are modeled using 3-D structural solid elements. The overpack closure bolts are modeled using uniaxial tension-compression 3-D spar elements. The nonlinear contact interface between the overpack base and lid at the bolting flange is modeled using 3-D surface-to-surface contact.

The overpack base and lid shell components are modeled with a density of 8,030 kg/m^3, Poisson's ratio of 0.3, and a modulus of elasticity of 198E9 Pa for the overpack shell stainless steel materials at -29°C. The overpack closure bolts are modeled using the material properties of SA-320, Grade L43 bolting steel at -29°C.

Symmetry boundary conditions are applied to the symmetry planes of the model (i.e., UX=0 at X=0 and UZ=0 at Z=0). In addition, a single node located on the bottom centerline of the overpack base is restrained in the vertical direction (i.e., UY=0) for numerical stability.

The applied loading for the NCT compression analysis consists of a uniform pressure load on the top surface of the overpack lid and the bottom surface of the overpack base equivalent to five times the weight of the package.

The results of the NCT compression linear-elastic static analysis show that the maximum primary membrane plus bending stress intensity (P_m+P_b) and the maximum primary plus secondary (P_m+P_b+Q) stress intensity in the overpack outer shell are 85 MPa and 111 MPa, respectively. The allowable P_m+P_b and P_m+P_b+Q stress intensities for the overpack shell at a bounding design temperature of 74°C are 207 MPa and 414 MPa, respectively. Therefore, the

minimum design margin in the overpack shells due to the NCT compression loading (due to primary membrane plus bending stress intensity) is +1.44.

The results of the NCT compression analysis show that the package satisfies the applicable NCT allowable stress design criteria. Furthermore, the maximum stress intensity in the overpack shells due to the NCT compression loading is lower than the material yield strength. Therefore, NCT compression loading will not cause any permanent deformation to the package.

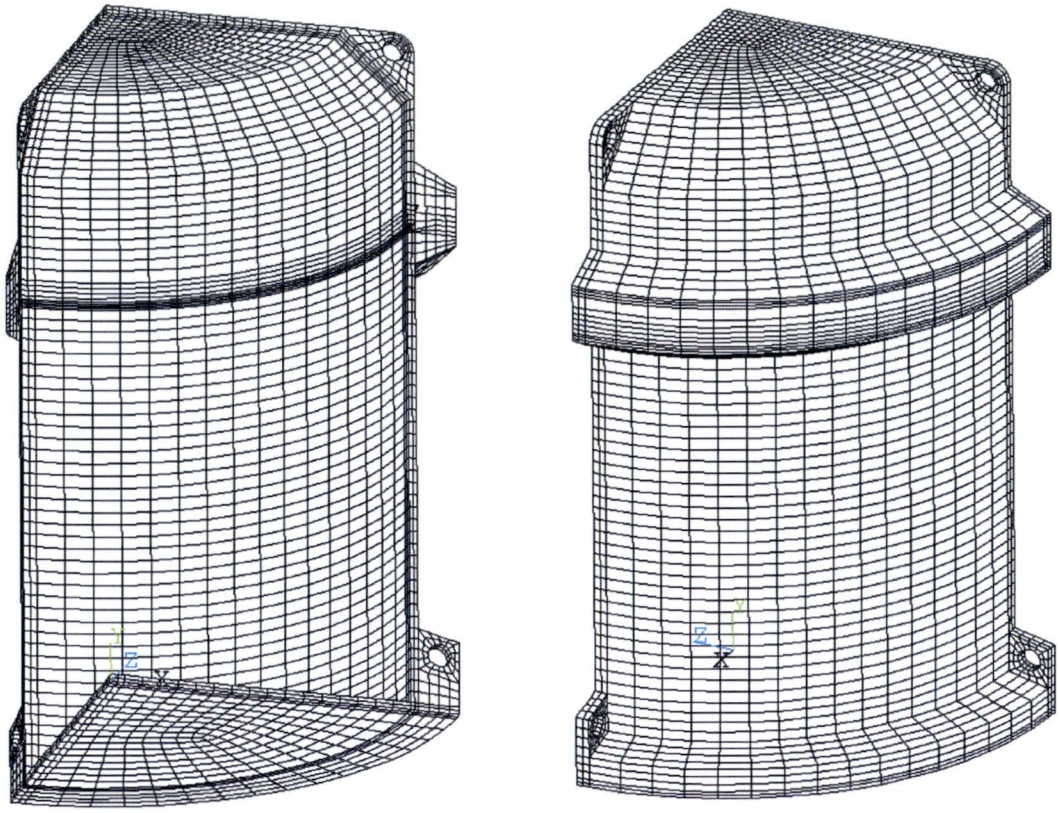

Figure 2-20 – MIDUS Overpack Outer Shell Finite Element Model

2.6.10 Penetration

In accordance with §71.71(c)(10), the package must be subjected to an impact of the hemispherical end of a vertical steel cylinder of 3.2 cm diameter and 6 kg mass. Per Regulatory Guide 7.8 [2.5], the penetration condition of §71.71(c)(10) is not structurally limiting for large packages without unprotected valves. Furthermore, the impact of the hemispherical end of a vertical steel cylinder of 3.2 cm diameter and 6 kg, dropped from a height of 1 meter will not penetrate 10 gage (3.4 mm thick) material. The outer shell of the overpack is 6.0 mm thick and has no valves. In addition, the package mass is over 50 times that of the steel penetration cylinder. Thus, the package need not be evaluated for NCT penetration.

2.7 Hypothetical Accident Conditions

The package meets the standards specified in §71.51 when subjected to the HAC tests specified in §71.73. In accordance with Regulatory Guide 7.6 [2.13], "design-by-analysis" is used for the structural evaluation of the package. The structural evaluation for HAC is based on sequential application of the HAC tests specified in §71.73 to determine the cumulative effect on the package, in accordance with §71.73(a). As discussed in Section 2.6, no significant package damage results from the NCT tests of §71.71. Thus, the evaluation of the package for the HAC test sequence is performed starting with an undamaged specimen. The package is evaluated for the most unfavorable initial conditions specified in §71.73(b). The HAC load combinations considered in the structural evaluation are developed in accordance with Regulatory Guide 7.8 [2.5] and summarized in Section 2.1.2.1.

The results of the structural evaluation show that the package satisfies the applicable allowable stress design criteria of the ASME Code when subjected to the HAC tests of §71.73. A summary of the cumulative package damage resulting from the HAC tests is provided in Section 2.7.8. The predicted package damage is considered in the package thermal, containment, and shielding HAC evaluations. The containment and shielding evaluations of the package show that the cumulative package damage resulting from the HAC test sequence results in no escape of other radioactive material exceeding a total amount of A_2 in one week and no external radiation dose rate exceeding 10 mSv/h at 1 m from the external surface of the package, in accordance with §71.51(a)(2).

2.7.1 Free Drop

In accordance with §71.73(c)(1), the package is subjected to a free drop through a distance of 9 m "*onto a flat, essentially unyielding, horizontal surface, striking in a position for which maximum damage is expected.*" The package is evaluated for a total of 26 different HAC free drop conditions, including thirteen different HAC free drop orientations. These HAC free drop conditions are summarized in Table 2-37 and shown in Figure 2-21. They include upper-bound and lower-bound analyses for a bottom end drop, a top end drop, a bottom corner drop, a top corner drop, a horizontal side drop, four different bottom-end oblique drop angles, and four different top-end oblique drop angles.

The dynamic response of the package to the HAC free drop test conditions is determined using explicit dynamic finite element analysis methods. The ANSYS LS-DYNA PC computer code, which is described in Section 2.12.2.2, is used for this analysis. In accordance with the requirements of Regulatory Guide 7.8 [2.5], the worst-case initial conditions are considered. For each HAC free drop impact orientation considered, upper-bound and lower-bound analyses are performed. The upper-bound analyses are performed using the overpack material upper-bound strength properties for the "cold" thermal condition temperature of -29°C with a lower-bound cask mass of 197 kg. The upper-bound analyses produces the maximum peak rigid-body cask accelerations that are used for the cask stress analysis. The lower-bound analyses are performed using the overpack material lower-bound strength properties for the "hot" thermal condition ambient temperature of 38°C, maximum decay heat, and insolation, combined with an

upper-bound cask mass of 207 kg. The lower-bound analyses, which produce the maximum overpack deformation and the lowest peak rigid-body cask acceleration, are evaluated to assure that the overpack will not "bottom-out," causing large impact loads to be imparted to the cask.

The explicit dynamic finite element analysis of the package is used to predict the rigid-body response of the cask to each HAC free drop test. In addition, this analysis demonstrates the structural adequacy of the overpack assembly for the HAC free drop tests. The maximum stresses in the overpack closure bolts are shown to satisfy the applicable allowable stress design criteria described in Section 2.1.2.2. Furthermore, the maximum crush depth of the overpack polyurethane foam due to each HAC free drop is shown to be less than the allowable crush depth. The drop loads analysis of the package for each HAC free drop impact orientation are discussed in the following sections.

Detailed stress analyses of the cask and shield lid for HAC free drop loading are performed using linear-elastic equivalent-static finite element analysis methods. The ANSYS Mechanical computer program, which is described in Section 2.12.2.1, is used for this analysis. Bounding equivalent-static acceleration design loads are applied to the cask finite element model for each HAC free drop orientation. The bounding equivalent-static acceleration design loads are determined by multiplying the cask peak rigid-body accelerations for each HAC free drop condition by a DLF to account for possible dynamic amplification within the cask.

In accordance with Regulatory Guide 7.8 [2.5], HAC free drop loads are evaluated in combination with internal pressure, thermal, and fabrication stresses. A bounding internal design pressure of 700 kPa gauge is conservatively used for the structural evaluation of the cask. NCT cold and NCT hot thermal loading are considered in combination with HAC free drop loading. Thermally induced stress intensities are classified as secondary in accordance with the ASME Code, since they are self-limiting, and do not require evaluation for HAC. Furthermore, the only significant stresses in the cask body due to NCT thermal loading result from differential thermal expansion of the closure bolts and closure lid. The stresses elsewhere in the cask are not significantly affected by NCT thermal loading, as shown by the results of the NCT end drop evaluation discussed in Section 2.6.7.2. Therefore, NCT thermal loading is not included in the HAC free drop load combinations. However, the effects of elevated temperature are considered for differential thermal expansion between the closure bolts and closure lid and for material properties and allowable stresses used for the HAC free drop evaluation. Furthermore, the only significant fabrication and assembly stresses in the cask are those resulting from closure bolt preload. Therefore, the following load combinations are considered for each HAC free drop load orientation evaluated:

(A) HAC Free Drop + Bolt Preload

(B) HAC Free Drop + Bolt Preload + Maximum Internal Pressure

The maximum stresses in the cask and shield lid due to each HAC free drop are calculated and shown to satisfy the applicable allowable stress design criteria of Subsection NF and Subsection WB of the ASME Code. In addition, the compressive stresses in the cask cylindrical shells due to each HAC free drop are evaluated in accordance with ASME Code Case N-284-1

and shown to satisfy the applicable buckling design criteria. The cask stress analysis and buckling analysis for each HAC impact orientation are discussed further in the following sections.

The results of the HAC free drop structural evaluation demonstrate that the cask satisfies the applicable HAC allowable stress design criteria. HAC free drop loading does not cause any significant permanent deformation of the cask, nor does it substantially reduce the effectiveness of the packaging. The evaluation shows that, under HAC free loading, the containment seal is maintained, and there is no loss or dispersal of radioactive contents. The damage to the overpack resulting from HAC free drop loading is considered in the HAC shielding evaluation, which demonstrates that the external dose rate limit requirement of §71.51(a)(1) is satisfied. Therefore, the package complies with the requirements of §71.51(a)(1) when subjected to the HAC free drop test of §71.73(c)(2).

Table 2-37 – Summary of HAC Free Drop Cases Evaluated

Case I.D.	Case Description	Mass Properties[1]	Thermal Condition[2]	Material Properties[3]	Impact Angle[4]
H1	Cold Bottom End Drop	Lower Bound	Cold	Upper Bound	0°
H2	Hot Bottom End Drop	Upper Bound	Hot	Lower Bound	0°
H3	Cold Top End Drop	Lower Bound	Cold	Upper Bound	180°
H4	Hot Top End Drop	Upper Bound	Hot	Lower Bound	180°
H5	Cold Bottom Corner Drop	Lower Bound	Cold	Upper Bound	44°
H6	Hot Bottom Corner Drop	Upper Bound	Hot	Lower Bound	44°
H7	Cold Top Corner Drop	Lower Bound	Cold	Upper Bound	140°
H8	Hot Top Corner Drop	Upper Bound	Hot	Lower Bound	140°
H9	Cold Side Drop	Lower Bound	Cold	Upper Bound	90°
H10	Hot Side Drop	Upper Bound	Hot	Lower Bound	90°
H11	Cold 5° Bottom Oblique Drop	Lower Bound	Cold	Upper Bound	85°
H12	Hot 5° Bottom Oblique Drop	Upper Bound	Hot	Lower Bound	85°
H13	Cold 10° Bottom Oblique Drop	Lower Bound	Cold	Upper Bound	80°
H14	Hot 10° Bottom Oblique Drop	Upper Bound	Hot	Lower Bound	80°
H15	Cold 15° Bottom Oblique Drop	Lower Bound	Cold	Upper Bound	75°
H16	Hot 15° Bottom Oblique Drop	Upper Bound	Hot	Lower Bound	75°
H17	Cold 20° Bottom Oblique Drop	Lower Bound	Cold	Upper Bound	70°
H18	Hot 20° Bottom Oblique Drop	Upper Bound	Hot	Lower Bound	70°
H19	Cold 5° Top Oblique Drop	Lower Bound	Cold	Upper Bound	95°
H20	Hot 5° Top Oblique Drop	Upper Bound	Hot	Lower Bound	95°
H21	Cold 10° Top Oblique Drop	Lower Bound	Cold	Upper Bound	100°
H22	Hot 10° Top Oblique Drop	Upper Bound	Hot	Lower Bound	100°
H23	Cold 15° Top Oblique Drop	Lower Bound	Cold	Upper Bound	105°
H24	Hot 15° Top Oblique Drop	Upper Bound	Hot	Lower Bound	105°
H25	Cold 20° Top Oblique Drop	Lower Bound	Cold	Upper Bound	110°
H26	Hot 20° Top Oblique Drop	Upper Bound	Hot	Lower Bound	110°

Notes:

1. Upper- and lower-bound mass properties are 2.5% higher and lower than the nominal values shown in Table 2-8.
2. A lower-bound uniform package temperature -29°C is assumed for the "cold" thermal condition. Upper-bound temperatures of 93°C for the overpack steel and 82°C for the overpack foam core are assumed for the "hot" thermal condition.
3. Upper- and lower-bound strength properties of the overpack materials are described in Section 2.2.1.
4. Impact angle is measured relative to the vertical upright package position (refer to Figure 2-21).

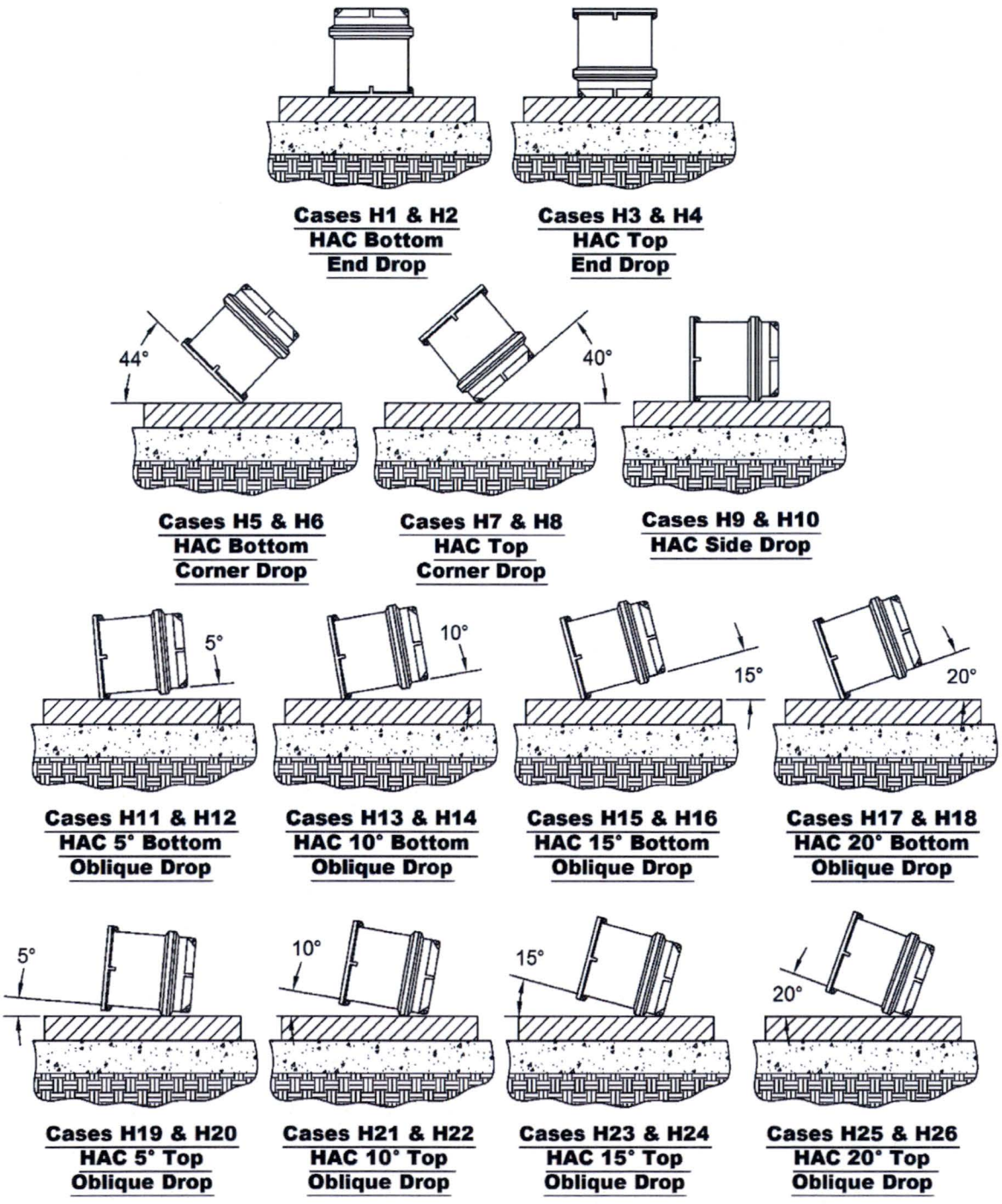

Figure 2-21 – HAC Free Drop Impact Orientations

2.7.1.1 End Drop

The package is evaluated for a 9 m HAC end drop, occurring on either the top or bottom end of the package, considering the worst-case initial conditions in accordance with Regulatory Guide 7.8 [2.5]. The structural evaluation of the package for the HAC bottom end and top end drop tests is described in the following sections.

2.7.1.1.1 Overpack Evaluation

The structural evaluation of the overpack for the HAC end drop orientations is performed using the ANSYS LS-DYNA PC finite element code and the 3-D half-symmetry finite element model described in Section 2.6.7.1. As discussed in Section 2.7.1, HAC drop analyses are performed for the bottom end impact and top end impact orientations for "cold" thermal conditions using the upper-bound strength properties of the overpack materials and the lower-bound mass of the cask to determine the maximum cask rigid-body accelerations for use in the cask stress analysis. In addition, analyses are performed for "hot" thermal conditions using the lower-bound strength properties of the overpack material and the upper-bound mass of the cask to determine the maximum possible crush of the overpack foam.

Each HAC end drop time-history analysis is started at the moment of initial contact between the package outer surface and the impact surface. An initial vertical velocity of 13.29 m/s, corresponding to a free-fall velocity from a height of 9 m, and a constant gravitational acceleration of 9.81 m/s^2 are applied to the package. Each HAC end drop time-history analysis is performed for a duration that is sufficient to capture the primary impact.

The maximum crush depth of the overpack foam, as a percentage of the total foam thickness, and the maximum peak rigid-body accelerations resulting from each HAC end drop test are summarized in Table 2-38. The highest peak rigid-body acceleration of the cask assembly due to the HAC bottom and top end drops are 424*g* and 419*g*, respectively. The results also show that the maximum foam crush due to all HAC end drop conditions is less than or equal to 70% of the foam thickness. This is within the acceptable crush range for the overpack foam material. Therefore, the overpack will not experience excessive deformation that would allow the cask to "bottom-out" under the most severe HAC end drop conditions. The overpack damage resulting from the HAC end drop test is described in Section 2.7.1.5.

The maximum shear stress and maximum axial strain in the overpack closure bolts resulting from each HAC end drop test are summarized in Table 2-39. The maximum shear stresses in the overpack closure bolts for each HAC end drop test are evaluated in accordance with the Service Level D allowable stress design criteria for Class 2 supports from Subsection NF of the ASME Code. As discussed in Section 2.1.2.2, the maximum axial strain in the overpack closure bolts under HAC loading is limited to 16% (i.e., the maximum specified elongation of the overpack closure bolt A320, Grade L43 bolting material) to assure that the overpack bolts do not experience any gross failure. The minimum design margin in the overpack closure bolts for the HAC end drop is +2.58 due to the maximum shear stress resulting from the cold bottom end

drop. Thus, the overpack closure bolts satisfy the applicable allowable stress design criteria for the HAC end drop.

2.7.1.1.2 Cask Stress Evaluation

The stresses in the cask and shield lid resulting from the HAC bottom end drop and top end drop loads are determined using equivalent-static linear-elastic finite element analysis methods. The equivalent-static acceleration load for each HAC end drop orientation is equal to the peak rigid-body acceleration of the cask multiplied by a DLF that accounts for possible dynamic amplification within the cask. As shown in Table 2-38, the cask peak rigid-body acceleration loads due to the HAC cold end drop conditions are much higher than those due to the HAC hot end drop conditions. Thus, bounding equivalent-static acceleration loads are calculated based on the peak rigid-body accelerations resulting from the HAC cold bottom and top end drops, which are 424*g* and 419*g*, respectively. As discussed in Section 2.12.3, a bounding DLF of 1.1 is conservatively used for all HAC end drop evaluations. Thus, the equivalent-static acceleration loads for the HAC cold bottom end drop and HAC cold top end drop are 466*g* and 461*g*, respectively. A bounding equivalent-static acceleration load of 470*g* is conservatively used for the HAC bottom end drop and HAC top end drop stress evaluations.

The stresses in the cask and shield lid due to a 470*g* HAC bottom end drop and a 470*g* HAC top end drop load are determined using the axisymmetric finite element model described in Section 2.6.1.3. The finite element model boundary conditions used for the HAC end drop stress analyses are the same as those used for the NCT end drop stress analyses, as described in Section 2.6.7.2. Also, the 470*g* HAC end drop loading is applied to the finite element model in the same manner as the loads for the NCT end drop stress analysis, as described in Section 2.6.7.2. As discussed in Section 2.7.1, bolt preload and internal pressure loads are evaluated in combination with the HAC end drop loading per the following load combinations:

H1-A: HAC Bottom End Drop + Bolt Preload

H1-B: HAC Bottom End Drop + Bolt Preload + Maximum Internal Pressure

H3-A: HAC Top End Drop + Bolt Preload

H3-B: HAC Top End Drop + Bolt Preload + Maximum Internal Pressure

For all load combinations, the maximum bolt preload of 7.2 kN per bolt is applied to the closure bolt elements on a 360° basis, producing a total preload (for eight closure bolts) of 57.8 kN on the closure lid. For load combinations H1-B and H3-B, the maximum internal pressure load of 700 kPa gauge is applied to the inner surfaces of the cask containment boundary. On the impacted end of the cask cavity, this pressure load is added to the applied pressure that accounts for the payload inertial load due to the HAC end drop acceleration. In addition, a uniform temperature of 75°C is applied to the model for all HAC end drop analyses to account for the cask material properties at elevated temperature

The maximum stress intensities in the cask's containment system and non-containment components due to the HAC bottom end drop and HAC top end drop, along with the corresponding allowable stress intensities and minimum design margins, are summarized in Table 2-40 and Table 2-41, respectively. The minimum design margin for the HAC bottom end drop is +0.44 for primary membrane stress intensity (P_m) occurring at the outer diameter of the cask outer bottom plate (section N2 in Figure 2-2). The minimum design margin for the HAC top end drop is +0.57 for primary membrane plus bending stress intensity (P_m+P_b) in the shield plug bottom casing plate (section N7 in Figure 2-2). The results of the HAC end drop stress evaluation show that the stresses in the cask and shield lid satisfy the applicable HAC allowable stress design criteria of the ASME Code.

To prevent inelastic deformation of the cask's containment system closure, the maximum stresses in the cask flange and closure lid in the region of the containment O-ring seal are limited to the yield strength of the cask material. The maximum stress intensity in the cask's closure seal region due to the HAC top end drop loading is 116 MPa. This is less than the 184 MPa yield strength of the cask body stainless steel material at the upper-bound design temperature of 74°C. Therefore, the HAC top end drop will not cause any plastic deformation in the region of the containment O-ring seal.

As discussed in Section 2.1.2.5, the DU alloy material used for the cask gamma shield components is not expected to experience brittle fracture failure if it does not undergo substantial plastic deformation. Therefore, the maximum stresses in the cask gamma shield are limited to the yield strength of the DU alloy material. The maximum stress intensity in the cask body DU shields due to the HAC top end drop, which occurs at the top end of the radial DU shield, is 152 MPa. This stress is much less than the 380 MPa yield strength of DU at an upper-bound temperature of 93°C. Therefore, the HAC top end drop is not expected to cause any plastic deformation or brittle fracture failure of the cask body DU shields.

In addition to the stress analysis of the cask and shield lid described above, a detailed stress analysis of the cask closure bolts for HAC top end drop loading is performed using the 3-D quarter-symmetry finite element model described in Section 2.5.1.2. The applied HAC top end drop loads are based on the maximum calculated equivalent-static longitudinal acceleration of 461*g*. The inertia load from the closure lid self-weight due to the HAC top end drop acceleration is accounted for by applying the 461*g* equivalent-static acceleration load to the model. In addition, a uniform pressure load is applied to the underside of the closure lid to account for the loading from the combined mass of the shield plug and payload.

For modeling simplicity, a uniform pressure load is applied over the entire area inside the containment O-ring diameter. Although the O-ring diameter upon which the pressure load is calculated is approximately 18% larger than the outside diameter of the shield plug, this does not significantly affect the solution results. In fact, the assumption of a uniform pressure distribution is conservative; the load from the shield plug will concentrate at its outer edge because it is relatively stiff compared to the closure plate. Thus, the prying moment resulting from the assumed uniform pressure load distribution is conservative.

The HAC top end drop loading is applied in combination with NCT heat temperature loading, maximum internal pressure, and maximum bolt preload. The NCT heat temperature loading is applied to the finite element model as a uniform temperature load of 68.3°C. The maximum bolt preload of 7.2 kN is applied to each bolt and a uniform pressure load of 700 kPa is applied on the inner surface of the closure plate over the area inside the containment O-ring.

The maximum average stress (i.e., axial stress) in the closure bolts due to HAC top end drop loading is 322 MPa. The average axial stress for HAC is limited to the less of $3S_m$ or $0.7S_u$. The values of S_m and S_u for SA-320, Grade L43 bolting steel at 68.3°C are 234 MPa and 862 MPa, respectively, based on linear interpolation of the values shown in Table 2-15. Therefore, the allowable average stress for HAC is 603 MPa. The corresponding minimum design margin in the closure bolt for the HAC top end drop loading is +0.87.

The maximum lid separation at the inside edge of the bolting flange resulting from the HAC top end drop loading is approximately 0.093 mm, or 10.5% of the O-ring compression. However, separation of the closure lid is not expected to occur during the HAC top end drop because the reaction pressure on the top end of the cask, which is conservatively neglected in the closure bolt evaluation, would compress the seal. Nevertheless, the maximum calculated lid separation is considered in the evaluation of the cask containment seal.

For the cask closure to maintain containment under these conditions, the elastomeric O-ring must have sufficient elasticity to expand to fill the gap, considering potential material degradation due to environmental effects such as radiation and temperature. This is satisfied provided that the maximum compression set does not exceed 89.4% (i.e., (0.88-0.093)/0.88). As shown in Section 3.9.14 of the Parker O-Ring Handbook [2.18], the compression set in ethylene propylene O-rings after exposure to 10^7 rads of gamma radiation at room temperature ranges from 28.6% to 46.6%, based on the compound. The data also shows that these materials will take on a compression set of less than 18% when exposed to a maximum temperature of 100°C for 70 hours ([2.18], Figure 2-13). This data shows that the maximum O-ring compression set due to the combined effects of temperature and radiation will be sufficient to maintain a tight seal for the HAC end drop loading.

2.7.1.1.3 Cask Shell Buckling Evaluation

Buckling evaluations of the cask's containment shell and outer shell are performed for the HAC bottom end drop and HAC top end drop tests in accordance with the requirements of ASME Code Case N-284-1 [2.7]. The maximum compressive stresses and shear stresses near the mid-lengths of the cask's inner shell and outer shell (i.e., Sections C5 and N5 in Figure 2-1 and Figure 2-2) are used for the cask shell buckling evaluation. As discussed in Section 2.1.2.3, elastic and inelastic buckling interaction ratios are calculated based on the HAC allowable buckling stresses shown in Table 2-7, which include a factor of safety of 1.34. The maximum interaction ratios must not exceed 1.0.

The maximum calculated cask shell stresses and the resulting maximum buckling interaction ratios for the HAC bottom end drop and HAC top end drop are summarized in Table 2-42. The maximum buckling interaction ratio in the cask's inner shell is 0.03, resulting from the HAC top

end drop. The maximum buckling interaction ratio in the cask's outer shell is 0.43, resulting from the HAC bottom end drop. Therefore, the cask satisfies the buckling design criteria of ASME Code Case N-284-1 for the HAC end drop test.

Table 2-38 – HAC End Drop Loads Summary

HAC Drop Case I.D.	Case Description[1]	Maximum Overpack Foam Crush[2]	Cask Peak Rigid-Body Accelerations[3]	
			Transverse	Longitudinal
H1	Cold Bottom End Drop	36%	[4]	424g
H2	Hot Bottom End Drop	70%	[4]	281g
H3	Cold Top End Drop	36%	[4]	419g
H4	Hot Top End Drop	65%	[4]	286g

Notes:
1. Impact orientations are shown in Figure 2-16.
2. Value equal to the maximum deformation divided by the nominal foam thickness in the corresponding direction.
3. The highest peak accelerations on either the top or bottom centerline of the cask/shield lid rigid-body in the transverse (X) and longitudinal (Y) directions are reported.
4. The transverse acceleration of the cask due to HAC end drop impacts is insignificant.

Table 2-39 – Overpack Closure Bolt HAC End Drop Stress Summary

HAC Drop Case I.D.	Case Description[1]	Maximum Shear Stress (MPa)	Maximum Axial Strain	Minimum Bolt Design Margin[2]
H1	Cold Bottom End Drop	101	0.5%	+2.58
H2	Hot Bottom End Drop	94	0.5%	+2.85
H3	Cold Top End Drop	24	0.3%	+14.1
H4	Hot Top End Drop	11	0.2%	+31.9

Notes:
1. Impact orientations are shown in Figure 2-16.
2. The minimum design margin is calculated as (Allowable Value/Maximum Value) – 1, where the allowable shear stresses for A320, Grade L43 bolting steel at an upper-bound temperature of 93°C is 362 MPa, and the allowable axial strain is equal to the maximum elongation of A320, Grade L43 bolting steel (i.e., 16%).

Table 2-40 – HAC Bottom End Drop Maximum Stress Summary

Cask Components	Stress Type	Maximum Stress Intensity (MPa)	Controlling Load Combination & Location[1]	Allowable Stress Intensity[2] (MPa)	Minimum Design Margin[3]
Containment System	P_m	191	H1-B, C7	331	+0.73
	P_m+P_b	313	H1-B, C7	492	+0.57
	P_m+P_b+Q	313	H1-B, C7	N/A[4]	N/A[4]
Non-Containment Components	P_m	153	H1-B, N2	221	+0.44
	P_m+P_b	187	H1-B, N13	332	+0.78
	P_m+P_b+Q	192	H1-A, N13	N/A[4]	N/A[4]

Notes:
1. Load combinations H1-A and H1-B are defined in Section 2.7.1.1. Containment system and non-containment component stress locations are shown in Figure 2-1 and Figure 2-2, respectively.
2. Allowable stress intensities are based on an upper-bound design temperature of 74°C.
3. Design margin is calculated as (Allowable S.I./Maximum S.I) – 1.
4. Evaluation of secondary stress is not required for HAC.

Table 2-41 – HAC Top End Drop Maximum Stress Summary

Cask Components	Stress Type	Maximum Stress Intensity (MPa)	Controlling Load Combination & Location[1]	Allowable Stress Intensity[2] (MPa)	Minimum Design Margin[3]
Containment System	P_m	55	H3-B, C15	331	+5.02
	P_m+P_b	91	H3-B, C15	492	+4.41
	P_m+P_b+Q	91	H3-B, C15	N/A[4]	N/A[4]
Non-Containment Components	P_m	88	H3-B, N9	221	+1.51
	P_m+P_b	212	H3-B, N7	332	+0.57
	P_m+P_b+Q	233	H3-B, N8	N/A[4]	N/A[4]

Notes:
1. Load combinations H3-A and H3-B are defined in Section 2.7.1.1. Containment system and non-containment component stress locations are shown in Figure 2-1 and Figure 2-2, respectively.
2. Allowable stress intensities are based on an upper-bound design temperature of 74°C.
3. Design margin is calculated as (Allowable S.I./Maximum S.I) – 1.
4. Evaluation of secondary stress is not required for HAC.

Table 2-42 – HAC End Drop Buckling Evaluation Summary

HAC End Drop Orientation	Inner Shell[1]				Outer Shell[2]			
	Maximum S.I.[3] (kPa)			Maximum Buckling IR	Maximum S.I.[3] (kPa)			Maximum Buckling IR
	Axial	Hoop	Shear		Axial	Hoop	Shear	
Bottom End (H1)	0[4]	0[4]	0	0.00	54,680	5	0	0.43
Top End (H3)	3,940	15	0	0.03	12,610	3	0	0.10

Notes:
1. Maximum stress intensities at section C5 in Figure 2-1.
2. Maximum stress intensities at section N5 in Figure 2-2.
3. The maximum compressive axial and hoop stress intensities and maximum in-plane shear stress intensities from load combinations "-A" and "-B" are reported.
4. Zero stress is assumed for the buckling evaluation since all stresses are tensile.

2.7.1.2 Side Drop

The package is evaluated for a 9 m HAC side drop considering the worst-case initial conditions in accordance with Regulatory Guide 7.8 [2.5]. The structural evaluation of the package for the HAC side drop test is described in the following sections.

2.7.1.2.1 Overpack Evaluation

The structural evaluation of the overpack for the HAC side drop orientation is performed using the ANSYS LS-DYNA PC finite element code and the 3-D half-symmetry finite element model described in Section 2.6.7.1. As discussed in Section 2.7.1, HAC side drop analyses are performed for "cold" thermal conditions using the upper-bound strength properties of the overpack materials and the lower-bound mass of the cask to determine the maximum cask rigid-body accelerations for use in the cask stress analysis. In addition, analyses are performed for "hot" thermal conditions using the lower-bound strength properties of the overpack material and the upper-bound mass of the cask to determine the maximum possible crush of the overpack foam.

Each HAC side drop time-history analysis is started at the moment of initial contact between the package's outer surface and the impact surface. An initial vertical velocity of 13.29 m/s, corresponding to a free-fall velocity from a height of 9 m, and a constant gravitational acceleration of 9.81 m/s^2 are applied to the package. Each HAC side drop time-history analysis is performed for a duration that is sufficient to capture the primary impact.

The maximum crush depth of the overpack foam (as a percentage of the total foam thickness) and the maximum peak rigid-body accelerations resulting from each HAC side drop test are summarized in Table 2-43. The highest peak rigid-body acceleration of the cask assembly due to the HAC side drop is 739*g*. The results also show that the maximum foam crush due to all HAC side drop conditions is 66%, which is less than the maximum acceptable crush of 70% for the overpack foam material. Therefore, the overpack will not experience excessive deformation that would allow the cask to "bottom-out" under the most severe HAC side drop condition. The extent of overpack damage resulting from the HAC side drop is discussed further in Section 2.7.1.5.

The maximum shear stress and maximum axial strain in the overpack closure bolts resulting from each HAC side drop test are summarized in Table 2-44. The maximum shear stresses in the overpack closure bolts for each HAC side drop test are evaluated in accordance with the Service Level D allowable stress design criteria for Class 2 supports from Subsection NF of the ASME Code. As discussed in Section 2.1.2.2, the maximum axial strain in the overpack closure bolts under HAC loading is limited 16% (i.e., the maximum specified elongation of the overpack closure bolt A320, Grade L43 bolting material) to assure that the overpack bolts do not experience any gross failure. The minimum design margin in the overpack closure bolts for the HAC side drop is +2.93 due to the maximum shear stress resulting from the HAC hot side drop (Case H10). Thus, the overpack closure bolts satisfy the applicable allowable-stress design criteria for the HAC side drop.

2.7.1.2.2 Cask Stress Evaluation

The stresses in the cask and shield lid resulting from the HAC side drop loads are determined using equivalent-static linear-elastic finite element analysis methods. The equivalent-static acceleration load for the HAC side drop is equal to the peak rigid-body acceleration of the cask multiplied by a DLF that accounts for possible dynamic amplification within the cask. As shown in Table 2-43, the cask peak rigid-body acceleration loads due to the HAC cold side drop conditions are much higher than those due to the HAC hot side drop conditions. The peak transverse rigid-body acceleration due to the HAC cold side drop varies from 739*g* at the top end of the shield lid to 292*g* at the bottom end of the cask. As discussed in Section 2.12.3, a bounding DLF of 1.13 is conservatively used for the HAC side drop evaluation. The resulting equivalent-static transverse acceleration load for the HAC cold side drop is 835*g* at the top end of the shield lid and 330*g* at the bottom end of the cask. The HAC side drop analysis is performed using bounding equivalent-static acceleration loads of 850*g* at the top end of the shield lid and 350*g* at the bottom end of the cask. These loads are applied as an average transverse linear acceleration of 5,886 m/s^2 (600*g*) and a rotational acceleration load of 14,135 rads/s^2 about the mid-length of the cask (i.e., 173.5 mm from the bottom end of the cask).

The stresses in the cask and shield lid due to the HAC side drop loading are determined using the 3-D half-symmetry finite element model described in Section 2.6.7.2. The finite element model boundary conditions used for the HAC side drop stress analyses are the same as those used for the NCT side drop stress analyses, as described in Section 2.6.7.2. Also, the HAC side drop loading is applied to the finite element model in the same manner as the loads for the NCT side drop stress analysis, as described in Section 2.6.7.2. As discussed in Section 2.7.1, bolt preload and internal pressure loads are evaluated in combination with the HAC side drop loading per the following load combinations:

H9-A: HAC Side Drop + Bolt Preload

H9-B: HAC Side Drop + Bolt Preload + Maximum Internal Pressure

The maximum bolt preload of 7.2 kN is applied to each closure bolt element (3.6 N for the bolts on the half-symmetry plane). For load combinations H9-B, the maximum internal pressure load of 700 kPa gauge is applied to the inner surfaces of the cask's containment boundary. On the impacted side of the cask cavity, this pressure load is added to the applied pressure that accounts for the payload inertial load due to the HAC side drop acceleration. In addition, a uniform temperature of 75°C is applied to the model for both HAC side drop analyses to account for the cask's material properties at elevated temperature

The maximum stress intensities in the cask's containment system and non-containment components due to the HAC side drop, along with the corresponding allowable stress intensities and minimum design margins, are summarized in Table 2-45. The minimum design margin for the HAC side drop is +0.40 for primary membrane stress intensity (P_m) occurring in the shield plug bottom plate (section N11 in Figure 2-2). The results of the HAC side drop stress evaluation show that the stresses in the cask and shield lid satisfy the applicable HAC allowable-stress design criteria of the ASME Code.

2.7.1.2.3 Cask Shell Buckling Evaluation

A buckling evaluation of the cask's containment shell and outer shell is performed for the HAC side drop test in accordance with the requirements of ASME Code Case N-284-1 [2.7]. The maximum compressive stresses and shear stresses near the mid-lengths of the cask's inner shell and outer shell (i.e., Sections C5 and N5 in Figure 2-1 and Figure 2-2) are used for the cask-shell buckling evaluation. As discussed in Section 2.1.2.3, elastic and inelastic buckling interaction ratios are calculated based on the HAC allowable buckling stresses shown in Table 2-7, which include a factor of safety of 1.34. The maximum interaction ratios must not exceed 1.0.

The maximum calculated cask-shell stresses and the resulting maximum buckling interaction ratios for the HAC side drop are summarized in Table 2-46. The maximum buckling interaction ratios in the cask's inner and outer shells, calculated using the bounding shell stresses from load combinations H9-A and H9-B, are 0.19 and 0.27, respectively. Therefore, the cask satisfies the buckling design criteria of ASME Code Case N-284-1 for the HAC side drop test.

Table 2-43 – HAC Side Drop Loads Summary

HAC Drop Case I.D.	Case Description[1]	Maximum Overpack Foam Crush[2]	Cask Peak Rigid-Body Accelerations[3]		
			Transverse		
			Top End	Bottom End	Longitudinal
H9	Cold Side Drop	32%	-739*g*	-292*g*[4]	[5]
H10	Hot Side Drop	66%	-534*g*	-342*g*	[5]

Notes:
1. Impact orientations are shown in Figure 2-16.
2. Value is equal to the maximum deformation divided by the nominal foam thickness in the corresponding direction.
3. The highest peak accelerations on either the top or bottom centerline of the cask/shield lid rigid-body in the transverse (X) and longitudinal (Y) directions are reported, unless otherwise noted.
4. Transverse acceleration on the cask bottom end at the time of the peak transverse acceleration at the cask top end.
5. The longitudinal acceleration of the cask due to HAC side drop impacts is insignificant.

Table 2-44 – Overpack Closure Bolt HAC Side Drop Stress Summary

HAC Drop Case I.D.	Case Description[1]	Maximum Shear Stress (MPa)	Maximum Axial Strain	Minimum Bolt Design Margin[2]
H9	Cold Side Drop	84	1.4%	+3.31
H10	Hot Side Drop	92	3.2%	+2.93

Notes:
1. Impact orientations are shown in Figure 2-16.
2. The minimum design margin is calculated as (Allowable Value/Maximum Value) – 1, where the allowable shear stresses for A320, Grade L43 bolting steel at an upper-bound temperature of 93°C is 362 MPa, and the allowable axial strain is equal to the maximum elongation of A320, Grade L43 bolting steel (i.e., 16%).

Table 2-45 – HAC Side Drop Maximum Stress Summary

Cask Components	Stress Type	Maximum Stress Intensity (MPa)	Controlling Load Combination & Location[1]	Allowable Stress Intensity[2] (MPa)	Minimum Design Margin[3]
Containment System	P_m	189	H9-A, C11, 37.5°	331	+0.75
	P_l	261	H9-B, C14, 0°	492	+0.89
	P_m+P_b	287	H9-A, C11, 37.5°	492	+0.71
	P_m+P_b+Q	568	H9-B, C13, 0°	N/A[4]	N/A[4]
Non-Containment Components	P_m	158	H9-B, N11, 0°	221	+0.40
	P_l	173	H9-B, N3, 0°	332	+0.92
	P_m+P_b	214	H9-B, N18, 180°	332	+0.55
	P_m+P_b+Q	228	H9-A, N3, 0°	N/A[4]	N/A[4]

Notes:
1. The load combination and the location of the maximum stress intensity (section number and circumferential location) is identified. Load combinations H9-A and H9-B are defined in Section 2.7.1.1. Containment system and non-containment component stress locations are shown in Figure 2-1 and Figure 2-2, respectively. The circumferential location is identified with 0° at the side of impact and 180° opposite the side of impact.
2. Allowable stress intensities are based on an upper-bound design temperature of 74°C.
3. Design margin is calculated as (Allowable S.I./Maximum S.I) – 1.
4. Evaluation of secondary stress is not required for HAC.

Table 2-46 – HAC Side Drop Buckling Evaluation Summary

	Inner Shell[1]				Outer Shell[2]			
	Maximum S.I.[3] (kPa)			Maximum Buckling IR	Maximum S.I.[3] (kPa)			Maximum Buckling IR
Load Case I.D.	Hoop	Axial	Shear		Hoop	Axial	Shear	
H9-A	3,039	17,349	18,624	---	31,837	10,191	8,714	---
H9-B	[4]	11,664	18,641	---	31,771	9,053	9,165	---
Bounding Values	3,039	17,349	18,641	0.19	31,837	10,191	9,165	0.27

Notes:
1. Maximum stress intensities at section C5 in Figure 2-1.
2. Maximum stress intensities at section N5 in Figure 2-2.
3. The maximum compressive axial and hoop stress intensities and maximum in-plane shear stress intensities from load combinations "-A" and "-B" are reported.
4. Zero stress is assumed for the buckling evaluation since all stresses are tensile.

2.7.1.3 Corner Drop

The package is evaluated for a 9 m HAC drop with the package center of gravity loaded directly over either the top or bottom corner of the package, considering the worst-case initial conditions in accordance with Regulatory Guide 7.8 [2.5]. The package orientations for the bottom corner drop and top corner drop, given as the angle of the package relative to the vertical upright orientation in which it is transported, are 44° and 140°, respectively. The structural evaluation of the package for the HAC bottom-corner drop and top-corner drop tests is described in the following sections.

2.7.1.3.1 Overpack Evaluation

The structural evaluation of the overpack for the HAC bottom corner drop and top corner drop tests is performed using the ANSYS LS-DYNA PC finite element code and the 3-D half-symmetry finite element model described in Section 2.6.7.1. As discussed in Section 2.7.1, HAC drop analyses are performed for "cold" thermal conditions using the upper-bound strength properties of the overpack materials and the lower-bound mass of the cask to determine the maximum cask rigid-body accelerations for use in the cask stress analysis, and for "hot" thermal conditions using the lower-bound strength properties of the overpack material and the upper-bound mass of the cask to determine the maximum possible crush of the overpack foam.

Each HAC corner drop time-history analysis is started at the moment of initial contact between the package's outer surface and the impact surface. An initial vertical velocity of 13.29 m/s, corresponding to a free-fall velocity from a height of 9 m, and a constant gravitational acceleration of 9.81 m/s^2 are applied to the package. Each HAC corner drop time-history analysis is performed for a duration that is sufficient to capture the primary impact.

The maximum crush depth of the overpack foam (as a percentage of the total foam thickness) and the maximum peak rigid-body accelerations resulting from the HAC bottom-corner drop and top-corner drop tests are summarized in Table 2-47. The highest transverse and longitudinal peak rigid-body acceleration of the cask resulting from the HAC cold bottom-corner drop are 171*g* and 211*g*, respectively. The highest transverse and longitudinal peak rigid-body accelerations of the cask resulting from the HAC cold top-corner drop are 272*g* and 298*g*, respectively. The maximum foam crush due to the HAC hot bottom-corner drop and HAC hot top-corner drop, given as a percentage of the overall foam thickness, are 77% and 71%, respectively. In both cases, the maximum foam crush results from localized deformation of the overpack outer shell at the location of an overpack lug. Due to the localized nature of the deformation, the volume of foam that is crushed beyond 70% is small and does not account for a significant portion of the overall energy absorption. As discussed in Section 2.1.2.2, the maximum localized foam crush is limited to 80% of the foam thickness. Therefore, the overpack foam meets the maximum crush acceptance criteria and will not experience excessive deformation that would allow the cask to "bottom-out" under the HAC hot bottom-corner drop and HAC hot top-corner drop tests. The extent of overpack damage resulting from the HAC corner drop is discussed further in Section 2.7.1.5.

The maximum shear stress and maximum axial strain in the overpack closure bolts resulting from each HAC bottom-corner and top-corner drop tests are summarized in Table 2-48. The maximum shear stresses in the overpack closure bolts for each HAC corner drop test are evaluated in accordance with the Service Level D allowable-stress design criteria for Class 2 supports from Subsection NF of the ASME Code. As discussed in Section 2.1.2.2, the maximum axial strain in the overpack closure bolts under HAC loading is limited to 16% (i.e., the maximum specified elongation of the overpack closure bolt A320, Grade L43 bolting material) to assure that the overpack bolts do not experience any gross failure. The minimum design margin in the overpack closure bolts for the HAC corner drop is +1.81 due to the maximum axial strain resulting from the HAC hot top-corner drop (Case H8). Thus, the overpack closure bolts satisfy the applicable allowable-stress design criteria for the HAC bottom-corner and top-corner drop tests.

2.7.1.3.2 Cask Stress Evaluation

As discussed in Section 2.7.1.4.2, the stress analysis of the cask and shield lid for the HAC oblique drops is performed using transverse and longitudinal equivalent-static-acceleration loads that bound the maximum equivalent-static accelerations for all HAC corner drop and HAC oblique drop tests. The results of that bounding evaluation show that the cask and shield lid satisfy the applicable HAC allowable-stress design criteria for all HAC corner drop and oblique drop tests.

A detailed stress analysis of the cask's closure bolts for HAC top-corner drop loading is performed using the 3-D quarter-symmetry finite element model described in Section 2.5.1.2. The applied HAC top-corner drop loads are based on the maximum calculated equivalent-static longitudinal acceleration of 328*g*. The inertia load from the closure lid self-weight due to the HAC top-corner drop acceleration is accounted for by applying the 328*g* equivalent-static acceleration load to the model. In addition, a uniform pressure load is applied to the underside of the closure lid to account for the loading from the combined mass of the shield plug and payload. For modeling simplicity, a uniform pressure load is applied over the entire area inside the containment O-ring diameter. Although the O-ring diameter upon which the pressure load is calculated is approximately 18% larger than the outside diameter of the shield plug, this does not significantly affect the solution results. The assumption of a uniform pressure distribution is conservative; the load from the shield plug will concentrate at its outer edge because it is relatively stiff compared to the closure plate. Thus, the prying moment resulting from the assumed uniform pressure load distribution is conservative.

The HAC top-corner loading is applied in combination with NCT heat-temperature loading, maximum internal pressure, and maximum bolt preload. The NCT heat-temperature loading is applied to the finite element model as a uniform temperature load of 68.3°C. The maximum bolt preload of 7.2 kN is applied to each bolt and a uniform pressure load of 700 kPa is applied on the inner surface of the closure plate over the area inside the containment O-ring.

The maximum average stress (i.e., axial stress) in the closure bolts due to the HAC top-corner drop loading is 270 MPa. The average axial stress for HAC is limited to the less of $3S_m$ or $0.7S_u$. The values of S_m and S_u for SA-320, Grade L43 bolting steel at 68.3°C are 234 MPa and

862 MPa, respectively, based on linear interpolation of the values shown in Table 2-15. Therefore, the allowable average stress for HAC is 603 MPa. The corresponding minimum design margin in the closure bolt for the HAC top-corner drop loading is +1.23.

The maximum lid separation at the inside edge of the bolting flange resulting from the HAC top-corner drop loading is approximately 0.004 mm, or 0.4% of the O-ring compression. This lid separation is much less than the maximum weld separation from the HAC end drop. As discussed in Section 2.7.1.1.2, the maximum compression set in the cask's containment O-ring seal due to the combined effects of radiation and temperature is sufficient to maintain a tight seal under the bounding HAC end drop test. Therefore, a tight containment seal will also be maintained under the most severe HAC top-corner drop test conditions.

Table 2-47 – HAC Corner Drop Loads Summary

HAC Drop Case I.D.	Case Description[1]	Maximum Overpack Foam Crush[2]	Cask Peak Rigid-Body Accelerations[3]	
			Transverse	Longitudinal
H5	Cold Bottom Corner Drop	47%	171g	211g
H6	Hot Bottom Corner Drop	77%	123g	149g
H7	Cold Top Corner Drop	50%	272g	298g
H8	Hot Top Corner Drop	71%	191g	214g

Notes:
1. Impact orientations are shown in Figure 2-16.
2. Value is equal to the maximum deformation divided by the nominal foam thickness in the corresponding direction.
3. The highest peak accelerations on either the top or bottom centerline of the cask/shield lid rigid-body in the transverse (X) and longitudinal (Y) directions are reported.

Table 2-48 – Overpack Closure-Bolt HAC Corner Drop Stress Summary

HAC Drop Case I.D.	Case Description[1]	Maximum Shear Stress (MPa)	Maximum Axial Strain	Minimum Bolt Design Margin[2]
H5	Cold Bottom Corner Drop	78	0.4%	+3.64
H6	Hot Bottom Corner Drop	56	0.3%	+5.46
H7	Cold Top Corner Drop	105	3.9%	+2.45
H8	Hot Top Corner Drop	108	5.7%	+1.81

Notes:
1. Impact orientations are shown in Figure 2-16.
2. The minimum design margin is calculated as (Allowable Value/Maximum Value) – 1, where the allowable shear stresses for A320, Grade L43 bolting steel at an upper-bound temperature of 93°C is 362 MPa, and the allowable axial strain is equal to the maximum elongation of A320, Grade L43 bolting steel (i.e., 16%).

2.7.1.4 Oblique Drops

The package is evaluated for HAC oblique drop loading resulting from bottom-end and top-end primary impact angles of 5°, 10°, 15°, and 20° from horizontal. The structural evaluation of the package for the HAC oblique drop considers the effects of both primary and secondary (slapdown) impact loadings. The structural evaluation of the package for the HAC oblique drop tests is presented in the following sections.

2.7.1.4.1 Overpack Evaluation

The structural evaluation of the overpack for the HAC bottom-oblique drop and top-oblique drop tests is performed using the ANSYS LS-DYNA PC finite element code and the 3-D half-symmetry finite element model described in Section 2.6.7.1. As discussed in Section 2.7.1, HAC drop analyses are performed for "cold" thermal conditions using the upper-bound strength properties of the overpack materials and the lower-bound mass of the cask assembly to determine the maximum cask rigid-body accelerations for use in the cask stress analysis, and for "hot" thermal conditions using the lower-bound strength properties of the overpack material and the upper-bound mass of the cask to determine the maximum possible crush of the overpack foam.

Each HAC oblique drop time-history analysis is started at the moment of initial contact between the package's outer surface and the impact surface. An initial vertical velocity of 13.29 m/s, corresponding to a free-fall velocity from a height of 9 m, and a constant gravitational acceleration of 9.81 m/s^2 are applied to the package. Each HAC oblique drop time-history analysis is performed for a duration that is sufficient to capture both the primary and secondary impact.

The maximum crush depth of the overpack foam (as a percentage of the total foam thickness) and the maximum peak rigid-body accelerations resulting from each of the HAC bottom-end oblique drop and top-end oblique drop tests are summarized in Table 2-49 and Table 2-50, respectively. The maximum foam crush resulting from the full range of HAC bottom-end oblique drop tests analyzed is 61% from the HAC hot 5° bottom-end oblique drop (Case H12). The maximum foam crush resulting from the full range of HAC top-end oblique drop tests analyzed is 57% from the HAC hot 5° top-end oblique drop (Case H20). The maximum foam crush due to all HAC bottom- and top-end oblique drop tests is within the acceptable crush range for the overpack foam material. Therefore, the overpack will not experience excessive deformation that would allow the cask to "bottom-out" under the most severe HAC oblique drop conditions. The extent of permanent damage to the overpack assembly resulting from the HAC oblique drop tests is discussed in Section 2.7.1.5.

As shown in Table 2-49, the HAC bottom-end oblique drop primary impacts produce the highest transverse accelerations at the cask bottom end, while the secondary impacts produce the highest transverse accelerations at the cask top end. The magnitude of the peak transverse acceleration resulting from the secondary impact is higher than that due to the primary impact in all cases. The highest transverse peak rigid-body acceleration of the cask for all HAC bottom-end oblique drop tests is 985*g* for the HAC cold 15° bottom-end oblique drop (Case H15). The highest

longitudinal peak rigid-body acceleration of the cask for all HAC bottom-end oblique drop tests is +433*g* for the HAC cold 20° bottom-end oblique drop (Case H17). This maximum peak longitudinal acceleration also occurs during the slapdown impact.

As shown in Table 2-50, HAC top-end oblique drop primary impacts produce the highest transverse accelerations at the cask top end, while the secondary impacts produce the highest transverse accelerations at the cask bottom end. The magnitude of the peak transverse acceleration resulting from the primary impact is higher than that due to the secondary impact in all cases. The highest transverse peak rigid-body acceleration of the cask assembly for all HAC top-end oblique drop tests is -898*g* for the HAC cold 15° top-end oblique drop (Case H23). The highest longitudinal peak rigid-body acceleration of the cask for all HAC top-end oblique drop tests is -258*g* for the HAC cold 20° top-end oblique drop (Case H25) secondary impact.

The maximum shear stress and maximum axial strain in the overpack closure bolts resulting from each HAC bottom-corner and top-corner drop tests are summarized in Table 2-51. The maximum shear stresses in the overpack closure bolts for each HAC oblique drop test are evaluated in accordance with the Service Level D allowable-stress design criteria for Class 2 supports from Subsection NF of the ASME Code. As discussed in Section 2.1.2.2, the maximum axial strain in the overpack closure bolts under HAC loading is limited to 16% (i.e., the maximum specified elongation of the overpack closure bolt A320, Grade L43 bolting material) to assure that the overpack bolts do not experience any gross failure. The minimum design margin in the overpack closure bolts for the HAC oblique drop is +0.45 due to the maximum axial strain resulting from the HAC cold 20° top-oblique drop (Case H25). Thus, the overpack closure bolts satisfy the applicable structural design criteria for the HAC oblique drop tests.

2.7.1.4.2 Cask Stress Evaluation

The stresses in the cask and shield lid resulting from the HAC bottom-oblique drop and HAC top-oblique drop loads are determined using equivalent-static linear-elastic finite element analysis methods. The equivalent-static acceleration load for each HAC oblique drop test is equal to the peak rigid-body acceleration of the cask multiplied by a DLF that accounts for possible dynamic amplification within the cask. As discussed in Section 2.12.3, a bounding DLF of 1.13 is conservatively used for all HAC oblique drop evaluations.

As shown in Table 2-49 and Table 2-50, the cask peak rigid-body acceleration loads due to the HAC cold oblique drop conditions are much higher than those due to the HAC hot oblique drop conditions. Thus, bounding equivalent-static-acceleration loads are calculated based on the peak rigid-body accelerations resulting from the HAC cold oblique drops.

As shown in Table 2-49, the HAC bottom oblique drop primary impacts produce the highest transverse rigid-body acceleration load at the bottom end of the cask, with a maximum value of -553*g* for the 20° drop orientation (case H17). The HAC bottom oblique drop secondary impacts produce the highest transverse rigid-body acceleration load at the top end of the cask, with a maximum value of -985*g* for the 15° drop orientation (case H15). Based upon the relative magnitudes of the primary and secondary impact acceleration loads, the cask stresses due to the HAC bottom oblique drop secondary impact are expected to bound those due to the primary

impact. A bounding HAC bottom oblique drop stress analysis is performed using transverse and longitudinal accelerations that envelope the secondary impact loads for all HAC bottom oblique drop orientations. These include a transverse acceleration load that varies linearly from -985*g* at the top end of the cask to -437*g* at the cask mid-length, and a longitudinal acceleration of +444*g*. Multiplying these values by the bounding DLF of 1.13 results in a transverse equivalent-static acceleration load that varies from -1,113*g* at the cask top end to -494*g* at the cask mid-length, and a longitudinal equivalent static acceleration load of +489*g*. The HAC bottom oblique drop stress analysis of the cask is performed using a bounding transverse acceleration load that varies linearly from -1,120*g* at the cask top end to -560*g* at the cask mid-length, and a longitudinal equivalent static acceleration load of +490*g*.

As shown in Table 2-50, the HAC top oblique drop primary impacts produce the highest transverse rigid-body acceleration load at the top end of the cask, with a maximum value of -898*g* for the 15° drop orientation (case H23). The HAC top oblique drop secondary impacts produce the highest transverse rigid-body acceleration load at the bottom end of the cask, with a maximum value of -592*g* for the 15° drop orientation (case H23). Based upon the relative magnitudes of the primary and secondary impact acceleration loads, the cask stresses due to the HAC top oblique drop primary impact are expected to bound those due to the secondary impact. A bounding HAC top oblique drop stress analysis is performed using transverse and longitudinal accelerations that envelope the secondary impact loads for all HAC top oblique drop orientations. These include a transverse acceleration load that varies linearly from -898*g* at the top end of the cask to -519*g* at the cask mid-length, and a longitudinal acceleration of -258*g*. Multiplying these values by the bounding DLF of 1.13 results in a transverse equivalent-static acceleration load that varies from -1,015*g* at the cask top end to -586*g* at the cask mid-length, and a longitudinal equivalent static acceleration load of -292*g*. The HAC top oblique drop stress analysis of the cask is performed using a bounding transverse acceleration load that varies linearly from -1,015*g* at the cask top end to -590*g* at the cask mid-length, and a longitudinal equivalent static acceleration load of -340*g*.

The stresses in the cask and shield lid due to the bounding HAC bottom oblique drop and top oblique drop loads are determined using the 3-D half-symmetry finite element model described in Section 2.6.7.2. The finite element model boundary conditions used for the HAC top and bottom oblique drop stress analyses are the same as those used for the NCT top and bottom corner drop stress analyses, as described in Section 2.6.7.2. Also, the loading due to the HAC top and bottom oblique drops is applied to the finite element model in the same manner as the loads for the NCT top and bottom oblique drop stress analysis, as described in Section 2.6.7.2. As discussed in Section 2.7.1, bolt preload and internal pressure loads are evaluated in combination with the HAC oblique drop loading per the following load combinations:

H11-18-A: HAC Bottom Oblique Drop + Bolt Preload

H11-18-B: HAC Bottom Oblique Drop + Bolt Preload + Maximum Internal Pressure

H19-26-A: HAC Top Oblique Drop + Bolt Preload

H19-26-B: HAC Top Oblique Drop + Bolt Preload + Maximum Internal Pressure

For all load combinations, the maximum bolt preload of 7.2 kN per bolt is applied to the closure bolt elements on a 360° basis, producing a total preload (for eight closure bolts) of 57.8 kN on the closure lid. For load combinations H11-18-B and H19-26-B, the maximum internal pressure load of 700 kPa gauge is applied to the inner surfaces of the cask's containment boundary. On the impacted end and side of the cask cavity, this pressure load is added to the applied pressures that account for the payload inertial loads due to the transverse and longitudinal accelerations. In addition, a uniform temperature of 75°C is applied to the model for all HAC oblique drop analyses to account for the cask's material properties at elevated temperature.

The maximum stress intensities in the cask's containment system and non-containment components from the bounding HAC bottom oblique drop and bounding HAC top oblique drop finite element analyses, along with the corresponding allowable stress intensities and minimum design margins, are summarized in Table 2-52 and Table 2-53, respectively. The minimum design margin for the bounding HAC bottom oblique drop is +0.20 for local membrane stress intensity (P_l) occurring in the cask containment shell (section C7 in Figure 2-1). The minimum design margin for the bounding HAC top oblique drop is +0.69 for primary membrane stress intensity (P_m) in the shield lid shear lip (section N19 in Figure 2-2). The results of the bounding HAC oblique drop stress evaluations show that the stresses in the cask and shield lid satisfy the applicable HAC allowable-stress design criteria of the ASME Code.

To prevent inelastic deformation of the cask's containment system closure, the maximum stresses in the cask flange and closure lid in the region of the containment O-ring seal are limited to the yield strength of the cask material. The maximum stress intensity in the cask's closure seal region due to the bounding HAC top oblique drop loading is 179 MPa. This is less than the 184 MPa yield strength of the cask-body stainless steel material at the upper-bound design temperature of 74°C. Therefore, the bounding HAC top oblique drop will not cause any plastic deformation in the region of the containment O-ring seal.

As discussed in Section 2.1.2.5, the DU alloy material used for the cask gamma shield components is not expected to experience brittle fracture failure if it does not undergo substantial plastic deformation. Therefore, the maximum stresses in the cask gamma shield are limited to the yield strength of the DU alloy material. The maximum stress intensity in the cask-body DU shields due to the bounding HAC top oblique drop, which is highly localized and occurs on the impacted side of the cask-body bottom DU shield, is 162 MPa. This stress is much less than the 380 MPa yield strength of DU at an upper-bound temperature of 93°C. Therefore, the bounding HAC top oblique drop is not expected to cause any plastic deformation or brittle fracture failure of the cask-body DU shields.

2.7.1.4.3 Cask Shell Buckling Evaluation

A buckling evaluation of the cask's containment shell and outer shell is performed for the HAC oblique drop tests in accordance with the requirements of ASME Code Case N-284-1 [2.7]. The maximum compressive stresses and shear stresses near the mid-lengths of the cask's inner shell and outer shell (i.e., Sections C5 and N5 in Figure 2-1 and Figure 2-2) are used for the cask-shell buckling evaluation. As discussed in Section 2.1.2.3, elastic and inelastic buckling interaction

ratios are calculated based on the HAC allowable buckling stresses shown in Table 2-7, which include a factor of safety of 1.34. The maximum interaction ratios must not exceed 1.0.

The maximum calculated cask-shell stresses and the resulting maximum buckling interaction ratios for the HAC bottom oblique drop and HAC top oblique drop tests are summarized in Table 2-46. The maximum buckling interaction ratios in the cask's inner and outer shells, calculated using the bounding shell stresses for the HAC bottom oblique drop (cases H11-16-A and –B) and HAC top oblique drop (cases H17-22-A and -B), are 0.21 and 0.70, respectively. Therefore, the cask satisfies the buckling design criteria of ASME Code Case N-284-1 for the HAC oblique drop test.

Table 2-49 – HAC Bottom Oblique Drop Loads Summary

HAC Drop Case I.D.	Case Description[1]	Maximum Overpack Foam Crush[2]	Cask Peak Rigid-Body Accelerations[3]		
			Transverse		
			Top	Bottom	Longitudinal
H11	Cold 5° Bottom Oblique Drop - Primary Impact - Secondary Impact	27%	+87g -853g	-503g -20g	+30g +75g
H12	Hot 5° Bottom Oblique Drop - Primary Impact - Secondary Impact - Tertiary Impact	61%	-39g -438g +51g	-215g -101g -260g	+8g +18g +19g
H13	Cold 10° Bottom Oblique Drop - Primary Impact - Secondary Impact	28%	+100g -920g	-513g +109g	+54g +208g
H14	Hot 10° Bottom Oblique Drop - Primary Impact - Secondary Impact	44%	+31g -595g	-272g +26g	+38g +104g
H15	Cold 15° Bottom Oblique Drop - Primary Impact - Secondary Impact	26%	+118g -985g	-543g +262g	+87g +361g
H16	Hot 15° Bottom Oblique Drop - Primary Impact - Secondary Impact	43%	+98g -599g	-277g +73g	+56g +178g
H17	Cold 20° Bottom Oblique Drop - Primary Impact - Secondary Impact	33%	+106g -898g	-553g +89g	+118g +433g
H18	Hot 20° Bottom Oblique Drop - Primary Impact - Secondary Impact	36%	+48g -515g	-184g +27g	+32g +169g

Notes:
1. Impact orientations are shown in Figure 2-16.
2. Value is equal to the maximum deformation divided by the nominal foam thickness in the corresponding direction.
3. Accelerations reported at the time that the peak transverse rigid-body acceleration is reached.

Table 2-50 – HAC Top Oblique Drop Loads Summary

HAC Drop Case I.D.	Case Description[1]	Maximum Overpack Foam Crush[2]	Cask Peak Rigid-Body Accelerations[3]		
			Transverse		
			Top	Bottom	Longitudinal
H19	Cold 5° Top Oblique Drop - Primary Impact - Secondary Impact	26%	-801g +174g	-106g -536g	-45g -107g
H20	Hot 5° Top Oblique Drop - Primary Impact - Secondary Impact	57%	-495g +45g	-22g -311g	-40g -49g
H21	Cold 10° Top Oblique Drop - Primary Impact - Secondary Impact	24%	-853g 90g	-113g -463g	-103g -86g
H22	Hot 10° Top Oblique Drop - Primary Impact - Secondary Impact	45%	-513g +50g	-17g -261g	-45g -68g
H23	Cold 15° Top Oblique Drop - Primary Impact - Secondary Impact	21%	-898g +209g	-114g -592g	-126g +124g
H24	Hot 15° Top Oblique Drop - Primary Impact - Secondary Impact	38%	-500g +49g	-27g -221g	-79g -73g
H25	Cold 20° Top Oblique Drop - Primary Impact - Secondary Impact	23%	-889g +126g	-148g -493g	-157g -258g
H26	Hot 20° Top Oblique Drop - Primary Impact - Secondary Impact	37%	-477g +62g	-27g -247g	-85g +74g

Notes:
1. Impact orientations are shown in Figure 2-16.
2. Value is equal to the maximum deformation divided by the nominal foam thickness in the corresponding direction.
3. Accelerations reported at the time that the peak transverse rigid-body acceleration is reached.

Table 2-51 – Overpack Closure-Bolt HAC Oblique Drop Stress Summary

HAC Drop Case I.D.	Case Description[1]	Maximum Shear Stress (MPa)	Maximum Axial Strain	Minimum Bolt Design Margin[2]
H11	Cold 5° Bottom Oblique Drop	107	1.5%	+2.38
H12	Hot 5° Bottom Oblique Drop	97	0.6%	+2.73
H13	Cold 10° Bottom Oblique Drop	113	1.2%	+2.20
H14	Hot 10° Bottom Oblique Drop	101	3.0%	+2.58
H15	Cold 15° Bottom Oblique Drop	116	6.2%	+1.58
H16	Hot 15° Bottom Oblique Drop	104	2.4%	+2.48
H17	Cold 20° Bottom Oblique Drop	169	4.9%	+1.14
H18	Hot 20° Bottom Oblique Drop	95	1.9%	+2.81
H19	Cold 5° Top Oblique Drop	87	1.0%	+3.16
H20	Hot 5° Top Oblique Drop	74	0.7%	+3.89
H21	Cold 10° Top Oblique Drop	107	2.8%	+2.38
H22	Hot 10° Top Oblique Drop	97	0.8%	+2.73
H23	Cold 15° Top Oblique Drop	120	7.4%	+1.16
H24	Hot 15° Top Oblique Drop	93	1.8%	+2.89
H25	Cold 20° Top Oblique Drop	132	11.0%	+0.45
H26	Hot 20° Top Oblique Drop	107	4.0%	+2.38

Notes:
1. Impact orientations are shown in Figure 2-16.
2. The minimum design margin is calculated as (Allowable Value/Maximum Value) – 1, where the allowable shear stresses for A320, Grade L43 bolting steel at an upper-bound temperature of 93°C is 362 MPa, and the allowable axial strain is equal to the maximum elongation of A320, Grade L43 bolting steel (i.e., 16%).

Table 2-52 – HAC Bottom Oblique Drop Maximum Stress Summary

Cask Components	Stress Type	Maximum Stress Intensity (MPa)	Controlling Load Combination & Location[1]	Allowable Stress Intensity[2] (MPa)	Minimum Design Margin[3]
Containment System	P_m	227	H11-16-B, C8, 30°	331	+0.46
	P_l	409	H11-16-B, C7, 67.5°	492	+0.20
	P_m+P_b	320	H11-16-A, C11, 37.5°	492	+0.54
	P_m+P_b+Q	624	H11-16-B, C7, 67.5°	N/A[4]	N/A[4]
Non-Containment Components	P_m	159	H11-16-A, N13, 60°	221	+0.39
	P_l	247	H11-16-A, N2, 37.5°	332	+0.34
	P_m+P_b	209	H11-16-A, N19, 22.5°	332	+0.59
	P_m+P_b+Q	334	H11-16-B, N12, 37.5°	N/A[4]	N/A[4]

Notes:
1. The load combination and the location of the maximum stress intensity (section number and circumferential location) is identified. Load combinations H11-16-A and H11-16-B are defined in Section 2.7.1.4.2. Containment system and non-containment component stress locations are shown in Figure 2-1 and Figure 2-2, respectively. The circumferential location is identified with 0° at the side of impact and 180° opposite the side of impact.
2. Allowable stress intensities are based on an upper-bound design temperature of 74°C.
3. Design margin is calculated as (Allowable S.I./Maximum S.I) – 1.
4. Evaluation of secondary stress is not required for HAC.

Table 2-53 – HAC Top Oblique Drop Maximum Stress Summary

Cask Components	Stress Type	Maximum Stress Intensity (MPa)	Controlling Load Combination & Location[1]	Allowable Stress Intensity[2] (MPa)	Minimum Design Margin[3]
Containment System	P_m	145	H19-26-A, C11, 30°	331	+1.28
	P_l	287	H19-26-A, C14, 0°	492	+0.71
	P_m+P_b	213	H19-26-A, C11, 37.5°	492	+1.31
	P_m+P_b+Q	402	H19-26-B, C17, 0°	N/A[4]	N/A[4]
Non-Containment Components	P_m	131	H19-26-A, N19, 22.5°	221	+0.69
	P_l	151	H19-26-A, N3, 0°	332	+1.20
	P_m+P_b	192	H19-26-A, N19, 22.5°	332	+0.73
	P_m+P_b+Q	221	H19-26-A, N3, 0°	N/A[4]	N/A[4]

Notes:
1. The load combination and the location of the maximum stress intensity (section number and circumferential location) is identified. Load combinations H17-22-A and H17-22-B are defined in Section 2.7.1.4.2. Containment system and non-containment component stress locations are shown in Figure 2-1 and Figure 2-2, respectively. The circumferential location is identified with 0° at the side of impact and 180° opposite the side of impact.
2. Allowable stress intensities are based on an upper-bound design temperature of 74°C.
3. Design margin is calculated as (Allowable S.I./Maximum S.I) – 1.
4. Evaluation of secondary stress is not required for HAC.

Table 2-54 – HAC Oblique Drop Buckling Evaluation Summary

Load Case I.D.	Inner Shell[1]				Outer Shell[2]			
	Maximum S.I.[3] (kPa)			Maximum Buckling IR	Maximum S.I.[3] (kPa)			Maximum Buckling IR
	Hoop	Axial	Shear		Hoop	Axial	Shear	
H11-18-A	2,503	19,465	15,170	---	34,744	80,332	20,216	---
H11-18-B	[4]	21,578	15,214	---	36,237	76,112	20,965	---
Bounding Values	2,503	21,578	15,214	0.21	36,237	80,332	20,965	0.70
H19-26-A	1,924	16,108	14,447	---	27,778	31,634	17,378	---
H19-26-B	[4]	10,729	5,861	---	28,131	34,082	17,370	---
Bounding Values	1,924	16,108	14,447	0.16	28,131	34,082	17,378	0.32

Notes:
1. Maximum stress intensities at section C5 in Figure 2-1.
2. Maximum stress intensities at section N5 in Figure 2-2.
3. The maximum compressive axial and hoop stress intensities and maximum in-plane shear stress intensities from load combinations "-A" and "-B" are reported.
4. Zero stress is assumed for the buckling evaluation since all stresses are tensile.

2.7.1.5 Summary of Results

The structural evaluation of the package for the HAC free drop test of §71.73(c)(1) shows that the applicable structural design criteria is satisfied for all cases analyzed. The HAC free drop does not cause any significant permanent deformation in the cask and shield lid. Furthermore, no inelastic deformation of the cask's closure bolts and containment sealing surfaces results from the HAC free drop tests analyzed. The only significant package damage resulting from the HAC free drop occurs in the overpack. The overpack damage resulting from each HAC free drop position is described as follows:

HAC End Drop

The permanently deformed shape of the overpack following the HAC hot bottom-end drop (Case H2) and HAC hot top-end drop (Case H4) is shown in Figure 2-22 and Figure 2-23, respectively. The HAC hot bottom-end drop results in a permanent deformation of the overpack base inner shell and foam toward the bottom end of approximately 45 mm, but no significant permanent deformation in the overpack lid. As shown in Figure 2-22, this results in the formation of a conical-shaped gap at the top of the overpack base leading into the overpack cavity. As shown in Figure 2-23, the HAC hot top-end drop results in a permanent deformation of the overpack lid inner shell and foam of approximately 56 mm over the entire cask diameter, but only minor permanent deformation in the overpack-base inner shell. This deformation creates additional air space at the interface between the overpack base and lid. The overpack deformation resulting from the HAC bottom-end drop and HAC top-end drop is considered in the package HAC thermal evaluation.

HAC Side Drop

The HAC hot side drop (case H10) results in the maximum damage to the overpack. The permanently deformed shape of the overpack following the HAC hot side drop is shown in Figure 2-24. It shows that the overpack-base side-wall foam crush on the impacted side ranges from approximately 35 mm at the top end of the overpack cavity to approximately 58 mm at the bottom end of the overpack cavity. Because the overpack crush is primarily inside-out, a gap forms between the overpack-base foam core and overpack-base inner shell the at the bottom end of the overpack cavity on the side opposite impact. The only significant damage to the overpack exterior surfaces occurs near the impacted portions of the overpack tie-down flange and bolting flange. As shown in Figure 2-24, a slight indentation of the flanges occurs on the side of impact. The overpack deformation resulting from the HAC side drop is considered in the package HAC thermal evaluation.

HAC Corner Drop

The permanently deformed shape of the overpack following the HAC hot bottom-corner drop (Case H6) is shown in Figure 2-25. The overpack base tie-down flange is permanently bent upward and the tie-down flange lug is permanently pushed into the overpack-base outer shell. The foam sidewall thickness in the region directly behind the overpack base lug is reduced from

104.5 mm to approximately 30 mm. The HAC hot bottom-corner drop also results in a permanent longitudinal shift of the overpack-base inner shell of approximately 15 mm toward the bottom end of the package. In addition, a gap of approximately the same size is formed around the entire circumference of the overpack-cavity top end due to this longitudinal shift. As shown in Figure 2-25, small gaps are also developed between the overpack foam core and the inner and outer shells at the bottom end of the package due to elastic spring-back effects in the overpack shells.

The permanently deformed shape of the overpack following the HAC hot top-corner drop (Case H8) is shown in Figure 2-26. The most significant damage to the package resulting from the HAC hot top-corner drop occurs in the local vicinity of the impacted overpack lid lug, which is permanently crushed into the overpack lid foam core. As discussed above, the region of maximum crush in the overpack lid foam core due to the HAC hot top-corner drop impact is very localized. The HAC hot top-corner drop impact also results in a permanent depression of the overpack lid inner shell of approximately 45 mm toward the top end of the package. In addition, the outermost portion of the lid lug (i.e., the material outside the lug hole) is shown to reach the ultimate strain, causing local failure.

HAC Oblique Drop

As discussed in Section 2.7.1.4.1, the maximum foam crush depths for the HAC oblique drop result from the HAC hot 5° bottom-end oblique drop (Case H12) and the HAC hot 5° top-end oblique drop (Case H20). These two cases also cause the greatest extent of permanent damage to the overpack for all HAC oblique drops evaluated.

The permanently deformed shape of the overpack resulting from the HAC hot 5° bottom-end oblique drop (Case H12) is shown in Figure 2-27. The HAC hot 5° bottom-end oblique drop causes damage to both the internal and external surfaces of the overpack on the impacted side of the package, with the maximum damage occurring at the bottom end of the overpack cavity. The most significant damage to the overpack due the HAC hot 5° bottom-end oblique drop results from inside-out crush. This is most evident at the bottom end of the overpack cavity where the sidewall foam crush is highest. The permanent crush of the overpack sidewall foam is approximately 40 mm at the top end of the overpack cavity and 60 mm at the bottom end of the overpack cavity. As shown in Figure 2-27, a large air gap is also developed between the overpack foam core and inner shell on the side opposite impact at the bottom end of the overpack cavity.

The permanently deformed shape of the overpack resulting from the HAC hot 5° top-end oblique drop (Case H20) is shown in Figure 2-28. The HAC hot 5° top-end oblique drop causes damage to both the internal and external surfaces of the overpack on the impacted side of the package, with the maximum damage occurring at the top end of the overpack cavity. The most significant damage to the overpack due the HAC hot 5° top-end oblique drop results from inside-out crush at the top end of the overpack cavity on the side of impact. The permanent crush of the overpack sidewall foam resulting from the HAC hot 5° top-end oblique drop (Case H20) is less than 44 mm over the entire length of the overpack cavity.

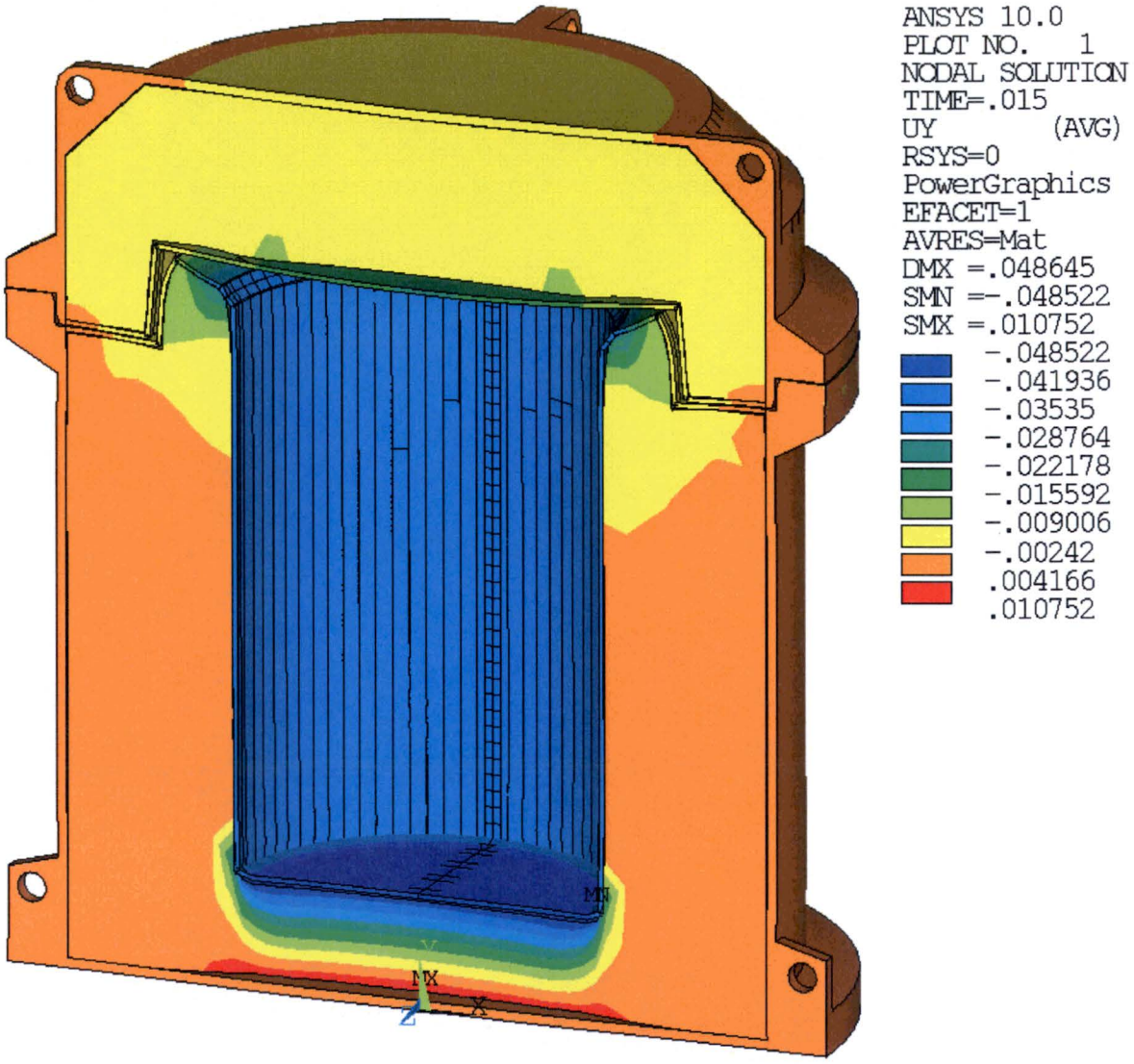

(Notes: Displacement units are meters. Deformed shape shown at 1:1 scale)

Figure 2-22 – Overpack Permanent Deformation, HAC Hot Bottom-End Drop (Case H2)

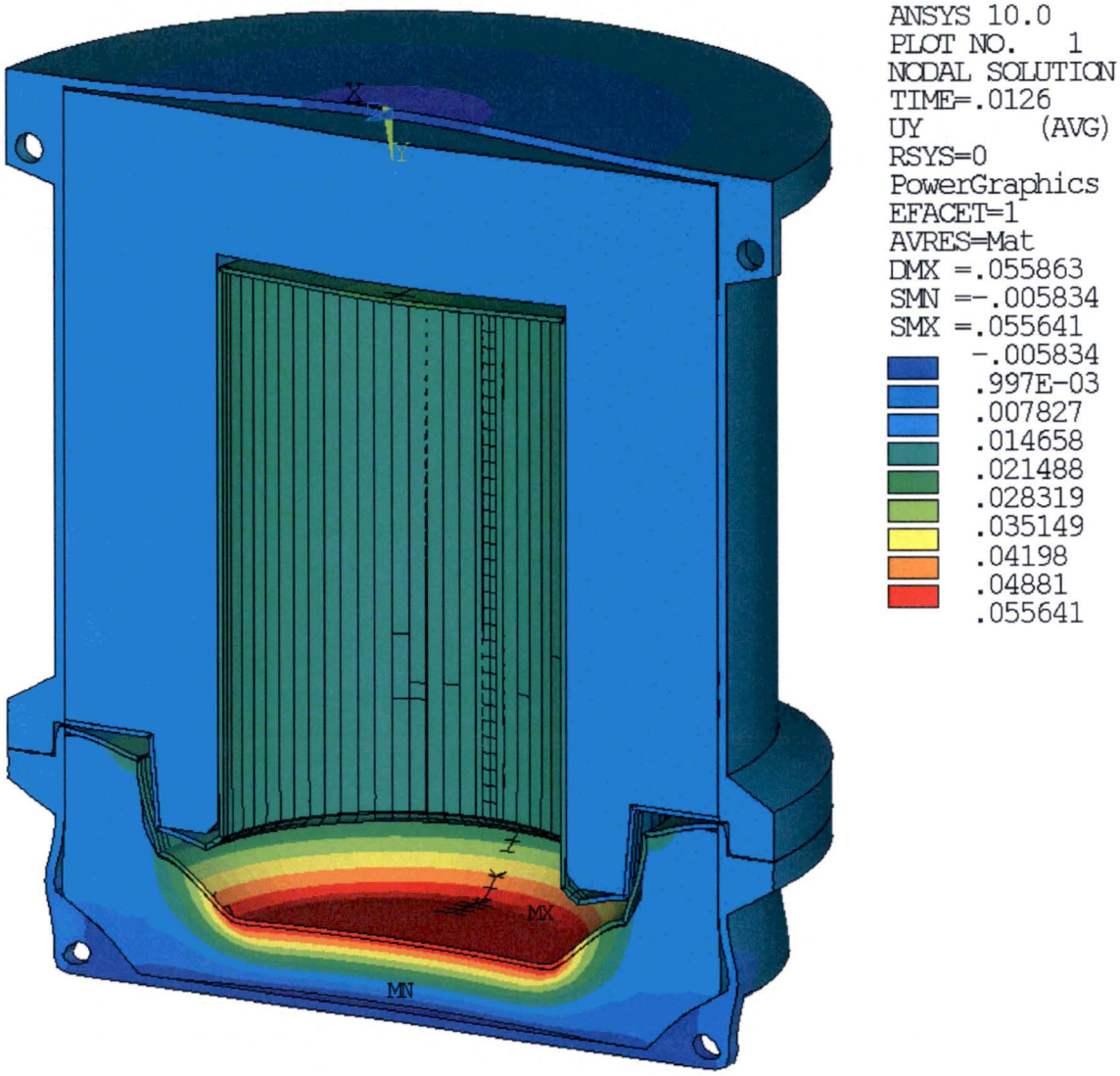

(Notes: Displacement units are meters. Deformed shape shown at 1:1 scale)

Figure 2-23 – Overpack Permanent Deformation, HAC Hot Top-End Drop (Case H4)

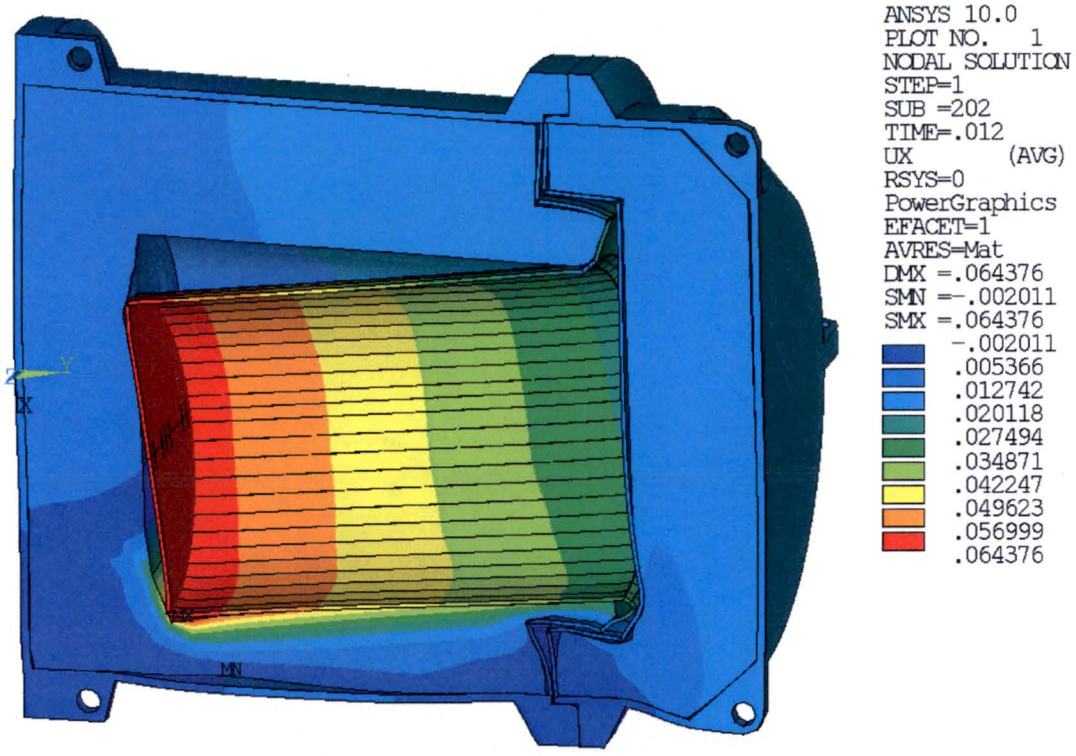

(Notes: Displacement units are meters. Deformed shape shown at 1:1 scale)

Figure 2-24 – Overpack Permanent Deformation, HAC Hot Side Drop (Case H10)

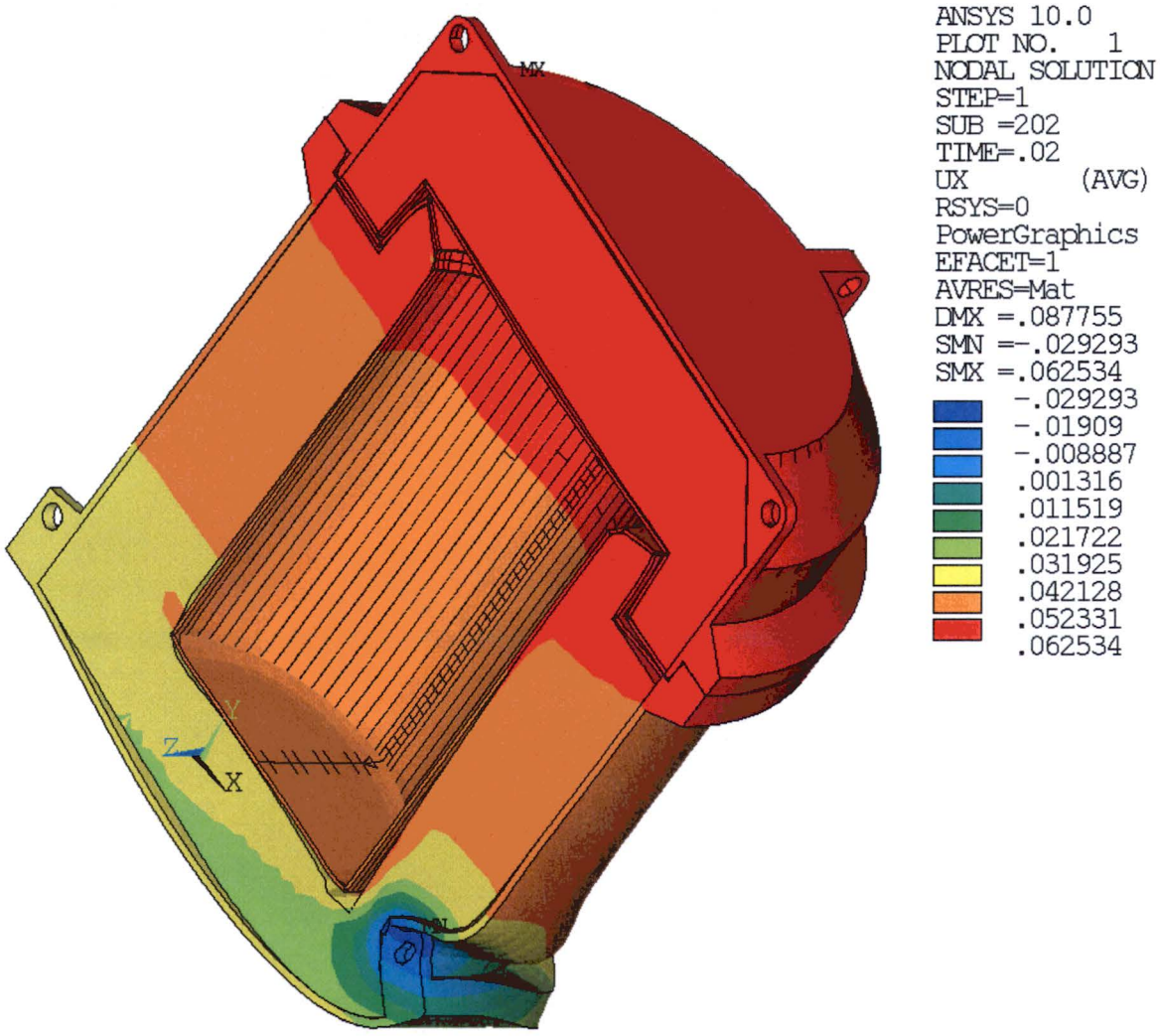

(Notes: Displacement units are meters. Deformed shape shown at 1:1 scale)

Figure 2-25 – Overpack Permanent Deformation, HAC Hot Bottom-Corner Drop (Case H6)

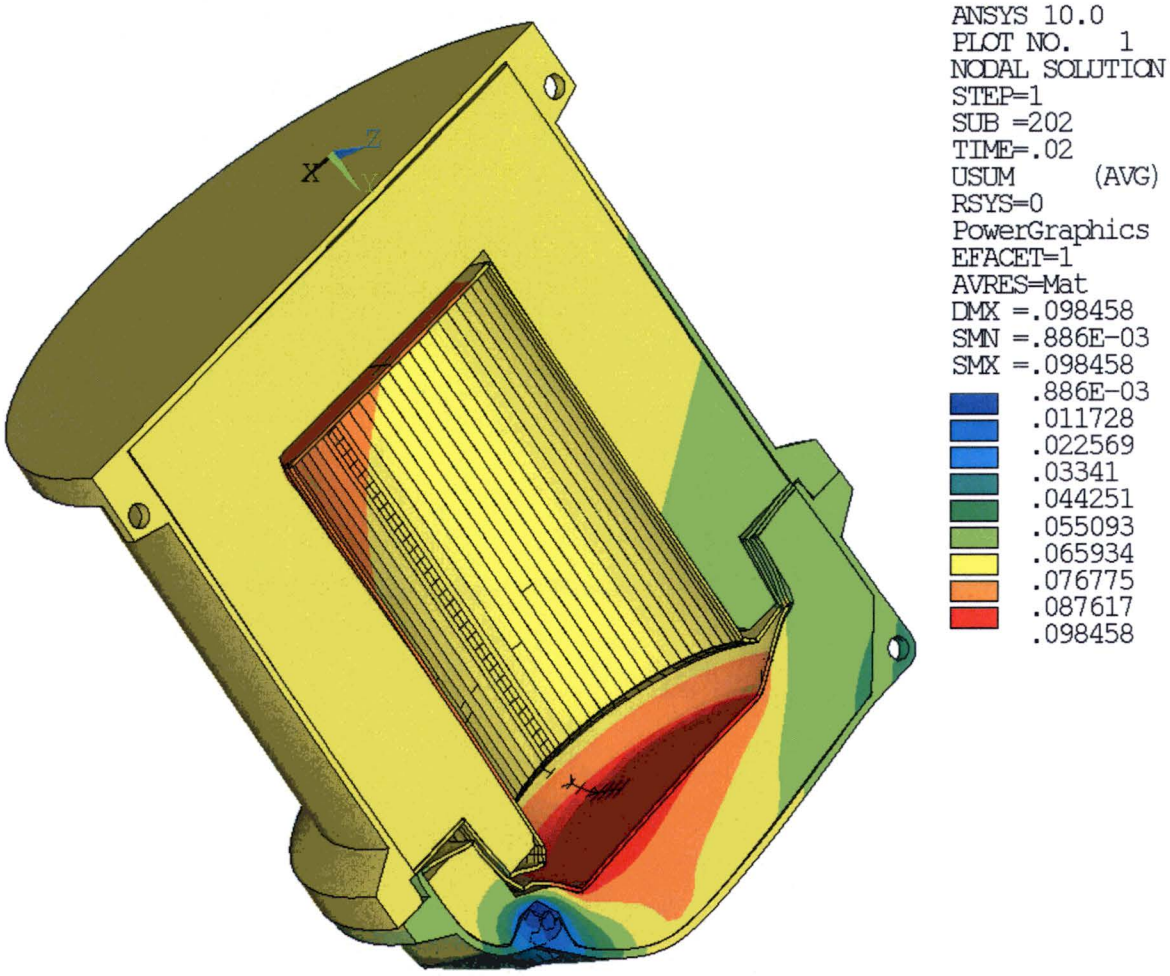

(Notes: Displacement units are meters. Deformed shape shown at 1:1 scale)

Figure 2-26 – Overpack Permanent Deformation, HAC Hot Top-Corner Drop (Case H8)

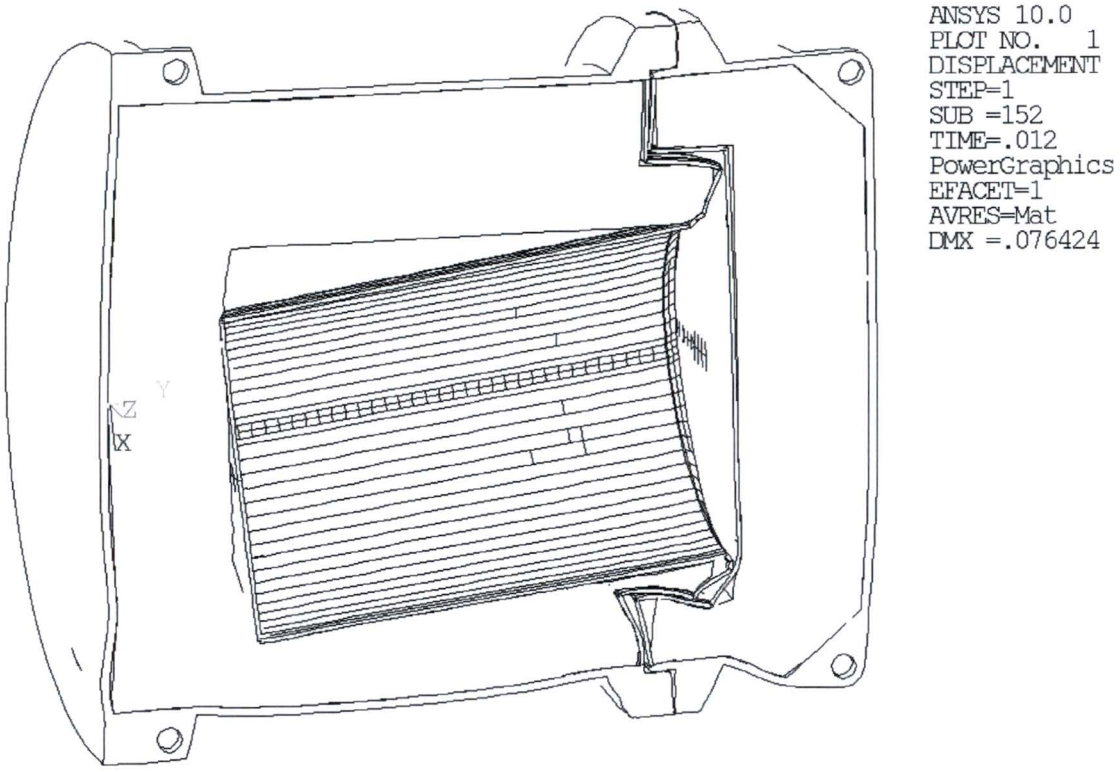

(Note: Deformed shape shown at 1:1 scale)

Figure 2-27 – Overpack Permanent Deformation, HAC Hot 5° Bottom-End Oblique Drop (Case H12)

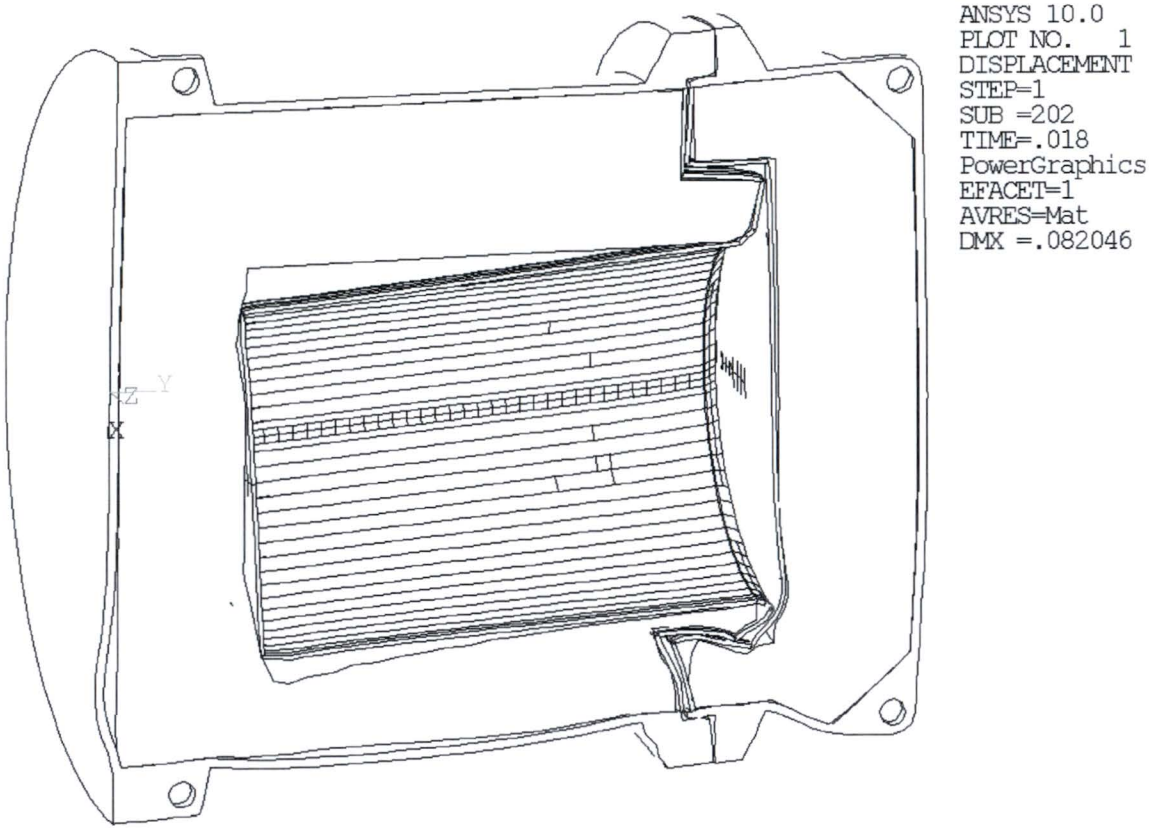

(Note: Deformed shape shown at 1:1 scale)

Figure 2-28 – Overpack Permanent Deformation, HAC Hot 5° Top-End Oblique Drop (Case H20)

2.7.2 Crush

The crush test of §71.73(c)(2) is required only when the specimen has a mass not greater than 500 kg (1,100 lb), an overall density not greater than 1,000 kg/m^3 (62.4 lb/ft^3) based on external dimensions, and radioactive contents greater than 1,000 A_2 not as a special form radioactive material. The A_2 value for ^{99}Mo is 16 Ci per Table A-1 of 10 CFR 71. Therefore, the crush test is required only if the maximum activity of the radioactive contents is greater than 16,000 Ci. Since the maximum activity of the product is limited to a maximum of 4,400 Ci, the crush test is not applicable.

2.7.3 Puncture

In accordance with §71.73(c)(3), the package is evaluated for "*a free drop through a distance of 1 m (40 in) in a position for which maximum damage is expected, onto the upper end of a solid, vertical, cylindrical, mild steel bar, mounted on an essentially unyielding horizontal surface. The bar must be 15 cm (6 in) in diameter, with the top horizontal and its edge rounded to a radius of not more than 6 mm (0.25 in), and a length as to cause maximum damage to the package, but not less than 20 cm (8 in) long.*" The puncture drop test is performed in sequence following the HAC free drop test in accordance with §71.73(a). Therefore, the package damage resulting from the HAC free drop is considered in the HAC puncture drop evaluation. The maximum extent of damage sustained by the overpack for each HAC free drop orientation is discussed in Section 2.7.1.5.

When subjected to the HAC puncture drop test, the outer shell of the overpack is designed to prevent penetration or perforation by the puncture bar. The maximum damage to the overpack and the greatest potential for penetration or perforation of the overpack outer shell exists under initial conditions for which the outer shell material and foam core material is weakest. Therefore, the HAC puncture drop analysis is performed using the overpack material lower-bound strength properties for the "hot" initial conditions (i.e., an ambient temperature of 38°C, maximum decay heat, and insolation) and an upper-bound cask mass of 207 kg. Since damage to the overpack foam core material (i.e., crushing) resulting from the HAC free drop generally results in local densification that effectively increases the foam crush strength, a subsequent HAC puncture drop impact on a damaged portion of the overpack would have less potential for maximum damage than the same HAC puncture drop with an undamaged package. Therefore, the HAC puncture drop analyses are performed with an undamaged overpack since it is expected to cause maximum damage.

Six HAC puncture drop orientations for which maximum damage is expected are considered in the evaluation of the package, as summarized in Table 2-55 and illustrated in Figure 2-29. These include three "center" impact orientations and three "oblique" impact orientations that are expected to cause maximum damage to the package. Each center impact orientation has the package center of gravity located directly over the centerline of the puncture bar and results in the outer surface of the overpack striking the top flat surface of the puncture pin. Each oblique impact orientation has the package center of gravity located directly over the struck corner of the puncture bar to impart maximum impact energy to the package.

The HAC puncture drop impact analysis are performed using the LS-DYNA finite element model described in Section 2.6.7.1. As discussed above, the HAC puncture drop analysis is performed using the overpack material lower-bound strength properties for the "hot" thermal condition and an upper-bound cask mass of 207 kg. In addition, a single puncture drop impact analysis is performed for the "cold" thermal condition with upper-bound material strength properties and lower-bound cask weight (Case P3B). This case is evaluated primarily to determine the highest peak rigid-body acceleration of the cask resulting from the top-end puncture drop impact for use in the cask closure bolt evaluation.

Each HAC puncture drop time-history analyses is started at or near the moment of initial contact between the package's outer surface and the top surface of the puncture bar. An initial vertical velocity of 4.43 m/s, corresponding to a free-fall velocity from a height of 1 m, is applied to the package in all cases. The time-history analysis durations used for the puncture drop impacts are sufficient to capture the entire duration of the primary impact between the package and puncture bar.

The maximum overpack foam crush, maximum total strain in the overpack shell, and peak rigid-body cask acceleration loads resulting from the HAC puncture drop orientations analyzed are summarized in Table 2-56. The overpack satisfies the applicable design criteria for the HAC puncture drop orientations expected to cause maximum damage. The maximum foam crush of 38%, resulting from the HAC hot top-oblique puncture drop (Case P4), is within the acceptable crush range for the foam material. The highest strain in the overpack outer shell for all HAC puncture drop impact orientations considered is 23% (Case P6), which is lower than the lowest maximum elongation (30%) of the overpack shell material. Therefore, the HAC puncture drop will not cause perforation or penetration of the overpack outer shell. The highest peak rigid-body longitudinal acceleration of 139*g* results from the HAC cold top-center puncture drop (Case P3B). As expected, the highest peak rigid-body cask accelerations due to the HAC puncture drop conditions are much lower than those resulting from the HAC free drop conditions.

Table 2-57 summarizes the maximum shear stress, maximum total strain intensity, and minimum design margins for the most heavily loaded overpack closure bolt in each HAC puncture drop analysis. The results show that the maximum total strain intensity in the most heavily loaded bolt never exceeds the yield strain (0.37%) of the overpack closure bolt A320, Grade L43 material at an upper-bound design temperature of 93°C. Therefore, the overpack closure bolts will not experience any plastic deformation due to the HAC puncture drop. The maximum shear stress in the most heavily loaded closure bolt is 32 MPa for cases P4, P5, and P6. The allowable bolt shear stress for HAC is $0.42S_u$, or 362 MPa for the overpack closure bolt A320, Grade L43 material at an upper-bound design temperature of 93°C. The corresponding minimum design margin in the overpack closure bolts for all HAC puncture drop impact orientations is +10.3. Therefore, the overpack closure bolts satisfy the applicable HAC structural design criteria for the HAC puncture drop impact.

The permanent deformation of the overpack following each HAC hot puncture drop tests (i.e., case P3B not included) are shown in Figure 2-30 through Figure 2-35. The results show that the

permanent deformation of the overpack resulting from the HAC puncture drop is small and localized in comparison to the permanent deformation resulting from the HAC free drop tests. As shown in Figure 2-30 and Figure 2-32, the damage to the overpack resulting from the HAC hot bottom and top center puncture drops (cases P1 and P3A) is similar. In these cases the package damage is limited to a circular-shaped dent centered on the bottom or top outer end plate of the overpack assembly that is approximately 150 mm in diameter (i.e., the puncture bar diameter) and 20 mm deep. For the HAC hot bottom and top oblique puncture drops (cases P2 and P4), the package damage is limited to a crescent-shaped dent in the impacted outer end plate of the overpack assembly with a maximum depth of approximately 30 mm, as shown in Figure 2-31 and Figure 2-33. The package damage resulting from the HAC hot side-center puncture drop (case P5), shown in Figure 2-34, is limited to a dent in the overpack base outer shell that is approximately 150 mm long (i.e., the puncture bar diameter) and 20 mm deep. The package damage resulting from the HAC hot side-oblique puncture drop (case P6), shown in Figure 2-35, is limited to a crescent-shaped dent in the overpack-base outer shell with a maximum depth of approximately 27 mm.

The structural evaluation of the overpack for the HAC puncture test demonstrates that the overpack outer shell will not be penetrated or perforated by the puncture bar, thereby preventing the puncture bar from impinging directly upon the exterior surface of the cask assembly. Furthermore, the cask peak rigid-body acceleration loads due to the HAC puncture tests are much lower than those resulting from the HAC free drop test. Therefore, a detailed structural evaluation of the cask and shield lid is not required for the HAC puncture test since the stresses in the cask and shield lid due to the HAC puncture test are expected to be much lower than those calculated for the HAC free drop test.

A detailed stress analysis of the cask closure bolts for HAC puncture test is performed using the 3-D quarter-symmetry finite element model described in Section 2.5.1.2. The evaluation is performed for the HAC cold top center puncture impact, which results in the maximum cask longitudinal peak rigid-body acceleration load of 139*g*. A 153*g* equivalent-static longitudinal acceleration load, which includes a DLF of 1.1 to account for possible dynamic amplification within the cask assembly, is used for the analysis. The inertia load from the closure lid self-weight due to the HAC puncture drop is accounted for by applying the 153*g* equivalent-static acceleration load to the model. A uniform pressure load of 22,832 kPa is applied over the center region of the closure plate to model the inward-acting reaction from the puncture bar. This pressure load is distributed over a circular area with a diameter of 126.95 mm, which is less than the 150 mm diameter of the puncture bar, resulting in a total load of 289 kN. A uniform pressure load is applied to the underside of the closure lid to account for the loading from the combined mass of the shield plug and payload. For modeling simplicity, a uniform pressure load is applied over the entire area inside the containment O-ring diameter. Although the O-ring diameter upon which the pressure load is calculated is approximately 18% larger than the outside diameter of the shield plug, it does not significantly affect the solution results. In fact, the assumption of a uniform pressure distribution is conservative since the load from the shield plug will concentrate at its outer edge because it is relatively stiff compared to the closure plate. Thus, the prying moment resulting from the assumed uniform pressure load distribution is conservative.

The HAC puncture loading is applied in combination with NCT heat temperature loading, maximum internal pressure, and maximum bolt preload. The NCT heat temperature loading is applied to the finite element model as a uniform temperature load of 68.3°C. The maximum bolt preload of 7.2 kN is applied to each bolt and a uniform pressure load of 700 kPa is applied on the inner surface of the closure plate over the area inside the containment O-ring.

The maximum average stress (i.e., axial stress) in the closure bolts due to HAC puncture loading is 212 MPa. The average axial stress for HAC is limited to the less of $3S_m$ or $0.7S_u$. The values of S_m and S_u for SA-320, Grade L43 bolting steel at 68.3°C are 234 MPa and 862 MPa, respectively, based on linear interpolation of the values shown in Table 2-15. Therefore, the allowable average stress for HAC is 603 MPa. The corresponding minimum design margin in the closure bolt for the HAC puncture loading is +1.84.

The maximum lid separation at the inside edge of the bolting flange resulting from the HAC top end drop loading is approximately 0.004 mm, or 0.4% of the O-ring compression. The maximum lid separation resulting from the HAC puncture test is not significant and no radioactive material is expected to escape from the cask containment system under HAC puncture loading.

Table 2-55 – Summary of HAC Puncture Drop Cases Evaluated

Case I.D.	Case Description	Mass Properties[1]	Thermal Condition[2]	Material Properties[3]	Impact Angle[4]
P1	Hot Bottom Center Puncture	Upper Bound	Hot	Lower Bound	0°
P2	Hot Bottom Oblique Puncture	Upper Bound	Hot	Lower Bound	25°
P3A	Hot Top Center Puncture	Upper Bound	Hot	Lower Bound	180°
P3B	Cold Top Center Puncture	Lower Bound	Cold	Upper Bound	180°
P4	Hot Top Oblique Puncture	Upper Bound	Hot	Lower Bound	155°
P5	Hot Side Center Puncture	Upper Bound	Hot	Lower Bound	90°
P6	Hot Side Oblique Puncture	Upper Bound	Hot	Lower Bound	105°

Notes:
1. Upper- and lower-bound mass properties are 2.5% higher and lower than the nominal values shown in Table 2-8.
2. A lower-bound uniform package temperature -29°C is assumed for the "cold" thermal condition. Upper-bound temperatures of 93°C for the overpack steel and 82°C for the overpack foam core are assumed for the "hot" thermal condition.
3. Upper- and lower-bound strength properties of the overpack materials are described in Section 2.2.1.
4. Impact angle is measured relative to the vertical upright package position (refer to Figure 2-29).

Table 2-56 – HAC Puncture Drop Summary

Case I.D.	Case Description[1]	Overpack Foam Maximum Crush[2]	Overpack Shell Maximum Total Strain	Cask Peak Rigid-Body Accelerations[3]	
				Transverse	Longitudinal
P1	Hot Bottom Center Puncture	24%	6%	---	83g
P2	Hot Bottom Oblique Puncture	37%	19%	37g	65g
P3A	Hot Top Center Puncture	22%	9%	---	72g
P3B	Cold Top Center Puncture	11%	8%	---	139g
P4	Hot Top Oblique Puncture	38%	21%	43g	50g
P5	Hot Side Center Puncture	22%	21%	96g	---
P6	Hot Side Oblique Puncture	30%	23%	66g	16g

Notes:
1. Puncture drop impact orientations shown in Figure 2-29.
2. Value is equal to the maximum deformation divided by the nominal foam thickness in the corresponding direction.
3. The highest peak accelerations on either the top or bottom centerline of the cask/shield lid rigid-body in the transverse (X) and longitudinal (Y) directions are reported.

Table 2-57 – Overpack Closure-Bolt HAC Puncture Drop Stress Summary

Case I.D.	Case Description[1]	Maximum Shear Stress (MPa)	Maximum Total Strain Intensity	Minimum Bolt Design Margin[2]
P1	Hot Bottom Center Puncture	<2	0.02%	Large[3]
P2	Hot Bottom Oblique Puncture	22	0.11%	+15.5
P3A	Hot Top Center Puncture	<4	0.05%	Large[3]
P3B	Cold Top Center Puncture	<4	0.05%	Large[3]
P4	Hot Top Oblique Puncture	32	<0.20%	+10.3
P5	Hot Side Center Puncture	32	<0.15%	+10.3
P6	Hot Side Oblique Puncture	32	<0.15%	+10.3

Notes:

1. Puncture drop impact orientations are shown in Figure 2-29.
2. The minimum design margin is calculated as (Allowable Value/Maximum Value) – 1, where the allowable shear stresses for A320, Grade L43 bolting steel at an upper-bound temperature of 93°C is 362 MPa, and the allowable axial strain is equal to the maximum elongation of A320, Grade L43 bolting steel (i.e., 16%).
3. The minimum bolt design margin for this case is greater than +50.0 and does not control the design.

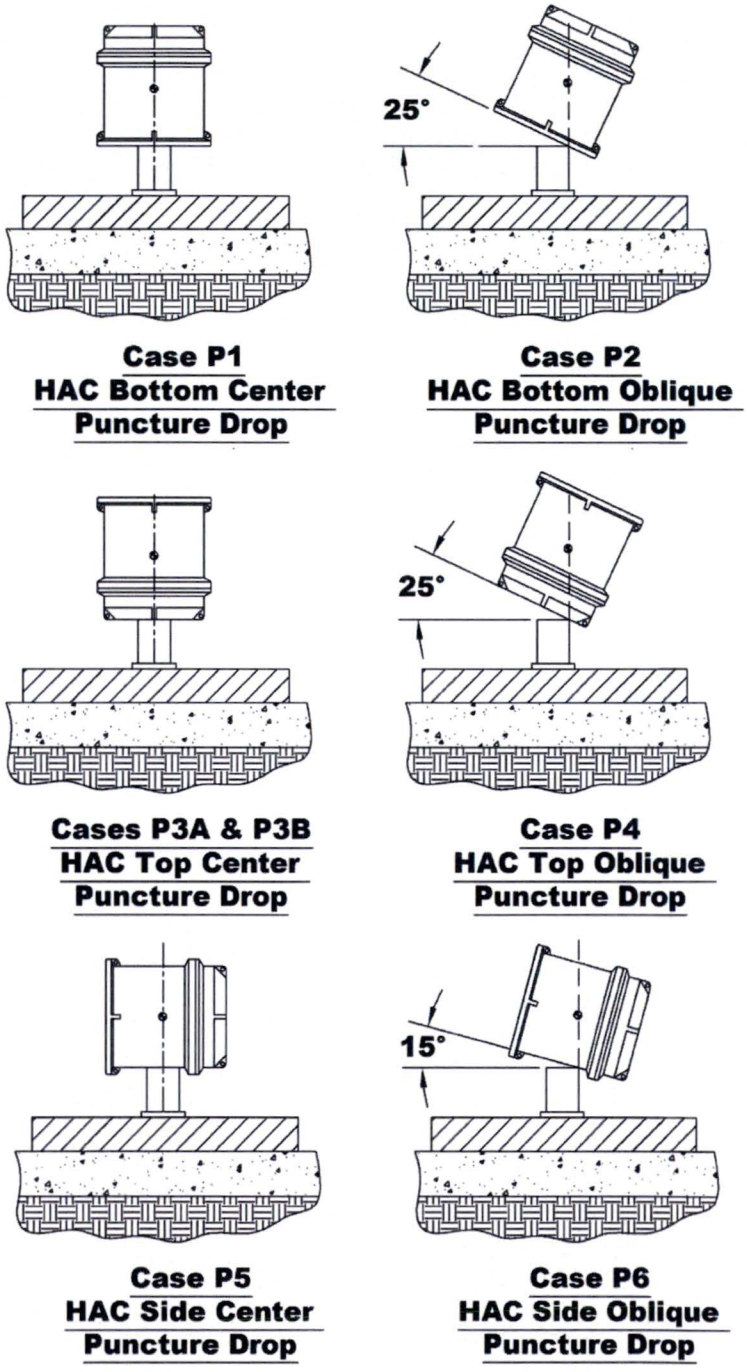

Figure 2-29 – HAC Puncture Drop Impact Orientations

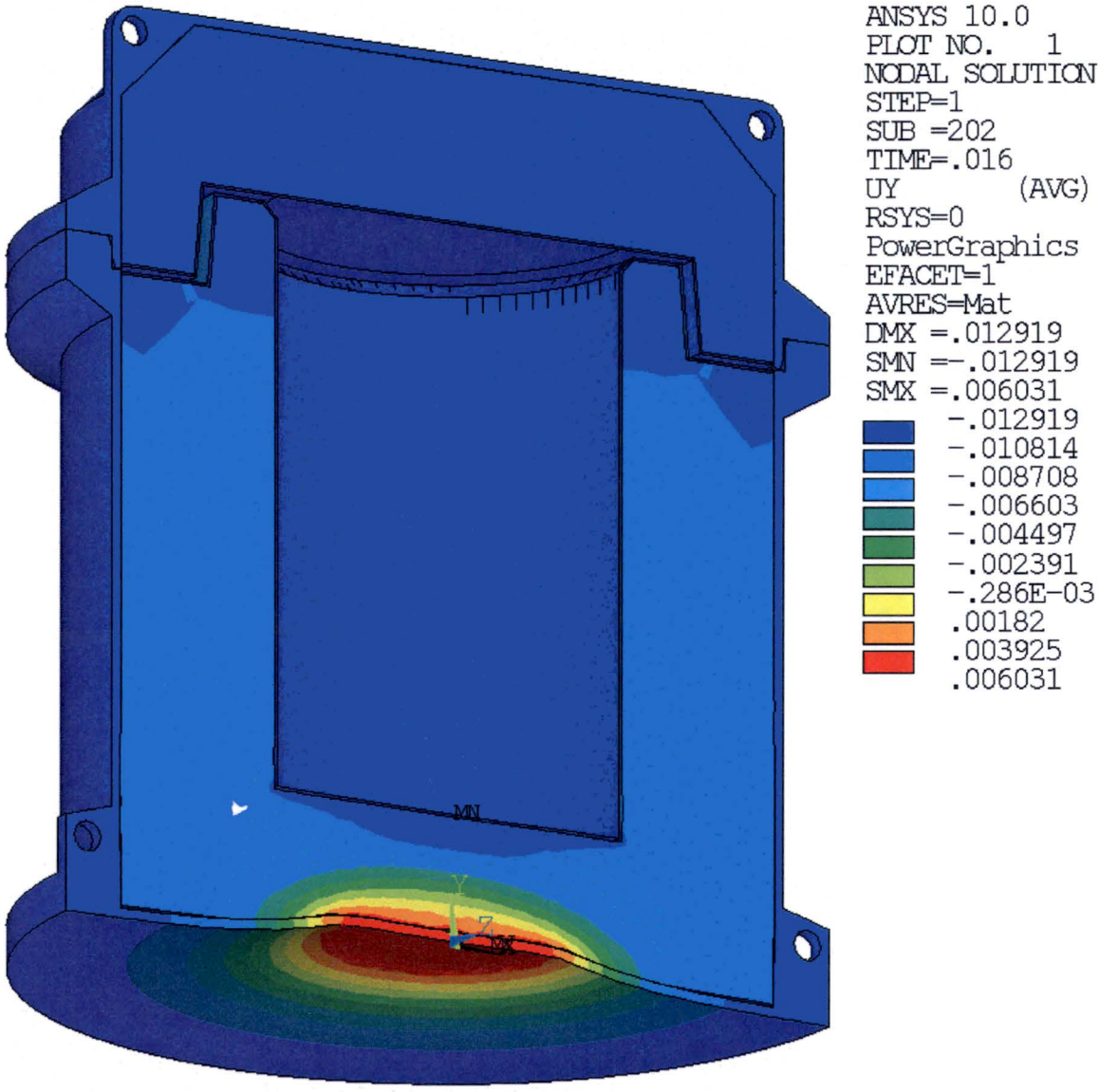

(Note: Displacement units are meters)

Figure 2-30 – Overpack Deformation, HAC Hot Bottom-Center Puncture (Case P1)

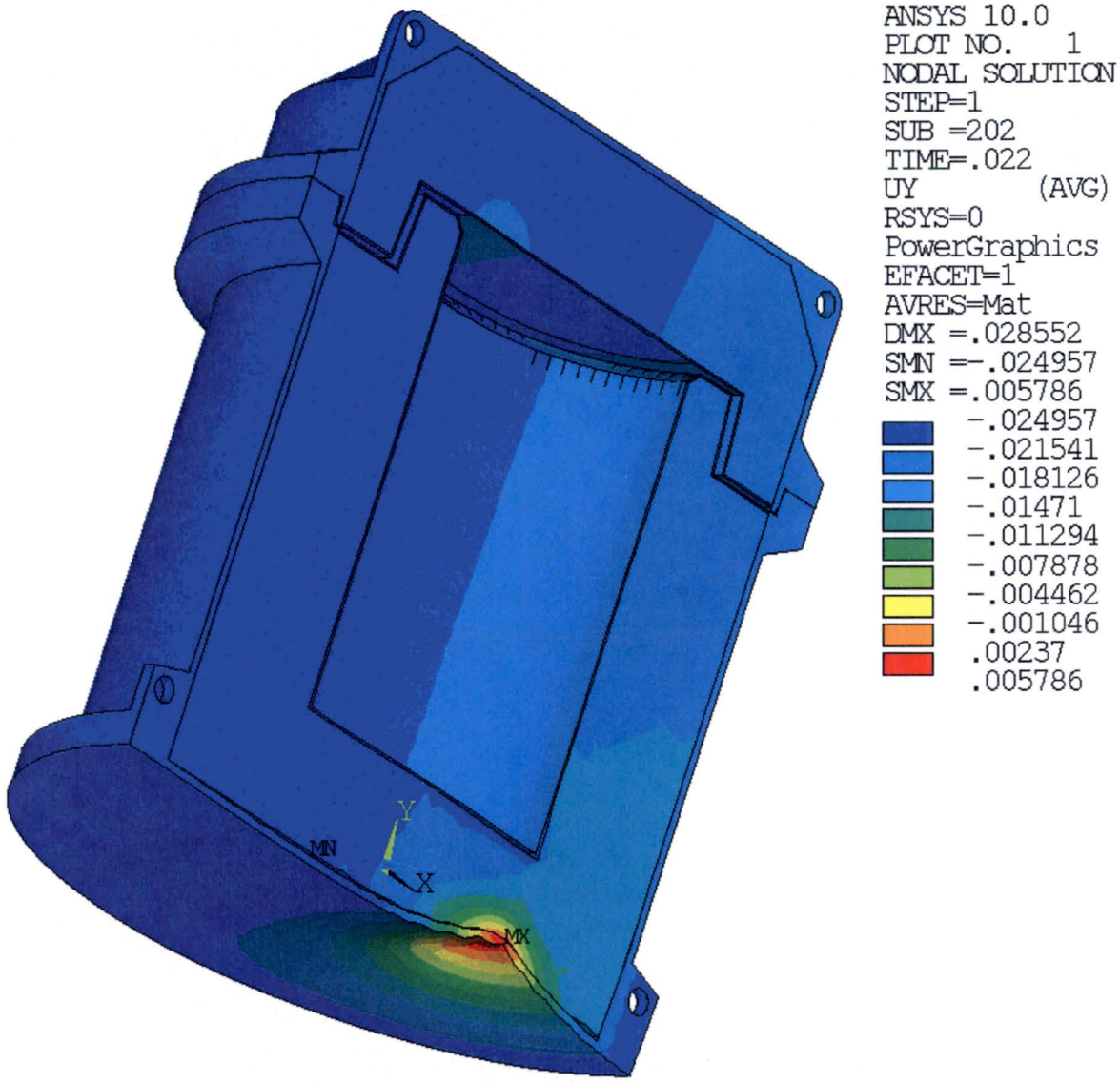

(Note: Displacement units are meters)

Figure 2-31 – Overpack Deformation, HAC Hot Bottom-Oblique Puncture (Case P2)

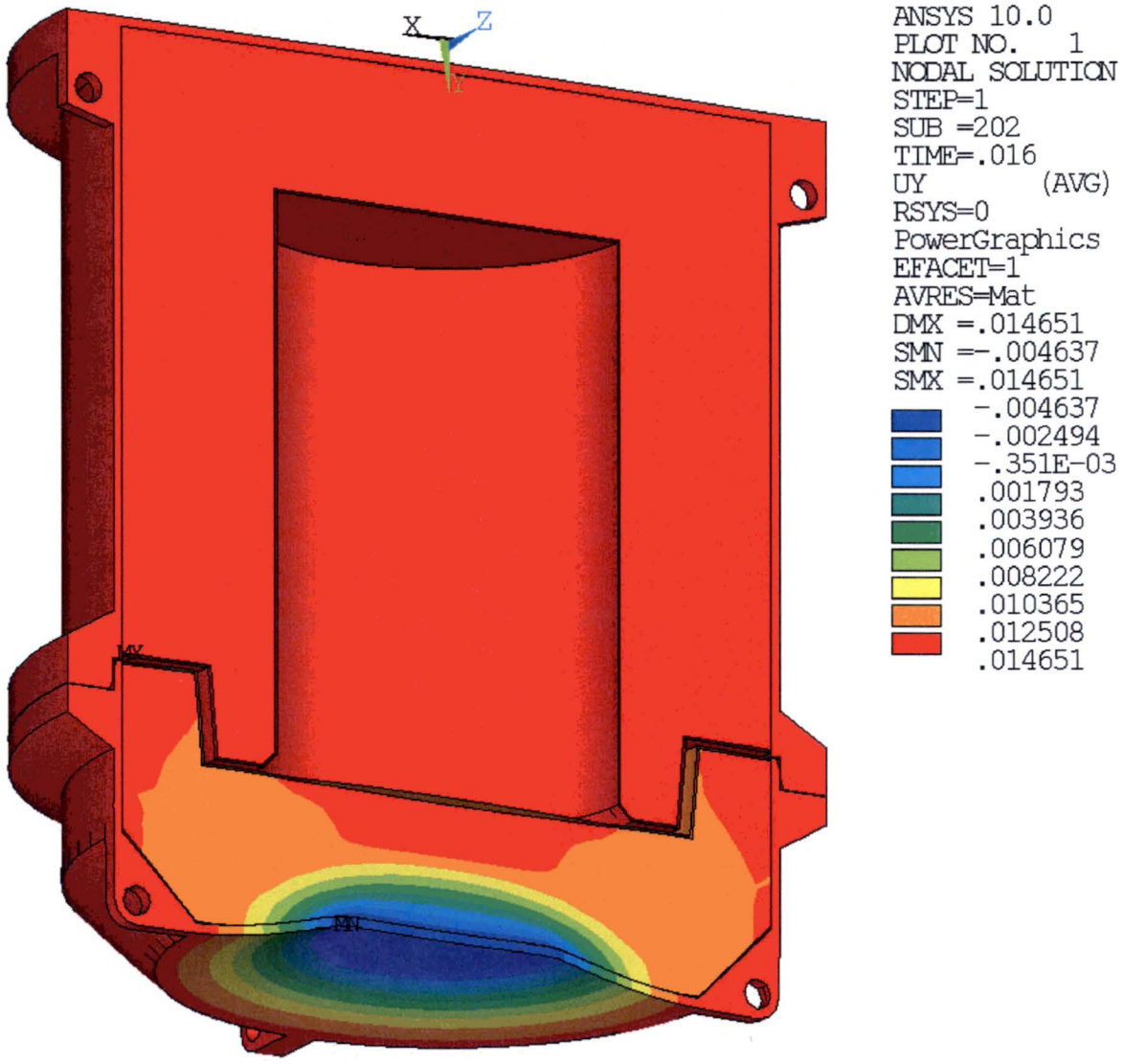

(Note: Displacement units are meters)

Figure 2-32 – Overpack Deformation, HAC Hot Top-Center Puncture (Case P3A)

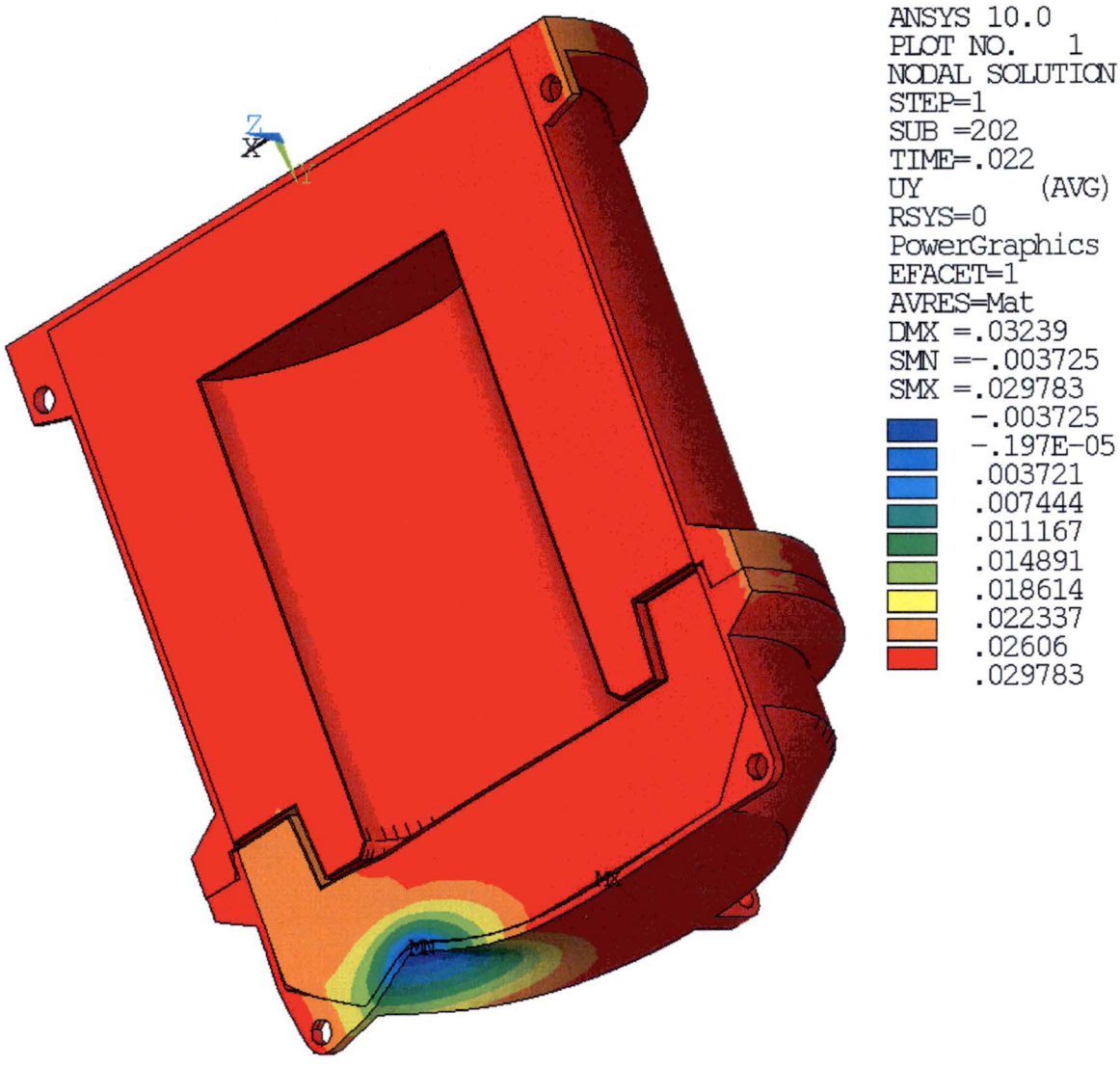

(Note: Displacement units are meters)

Figure 2-33 – Overpack Deformation, HAC Hot Top-Oblique Puncture (Case P4)

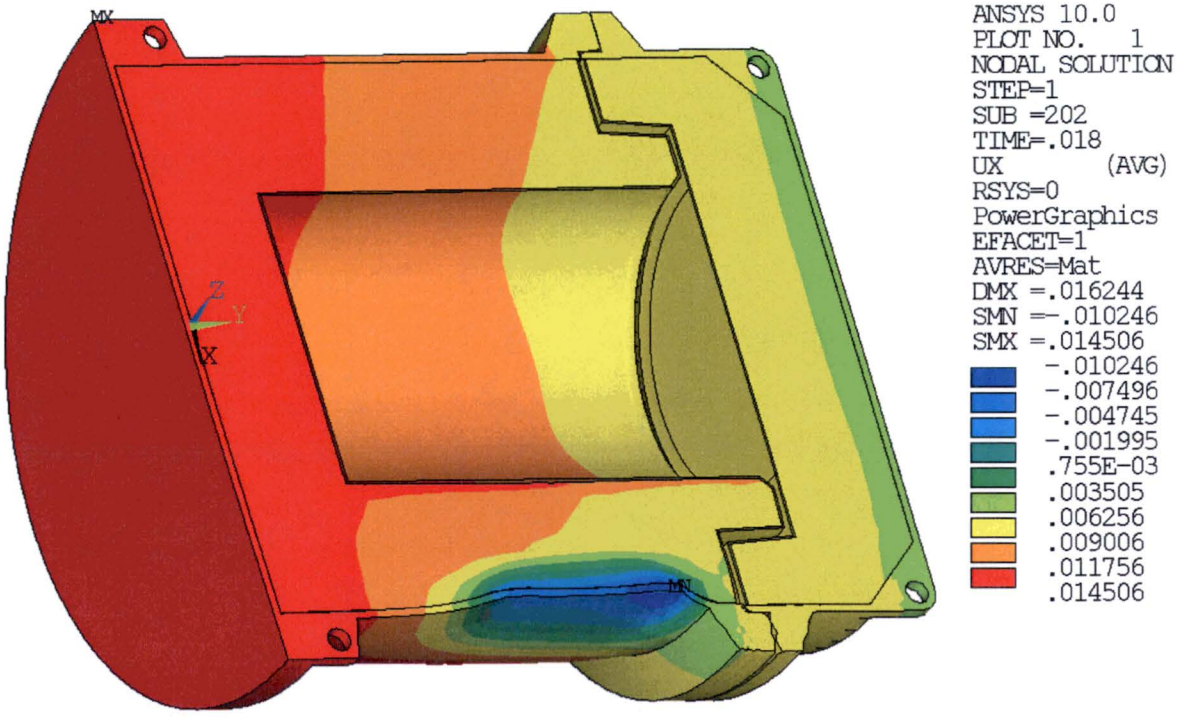

(Note: Displacement units are meters)

Figure 2-34 – Overpack Deformation, HAC Hot Side-Center Puncture (Case P5)

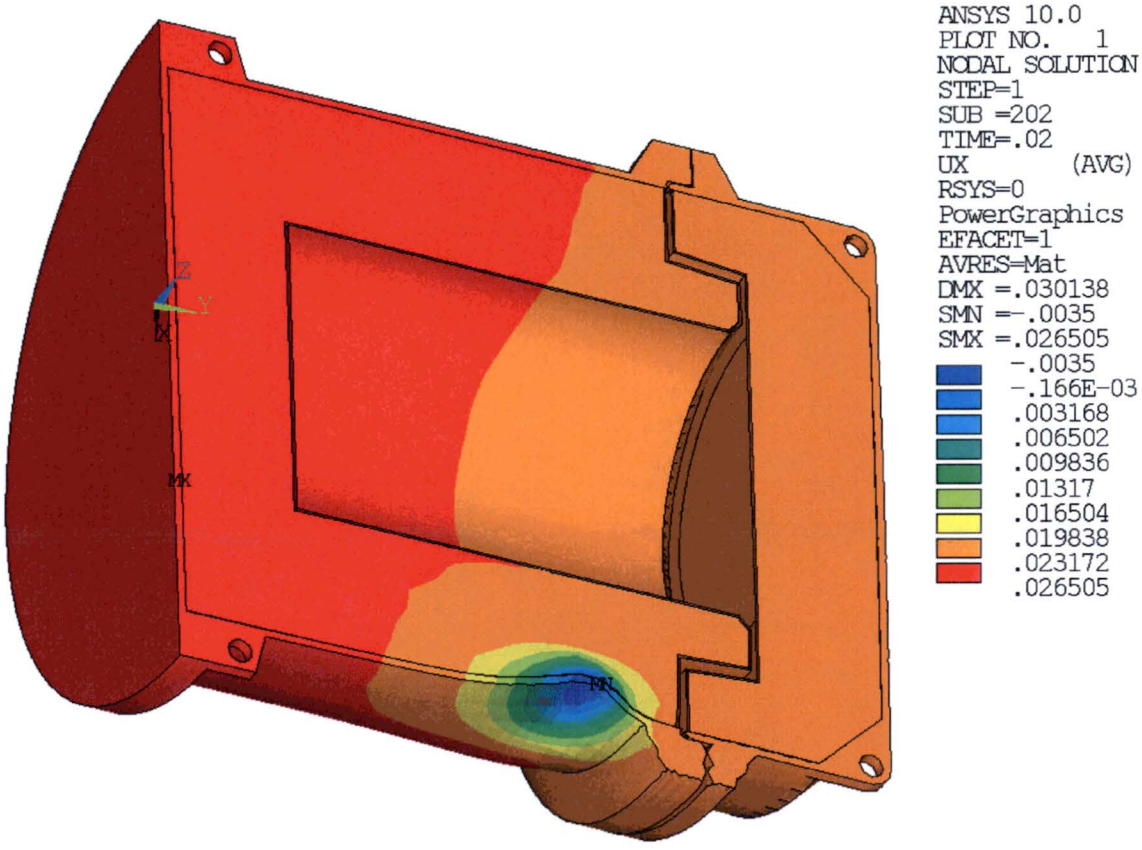

(Note: Displacement units are meters)

Figure 2-35 – Overpack Deformation, HAC Hot Side-Oblique Puncture (Case P6)

2.7.4 Thermal

In accordance with §71.73(c)(4), the package is designed to withstand the 30-minute fire with the flame temperature of 800°C. This section presents the structural evaluation of the cask for the HAC thermal loading. The package temperatures and pressure resulting from the HAC thermal test are discussed in Section 2.7.4.1. Differential thermal expansion between the components of the package due to the HAC thermal loading is discussed in Section 2.7.4.2. The stresses in the cask due to the HAC thermal loading are evaluated in Section 2.7.4.3. Compliance with the applicable structural design criteria and the applicable regulatory performance requirements is discussed in Section 2.7.4.4.

2.7.4.1 Summary of Pressures and Temperatures

The cask is insulated from the full effects of the HAC fire by the overpack. The thermal evaluation of the package for the HAC fire shows that, while the outer shell of the overpack reaches a peak temperature of approximately 782°C during the HAC fire transient, the peak temperature of the cask only reaches 221°C. The cask maximum internal pressure during the HAC fire is 12.6 bar or 1,260 kPa gauge.

2.7.4.2 Differential Thermal Expansion

Differential thermal expansion in the cask due to the HAC thermal loading causes the clearances between the cask components to increase. The HAC thermal evaluation shows that the pre-fire temperature gradient between the cask's inner and outer shells is essentially reduced to zero during the fire and remains lower over the post-fire transient. Therefore, the differential thermal expansion between the cask shells and DU during the HAC fire is expected to be bounded by the results for NCT heat from Section 2.6.1.2.

2.7.4.3 Stress Calculations

With the exception of closure-bolt stresses, the stresses in the package resulting from temperature loading are classified as secondary and need not be evaluated for HAC in accordance with the ASME Code. The HAC thermal evaluation of the package shows that the thermal gradients within the cask during the HAC fire are much greater than those due to NCT conditions. For instance, the temperature gradient between the cask's inner and outer shells is approximately +3.7°C for the NCT hot thermal condition and approximately -83.8°C for the HAC fire (bottom end drop damage case). However, due to the construction of the cask, these thermal gradients are not expected to cause significant thermal stresses in the cask. The through-wall gradient results in free thermal longitudinal thermal expansion of the cask's inner and outer shells. The only significant thermal stresses in the cask body are expected to occur in the closure bolts (due to differential thermal expansion of the closure bolts and closure lid) and at the cask outer shell-to-flange junctions. However, HAC fire is not expected to cause any permanent deformation or gross structural failure in the cask.

The stresses in the cask closure bolts due to HAC thermal loading are determined using the 3-D quarter-symmetry finite element model described in Section 2.5.1.2. The HAC thermal temperature loading for the cask closure-bolt analysis is applied as a uniform elevated temperature load of 204°C, which bounds the peak temperature of the cask closure bolt for the HAC thermal of 147.4°C. Elevated temperature produces differential thermal expansion between the closure bolts and closure lid, due to the differences in their material model coefficient of thermal expansion values, causing thermal stress. Thermal stresses in the closure bolts due to closure plate through-thickness temperature gradients are not considered since these temperature gradients are small. In combination with the HAC thermal temperature loading, a maximum bolt preload of 7.2 kN is applied to each closure bolt and a bounding accident internal pressure load of 1,800 kPa is applied on the inner surface of the closure plate over the entire area inside the containment O-ring.

The maximum average stress (i.e., axial stress) in the closure bolts due to HAC thermal loading is 486 MPa. The average bolt axial stress for HAC is limited to the lesser of $3S_m$ or $0.7S_u$. The values of S_m and S_u for SA-320, Grade L43 bolting steel at a bounding closure-bolt design temperature of 204°C are 234 MPa and 862 MPa, respectively. Therefore, the allowable average stress for HAC is 603 MPa, and the corresponding maximum closure bolt stress ratio is 0.81.

2.7.4.4 Comparison with Allowable Stresses

The results of the structural evaluation for the HAC thermal test demonstrate that the cask satisfies the applicable HAC allowable-stress design criteria. The HAC thermal loading does not cause any significant permanent deformation of the cask or shield lid, nor does it substantially reduce the effectiveness of the packaging. The evaluation shows that no inelastic deformation of the closure bolts results from the HAC thermal loading. Thus, the containment seal will be maintained under HAC thermal loading, and there will be no loss or dispersal of radioactive contents. The damage to the overpack resulting from HAC free drop loading is considered in the HAC shielding evaluation, which demonstrates that the external dose-rate limit requirement of §71.51(a)(1) is satisfied. Therefore, the package complies with the requirements of §71.51(a)(1) when subjected to the HAC thermal test of §71.73(c)(4).

2.7.5 Immersion — Fissile Material

Not applicable.

2.7.6 Immersion — All Packages

In accordance with §71.73(c)(6), an undamaged package is subjected to a water pressure equivalent to immersion under a head of water of at least 15 m, or an equivalent external pressure load of 150 kPa gauge. In addition to the external pressure loading, the quenching effects of immersion in water are considered.

The stresses in the cask and shield lid resulting from "HAC immersion - all packages" loading are determined using the axisymmetric finite element model described in Section 2.6.1.3. The applied loads and boundary conditions for the "HAC immersion - all packages" analysis are

shown in Figure 2-36. An external pressure load of 150 kPa gauge is applied to the outer surfaces of the cask's containment system, conservatively taking no credit for any pressure-retaining ability of the package non-containment components. Zero internal pressure is assumed in combination with the immersion external pressure load to maximize the net pressure load acting on the containment system. The temperature gradient applied to the model for the "HAC immersion - all packages" analysis is the same as the bounding NCT heat temperature gradient discussed in Section 2.6.1.3, except that the temperatures of the outer shells of the cask and shield lid are conservatively set to 21°C to account for the quenching effect of water. This is conservative since it neglects the relatively large thermal mass of the cask and assumes an instantaneous temperature change on the outside of the cask and no temperature change in the rest of the cask.

The maximum stresses in the cask's containment system and non-containment components due to the "HAC immersion - all packages" loading, along with the corresponding allowable stress intensities and minimum design margins, are summarized in Table 2-58. The minimum design margin is +1.63 for primary membrane plus bending stress intensity (P_m+P_b) at the bottom end of the cask-body outer shell (section N3 in Figure 2-2). Thus, the cask satisfies the applicable HAC allowable-stress design criteria for the "HAC immersion - all packages" test.

A buckling evaluation of the cask's containment shell and outer shell is performed for the "HAC immersion - all packages" loading in accordance with the requirements of ASME Code Case N-284-1 [2.7]. The maximum compressive stresses and shear stresses near the mid-lengths of the cask's inner shell and outer shell (i.e., Sections C5 and N5 in Figure 2-1 and Figure 2-2) are used for the cask-shell buckling evaluation. As discussed in Section 2.1.2.3, elastic and inelastic buckling interaction ratios are calculated based on the HAC allowable buckling stresses shown in Table 2-7, which include a factor of safety of 1.34. The maximum interaction ratios must not exceed 1.0.

The maximum calculated cask-shell stresses and the resulting maximum buckling interaction ratios for the "HAC immersion - all packages" loading are summarized in Table 2-59. The maximum buckling interaction ratios in the cask's inner and outer shells are 0.03 and 0.00, respectively. Therefore, the cask satisfies the buckling design criteria of ASME Code Case N-284-1 for the "HAC immersion—all packages" test.

Table 2-58 – "HAC Immersion - All Packages" Maximum Stress Summary

Cask Components	Stress Type	Maximum Stress Intensity (MPa)	Controlling Location[1]	Allowable Stress Intensity[2] (MPa)	Minimum Design Margin[3]
Containment System	P_m	99	C21	331	+2.34
	P_m+P_b	106	C21	492	+3.64
	P_m+P_b+Q	109	C21	N/A[4]	N/A[4]
Non-Containment Components	P_m	84	N3	221	+1.63
	P_m+P_b	140	N3	332	+1.37
	P_m+P_b+Q	141	N3	N/A[4]	N/A[4]

Notes:
1. Containment system and non-containment component stress locations are shown in Figure 2-1 and Figure 2-2, respectively.
2. Allowable stress intensities are based on an upper-bound design temperature of 74°C.
3. Design margin is calculated as (Allowable S.I./Maximum S.I) – 1.
4. Evaluation of secondary stress is not required for HAC.

Table 2-59 – Cask-Shell Buckling Stresses, Immersion - All Packages

Stress Type	Calculated Stresses[1], kPa	
	Inner Shell[2]	Outer Shell[3]
Axial Stress, SY (σ_ϕ)	1,389	0[4]
Hoop Stress, SZ (σ_θ)	2,706	-103
Shear Stress, SXZ ($\sigma_{\phi\theta}$)	0	0

Notes:
1. The maximum compressive axial and hoop stress intensities and maximum in-plane shear stress intensities are reported.
2. Maximum stress intensities at section C5 in Figure 2-1.
3. Maximum stress intensities at section N5 in Figure 2-2.
4. Zero stress is assumed for the buckling evaluation since the stress is tensile.

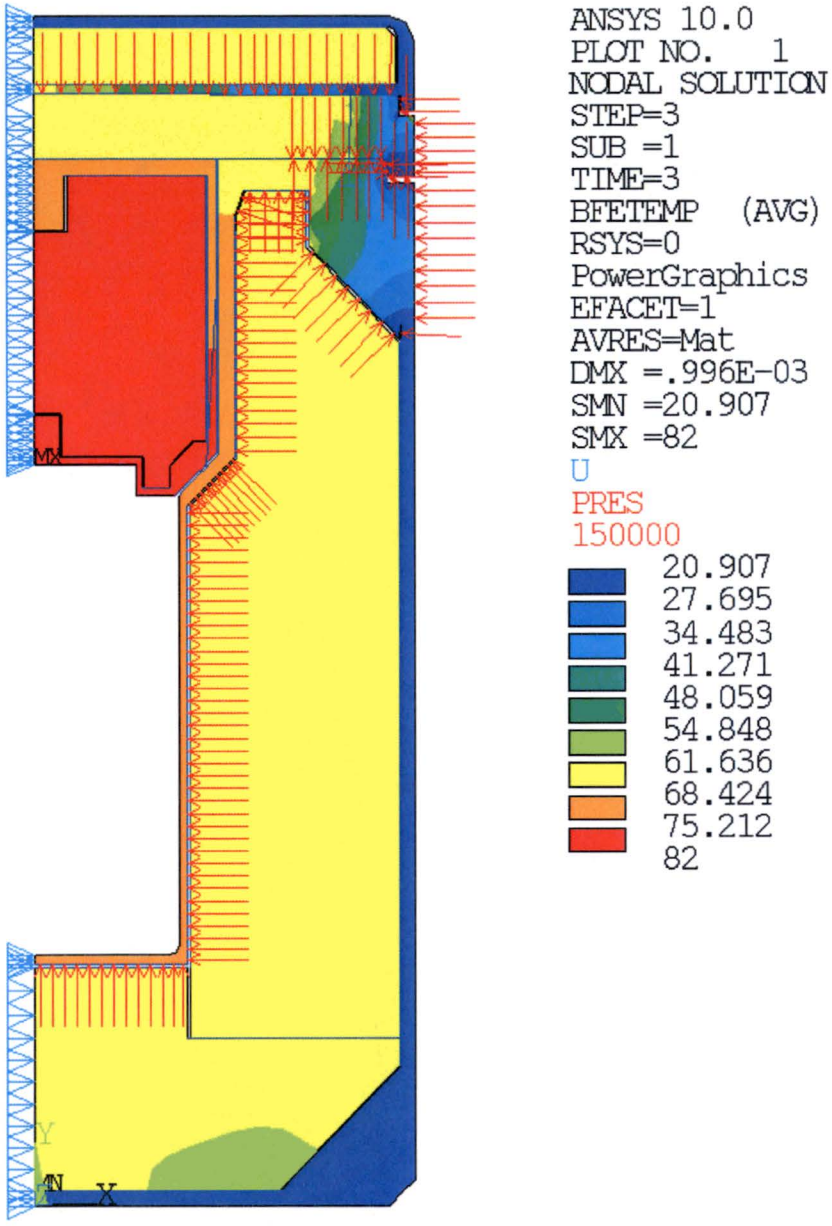

(Note: Temperatures in °C and pressure in units of Pa)

Figure 2-36 – Immersion - All Packages, Applied Pressure and Temperature Loads

2.7.7 Deep Water Immersion Test (for Type B Packages Containing More than 10^5 A_2)

Not applicable.

2.7.8 Summary of Damage

The preceding structural evaluation demonstrates that the package satisfies the applicable structural design criteria and the performance requirements of 10 CFR 71 for the HAC test sequence of §71.73. The condition of the package after each test of the HAC sequence, based on the sequential application of the free drop, puncture, and thermal tests, is summarized as follows.

HAC Free Drop

The HAC free drop does not cause any significant permanent deformation in the cask assembly and shield lid assembly. No inelastic deformation of the cask closure bolts and containment sealing surfaces results from the HAC free drop test. The only significant package damage resulting from the HAC free drop occurs in the overpack assembly. The overpack damage resulting from each of the HAC free drop orientations is discussed in Section 2.7.1.5. The HAC end drops and side drop are shown to cause the greatest extent of damage to the overpack. The HAC hot bottom end drop results in 45 mm of permanent crush in the bottom end of the overpack base, or 47% of the overpack bottom end thickness. The HAC hot top end drop results in 56 mm of permanent crush in the top end of the overpack lid, or 54% of the overpack top end thickness. The overpack side wall thickness is permanently reduced by about 40 mm, or 35% of the overpack side wall thickness, as a result of the HAC hot side drop.

HAC Puncture

The package is subjected to the HAC puncture test of §71.73(c)(1), considering the damage sustained from the HAC free drop of §71.73(c)(3). The damage to the package resulting from the HAC free drop does not affect the package's ability to withstand the HAC puncture. As discussed in Section 2.7.3, the extent of package damage resulting from the HAC puncture test is limited to local deformation (i.e., denting) of the overpack outer shell. The puncture bar will not pierce the overpack outer shell or cause any significant damage to the bolted closure of the overpack assembly.

The cumulative damage of the overpack resulting from the HAC free drop and HAC puncture tests is considered in the HAC thermal evaluation presented in Section 3.4. The HAC thermal evaluation is performed for three separate bounding damage scenarios: bottom end impact damage, top end impact damage, and side impact damage. The extent of overpack damage assumed in the HAC thermal analysis bounds the effects of the cumulative damage that result from the HAC free drop and HAC puncture tests. The results of the HAC thermal evaluation demonstrate that the cumulative damage does not affect the overpack's ability to satisfy the performance requirements of 10 CFR 71.

HAC Fire

The package is subjected to the HAC thermal test of §71.73(c)(4), considering the damage sustained from the HAC free drop of §71.73(c)(1) and HAC puncture of §71.73(c)(3). The extent of package damage resulting from the HAC free drop and HAC puncture tests does not affect the package's ability to withstand the HAC thermal test. This is demonstrated by the HAC thermal evaluation, which considers the cumulative package damage resulting from the HAC free drop and HAC puncture tests. The overpack thermal relief plugs are designed to fail during the HAC thermal test to allow gases generated by the foam material to escape. The HAC thermal test will cause some charring to the outer portion of the overpack foam. However, the foam will provide sufficient thermal protection to prevent the cask temperatures from exceeding any of the cask component temperature limits. The structural evaluation of the package for the temperature and pressure loads resulting from the HAC thermal test shows that no additional damage of the cask and shield lid will result from the HAC thermal test. As discussed in Section 2.7.4.3, the cask closure bolts satisfy the applicable HAC allowable stress design criteria and will maintain leak-tight containment under the worst-case HAC thermal loading.

2.8 Accident Conditions for Air Transport of Plutonium

Not applicable.

2.9 Accident Conditions for Fissile Material Packages for Air Transport

Not applicable.

2.10 Special Form

Not applicable.

2.11 Fuel Rods

Not applicable.

2.12 Appendix

2.12.1 References

[2.1] American Society of Mechanical Engineers (ASME) Boiler and Pressure Vessel Code, Section III, Division 3, *Containment Systems for Storage and Transport Packagings of Spent Nuclear Fuel and High Level Radioactive Material and Waste*, 2001 Edition with Addenda through July 1, 2003.

[2.2] American Society of Mechanical Engineers (ASME) Boiler and Pressure Vessel Code, Section III, Division 1, Subsection NF, *Supports*, 2001 Edition with Addenda through July 1, 2003.

[2.3] Regulatory Guide 7.9, *Standard Format and Content of Part 71 Applications for Approval of Packages for Radioactive Material*, Revision 2, March 2005.

[2.4] Interim Staff Guidance – 21 (ISG-21), *Use of Computational Modeling Software*, U.S. Nuclear Regulatory Commission, Spent Fuel Project Office, April 2006.

[2.5] Regulatory Guide 7.8, *Load Combinations for the Structural Analysis of Shipping Casks for Radioactive Material*, Revision 1, U.S. Nuclear Regulatory Commission, Office of Standards Development, March 1989.

[2.6] American Society of Mechanical Engineers (ASME) Boiler and Pressure Vessel Code, Section III, Division 1, Appendix F, *Rules for Evaluation of Service Loadings with Level D Service Limits*, 2001 Edition with Addenda through July 1, 2003.

[2.7] American Society of Mechanical Engineers (ASME) Boiler and Pressure Vessel Code, Section III, Division 1, Code Cases: Nuclear Components, Case N-284-1, *Metal Containment Shell Buckling Design Methods, Class MC*, 2001 Edition with Addenda through July 1, 2003.

[2.8] American Society of Mechanical Engineers (ASME) Boiler and Pressure Vessel Code, Division 1, Appendix I, *Design Stress Intensity Values, Allowable Stresses, Material Properties, and Design Fatigue Curves*, 2001 Edition with Addenda through July 1, 2003.

[2.9] Regulatory Guide 7.11, *Fracture Toughness Criteria of Base Material for Ferritic Steel Shipping Cask Containment Vessels with a Maximum Wall Thickness of 4 Inch (0.1 m)*, U.S. Nuclear Regulatory Commission, Office of Standards Development, June 1991.

[2.10] Holman, W. R., and Langland, R. T., *Recommendations for Protecting Against Failure by Brittle Fracture in Ferritic Steel Shipping Containers Up to Four Inches Thick*, NUREG/CR-1815, UCRL-53013, U.S. Nuclear Regulatory Commission, August 1981.

[2.11] American Society of Mechanical Engineers (ASME) Boiler and Pressure Vessel Code, Section II, Part D, *Materials*, 2001 Edition with Addenda through July 1, 2003.

[2.12] Eckelmeyer, K. H., *An Investigation of the Mechanical Behavior of Cast U-2 wt. % Mo for Breeder Reactor Spent Fuel Shipping Cask–Radiation Shielding*, SANDIA Report SAND80-1836, February 1982.

[2.13] Regulatory Guide 7.6, *Design Criteria for the Structural Analysis of Shipping Cask Containment Vessels*, Revision 1, March 1978.

[2.14] Fischer, L. E., and Lai, W., *Fabrication Criteria for Shipping Containers*, NUREG/CR-3854, UCRL-53544, U.S. Nuclear Regulatory Commission, March 1985.

[2.15] Gerber, T. L., et. al., *Evaluation of High-Energy Pipe Rupture Experiments*, EPRI Report No. NP-5531, January 1988.

[2.16] General Plastics Manufacturing Co., Design Guide for Use of LAST-A-FOAM® FR-3700 for *Crash and Fire Protection of Radioactive Material Shipping Containers*, Revision iss001.

[2.17] American Society of Mechanical Engineers Boiler and Pressure Vessel Code, Section II, *Materials*, Part B, *Nonferrous Material Specifications*, 2001 Edition with Addenda through July 1, 2003.

[2.18] Parker Hannifin Corporation, *Parker O-Ring Handbook*, ORD 5700/USA, 2001.

[2.19] American Society of Mechanical Engineers Boiler and Pressure Vessel Code, Section II, *Materials*, Part A, *Ferrous Material Specifications*, 2001 Edition with Addenda through July 1, 2003.

[2.20] Penton Publications, *Materials Engineering, Materials Selector 1990*, December 1989.

[2.21] Weakley, E. A., *Fuels Engineering Technical Handbook*, UNI-M-61, April 1979.

[2.22] American Society of Mechanical Engineers (ASME) Boiler and Pressure Vessel Code, Section IX, *Welding and Brazing Qualifications.* Latest Edition.

[2.23] ANSI N14.23, *Design Basis for Resistance to Shock and Vibration of Radioactive Material Packages Greater Than One Ton in Truck Transport*, American National Standards Institute, Inc., New York, 1980.

[2.24] Blevins, R. D., *Formulas for Natural Frequency and Mode Shape*, Van Nostrand Reinhold Company, 1979.

[2.25] NUREG/CR-3966, *Methods for Impact Analysis of Shipping Containers*, UCID-20639, U. S. Nuclear Regulatory Commission, November 1987.

2.12.2 Computer Code Descriptions

The structural evaluation of the package includes analyses performed using the ANSYS/Mechanical and ANSYS LS-DYNA PC modules of the ANSYS Release 10.0 computer program. These programs are both run on a PC platform under the Windows XP operating system. Descriptions of the models used to perform the structural analyses are provided in the respective sections of this chapter. Descriptions of these computer codes are provided in this section and the sections that follow.

The ANSYS computer code is acquired from and supported by ANSYS Incorporated as a fully-compiled executable program. The ANSYS/Mechanical and ANSYS LS-DYNA PC modules of the ANSYS computer code are tested, installed, operated, and maintained in accordance with the requirements of the Energy*Solutions* QA program. Prior to use for quality-affecting work, several validation test problems are solved using the ANSYS ANSYS/Mechanical and LS-DYNA PC computer codes. The validation tests include a large number of test problems included in the ANSYS Verification Manual and other independent test problems with solutions that are known either by classical means or by comparison to computer solutions that have been reviews and accepted by Energy*Solutions*. The validation tests demonstrate that the computer codes correctly solve the general classes of problems for which they will be used.

Errors in the ANSYS computer codes are identified and controlled in accordance with the requirements of the Energy*Solutions* QA program. All errors that are discovered either internally or externally are reviewed for impact on past and present work, and potential impact on future work. Errors that are identified to have potential impact on work are evaluated using the Corrective Action Process of the Energy*Solutions* QA program.

2.12.2.1 ANSYS Mechanical

The ANSYS/Mechanical computer code is an implicit finite element program that is used to solve a wide range of structural, heat transfer, and electromagnetic problems. The use of the ANSYS/Mechanical computer code for the structural analysis of the package is limited to mode-frequency analysis, and static structural analysis using linear-elastic material properties and non-linear contact behavior.

2.12.2.2 ANSYS LS-DYNA PC

The ANSYS LS-DYNA PC computer code combines the LS-DYNA explicit finite element program with the pre- and post-processing modules of the ANSYS program. The ANSYS LS-DYNA PC computer code is well-suited to simulate short-duration, large deformation dynamic impacts and complex contact problems. The code has been well benchmarked and is widely used for the structural analysis of transportation package drop tests.

2.12.3 Dynamic Load Factors

The stresses in the cask and shield lid due to NCT and HAC free drop loading are calculated using equivalent-static linear-elastic finite element analyses. The equivalent-static acceleration loads for each NCT and HAC free drop test are equal to the peak rigid-body accelerations of the cask multiplied by a DLF that accounts for possible dynamic amplification within the cask. The DLF is a function of the general shape of the rigid-body acceleration time-history pulse and the ratio of the duration of the rigid-body acceleration time-history to the cask period (t/T).

The longitudinal vibration modes of the cask that are of interest for the NCT and HAC free drop analyses include the axial compression/extension mode of the cask's outer shell and the plate bending mode of the closure lid.

The natural frequency of the cask's outer shell in compression is determined using classical hand calculations. The cask's outer shell is idealized as a linear spring with the bottom end fixed and a mass attached to the top end. The mass supported by the outer shell is equal to the total mass of cask assembly, less the mass of the cask-body DU shields and the cask's bottom plate, or 48.4 kg. The natural frequency of the cask's outer shell in compression is calculated using case 1 in Table 6-2 of Blevins [2.24] to be 1,121 Hz based on the nominal design dimensions and the elastic modulus of the cask's outer shell material at a bounding temperature of 93°C. This corresponds to a closure-lid natural period (T) of 0.000892 seconds.

The natural frequency of the closure lid in bending is determined using classical hand calculations. The closure plate is idealized as a 19 mm thick circular plate having a clamped edge at the bolt circle radius and a 15.3 kg point mass (i.e., the mass of shield plug and payload) at its center. The lowest natural frequency of the closure plate is calculated using case 12 in Table 11-1 of Blevins [2.24] to be 1,066 Hz based on the elastic modulus of the cask closure lid material at a bounding temperature of 93°C. This corresponds to a closure-lid natural period (T) of 0.000938 seconds.

The transverse vibration mode of the cask that is of interest for the NCT and HAC free drop analyses is the cantilever beam bending mode of the cask's inner containment shell. A finite element modal analysis of the cask is performed to determine the natural frequency of the cask for the inner-shell cantilever bending mode. The 3-D half-symmetry finite element model used for this analysis is shown in Figure 2-37. This model is essentially the same as the 3-D half-symmetry finite element model that is used for the detailed stress analysis of the cask assembly for those conditions that include transverse loading. The main difference between the two models are that the model used for the modal analysis does not include the shield lid assembly and that the nonlinear contact elements, which are not permitted for modal analyses, are deleted from the model. Instead, coupled nodes and displacement constraints are applied to the model to account for the expected boundary conditions under transverse impact loading conditions. The results of the analysis show that the natural frequency of the cask for the inner shell cantilever bending mode shown in Figure 2-38 is 897 Hz (i.e., T = 0.001115 s).

The general shape of the rigid-body acceleration time-history curve for all NCT and HAC free drop tests are characterized as a half-sine wave. The DLF for a half-sine wave pulse is shown in Figure 2.15 of NUREG/CR-3966 [2.25]. It shows that the DLF curve for a half-sine wave peaks at a maximum value of approximately 1.75 at t/T equal to 0.8 and reduces to 1.13 for t/T ratios of 2.5 and higher. Thus, the highest DLF results from the shortest acceleration time-history pulse duration and the longest natural period (i.e., the lowest natural frequency) of the cask. The NCT and HAC oblique drop acceleration time-histories have the shortest durations for all free drops at approximately 0.0035 seconds. Using the lowest natural frequency of the cask of 897 Hz (T = 0.001115 s) yields the lowest t/T ratio of 3.1 for all NCT and HAC free drop tests. Thus, a bounding DLF of 1.13 is conservatively used for all NCT and HAC free drop evaluations. The only exception to this is for the HAC end drop orientations, for which the shortest acceleration time-history pulse duration is approximately 0.004 seconds and the lowest longitudinal response frequency is 1,066 Hz, yielding a lower bound t/T ratio of 4.3. Based on the Figure 2.15 of NUREG/CR-3966 [2.25], the DLF for a t/T ratio of 4.3 is less than 1.1.

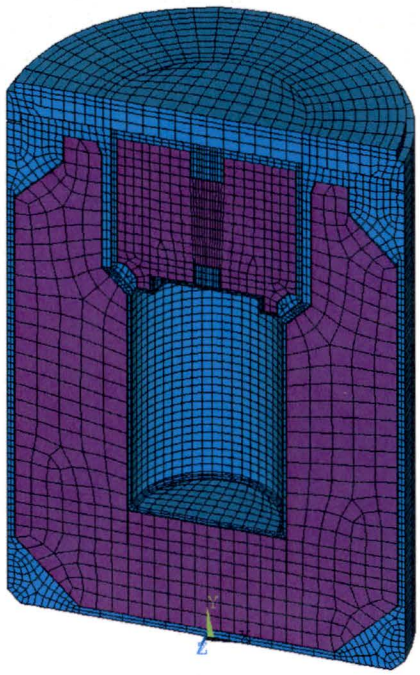

Figure 2-37 – MIDUS Cask Modal Analysis FE Model

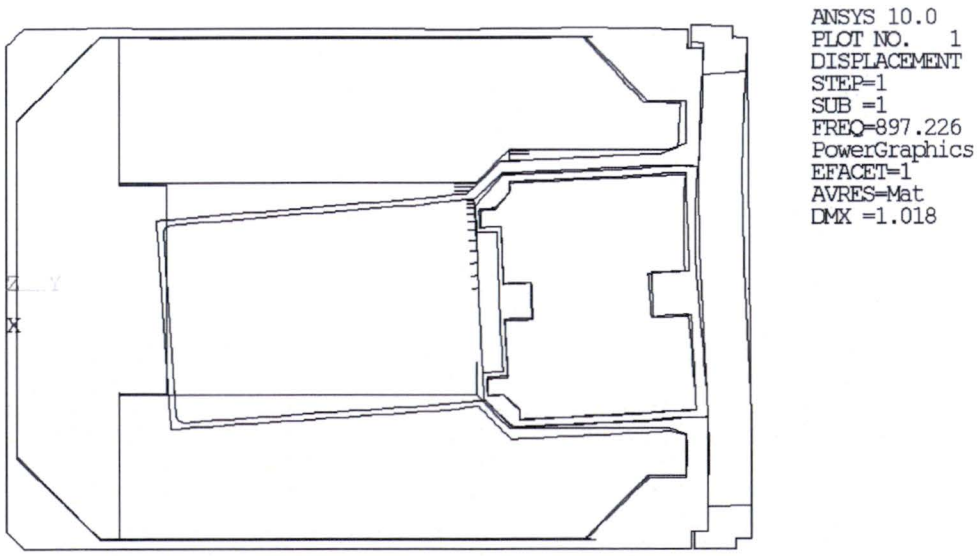

Figure 2-38 – Cask Body Containment Shell Cantilever Bending Mode Shape

2.12.4 Confirmatory Tests

2.12.4.1 Confirmatory Test Report

This section includes the confirmatory test report that provides a summary of the confirmatory testing performed to demonstrate the adequacy of the analytical methodologies used to predict the structural and thermal response of the package for the NCT free drop, HAC free drop, HAC puncture, and HAC thermal tests. The results of the confirmatory tests are summarized and compared to pre-test predictions determined using the same analytical methodology as the safety analyses. In general, the results of the confirmatory tests show good agreement with the pre-test predictions. In those instances where the test conditions deviated from the test plan or significant differences existed between the test results and the pre-test predictions, a reconciliation analysis was performed. The confirmatory drop test reconciliation analysis is included in Section 2.12.4.2.

(Attachment: Report No. TYC01.1071, Revision 0, *MIDUS Transportation Package Confirmatory Test Report*)

2.12.4.2 Confirmatory Test Reconciliation Analysis

(Attachment: Calc No. TYC01.1114, Revision 0, *MIDUS Confirmatory Drop Test Reconciliation Analysis*)